The synthesis and study of novel fluorescence probes for Nitroreductase

A thesis submitted to the National University of Ireland in fulfilment of the requirements for the degree of

Master of Science

By

Xiang Ao, B.Sc.

Department of Chemistry,

Maynooth University,

Maynooth, Co. Kildare,

Ireland.

December 2017

Research supervisor: Dr. Robert Elmes

Head of Department: Dr. Jennifer McManus

Declaration

I hereby certify that this thesis has not been submitted before, in whole or in part, to this or any university for any degree and is, except where otherwise stated, the original work of the author.

Signed:_____ Date:_____

Maynooth University

Acknowledgements

First of all, I would like to extend my sincere gratitude to my supervisor, Dr . Robert Elmes, For his instructive advice and useful suggestions on my project during the past two years. I am deeply thankful of his help in the completion of this thesis. His unselfish help and his profound knowledge of chemistry are the cornerstones for me to finish my study; his humorous personality and his skilful control over the language are the catalyst of my progress. I will not have any achievements without you. So I really want to say thank you very much! I would also like to thank Maynooth Chemistry Department for providing such a great place for me to study.

To all members of the Elmes research group, Anto, Nan and Michelle, thank you all for the laughs and good suggestions that made me a great person in the laboratory and in the life. Especially Anto, my partner in the lab and also the first friend I have ever met in Ireland who gave me many advises in chemistry and the way to live in Ireland. Michelle is also my best friend and I really thank her for helping me handling the biotechnology. Nan is not only my lab partner but also my roommate, we have a great time studying together and living together. And to the newest member of this group, Luke, I am pretty sure you can make it because you are so clever and you have the best supervisor to looks after you.

Thanks to all the academic and technical staff in the department, to, Ollie, Barbara and Walter for their help and the mass spec stuffs. Thanks to Dr . Ken Maddock for the instruction of NMR and the great advises for applying a job. A special thanks to Anne for guiding me experiments when I first came to Ireland. Very special to Ria for personally guiding me the use of various chemical instruments and helped me find the various things I needed. Thanks Donna and Carol for their help with my stuff number and all the things I needed. Thanks to Neol for fixing my laptop and installing all kinds of study software.

To the rest of the postgrads that I haven't mentioned, Jack, Sam, Justin, Muhib, Mathew, Harlie, Jessica, Mark K, Amanda, Mark G, Lucy, Caroline and Stephen, thanks for your friendship and very good suggestions during in the lab and good luck with your research.

I want to thank my family for the financial support and the confidence you gave me. Thank you for always trust me that I can do it and I love you so much!

I also want to thank all my friends who always be friendly with me and still be with me during the past two years. Thanks to Sheng, Dongyue, Qin, Nan, Jie and Sylvia, we are family forever!

Finally I want to thank myself for making decision to study abroad and never give up during this two years.

Abstract

This Thesis entitled ‘The synthesis and study of novel fluorescence probes for NTR’ is divided in 7 chapters. Chapter 1, provides an introduction to cancer, reductive stress and some techniques to detect the tumour cells. A range of relevant examples of fluorescence sensors for NTR are also given. This Chapter also includes the objectives for the research conducted in Chapters 2, 3 and 4.

Chapter 2 describes the synthesis of a set of novel fluorescence sensors where variation of naphthalimide substituents is described. The synthesis of each compound is discussed, followed by an evaluation of their photophysical characteristics and response to nitroreductase (NTR) in a biological setting.

Chapter 3 explores synthetic modifications to the compounds described in Chapter 2 in order to increase NTR sensitivity. A set of novel fluorescence sensors are described where the sensitivity is modulated using a range of reducible nitroaromatic moieties. The synthesis of each compound is also discussed, in addition to the preliminary test for NTR.

Chapter 4 discusses a novel family of NTR sensors amenable to bioconjugation through various biocompatible linkages. Structural modification of compounds described in Chapter 2 provides access for conjugation to peptides, sugars, oligonucleotides and various other important biomolecules. The synthesis of each compound is discussed.

Chapter 5 outlines the overall conclusion of the work carried out during this research.

Chapter 6 describes general experimental procedures and the characterisation of each compound discussed throughout the thesis.

Finally, in Chapter 7, the Appendix shows all supporting information.

Abbreviations

$CHCl_3$	chloroform
conc.	concentration
d	doublets
dd	doublets of doublets
σ	chemical shift
DCM	dichloromethane
DMF	N, N-dimethylformamide
DMSO	dimethyl sulfoxide
Eq.	equivalents
Et_3N	triethylamine
Et_2O	diethyl ether
EtOH	ethanol
HRMS	high resolution mass spectroscopy
Hrs	hours
Hz	hertz
IR	infrared
J	coupling constant
KOH	potassium hydroxide
λ	wavelength

MeOH	methanol
m/z	mass charge ratio
NMR	nuclear magnetic resonance
nm	nanometre
ppm	parts per million
q	quartet
t	triplet
s	singlet
UV/Vis	ultraviolet/visible

Contents

Chapter 1 Introduction

1.1 Cancer

1.1.1 What is cancer

Cancer is a disease of human cells. Our body is made up of countless cells. The body will automatically reproduce new cells, so that we can grow, replace old cells, or repair damaged cells due to injury. This mechanism is controlled by genes. But if the control mechanism of those genes are damaged, cancer will appear. Cancer can appear anywhere in human bodies. This damage have the opportunity to occur in our lifetime, and a small number of people are inherited from their parents to the damaged genes [1]. Normally, the cells will split and multiply in a very orderly manner. These cells can grow and divide to form new cells or tissues when our bodies need them. When cells get older or become damaged, they will die and new cells take their place. But once the cells loss of control, it will continue to reproduce, accumulate in the body into a tumor. When tumors develop, cells become more and more abnormal, and the fresh cells form when there is no space for them. These extra cells can divide and grow themselves without stopping and may form growths. Tumors can be divided into benign and malignant, malignant tumors commonly known as cancer [2]. Benign tumor cells will stay at their position and will not spread to other parts of the body. Malignant tumors contain cancer cells. When it is initially formed, it will keep in the original position, which is called in situ cancer. But if the cancer cells are not treated well, it will destroy the surrounding tissue and spread to other organs to become invasive cancer (Figure 1-1).

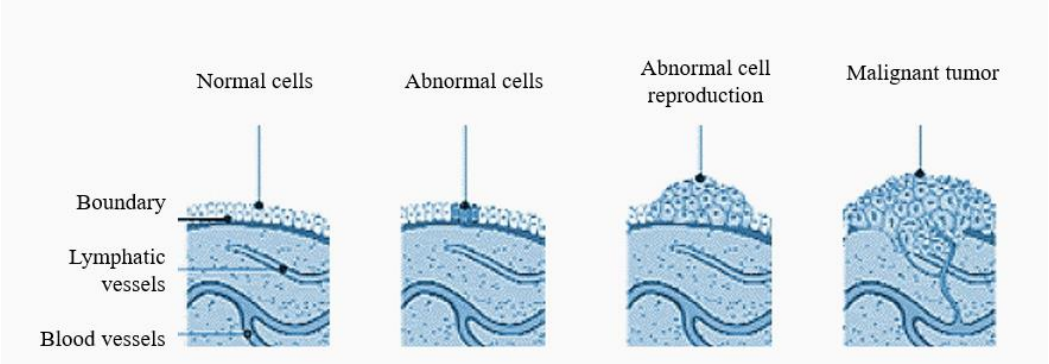

Figure 1-1: The growth of cancer cells affects the surrounding tissue

1.1.2 The characteristics of cancer

In 2000, Douglas Hanahan and Robert A. Weinberg published an article in Cell: The Hallmarks of Cancer [3], a review of the six basic characteristics of tumor cells: self-sufficient growth signal; anti-growth signal is not sensitive; resistance to cells death; unlimited ability to replicate; persistent angiogenesis; tissue infiltration and metastasis. In March 2011 issue of Cell magazine, this two professors had published an updated version of the overview: Hallmarks of Cancer: The Next Generation [4], which outlined the hot spots in oncology and progress of last 10 years, based on the original six characteristics, they added four characteristics, including to avoid immune destruction, promote tumor inflammation, cell energy abnormalities and genomic instability and mutation.

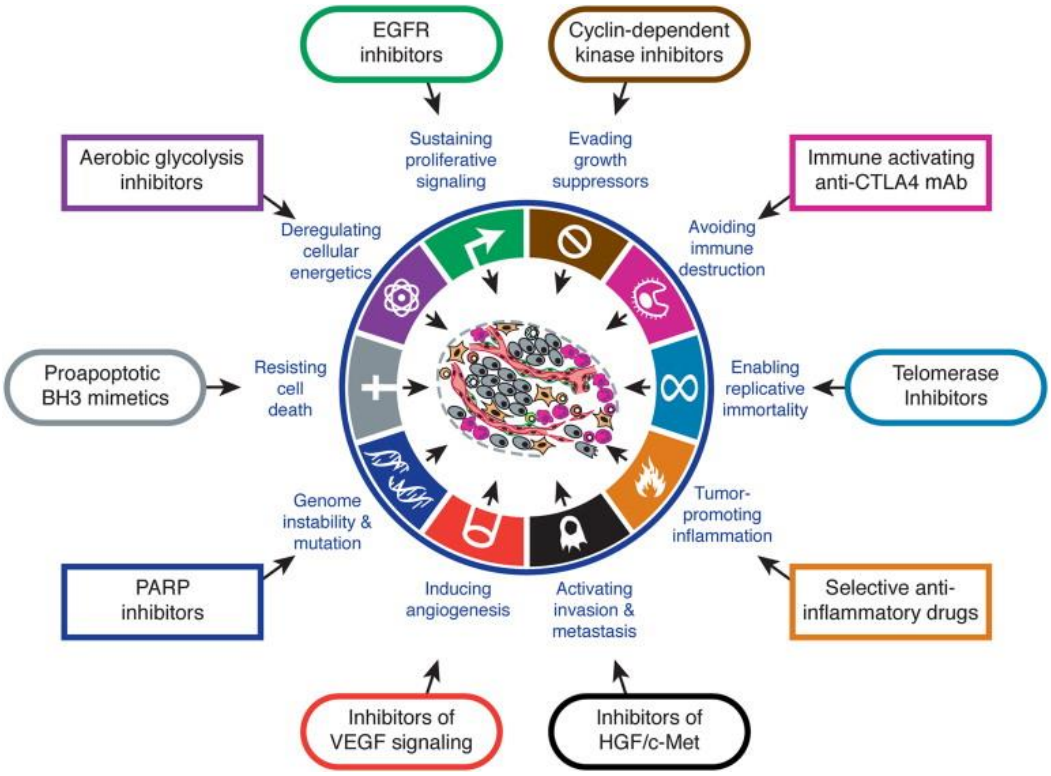

Figure 1-2: The characteristics of cancer and its targeted therapy

These ten characteristics which distinct tumor cells from normal cells were the target of treatment of cancer, and were the basis of biological targeted therapy (Figure 1-2). It is well known that cancer cells are almost rampant in every part of the body, from the brain to the various organs, from the epidermis to the bones. Cancer cells are not invaded from the outside, they are the same as the normal cells that make up the organs of the human body, but the difference is that the changes in the structure and function of the cancer cells make them aggressive and destructive.

Self-sufficient growth signal

If a cell wants to change its current state, it must receive a series of related instructions, then the process can be carried out. This instructions are called signal molecules. Signal molecules are carried out by binding to the receptors on the target cells and changing the state of the cells.

In this respect, cancer cells are distinctly different. Cancer cells have the ability to make their own orders, that is to say, they can be their own synthetic growth and differentiation of the growth signal required, without relying on exogenous signals.

Scientists have found that the ability to synthesize PDGF (platelet-derived growth factor) and TGFα (tumor growth factor alpha) is found in cancer cells in Neuroblastoma and Malignant Sarcoma, respectively [5].

Anti-growth signal is not sensitive

In addition to the growth of the human body signal, there is still a growth inhibition signal. At different stages of cell division, some molecules detect the status of these cells, depending on the circumstances to determine the development of cells: continuing to grow differentiation, or still at rest, or loss the ability of growth and differentiation into the late mitosis. So that the normal cells maintain a dynamic balance of the state, the orderly growth and differentiation. For cancer cells, if they want to continue to grow and divide, they must escape the monitoring of these molecules. Their primary strategy is to mutate these molecules through gene mutations to achieve the purpose of suppressing anti-growth signals [6].

Resistance to cells Death

Escape apoptosis is the ability almost all types of cancer cells have. Signal molecules responsible for apoptosis can be broadly divided into two categories: a class of monitoring molecules as described above, such as a protein called p53 which is one of the most important members [7]; the other is responsible for the implementation of cell apoptosis death. The former monitor the cells inside and outside the environment, once they found abnormal cells, the latter command. Apoptosis is the main barrier for people against cancer. Cancer cells are state of abnormal cells to monitoring molecules, and the main method for cancer cells to escape apoptosis is to mutate the p53 protein and make it inactive.

Unlimited ability to replicate

In cell culture experiments, it was observed that most normal cells can only divide around 60 times. Scientists have confirmed that cell division is related to the sequence of thousands of bases at the end of chromosome [8]. This sequence becomes telomeres, and the sequence will decrease by 50 to 100 bases every time a fraction is divided. As the number of fractions increases, telomeres become

shorter and shorter, and the result is that it can no longer protect the chromosome Of the end, the chromosome cannot be successfully copied, leading to cell aging.

The results show that all types of cancer cells (Figure 1-3) have the ability to maintain telomeres [9]. This ability is mainly achieved by overexpression of telomerase. The primary function of telomerase is to add the desired base to the end of telomeres to ensure that telomeres are not reduced by replication.

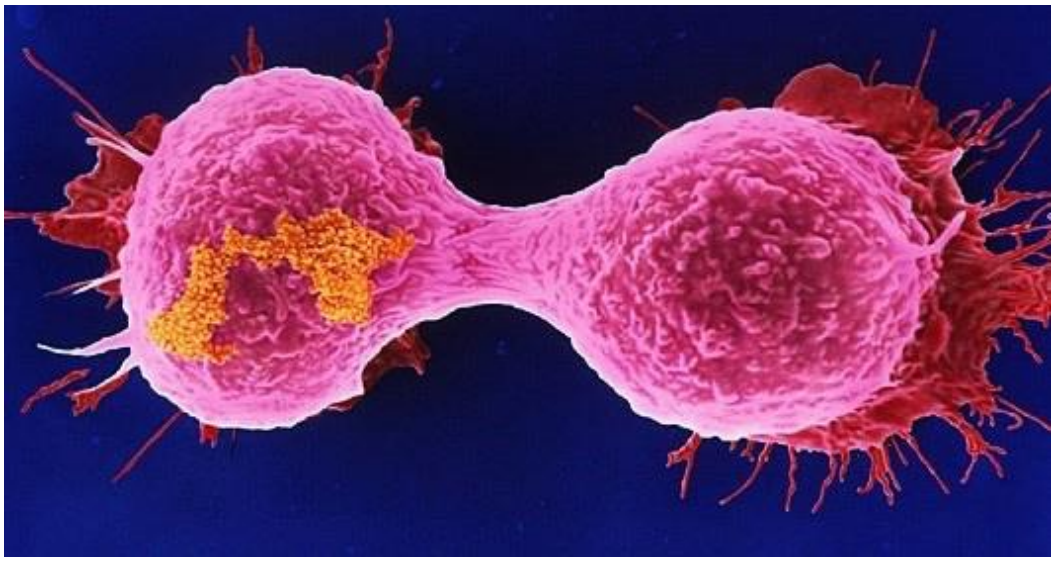

Figure 1-3: Breast cancer cells are splitting

Persistent angiogenesis

Blood vessels is very important to cells. In general, angiogenesis is finely regulated during tissue formation and organogenesis, and angiogenesis is temporary in this case, and angiogenesis is stopped when the physiological process is complete. The signal molecules that promote and inhibit angiogenesis are usually in a balanced state.

Cancer cells to achieve the ability of sustained neovascularization is to break through this balance. Scientists have found in many types of tumors that some of the signal molecules that promote angiogenesis, such as VEGF (vascular endothelial growth factor) and FGF (fibroblast growth factor), are much higher than the corresponding normal tissue controls. The expression of signal molecules such as thrombospondin-1 or beta-interferon decreases [10].

Tissue infiltration and metastasis

Most of the cells in the human body need to adhere to a specific extracellular matrix to survive and function properly, such as epithelial cells and endothelial cells. Once out of the cell extracellular matrix it will occur apoptosis. The molecule that adhere these cells to the extracellular matrix or molecules is called cell adhesion molecules, which act as anchors in the port.

E-cadherin is one of the most deeply studied cell adhesion molecules [11]. It is widely expressed in epithelial cells, and found in the loss of activity in most epithelial cell carcinoma. Scientists believe that E-cadherin plays an important role in inhibiting the invasion and metastasis of cancer cells in epithelial cell carcinoma. The loss of activity indicates that cancer can develop to other places.

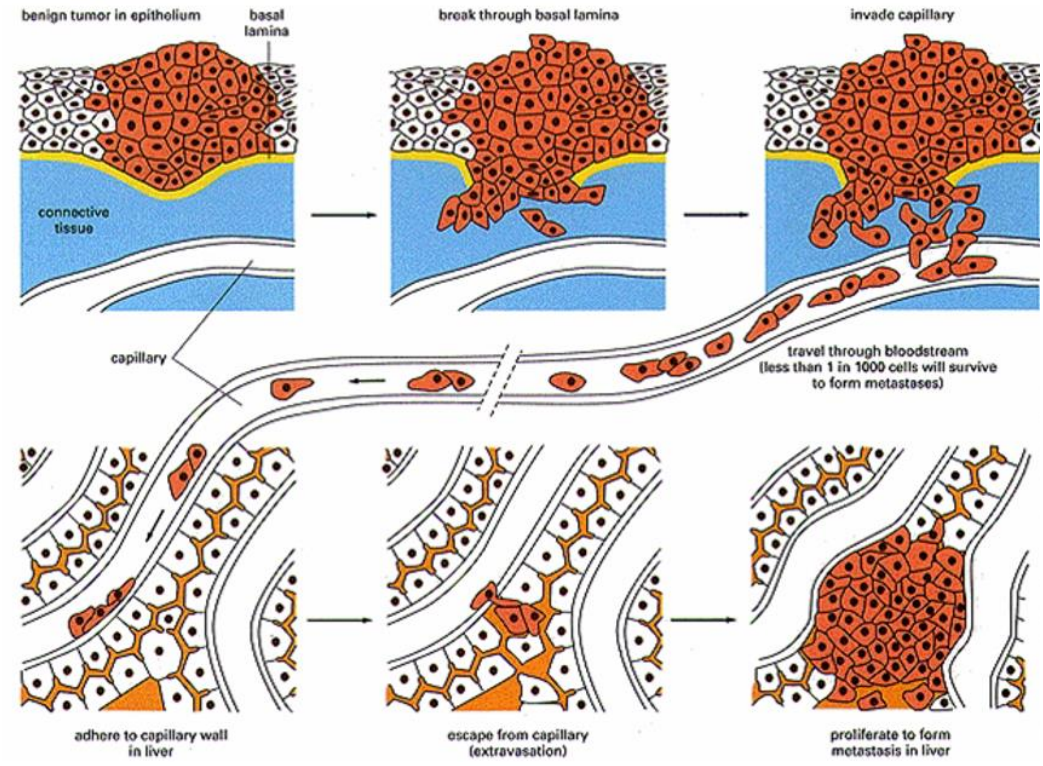

Figure 1-4: How tumor cells are transferred to other tissues (from the Art of MBoC3 1995 Garland Publishing, Inc)

Avoid immune destruction

Both the innate immune and the adaptive immune system play an important role in tumor clearance. While solid tumors have different functions to escape the

immune system of the human body, ensuring that they are not killed and cleared by immune cells such as T cells, B cells, macrophages and natural killer cells.

Promote tumor inflammation

Over the past several decades, a number of studies have confirmed the relationship between the inflammatory response and the pathogenesis of cancer: the inflammatory response can provide various biological activating molecules for the tumor microenvironment, including, for example, growth factors which can maintain the proliferation signal of cancer cells , Survival factors which inhibit cell death, angiogenic factors and extracellular matrix modulating enzymes which may favor vascular growth, cancer cell infiltration and metastasis, and other induction signals which may activate other characteristics of EMT and cancer cells.

Genomic instability and mutation

The complex process of tumors can be rooted in the continuous mutation of cancer cell genes. When a large number of gene mutations happen to induce tumorigenesis, cancer cells often increase their susceptibility to inducible gene mutations, thereby speeding up their gene mutation [12]. Although the types of gene mutations in different types of tumors are different, they can be found to be stable and to repair functional deficiencies in genomic DNA. Suggesting that a major feature of tumor cells is the inherent genomic instability.

Cell energy abnormalities

Even in the presence of oxygen, cancer cells produce energy mainly from anaerobic glycolysis.

Through the above, we know that one of the characteristics of cancer cells is uncontrolled reproduction. In the process of cell proliferation, the tumor cells will absorb nutrients and oxygen to suit their own growth. Since the body's blood oxygen content is fixed, when the tumor cells are infinitely replicated, it is bound to absorb a lot of oxygen and thus cause oxygen concentration around tumor cells gradually decreased, which formed a tumor hypoxia. In fact, tumor hypoxia occurs

in the vast majority of tumor cells, and is another major feature of the tumor microenvironment.

1.2 Tumor hypoxia

Tumor hypoxia is the situation which tumor cells have used all of the oxygen. As the tumor grows, it rapidly consuming the blood supply, and leave oxygen concentration of some parts of the tumor much lower than in healthy tissues. Just like the Figure 1-5, the oxygen concentration of hypoxic area is much lower than it in normal cells. The hypoxic microvascular disease in solid tumors is due to the rapid proliferation of tumor cells has consumed the available oxygen in tumor vasculature [13]. This causes solid tumors that have reduced oxygen availability to proliferate uncontrollably and show unusual structural and functional behaviour. The longer distance from the nearest blood vessels, the less chance to get the available oxygen (Figure 1-5). The distance between tumor hypoxic area and disorganized vascular is longer than the distance of diffusion oxygen (which is around 100 to 200 μm, depending on the oxygen concentration in the local tissue) [14].

When the partial pressure of oxygen (PO_2) is lower than the normal physiological level, the tumor microenvironment will show hypoxia. Studies have shown that most of the tumor cells around the oxygen partial pressure of 7.5 mm Hg [15], while the PO_2 value of normal tissue is more than 40 mm Hg, so hypoxia is a common phenomenon in the tumor microenvironment. There are many reasons for hypoxia in microenvironment, mainly in the following cases: (1) because most tumor cells are in high metabolic and rapid proliferative state, oxygen consumption is much larger than supply, resulting in a decrease in oxygen content in microenvironment, and ultimately the formation of hypoxia microenvironment. (2) hypoxia of tumor cells will cause secretion of vascular endothelial growth factor (vascular endothelial growth factor, VEGF) and other vascular factors, which can speed up tumor angiogenesis and increase the density of tumor microvessels that cannot regulate the blood flow, resulting in excessive perfusion hypoxia; in addition, microvessels within the tumor are not evenly distributed, the distance

between microvascular tend to exceed the oxygen diffusion distance, resulting in oxygen cannot be effectively transported to the hypoxic site [16]. (3) Some of the tumor itself and radiation therapy can lead to anemia in the body, haemoglobin reduction is a common phenomenon for cancer patients. One study found that when the haem is less than 10 ~ 12 g / d, the tumor supply of oxygen will be significantly declined and cause hypoxia [17].

It has been found that hypoxic tumor cells have a blocking effect on chemotherapy and radiation treatment and presents a huge challenge to cancer therapy for the following reasons: (1) since hypoxic tumor cells are very far away from blood vessels that anticancer drugs cannot reach to these areas; (2) the hypoxic tumor cells which can survive in hypoxic environment can show much more tolerance to hypoxia and might upgrade or renew to more malignant tumor cells; (3) when a treatment kills oxygenated cells, it will allow hypoxic cells to be reoxygenated and start to grow, which make a very important contribution to the growth of tumor cells [18].

On the other hand, hypoxic environments also help us identify and distinguish the tumor cells. Therefore, estimating the tumor hypoxia degree is one of the most important ways to predict therapy efficacies [19].

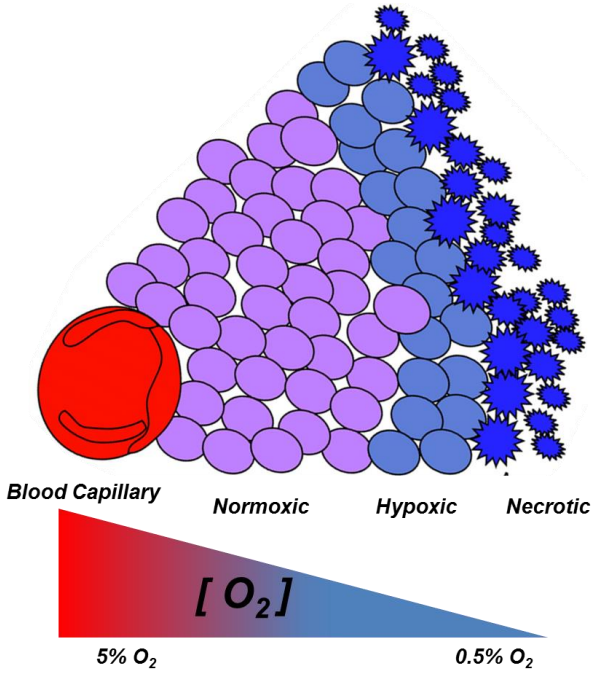

Figure 1-5: Oxygen concentration in hypoxic cells and normal cells

The formation of hypoxia in the tumor leads to a reduction of oxygen in the tumor. In this case, the nicotinamide adenine dinucleotide (NAD) in the molecule is converted into its reduced form (NADH) due to insufficient oxygen concentration, which leads to a new situation, reductive stress.

1.3 Reductive stress

Nicotinamide adenine dinucleotide (NAD) is a widespread biological redox cofactor in cells. The oxidized form of NAD carries a positive charge and is written as NAD^+ while the reduced form is NADH (Figure 1-6). Reductive stress is induced by conditions which promote the formation of excessive intracellular NADH.

In aerobic cells the decomposition of fuel molecules is associated with the reduction of NAD^+ to NADH (Figure 1-6). Because during the transition which the oxygen growth was limited, an increased level of NADH builds up, and it is less efficient to oxidize NAD+ again because of reduced aerobic respiration.

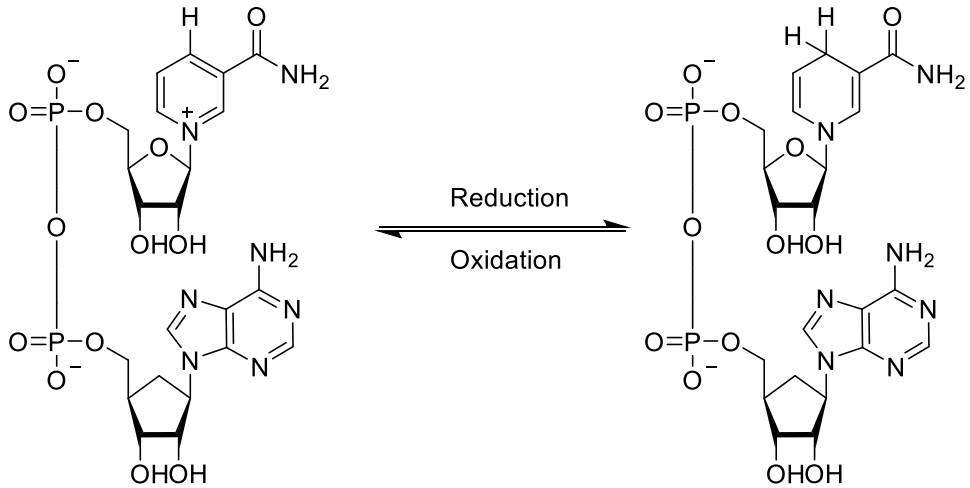

Figure 1-6: Transfer from NAD^+ to NADH

Therefore, reductive stress is related to respiratory inhibition and also it is related to the situation of cells become more reduced than the condition of normal cells.

Through the study of the reductive stress in the tumors, we found that it is particularly present in the case of tumor hypoxia, so it is very meaningful to use the appropriate methods to detect tumor hypoxia. The next section will be the discussion of the approaches for tumor hypoxia detection.

1.4 Approaches for detection

In 1955, Thomlinson and Gray found that there are hypoxic cells in malignant tumors; and in 1979, Brown and other scientists confirmed that the tumor hypoxia is divided into acute hypoxia and chronic hypoxia. This two different types can lead to different hypoxia related responses within the tumor, which can have an obvious and fast effect on tumor development and response to treatment [20]. Tumor hypoxia is divided into two parts, chronic hypoxia and acute hypoxia. Chronic hypoxia is when the tumor cells is too far away from the blood vessel under hypoxia situation because it is out of the distance of effective dispersion. On the other hand, acute hypoxia is because by tumor vascular network structure and function or intravascular blood reduced by or blocked. In addition, this status is caused by effective oxygen supply leads to functional oxygen deficiency and chronic hypoxia. The hypoxia caused by short-term blood flow interruption is known as acute hypoxia [21]. After many years of research, there is evidence to show that the presence of tumor hypoxic cells not only enhances the resistance of tumor to radiotherapy and chemotherapy but also makes the tumor more aggressive. Although people tried different methods to prevent tumor hypoxia, the clinical results are in need of further development. In recent years, many new methods have been developed to detect hypoxia, such as tumor vascular analysis, tumor metabolic degree determination, tumor cell DNA damage, hypoxic stress proteins analysis, radiotherapy assessment, radioactivity/ fluorescence staining labeling method, determination of oxygen pressure within tumors etc. Among these, three methods that are widely used today are: 1. Oxygen electrode direct measure; 2. Histomorphometric analysis; 3. Tumor markers [22].

Oxygen electrode

The oxygen electrode is one of the most widely used methods to detect hypoxia. This is the only method that directly determines tumor hypoxia, which reflects the oxygen concentration in tumor microenvironment. Now it is considered the gold standard to determine tumor hypoxia. At present, there are many clinical reports showing that oxygen electrode measurement is reliable, and the test result matches the tumor treatment effect. However, there are still many limitations: 1. Multi-channel determination is necessary due to the tumor oxygen distribution of significant heterogeneity. 2. It is unable to distinguish between the tumorous and necrotic tissue within the hypoxic environment. 3. It will increase the rate of tumor transfer because the test requires insertion into the tumor microenvironment.

This technology is measured by putting the cathode probe into the tumor, and measuring the oxygen partial pressure in a region of the tumor by detecting the current generated during the ionization of oxygen. Through the computer real time monitoring, it can be measured every 10 seconds.

Histomorphometric analysis

Histomorphometric analysis is the first method used in clinical practice. As the oxygen content of the tumor mainly depended on the blood supply of the tumor, so the hypoxia condition of the tumor is estimated indirectly by analysing the tumor tissue capillary space, vascular density, tumor necrosis and the closest distance between surrounding normal tissue blood vessels and tumor. It is relatively reliable to use this method to detect tumor hypoxia [23].

However, using this method to detect tumor hypoxia also has some disadvantages: 1. it requires large tumor tissue blocks for analysis so will cause great pain for patients and increase the chance of cancer cell metastasis. 2. The main drawback is that the measurement was indirectly to tumor oxygenation and it cannot reflect the oxygen content of the tumor duo to the stopped flow or because of the oxygen-depleted hemoglobin. [24]

Tumor markers

Tumor markers are when cancer cells are in the process of occurrence, proliferation, differentiation, metastasis, necrosis and disintegration, it releases some substances due to the abnormal transcription, expression or secretion, the human body will also react abnormal to tumor growth and release some physiological substances such as proteins, peptides, hormones, enzymes, polyamines, oncogene products, viral antigens, etc., their presence or quantitative changes can prompt the nature of the tumors. Tumor markers can be used to identify cancer types, determine cancer staging, predict cancer growth rate, drug response selection, observation of treatment and prognosis etc.

The ideal tumor markers must have the following characteristics: 1. High specificity, for tumor and non-tumor, it can identify accurately of up to 100%. 2. High sensitivity, it can be found in the very early stage of tumor. 3. The concentration of tumor marker in the body fluid is closely related to tumor size and clinical stage, and can be judged according to the prognosis. 4. Half-life is short, according to its level of monitoring, it can reflect the effect of treatment and whether the tumor recurrence or metastasis. 5. Easy to detect.

Some common tumor markers are classified as:

1. Embryonic antigen such as Carcinoma embryonic antigen, CEA for lung cancer detection [25]. The level of serum CEA in patients with lung cancer was significantly higher than that in normal control group and benign lung disease group, the positive rate of adenocarcinoma was more than 70% [26].

2. Protein markers such as inhibitor of apoptosis proteins, IAP. Surviving is one of the most important member in IAP family, and it plays a significant role in the development of tumor. Surviving protein is almost expressed in all malignancies, whereas it doesn't expressed in adult terminal differentiation tissues. Scientists Yagihashi et. using indirect ELISA to test the Surviving autoantibodies in 31 cases of NSCLC patients, and the positive rate was 58.1% [27].

3. Carbohydrate markers. The glycosylation process in tumor cell was mutated, resulting in the change of glycoprotein of cell membrane or the change of the glycosyl sequence of glycolipid, and formatting a specific antigen which is different from normal antigen.

4. Enzyme markers. When the tumor occurs, the activity of the enzyme often changes greatly because: 1. The tumor cells or tissue itself will induce other cells produce abnormal content of the enzyme. 2. Tumor cell metabolism is very strong and increases cell permeability, making the enzyme of the tumor cells get into the blood. 3. The tumor makes some organs dysfunction, resulting in enzyme inactivation and excretion obstacles. Take Neuron-specific enolase, NSE as an example, NSE is an acidic protease that exists only in neurons and neuroendocrine cells. SCLC is a neuroendocrine-derived tumor, so NSE is one of the most valuable serum tumor markers of SCLC, the sensitivity is up to 40% to 70%, the specificity is up 65% to 80% [28].

5. Hypoxia markers. Reductase overexpression is an important feature of tumor hypoxic cells, including nitroreductase, quinone reductase, azo reductase and so on. Reductive dependent hypoxia markers are mainly reduced by the fact that the probe is reduced by the reductase in the hypoxic region and the fluorescence changes. The hypoxia-sensitive groups used to reduce the dependent oxygen-deficient probes mainly include nitro, quinone and azo. The principle is that with the great ability of reduction of tumor cells, when the electron affinity of nitro functional group such as nitroimidazole or quinone and azo active diffusion through the cell membrane, the functional groups were reduced under the reductase in cell, the reduced product is irreversibly bound to the macromolecular substance and remains in the tissue.

Take nitroimidazole as an example (Figure 1-7), in the case of hypoxia area, the nitro group was reacted under the reaction of xanthine oxidase to form free anion, and then reduced by the nitroreductase into amino group, and bind with the biomolecule in the body to finally stay in the cell. While in the case of normal oxygen concentration, free anions will be oxidized into nitro group and excreted out of the body, resulting in the molecules unchanged. In this thesis, we are more focus on using Nitro reductase to detect tumor hypoxia.

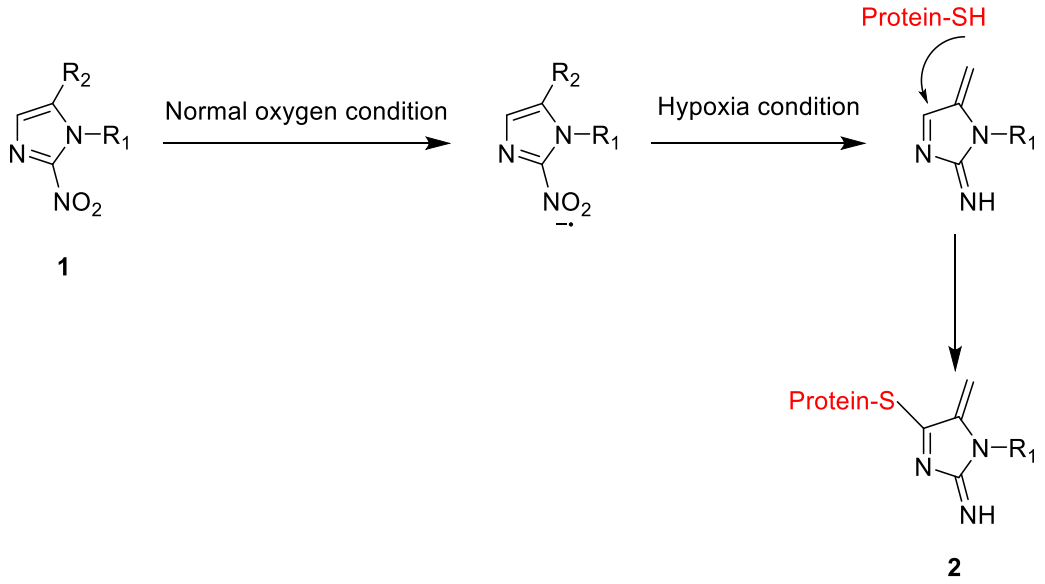

Figure 1-7: Reaction of nitroimidazole under hypoxia

In this thesis, we had introduced the classification of the methods for detecting hypoxia in the tumor, each method has its advantages and disadvantages, among them, hypoxia markers took a very important position in tumor hypoxia detection. Next we discussed some of the hypoxia markers that have been successfully developed.

1.5 Hypoxia markers and fluorescence detection

In 1976, Varghese et al. found that 2-nitroimidazoles are able to react with intracellular nucleophilic compounds to form novel molecules in hypoxia area as shown in Figure 1-7 [29]. The principle of nitroimidazole can act as a hypoxia activated prodrugs is that an enzymatic bioreduction resulting in the delivery of an electron to nitro group to activate it to a nitro radical. In normal conditions, the nitro group is back oxidized by oxygen in aerobic area which is changed to a superoxide anion and then transformed to hydrogen peroxide by superoxide dismutase (SOD) [30]. On the other hand, the pressures of oxygen can fall to below 2.5 mmHg in hypoxia area [31], which inhibit the back oxidation and promote the further reduction of nitro radical to nitroso and finally amine derivatives. This reduction of the amine derivative can be used as a perfect substrates for covalent

attachment to intracellular nucleophilic compounds and remain in hypoxic cells compare to normoxic cells.

In organisms, there are many reductase enzymes relating to the bioreduction of 2-nitroimidazoles, which include one electron reductases such as NADPH-cytochrome P450 reductase, cytochrome b5 reductase, xanthine oxidase and NADPH-nitroreductase, and two-electron reductases such as DT-diaphorase [32]. Instead of 2-nitroimidazole, there are still many functional groups that can be reduced by the various reductases such as 4-nitrobenzenes, nitrofuran, nitrothiofuran, azo linkages, quinones and 4-nitroimidazole. In fact, so many substrates and enzymes provide a variety of opinions for testing, we can not only synthesis the hypoxia targeting agents but also find out a way to selectively target tissues in which the aforementioned enzymes is located.

With further research, we notice that the bio reduction method is always amenable to fluorescence detection. Fluorescence signals are widely used as an analytical tool for monitoring many biological processes in vitro and in vivo [33] [34], The biologically active probes provided herein utilize various functions such as nitroaromatic compounds, azo bonds, quinolones and N-oxides and it will be more focused on the detection of nitroaromatic compounds for hypoxia.

The principle of the reaction of aromatic nitro compounds is the reduction of a nitroaromatic moiety present in the compound of a fluorophore. The electron of the nitro group is easy to be reduced by nitroreductase (NTR) enzymes [35]. This nitroreductase can be divided into two parts. First is oxygen insensitive nitroreductase, which means it can reduce nitro functional group in the presence of molecular oxygen; while the second is oxygen sensitive nitroreductase and it only works in extreme hypoxic area [36]. When there is a tumor, there is a hypoxia area and the concentration of the oxygen sensitive NTRs is getting higher. Due to its own characteristic, oxygen sensitive NTRs are of particular significance to the design of hypoxia sensitive fluorescent imaging agents [37].

In 1983, Olive and Durand found out the use of nitroaromatics for hypoxia imaging so they reported a family of 4 nitrofurans **3-6** (Figure 1-8).

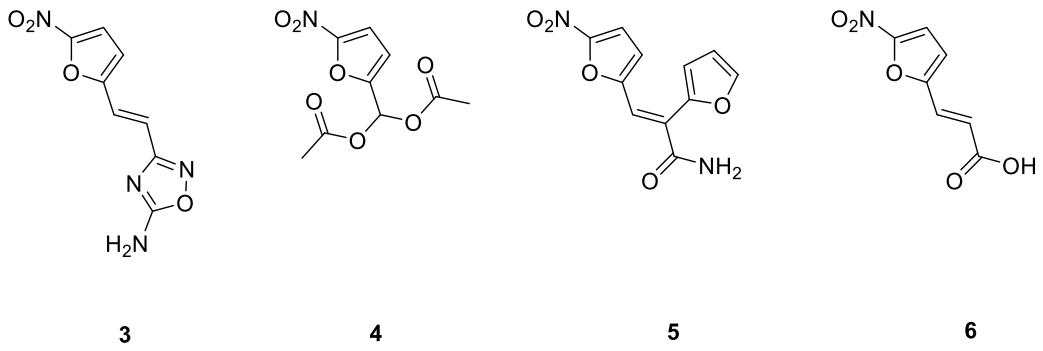

Figure 1-8: fluorescence sensors based on nitrofuran

They treated those 4 compounds into Chinese hamster V79 cells and observed their fluorescence change (Figure 1-9), because they found the mean cellular fluorescence can be used to predict the survival of single-cells, regardless of time of exposure or concentration of those compounds.

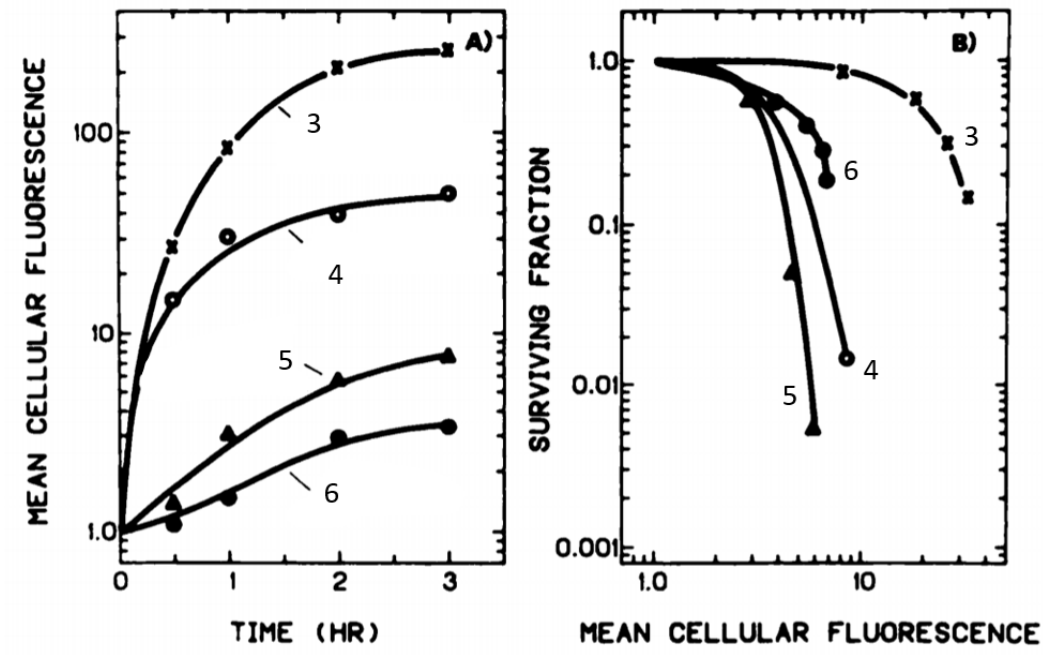

Figure 1-9: Fluorescence intensity change of 4 sensors treated in cells (left) and the surviving test of those 4 compounds (right).

The figure above showed the fluorescence change for those four compounds when the Chinese hamster V79 cells was exposed to each compound. Compound **3** showed the greatest fluorescence intensity (on the left) and the least toxicity (on the right) among four compounds.

From the conclusion, compound **3** could be used to estimate the fraction of hypoxic cells in multicellular and also they found that the fluorescence intensity of 3 was

highly responsive to cell oxygen concentration. All these results show that nitroheterocycles can be used as hypoxia sensors and the potential application of nitrofurans as fluorescent hypoxic cell markers [38].

The presence of hypoxia cause the bioactivity of nitroreductase to show a higher level. And under the hypoxic environment, nitro groups of compounds can be reudced to amino grouos by NTR. A lot of fluorescent probes have been made for hypoxia detection, however most of them are excited by one photon (with less than 500 nm emission wavelength), and this property has limited the applications for the probes. Therefore, it is important to develop a new probe for monitoring NTR for detecting the occurrence and progress of tumors. Zhan Rong Liu and Co. workers synthesized a novel two-photon (TP) fluorescence turn on NTR probe compound **7** as a new TP fluorescent probe for sensing and imaging NTR, which used compound **8** including an optically tunable hydroxyl group as the fluorescence marker, and use p-nitrobenzyl moiety as the recognition position for NTR. When it treated with NTR under the NADPH (Figure 1-10), the nitro group would be reduced to the amino group, after the 1,6-rearrangement-elimination reaction to release compound **8** [39].

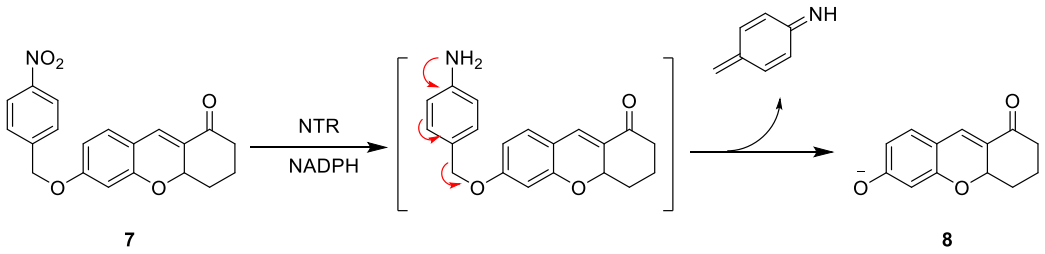

*Figure 1-10: The TP fluorescence turn-on NTR probe compound **7** and how it reacts with NTR.*

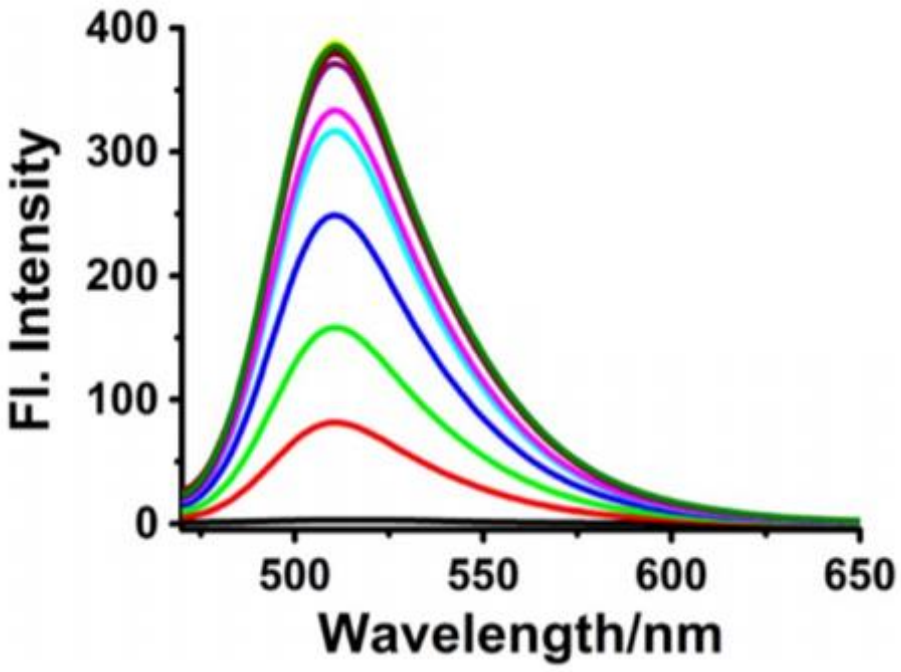

*Figure 1-11: The fluorescence response of the compound **7** to NTR at different concentration in PBS (pH 7.4, 5% DMSO).*

The experiment was conducted by treating the compound **7** (5 μM) with NTR (0-4.0 μg/mL) in the presence of NADH, and here was the emission spectrums for this reaction (Figure 1-11). As we can see from the figure, compound **7** was non-fluorescent at beginning, once the NTR was treated in the presence of NADH, there was a very obvious increasing in fluorescence intensity at 510 nm. This result showed that the compound **7** had a very high sensitivity for NTR.

In the cell experiment, the compound **7** was injected into HeLa cells, and the fluorescence images of the reaction were recorded at different oxygen concentrations.

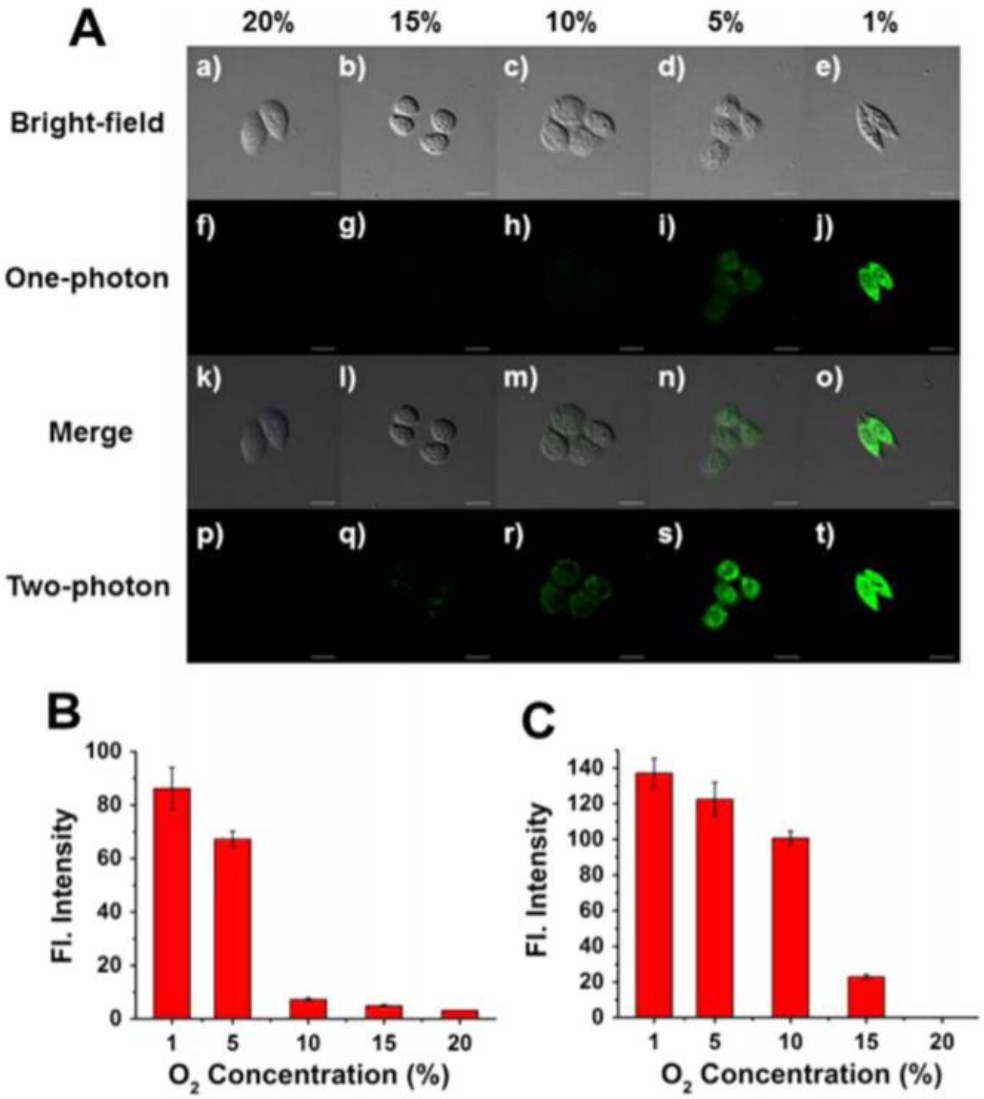

*Figure 1-12: (A) Fluorescence imaging of compound **7** with NTR in the living HeLa cells under normoxic (20% O2) and different hypoxic (15%, 10%, 5%, and 1% O2) conditions. (B) Imagines of one-photon fluorescence intensity change of Hela cells. (C) Imagines of two-photon fluorescence intensity change of Hela cells.*

As compound **8** was a powerful two-photon dye, so they treated the compound for imaging NTR in the living HeLa cells by one-photon and two-photon modes. In the Figure 1-12, compound **7** was treated in cells under 20 % of oxygen and it did not show any fluorescence signal (f and p). Then they switched the compound **7** in HeLa cells to different hypoxic condition (from 15 % to 1 %). With the oxygen concentration decreased, the fluorescence signal increased gradually as showed in figure B. C. This results showed that compound **7** was able to detect NTR in cells

in both one photon and two photon modes. And compound **7** was more sensitive when it was in two photon mode.

The recent development of ratiometric fluorescent sensor for hypoxia is the synthesis of naphthalimide sensor, which based on a p-nitrobenzyl functional group connected to the naphthalimide fluorophore through a carbamate linker [40]. This kind of nitro reductase based fluorescent sensor was designed by setting nitro recognition groups in the fluorophore, using the endogenous NADPH contained in the biological system as electron donor, and the electron withdrawing group nitro group of the sensor is reduced to the electron donating group amino group to form the 4-amino naphthalimide derivative by the presence of NTR. So that the sensor molecules internal charge transfer and lead to the change in optical signals with an obvious blue fluorescence to green fluorescence shift, and thus to achieve the detection of nitroredutase.

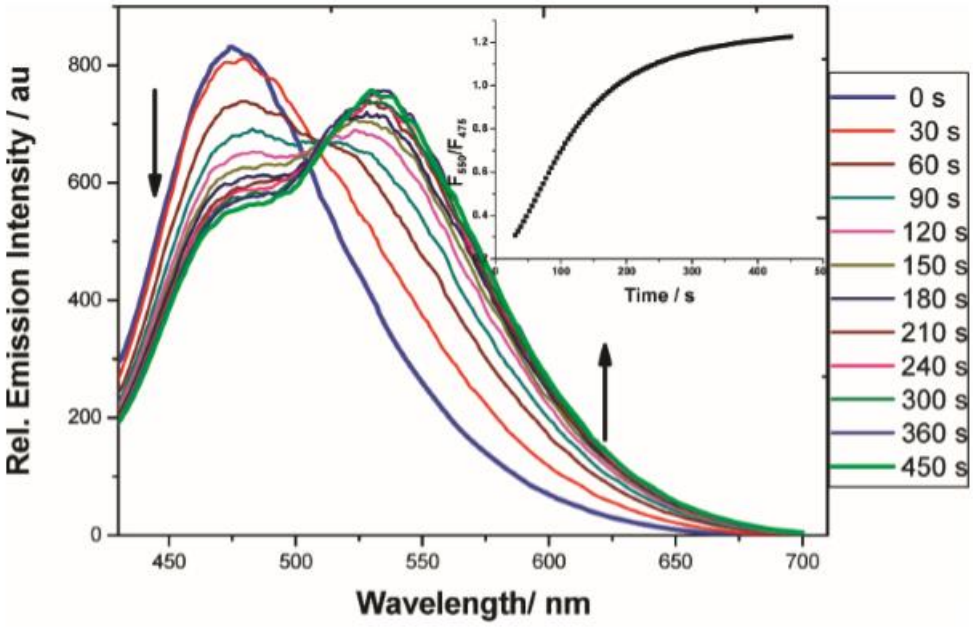

Figure 1-13: fluorescence spectrum of compound ***9*** *(10 μM) in PBS with 1% DMSO treated with NTR (10 μg/mL) with excitation wavelength of 410 nm. Inset: the emission ratio (F550/F475) verse time.*

In the fluorescence experiments of compound **9** with NTR (Figure 1-13), the compound **9** was injected into *Escherichia coli* and reacted with NTR. The

experimental results showed that the signal intensity decreases at 475 nm in 10 minutes with the signal at 550 nm increased, and 80% of the compound **9** was converted to compound **10**. The fluorescence signal of the reaction also undergoes a great change in the reaction process from blue to green.

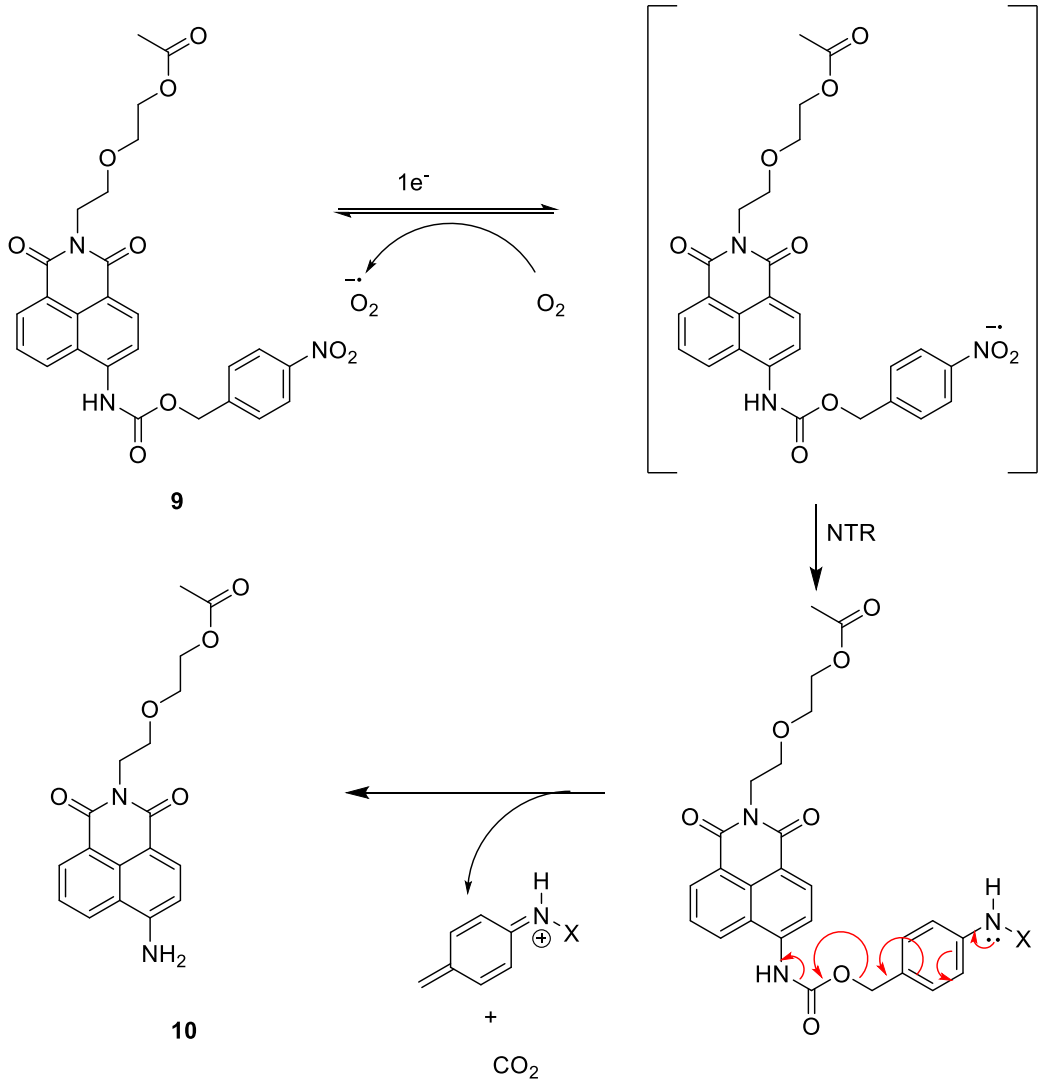

*Figure 1-14: Mechanism of compound **9** when treated with NTR.*

The development of the compound **9** indicates that a selective ratiometric fluorescent probe has been successfully made and its color change in the solution also illustrated that the compound **9** can be used as an NTR fluorescent probe.

Another example is that Ma et al. used resorufin as the fluorophore and conjugated 5-nitrofuran and 5-nitrothiophene into the resorufin as recognition groups of NTR to develop two sensitive turn-on nitroreductase optical sensors 11 and 12 [41]. The reason they chose resorufin as fluorophore is that resorufin has a relative long

analytical fluorescence wavelength, excellent water solubility and its fluorescence can be quenched by substitution of its 7-hydroxy functional group.

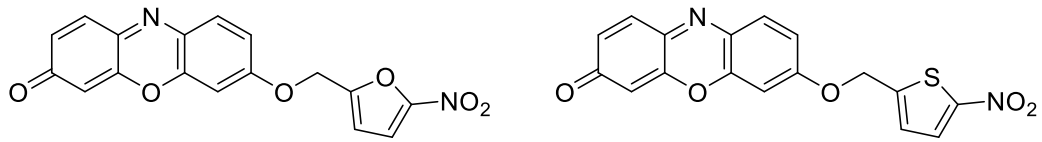

11 **12**

*Figure 1-15: The resorufin based fluorescence probes compound **11** and compound **12**.*

When under the environment of NADPH, the nitro groups of **11** and **12** can be reduced by NTR to form hydroxylamine or amino groups and subsequently 1,6-rearrangement and elimination reactions to release resorufin and bright the fluorescence (Figure 1-16). The color change from colorless to pink.

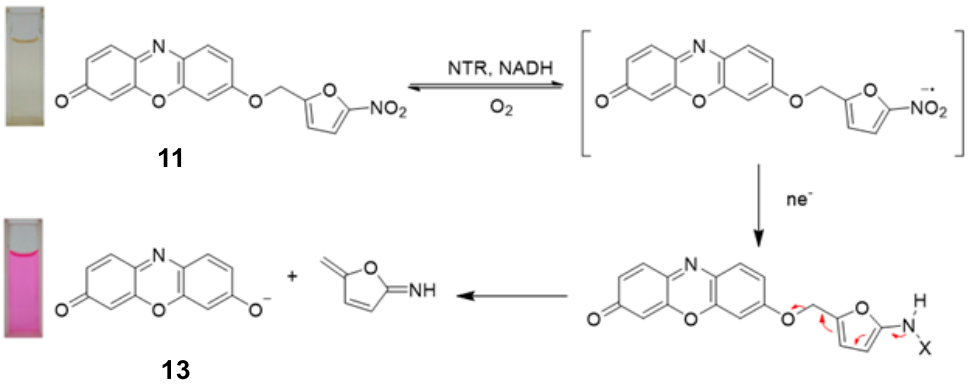

*Figure 1-16: The mechanism of compound **11** reacted with NTR. Insert, the color of compound **11** and compound **13** with naked eyes.*

From the research, these sensors showed no toxic to other endogenous substances in the cells, according to that, a highly selective and highly sensitive method for the detection of NTR in cells was constructed. Meanwhile, people can also visually examine NTR and hypoxia cells based on the color change.

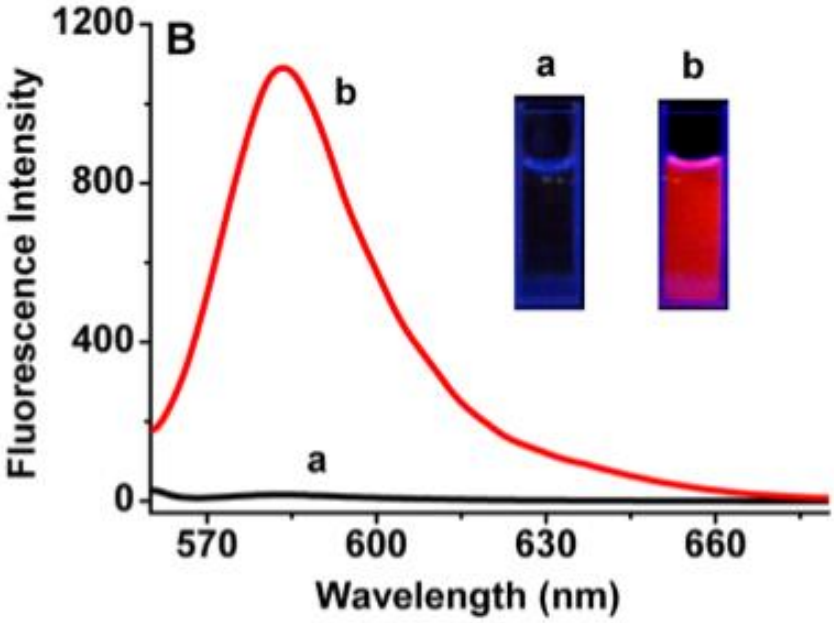

*Figure 1-17: Fluorescence emission spectrum of compound **11** (5 μM) (a) before and (b) after reaction with NTR (0.20 μg/mL) in the presence of 500 μM NADH at 37 °C for 30 min. Insert: The color and fluorescence changes of compound **11** before and after the reaction.*

The spectroscopic response of compound **11** to NTR was showed in Figure 1-17. Compound **11** had no fluorescence emission at 585 nm, however, after the reaction with NTR, the fluorescence intensity had a 100 fold enhancement, and achieved a great fluorescence colour change from no fluorescence to red fluorescence. The result of the fluorescence spectrum from the reaction system was similar to those of resorufin [42] [43]. This result can also evident that the NTR causes the release of resorufin functional group. Compound **12** had the silimar selectivity to NTR but it had a higher sensitivity to NTR. Since it can quantitatively determine the concentration of NTR produced by *Escherichia coli*, compound could be the first probe which can quantitative determine the NTR of cells for real time.

In most nitro-fluorescent probes, the nitro group is not directly attached to the fluorophore as an NTR recognition factor, most of which is indirectly connected to the fluorophore via an alkyl bridge. The probe that the nitro group is directly attached to the fluorophore is difficult to synthesize. However, in 2008, Qian [44]

and co-workers report about this new fluorescent sensors for NTR with a nitro group directly connect to the fluorophore (Figure 1-18). According to their reports, nitro can not only act as a fluorescence quencher, but also help to enhance fluorescence.

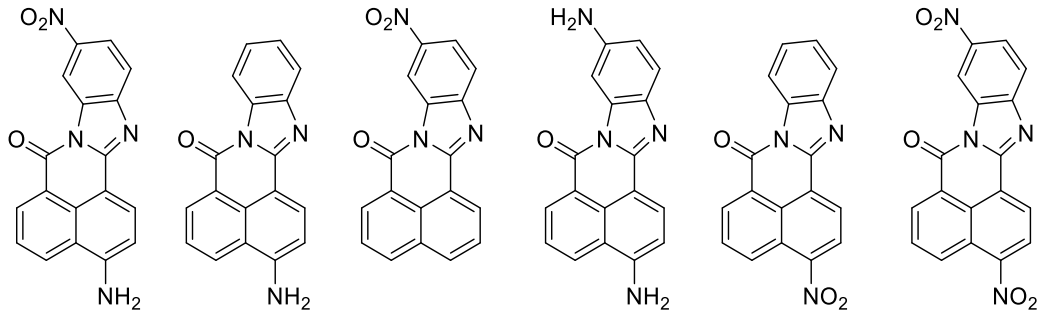

Figure 1-18: The new hypoxia sensors while nitro groups directly connect to fluorophore.

In their studies, they synthesised several compounds with nitro groups directly connected. First, they tested the fluorescence of the various compounds in a methanol solution. The result showed that compound **14** and **15** had very high fluorescence intensity while the rest compounds showed very weak fluorescence intensity (Figure 1-19).

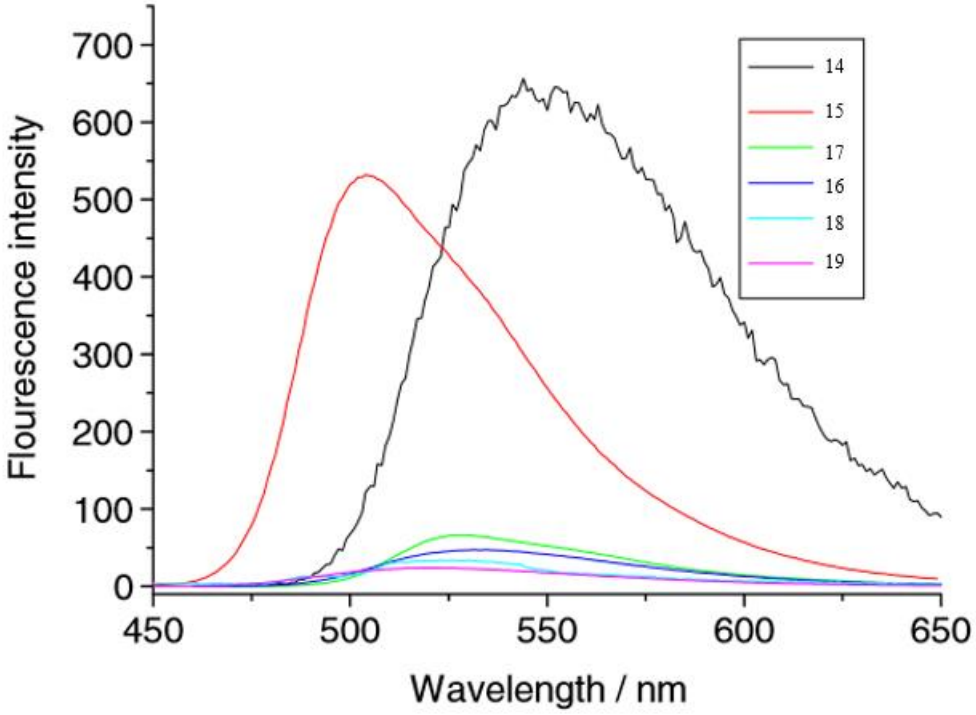

*Figure 1-19: The emission spectrum of compound **14** to **19** with the concentration of 10^{-5} mol / L in methanol.*

Among them, the nitro group of compound **14** was attached to the benzoimidazole ring and the nitro group of compound **15** was attached to the naphthalene ring.

In general, nitro group usually worked as fluorescence quencher because it is an electron withdrawing group and reduced the conjugation of the compound to quench the fluorescence. In order to explain the high fluorescence intensity of compound **14**, they designed an infrared experiment to prove the nitro group of compound **14** was highly conjugated with the compound. Since the nitro group increased the conjugation of the compound, it can improve the fluorescence as an electron acceptor.

Compound	A_{AS}/A_0	A_S/A_0
14	0.48	0.77
19	1.95	2.94
18	0.96	1.82
16	0.82	1.66

*Table 1-1: Spectra data of compound **14**, **19**, **18** and **16***

A_{AS} Peak area of the anti-stretching vibration of nitro groups

A_S Peak area of the stretching vibration of the nitro groups

A_0 Peak area of the stretching vibration of the C=O group of the corresponding compounds

While the nitro group of compound **14** was reduced to amino group, which means the compound **14** converted to compound **17**, the fluorescence had been quenched. On the other hand, the nitro group of compound **18** was worked as fluorescence quencher. There was no fluorescence of compound **18**, when it was reduced to amino group, which means compound **18** had changed to compound **15**, the fluorescence had increased.

In addition, they modified the compound **14** and finally yield the compound **20**

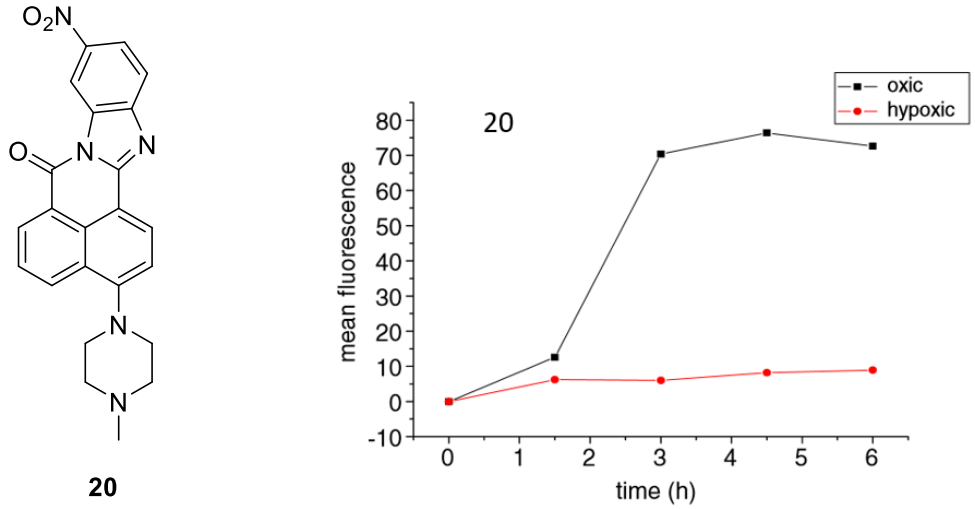

*Figure 1-20: The structure of compound **20** and the emission spectrums of compound **20** in V79 379A Chinese hamster cells under different oxygen concentration.*

According to the cell experiment, they treated compound **20** in V79 379A Chinese hamster cells under a hypoxia environment and a normoxic environment to observe the fluorescence change over time. After 4.5 hr, there was a large fluorescence enhancement for compound **20** under normoxic environment (Figure 1-20). By comparing the sensitivity of compound **14** and **20**, they found that compound **20** showed a higher fluorescence intensity than compound **14** because the introduction of the methlpierazine functional group had improved the hydrophilicity and the solubility in cell culture media, thereby improving cell uptake.

Another turn-on fluorescence probe for NTR is synthesised by Shao, Li and co-workers [45]. They used a quaternized 4-pyridinyl-substituted fluorophore to increase the water solubility and also to increase the cells permeability. The fluorophore was conjugated to 5-nitrofuran to form a novel fluorescence probe compound **21** (Figure 1-21).

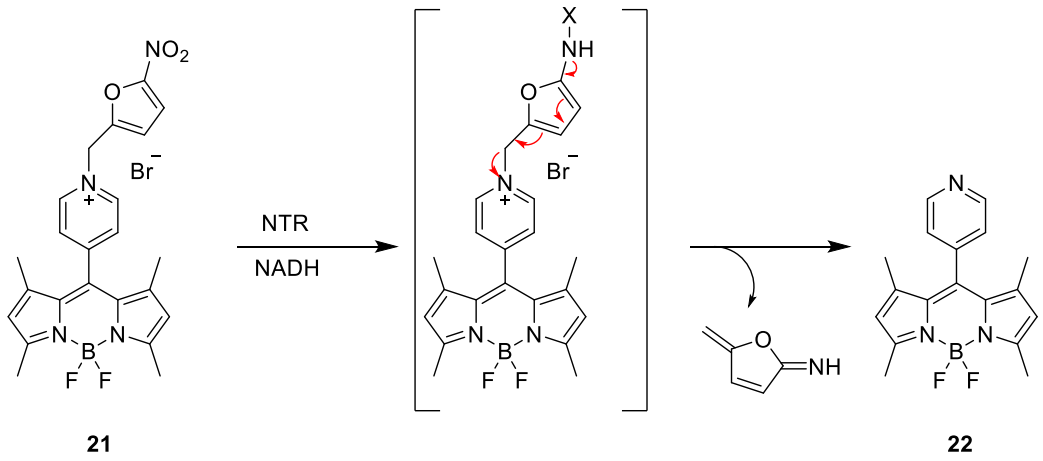

*Figure 1-21: The novel fluorescence probe compound **21** and the mechanism when it reacts with NTR.*

In their studies, compound **21** showed a very weak fluorescence signal because of the photo-induced electron transfer (PET) process [46] [47] [48]. By reacting the compound **21** with NTR in the presence of NADH, the nitro group was reduced to the amino group, and after the electron transfer, followed by a 1,6-rearrangement and elimination reaction the furan moiety was eliminated and finally release the fluorescent group compound **22**, which showed a fluorescence change from no fluorescence to green fluorescence.

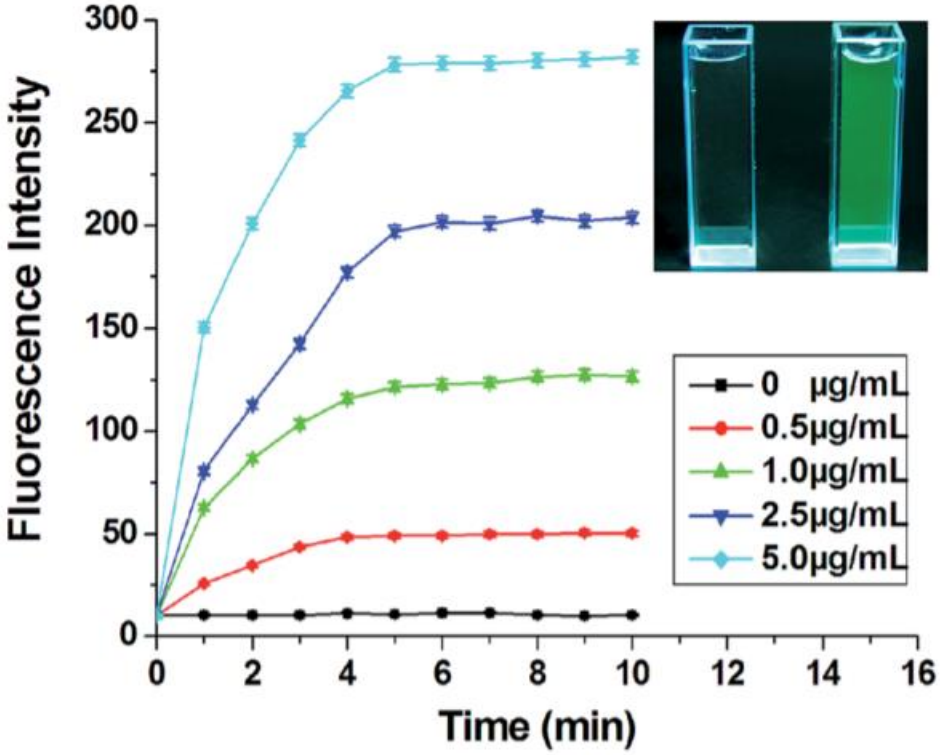

*Figure 1-22: The fluorescence intensity change of compound **21** (5 μM) with different concentration of NTR (0-5 μg mL^{-1}). Insert: fluorescence photograph of compound **21** with NTR.*

In the fluorescence emission spectrum of compound **21** (Figure 1-22), there was no fluorescence for compound **21** when none NTR was treated while when treated NTR with the compound **21**, there was a dramatic increase of fluorescence intensity at 520 nm with a very clear green fluorescence can be observed. This not only showed that the compound **21** can react as a hypoxia fluorescence probe for NTR, but also indicated the reaction rate of compound **21** with NTR increaseed as the concentration of NTR increased.

The last example was a series of compounds reported by Feng [49]. They had developed an effective sensor which allows optical detection of NTR for *in vivo* imaging. These compounds were based on cyanine conjugates with nitro aromatic groups showed on Figure 1-23.

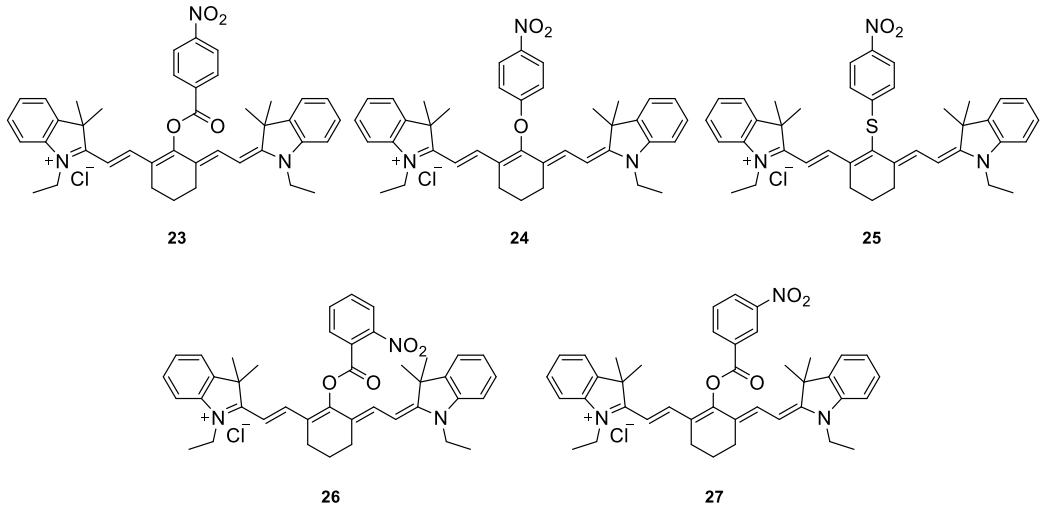

*Figure 1-23: Nitro aryl–cyanine conjugates compound **23**, **24**, **25**, **26** and **27**.*

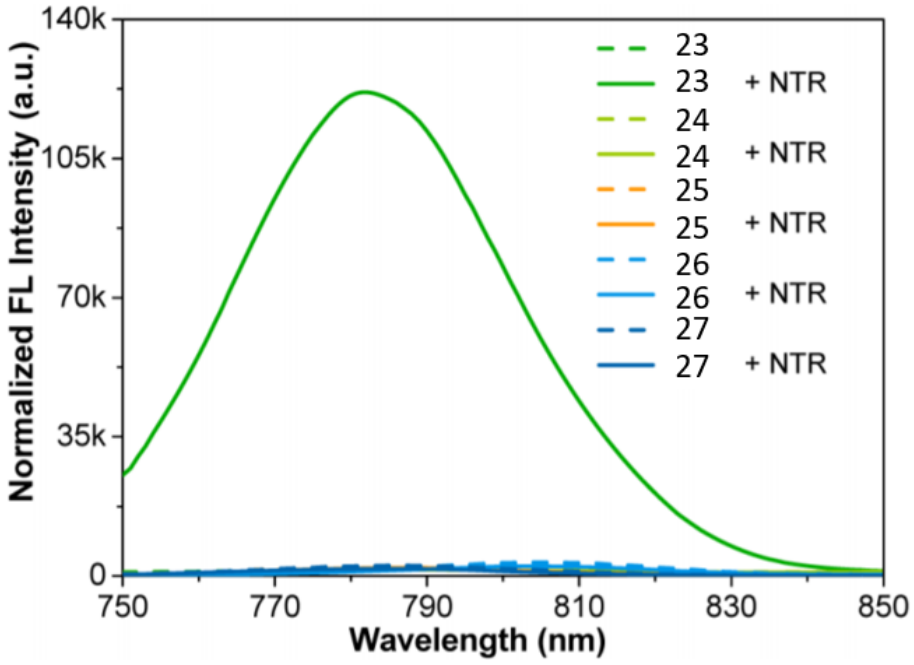

*Figure 1-24: The fluorescence emission spectrum of compound **23-27** reacted with NTR.*

In the NTR response experiment (Figure 1-24), they treated those 5 compounds with NTR and observed the fluorescence intensity change for each compound. Figure. As we can see from the spectrum, compound **24** – **27** did not show any significant change in the fluorescence, while a dramatic enhancement of about 110-fold in fluorescence intensity signal was observed for compound **23**.

Compound **23** was used as tumor hypoxia sensor for NTR from this spectrum. And an in vitro imaging of hypoxic A549 cells with compound **23** was also conducted (Figure 1-25). The part (a) was the fluorescence imaging of an A549 tumor mode in a mice, the tumor was in the top right of the mice. And the part (b) was the fluorescence imagines of the tumor mode when treated with compound **23**, as we can see in the figure, the fluorescence signal showed up once the compound **23** was injected, and the fluorescence signal can be observed increased during time with naked eyes. Part (c) was the average fluorescence intensity of the tumor during time. The fluorescence reached to the peak at 70 s and stay constantly for a long while. This example demonstrated the ability of compound **23** to be an *in cellulo* imaging agent for hypoxia.

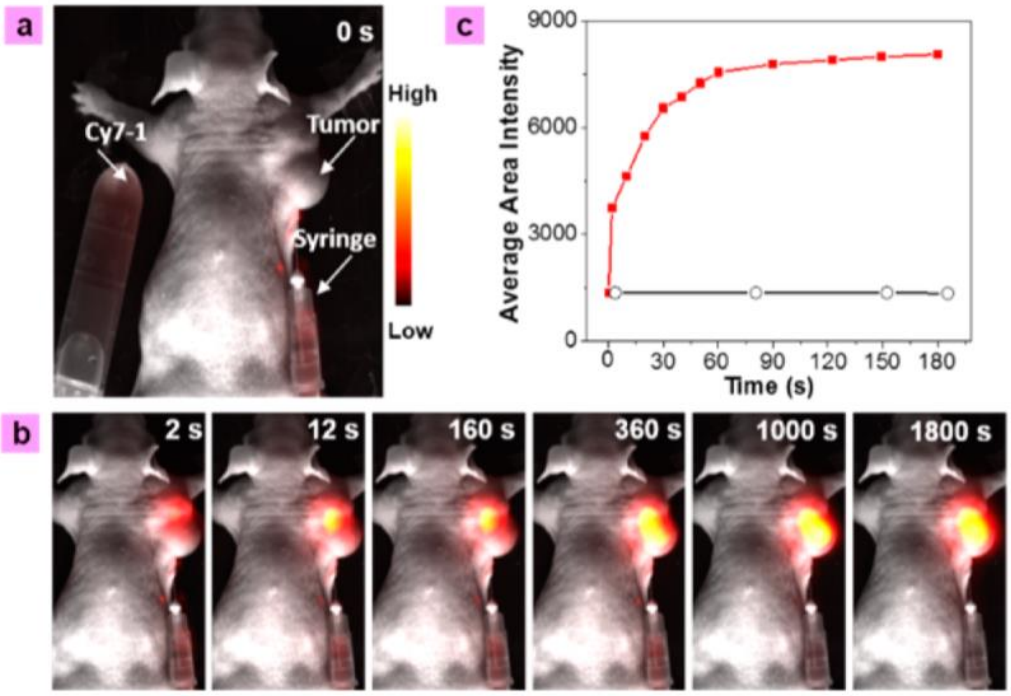

*Figure 1-25: In vivo fluorescence imaging of an A549 tumor mode (a) before and (b) after injecting compound **23**. (c) The fluorescence intensity time-dependent experiment of compound **23** in solution (black) and when it was injected to the tumor region (red) from 0 to 180 seconds. (Reproduced from J. Am. Chem. Soc., 2015, 137, 6407–6416. r 2015 American Chemical Society).*

We have described the characteristics of cancer, introduced the nature of tumor hypoxia and the methods for tumor hypoxia detection. Also we have cited a lot of

examples of fluorescence probes for the detection of tumor hypoxia. The next section will be the introduction of the thesis research objectives.

1.6 Research Objectives

Tumor hypoxia, where the oxygen concentration become less than normal, can result in reductive stress where the concentration of many reducing species such as reduced glutathione, NADPH and many oxidoreductases increase rapidly. Among them, oxygen sensitive nitroreductase is a critial marker for reductive stress as it can selectively reduce the nitro group of compounds to an amino group. This feature has already been used in both prodrug strategies and in approaches for tumor hypoxia detection. The study of the fluorescence probes for NTR in hypoxic environment is always hampered and limited, and the fluorescence probes are only studied in recent years. Many other research groups [50] [51] [52]have already reported their fluorescence probes for tumor hypoxia detection while most of them taking nitrothiophene, nitrofuran or nitrobenzene as the nitro aromatic functional groups to recognize NTR in tumor. However, another nitro aromatic substrate that is seldom mentioned in the synthesis of fluorescence probes, 2-nitroimidazole, is often used in prodrug strategies. It appears that, to date, 2-nitroimidazoles have been neglected as potential markers for fluorescence NTR recognition. Therefore, the thesis aims to evaluate 2-nitroimidazoles as markers in fluorescence detection of NTR and compare its sensitivity and selectivity to other more common nitroaromatics.

In the compound design stage, we envisioned the use of amino naphthalic anhydride as a fluorophore with 2-nitroimidazole connected to the fluorescent group through carbamate linker would furnish new fluorescent probes compound **28** and compound **29** (Figure 1-26).

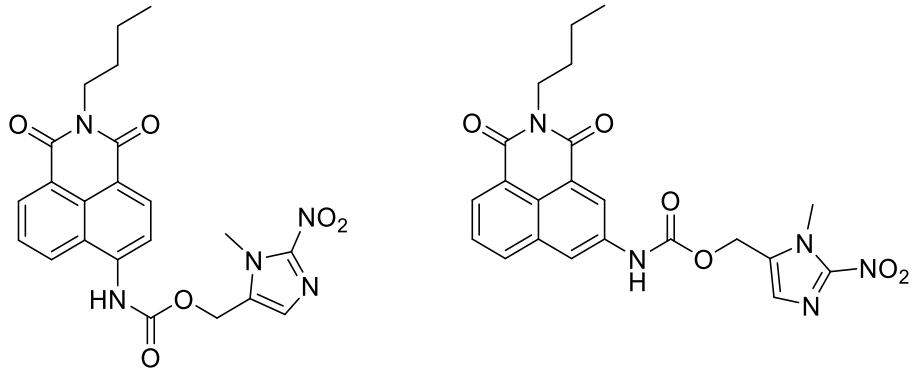

28 **29**

*Figure 1-26: The novel fluorescence probes compound **28** and compound **29** of this thesis.*

In our hypothesis, the nitro groups of this two compounds will be reduced to amino group with NTR in cells and the rearrangement reaction will lead to the cleavage of imidazole moiety and carbamate linker, finally it will release the amino naphthalimide as fluorophore to modulate fluorescence characteristics (Figure 1-27).

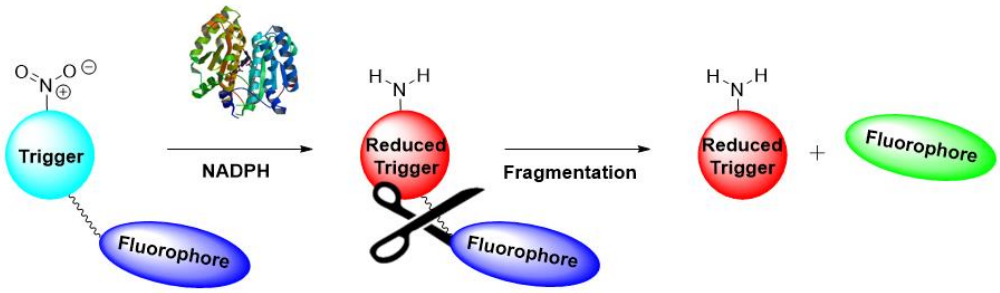

Figure 1-27: Mechanism of the novel fluorescence probe reacted with NTR.

After those two fluorescence probes have been made, our next object is to vary different nitroaromatic triggers as NTR recognition targets to increase the sensitivity to NTR and compare the abilities of various nitroaromatics such as nitrofuran, nitrobenzene and nitrothiophene to act as markers for reductive stress. (Figure 1-28).

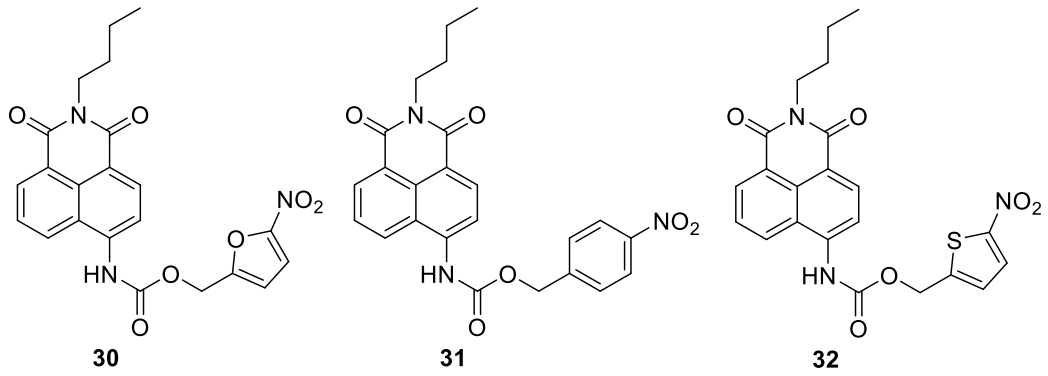

Figure 1-28: Novel compounds for sensitivity improvement

Finally, once the most sensitive compound to NTR has been identified, we will modify the compound to make it amenable to bioconjugation and also allow site selective uptake of the sensor to enable reductive stress measurements at organelle specific locations.

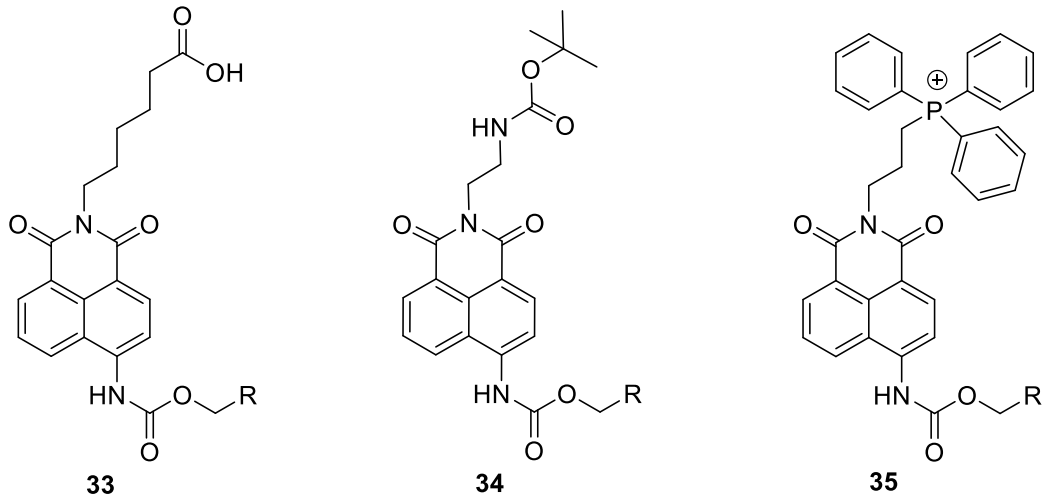

Figure 1-29: Novel compounds for bioconjugation and mitochondrial targeting.

In this thesis, we will report the synthesis of the novel sensors and a discussion of the photophysical characteristics in addition to the spectroscopic response to NTR. In some cases, preliminary cellular experiments have been carried out. Finally, based on our findings we will propose some improvements and modifications to ensure the most selective and sensitive fluorescent sensors for NTR.

Chapter 2 : 2-Nitroimidazole-naphthalimide conjugates as fluorescent sensors for nitroreductase.

2.1 Introduction

Since the first reported example of a fluorescent ratiometric probe in solid tumors in 2011 [53], improvements have been made in fluorescence detection of tumor hypoxia in vivo. The development of fluorescent probes for NTR has already become a burgeoning area of research interest. With the discussion in Chapter 1, we knew this kind of ratiometric probes require a nitroaromatic trigger to initiate the reduction reaction in cells with NTR and finally release the fluorophore to shift the fluorescence signal. In recent years, the research on ratiomatic triggers was limited to nitrobenzene, nitrofuran or nitrothiophene due to their relative ease of reduction. However, there is one compound that has not be used as nitroaromatic trigger despite it was widely used in the development of bioreductive prodrugs. The compounds with nitroimidazole as the parent nucleus have a very important role in the study of hypoxia imaging agents due to their ability of hypoxia targeting. And the tumor hypoxia targeting of nitroimidazoles is mainly based on the reduction susceptibility of nitroimidazole at different oxygen concentrations. In the cells with normal oxygen content, the nitro groups of these compounds generate free radical anions under the reaction of xanthine oxidase and rapidly reoxide to nitro group to diffuse out of the cells. While under hypoxic conditions, the free radicals are further treated with nitro reductase and the products bind to the intracellular component and remains in the cell [11]. The position of the nitro group on the imidazole ring mainly includes 2-nitroimidazole (2-N), 4-nitroimidazole (4-N), 5-nitroimidazole (5-N). Among them, 2-nitroimidazole has the highest reduction potential, which means that it is most likely to be reduced in an oxygen-free environment.

The objective of the research presented in this Chapter was developing a series of fluorescence detection probes based on naphthalimide and 2-nitroimidazole functional group, compound **28** and compound **29**. Compound **28** and compound

29 were two new fluorescently responsive NTR sensors that we envisaged a 2-nitroimidazole group coupled to a naphthalimide fluorophore through a carbamate linker so that they may afford ratiometric probes with sensitivity to NTR.

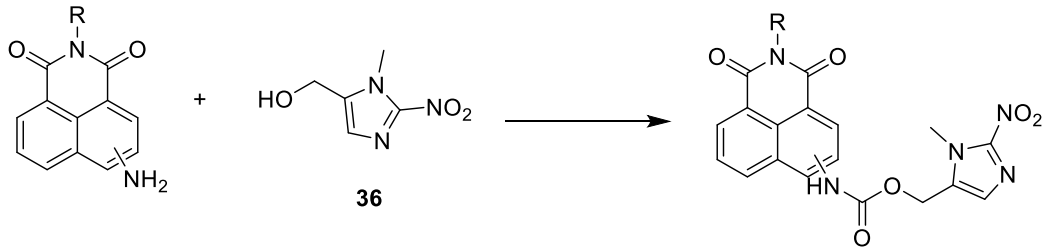

Scheme 2-1: Synthesis of novel fluorescence sensors

The purpose of designing these compounds was to develop sensitive fluorescent probes for cellular reductive stress. As we thought 2-nitroimidazole group (**36**) would have a great performance in a reductive environment by reducing the nitro group to amino group through NTR in cells consider its high reductive potential. In the design of these compounds, carbamate linker was used to connect the fluorophore and the nitroaromatic trigger, because carbamate linker could change the functional group attached to the fluorophore from electron donating group to electron withdrawing group, which can change the fluorescence signal. We envisaged that when treated with NTR in cells, both compound **28** and compound **29** would be reduced and given rise to a fragmentation of the parent molecule and release of the well-known amino-1,8-naphthalimide fluorophores as shown below of scheme 2-2. It was expected that the conversion of the electron-withdrawing carbamate linker to the electron-donating amino functional group would lead to significant modulation of their optical properties and lead to a fluorescence shift visible to the naked eye.

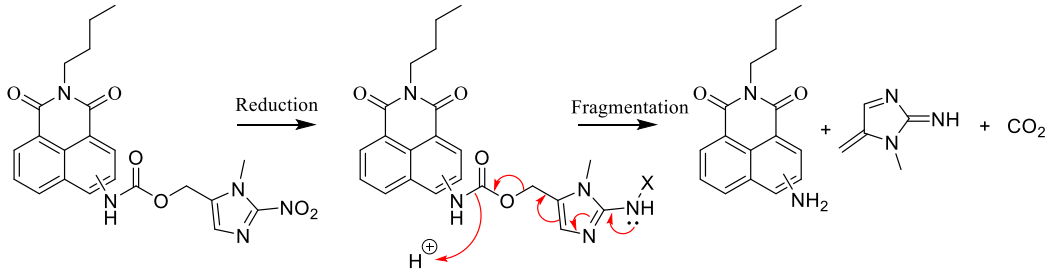

Scheme 2-2: Reaction mechanism of novel fluorescence sensors

The overall aim of the work presented in this chapter is to explore the various properties of the compound **28** and **29**. Firstly, there will be a brief description of the synthesis and characterization of each compound. This is followed by a discussion of the photophysical properties of these compounds. Then comes the discussion of the response of the probes to the enzyme NTR. Finally, preliminary biological studies will be described, cellular uptake and localization as well as cellular toxicity studies.

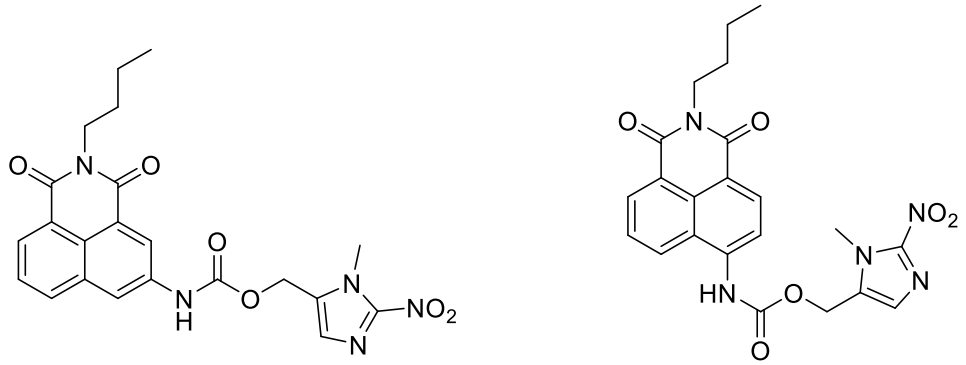

29 **28**

Figure 2-1: Two novel fluorescence sensors

2.2 Synthesis

2.2.1 Synthesis of compound 36

The synthesis of compound **29** was achieved using an intermediate in the synthetic pathway of 2-nitro-imidazole (**36**) as outlined in scheme 2-3 and scheme 2-4. Both compound **28** and compound **29** were synthesized by reaction with compound **36**. Therefore, to successfully synthesise compound **36** was the first step in the whole scheme. In this section, we discussed the conventional synthesis procedure (Scheme 2-3) of compound **36** and compared it with novel synthetic methods (Scheme 2-4), followed by identification of the intermediate product during the reaction to determine the progress of the reaction.

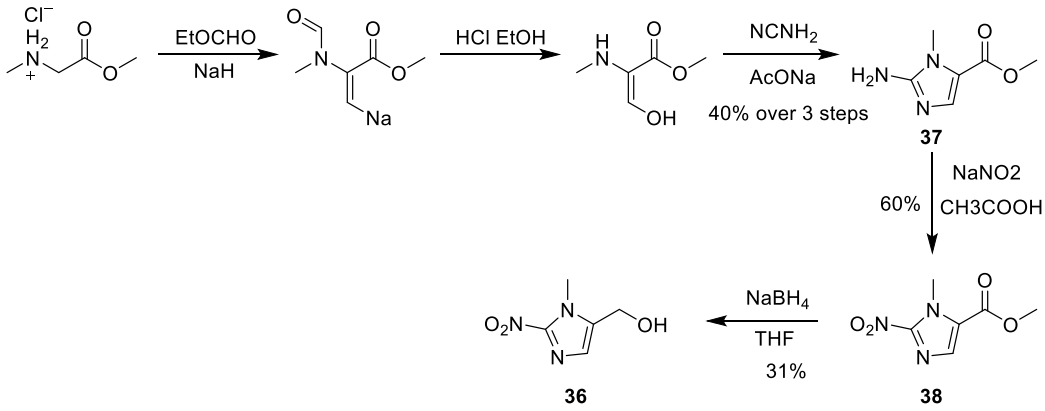

*Scheme 2-3: The conventional synthesis procedure of compound **36**.*

For the conventional synthesis of compound **36** shown in Scheme 2-3 [54], sarcosine methyl ester hydrochloride was chosen as starting material, which was reacted with NaH in ethyl formate to have the di-substitution reaction. The mixture was acidified and heated to afford elimination of a single aldehyde. Then the mixture had a ring forming reaction with cyanamide to form compound **37**. Compound **37** was going through an oxidation reaction and an ester reduction reaction to form the final product compound **36**.

If we turn back and have a look at the above reaction, we can see many shortcomings for this reaction. First of all, the raw material was sarcosine methyl ester hydrochloride, which was not very soluble in ethyl formate, and this largely restricted the yield of the reaction (35 % yield). Second, sodium hydride we used was 60 % present in mineral oil, so the amount required was very large and the reaction produced a sticky solid that is difficult to handle. More importantly, the hydrogen produced during the process is dangerous. The next shortcoming was that the reaction time was quite long. Finally, the post treatment of the reaction was very complicated (evaporated 7/8 of the solvent and then titration to adjust the reaction conditions).

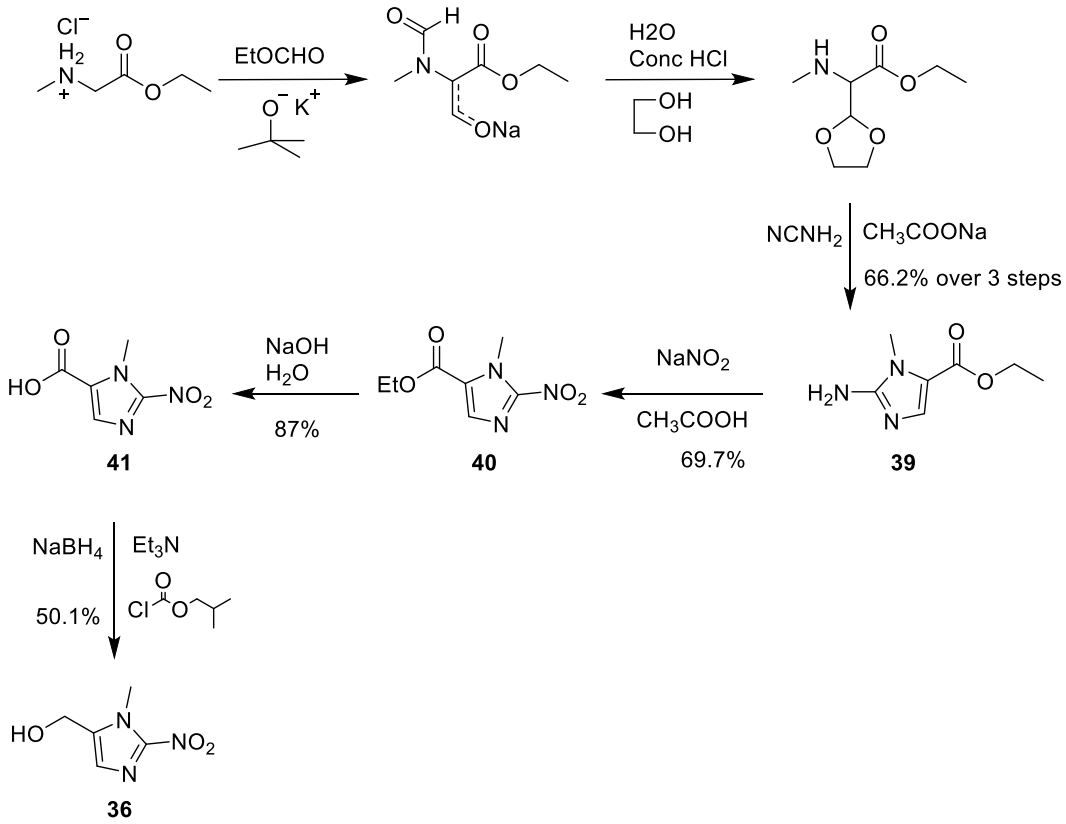

*Scheme 2-4: The novel synthesis procedure of compound **36**.*

Therefore, we had improved the reaction based on the shortcomings. We replaced some reactants and changed the reaction conditions and eventually formed the following reaction process (scheme 2-4): We used sarcosine ethyl ester hydrochloride as starting material, reacted with potassium tert-butoxide in ethyl formate at room temperature to have the di-substitution reaction. Then the mixture had elimination reaction with concentrated HCl and had the ring close reaction with ethylene glycol. After that used cyanamide to form compound **39**. Similar to the conventional synthesis, compound **39** had a diazonium reaction through sodium nitrite to compound **40** and the ester function group of compound **40** was reduced to carboxyl group to form compound **41**. Finally, compound **41** was reduced by sodium borohydride to form compound **36**.

With two different procedure in hand, we had a comparison of this two procedures. Instead of using sarcosine methyl ester hydrochloride, we chose sarcosine ethyl ester hydrochloride as our starting material in novel synthesis procedure because sarcosine ethyl ester hydrochloride was much more soluble in ethyl formate. It

only took 3 hr to complete the first step of this procedure while it required overnight reacting with sarcosine methyl ester hydrochloride, which saved much more time for this reaction. And the new method was using potassium tert-butoxide as a strong base while the sodium hydride was used in the conventional one. The advantage of doing so was that it does not produce gas, made the experiment safer, and it does not produce sticky solid, made the reaction easier to handle. Then, in the conventional synthetic method, the final compound **36** was obtained by direct reduction of its ester form, and the yield was only 28 %. While in the novel synthetic method, we reduced the ester to acid first, then yielded the final product compound **36** by reducing the acid. Although the number of reaction step was increased, the overall yield was improved (50.1 % yield). Last but not least, the new experimental program does not require a change of solvent during the reaction, sequence thereby simplifying the reaction procedure.

By comparison, we knew that the new method shown in scheme 2-4 can effectively improve the reaction yield and simplify the reaction step, making the experiment safer and faster. Therefore, for the synthesis of compound **36**, we were more inclined to use the new method. After that, we detected the synthesized compounds from the new method according to characterisation.

Since the first and the second step in scheme 2-4 was inseparable, our detection was started from compound **39**.

Compound **39** was characterised by ^{1}H NMR, melting point analysis, mass spectrometry, ^{13}C NMR and IR spectroscopy. The ^{1}H NMR spectrum is shown in figure 2-2. Assignment of the peaks was achieved by H-H COSY and C-H COSY analysis.

In the Figure 2-2, we can clearly see 5 signals which perfectly matched the H of compound **39**. The peak at 7.28 ppm which integrated as 1 H represents the H in the imidazole group, and the signal at 6.189 ppm stands for the NH_2 of compound **39** because this peak was singlet and integrated as 2. Peaks at 4.15 ppm and 1.24 ppm represent the ethyl group of compound **39**, and at last, peak at 3.52 ppm stands for the CH_3 group on the N. Also from the MS, the formula of compound **39** was $C_7H_{11}O_2N_3$, the mass we calculated was 169.0851 while with the machine the tested result was 169.0851. the PPM was 0.01, which perfectly matched the result

calculated. Therefore, with the ^{1}H NMR and MS, we can admit that compound **39** was made successfully.

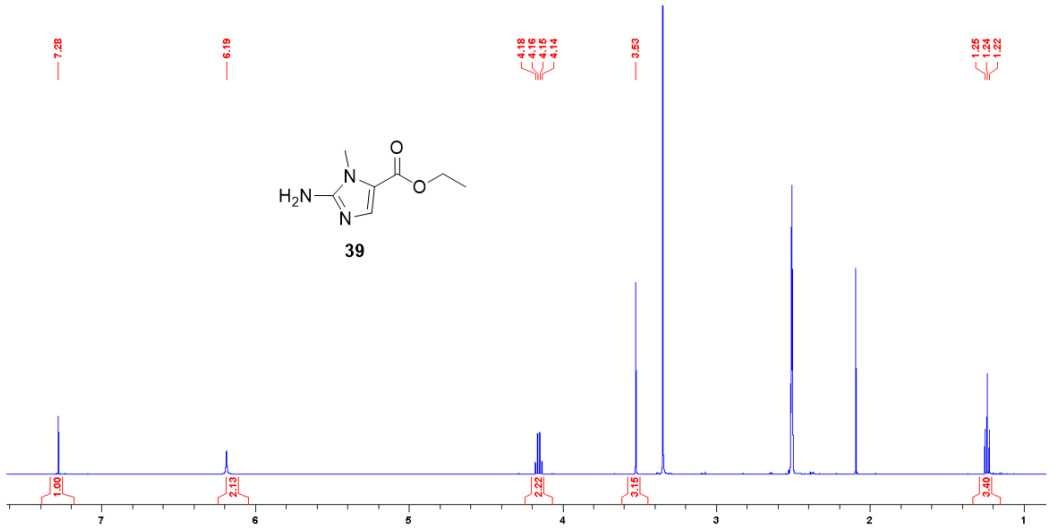

*Figure 2-2: The ^{1}H NMR spectrum of compound **39** (500 MHz, DMSO-d_6)*

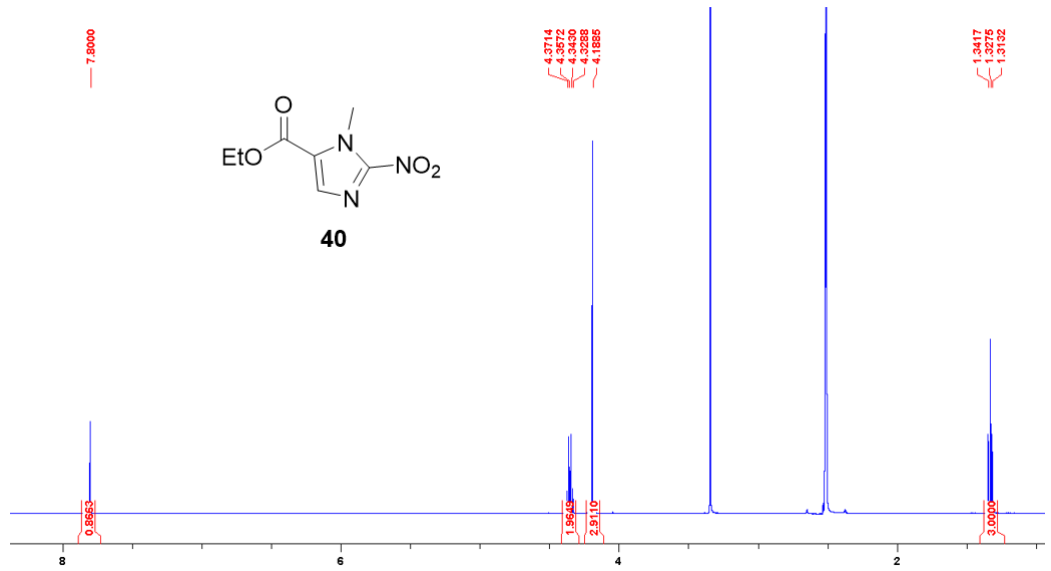

*Figure 2-3: The ^{1}H NMR spectrum of compound **40** (500 MHz, DMSO-d_6)*

Compound **40** was characterised by ^{1}H NMR, melting point analysis, mass spectrometry, ^{13}C NMR and IR spectroscopy. The ^{1}H NMR spectrum is shown in figure 2-3. In this spectrum, peak at 7.8 ppm stands for the H of the imidazole group. The chemical shift was moved to left side compared with the H in the same position of compound **39** which had 7.28 ppm chemical shift. This was because the amino group was changed to nitro group whereas it converted an electron donating group to an electron withdrawing group and decreased the electron density to deshield the H. Also the signal at 6.19 ppm which represent the NH_2 group disappeared in the spectrum of compound 66, this proved the compound **40** was successfully made from compound **39**. Finally, peaks at 4.34 ppm and 1.32 ppm stand for the ethyl group just similar to compound **39**. In compared with this two spectrums, we can see compound **39** was made successfully and compound **40** was changed from compound **39** by switching the amino group to nitro group.

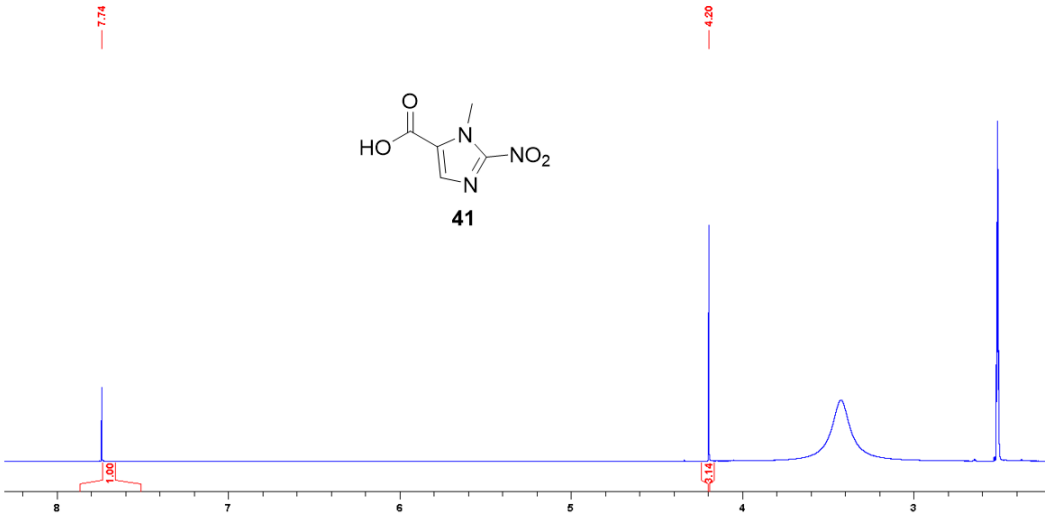

*Figure 2-4: The ^{1}H NMR spectrum of compound **41** (500 MHz, DMSO-d_6)*

After the oxidising of the amino group to nitro group, compound **40** was reduced to compound **41**. The ethyl group was disappeared so we cannot see the signals at 4.34 ppm or 1.32 ppm from figure 2-4. However the signal at 7.73 ppm and 4.19 ppm stand for the H in imidazole and the CH_3 group on the imidazole group separately was still the same as figure 2-3, which means the main structure of

compound **40** was not changed, the only change was the ester group was reduced to a carboxyl group.

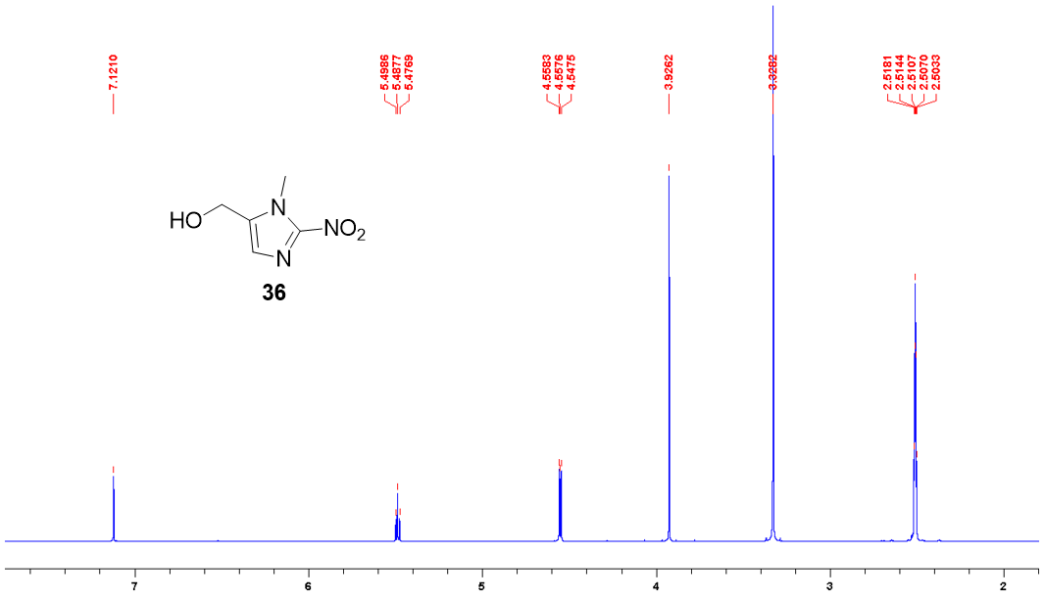

*Figure 2-5: The [1]H NMR spectrum of compound **36** (500 MHz, DMSO-d_6)*

Compound **39** was characterised by ^{1}H NMR, melting point analysis, mass spectrometry, ^{13}C NMR and IR spectroscopy. The ^{1}H NMR spectrum is shown in Figure 2-5. Assignment of the peaks was achieved by H-H COSY and C-H COSY analysis. Successful formation of compound **39** was also evident from accurate mass spectrometry.

Compound **41** was reduced to compound **36**, we can see in the spectrum, two new signals appeared, peak at 5.48 ppm integrated as 1 represents the OH signal and peak at 4.55 ppm integrated as 2 represents the CH_2 group. The chemical shift at 7.12 ppm stands for the H in the imidazole was shifted highfield, and the signal at 3.92 ppm stands for the CH_3 group also shifted to Highfield compared to compound **41**. The reason was the carboxyl group was electron withdrawing group, when it converted to an alcohol group, it was changed to an electron donating group compared to a carboxyl group. This increase the electron density and caused the shield of the hydrogen and finally, the peak shifted to left.

2.2.2 Synthesis of compound 29

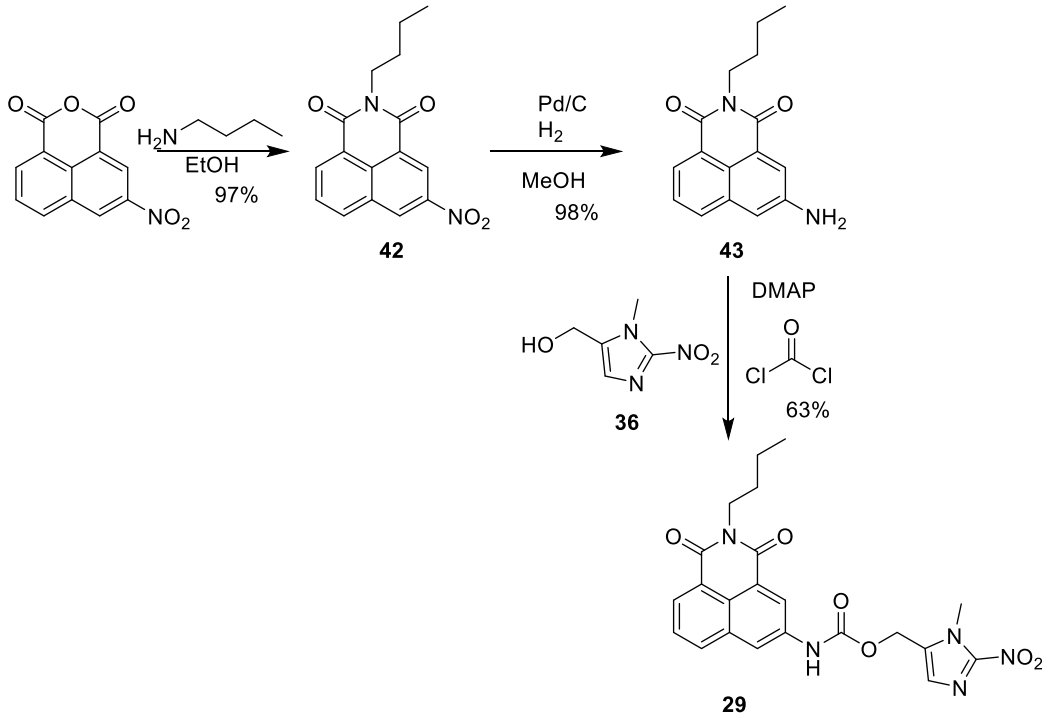

*Scheme 2-5: The synthesis of compound **29***

With the compound **36** in hand, our next step was to synthesis the two different fluorophores and connect the two fluorophores with compound **36** through a carbamate linker.

In order to synthesis compound **29**, 3-nitro-1,8-naphthalic anhydride and butyl amine were heated under microwave irradiation to yield compound **42**. Then compound **42** had the reduction, making the nitro group to amino group to form a bright yellow solid compound **43** at 98% yield. Finally, to get the final product, compound **43** was reacted with phosgene in the presence of DMAP first and then reacted with compound **36** to yield a beige solid compound **29** at 63% yield.

In order to make sure all steps were successfully proceeded, we compared the ^{1}H NMR spectrums of each intermediate.

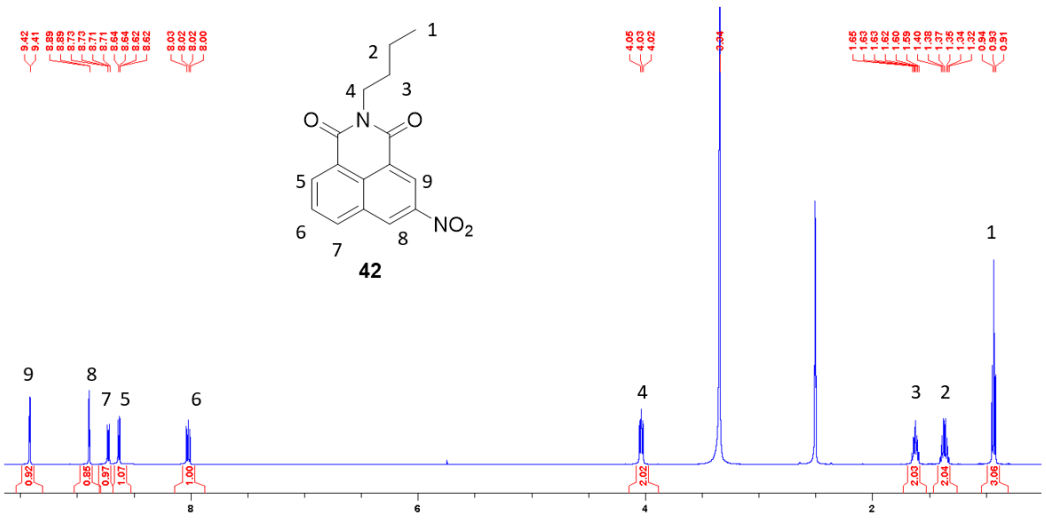

*Figure 2-6: The ^{1}H NMR spectrum of compound **42** (500 MHz, DMSO-d_6)*

From the spectrum of compound **42** in figure 2-6, we can clearly see that there were 9 signals which represent 9 kinds of H of compound **42**. Peaks from 7 ppm to 10 ppm were the aromatic H and peaks between 1 and 5 ppm were the aliphatic H. Peak at 0.93 ppm integrated 3 stands for the H1 and peaks at 1.34 ppm and 1.62 ppm which both integrated 2 represented H2 and H3 respectively. The chemical shift of H4 was 4.03 ppm, which shifted to downfield compared to the rest CH_2 groups. The reason was that this CH_2 group was attached to two carbonyl groups which were electron withdrawing groups, and those carbonyl groups decreased the electron density of H4, caused de-shield and finally made the H4 move to down field. The peak at 8.89 ppm was a singlet, means this H did not attach with other H, so peak at 8.89 ppm stands for H9. H5 was attached to one H and it was closed to a carbonyl group, therefore the signal of H5 should be downshield and doublet, also known as 9.42 ppm. H6, H7, and H8 were confirmed by H-H COSY and C-H COSY analysis.

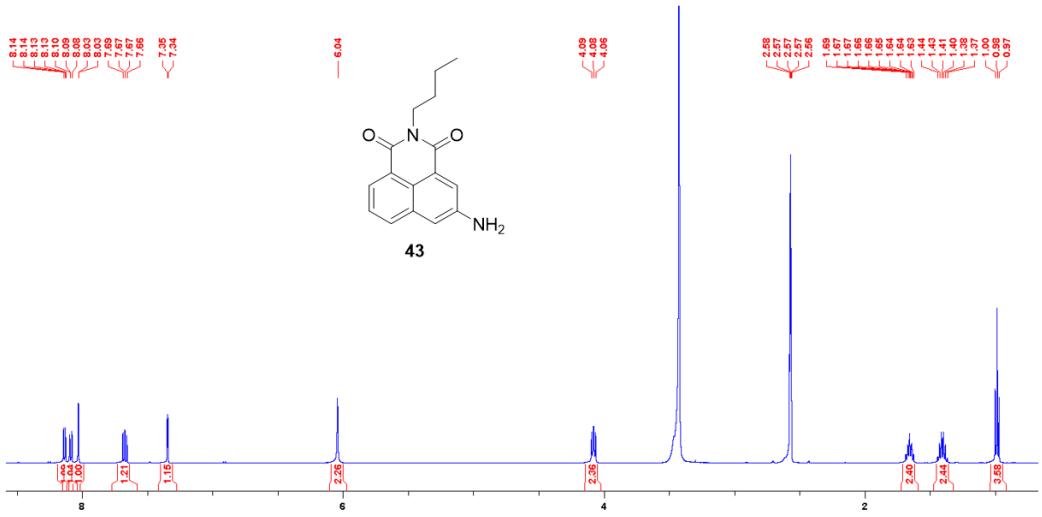

*Figure 2-7: The ^{1}H NMR spectrum of compound **43** (500 MHz, DMSO-d_6)*

Compared with compound **42**, there was very little change from figure 2-7. First of all, the aliphatic H did not change, it stayed with same chemical shift. Then, there was one new signal shown up. Peak at 6.04 ppm integrated 2 stands for the NH_2 group. Last, all the aromatic H had shifted to high field because once the nitro group changed to amino group, the electron withdrawing group had changed to electron donating group, this change increased the electron density of the aromatic ring and caused shield of the proton. According to the above description, we can be sure that compound **43** had been made successfully and was ready for the next synthesis.

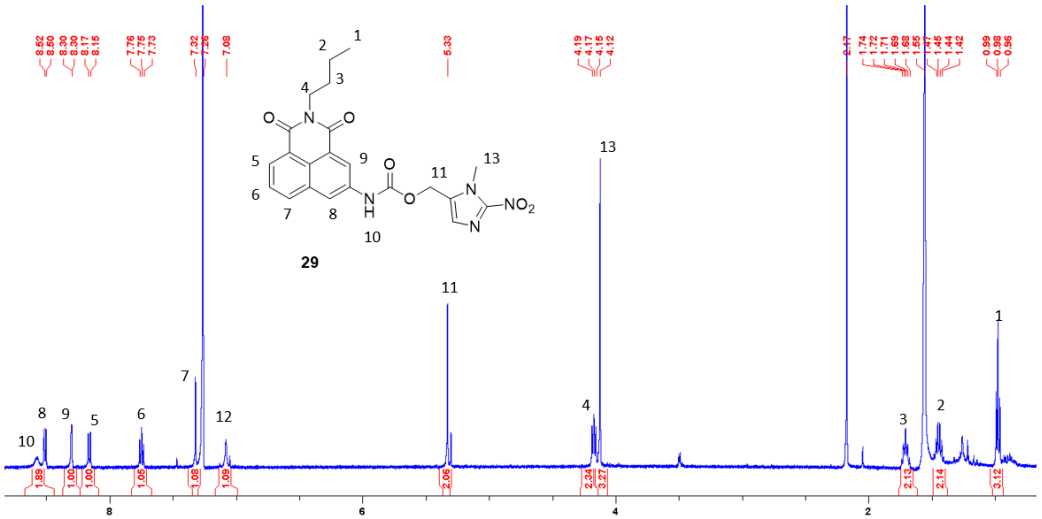

*Figure 2-8: The ^{1}H NMR spectrum of compound **29** (500 MHz, $CDCl_3$)*

Compound **29** was characterised by ^{1}H NMR, melting point analysis, mass spectrometry, ^{13}C NMR and IR spectroscopy. The ^{1}H NMR spectrum is shown in figure 2-8. Assignment of the peaks was achieved by H-H COSY and C-H COSY analysis.

As we see in the spectrum of figure 2-8, peaks at 7 ppm to 9 ppm represent the aromatic peaks and peaks between 1 ppm and 6 ppm were aliphatic H. There were 13 different kinds of H in compound **29**, if we compared it with compound **43**, there was a broad peak shown up at 8.56 ppm which stands for the NH of compound **29** and the chemical shift moved downfield because the NH group was connected with ester group which was electron withdrawing group, causing deshield to shift the peak to down field. There were 6 aromatic H while compound **43** only had 5, so the extra aromatic H stands for the H in imidazole functional group. If we combined those two spectrums of compound **43** and compound **29**, we can find out that the chemical shift of butyl group of compound **43** was much similar as the chemical shift of butyl group of compound **29**, therefore the peaks at 0.94 ppm, 1.44 ppm, 1.71 ppm and 4.16 ppm stand for the butyl group of compound **29**. The peak at 4.1 ppm integrated 3 represents the CH_3 group on the imidazole functional group. Finally, the peak at 5.32 ppm can only stand for the CH_2 group beside the imidazole group, shifted to downfield because the electron withdrawing group ester group connected by.

According to the comparation with the ^{1}H NMR spectrum, we were very confident that compound **29** had been produced. Our next aim was to synthesis the other fluorescence sensor compound **28**.

2.2.3 Synthesis of compound 28

The procedure to synthesis compound **28** (Scheme 2-6) was just the same as compound **29**, 4-nitro-1,8-naphthalic anhydride was chosen as the starting material. After the reaction with butylamine, it went through a reduction reaction of the nitro group to amino group. Then connected the naphthylamide with the trigger through the carbamate linker to yield the product compound **28**.

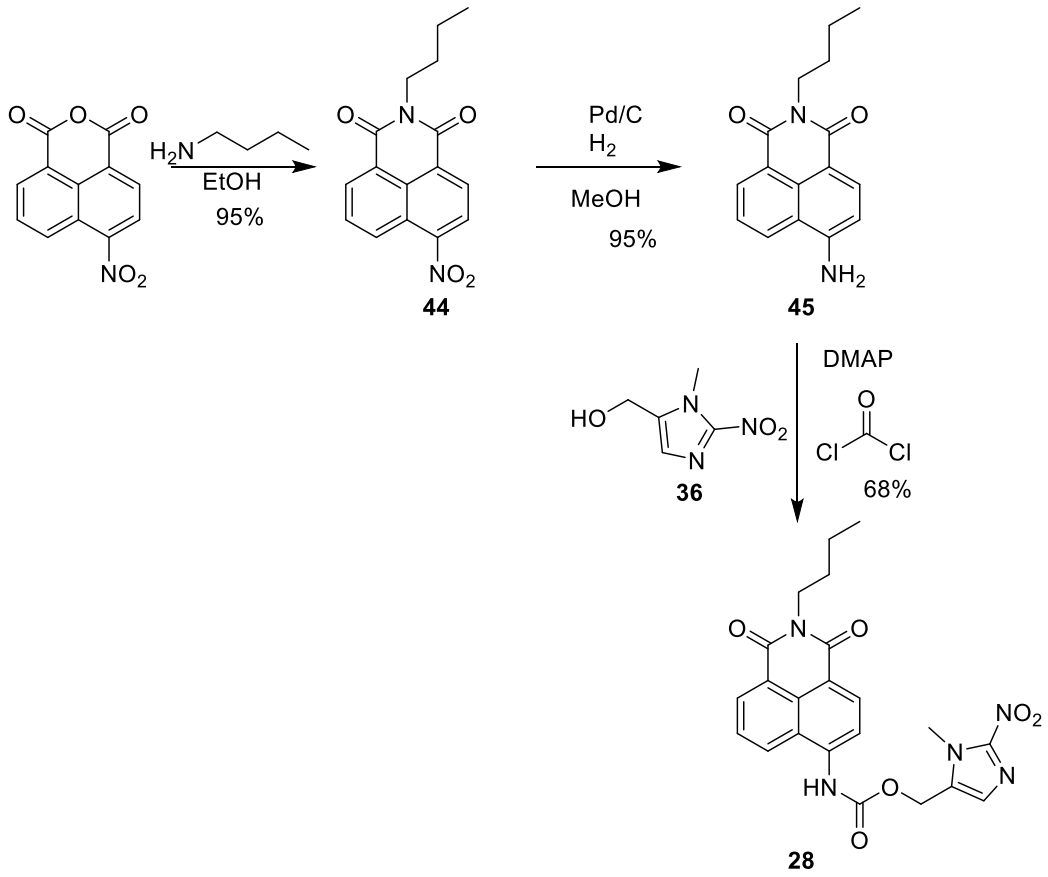

*Scheme 2-6: The synthesis of compound **28***

Compound **28** was characterised by ^{1}H NMR, melting point analysis, mass spectrometry, ^{13}C NMR and IR spectroscopy. The ^{1}H NMR spectrum is shown in figure 2-9. Assignment of the peaks was achieved by H-H COSY and C-H COSY analysis. Compound **28** had 13 different kinds of H, and the only different between compound **28** and compound **29** was the substitution potion. Therefore, the different between this two compounds on the spectrums was the chemical shift and the multiple of aromatic H. In the spectrum of compound **28**, there was only one singlet aromatic H which represents the H on imidazole group while there were two singlet peaks in compound **29**. In addition of this, there was little different between compound **28** and compound **29**. The peak at 0.92 ppm, 1.35 ppm, 1.63 ppm and 4.06 ppm represent the butyl group of compound **28**. The peak at 4.04 ppm integrated 3 stands for the CH_3 group on the imidazole group and peak at 5.39 ppm stands for the CH_2 group on the imidazole group.

Due to the overall similarity of this two spectrums and the difference in aromatic region, we can be sure the compound **28** had been made successfully.

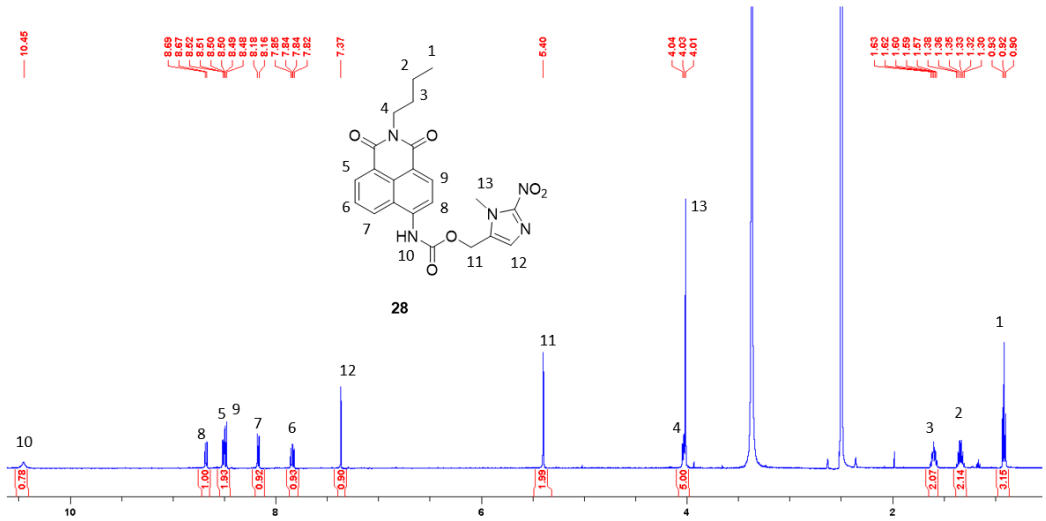

*Figure 2-9: The ^{1}H NMR spectrum of compound **28** (500 MHz, DMSO-d_6)*

Through the discussion of the synthesis procedure and the analysis of the ^{1}H NMR spectra, we had successfully synthesized the compounds. However we did not know too much about the photophysical properties of this compounds while the fluorescence properties of this compounds were important for exploring them as hypoxia fluorescent sensors. Therefore, our next aim was to detect the photophysical properties of these compounds.

2.3 Photophysical characterisation of compound 28 and compound 29

2.3.1 Absorption and emission spectra of compound 28 and compound 29

The absorption and emission spectra of compound **29** and compound **28**, recorded at pH 7.4 in 10 mM phosphate buffer with 0.5% DMSO as co-solvent were shown in below.

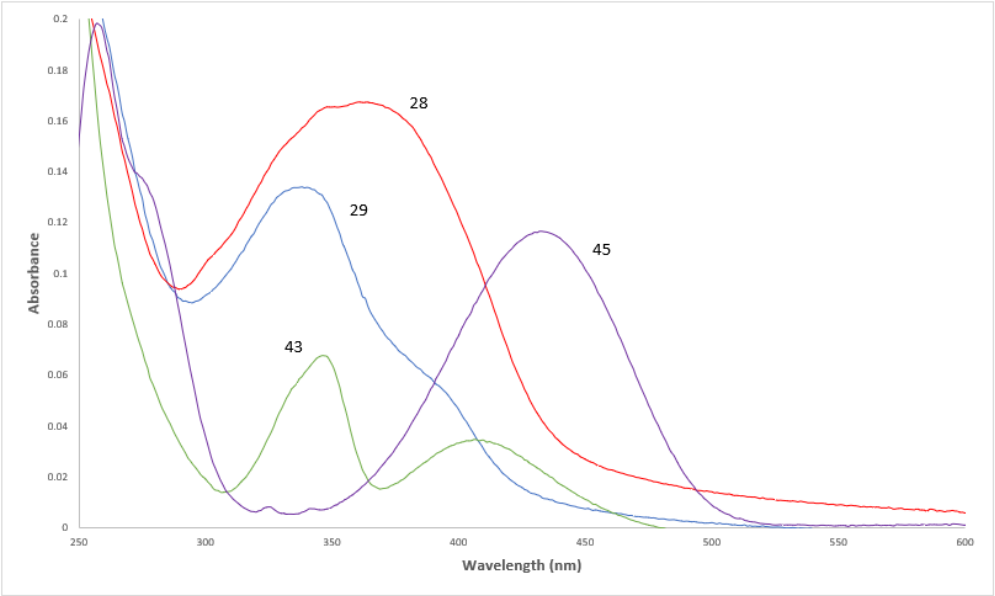

*Figure 2-10: The UV/Visible spectra of compound **28** and compound **29** and their reference fluorophores. **28** (red), **29** (blue), **45** (purple) and **43** (green).*

The absorption spectrum of compound **28** (figure 2-10) showed a λ_{max} at ca. 360 nm while compound **29** showed a λ_{max} at ca. 345 nm with a broad shoulder centred at 390 nm. So we chose 345 nm as our excitation wavelength cause the absorption at 345 nm were relatively high for both compound **29** and compound **28**. Therefore, the excitation (λ_{exc} = 345 nm) compound **28** (Figure 2-11)showed rise to emission with λ_{max} at 475 nm while compound **29** yielded emission spectrum (Figure 2-12) with λ_{max} at 460 nm. The value of the max intensity of compound **29** was 3 fold less than that of compound **28** when treated with same concentration. One possible reason is the fluorescence intensity could be changed by the anion's electronegativity and the fluorescence behaviour of compounds depending on their electronegativity [54]. We suggested compound **28** and compound **29** were treated with NTR in cells to make nitro group to amino group and then yield the corresponding amino-derivatives compound **45** and **43** thus causing significant shifting of spectral characteristics. Because of this, we also need to compare the photophysical characteristics of compound **28** and compound **29** with those of compound **45** and compound **43**.

The absorption spectrum of compound **45** (Figure 2-10) showed a λ_{max} at ca. 435 nm while compound **43** showed λ_{max} at ca. 345 nm and 410 nm (Figure 2-10). Emission from compound **45** (λ_{exc} = 435 nm) showed a λ_{max} at 550 nm while that of compound **43** (λ_{exc} = 345 nm) showed a λ_{max} at 590 nm, again demonstrating a lower level of emission when compared against the 4-substituted derivative. If we compare the emission spectrums of compound **28** and **45** we can see that the maxima peak signal was shifted about ca. 75 nm while that of compound **29** and **43** was 130 nm but still with low emission intensity. This result is consistent with the previous observations of the absorption spectrums.

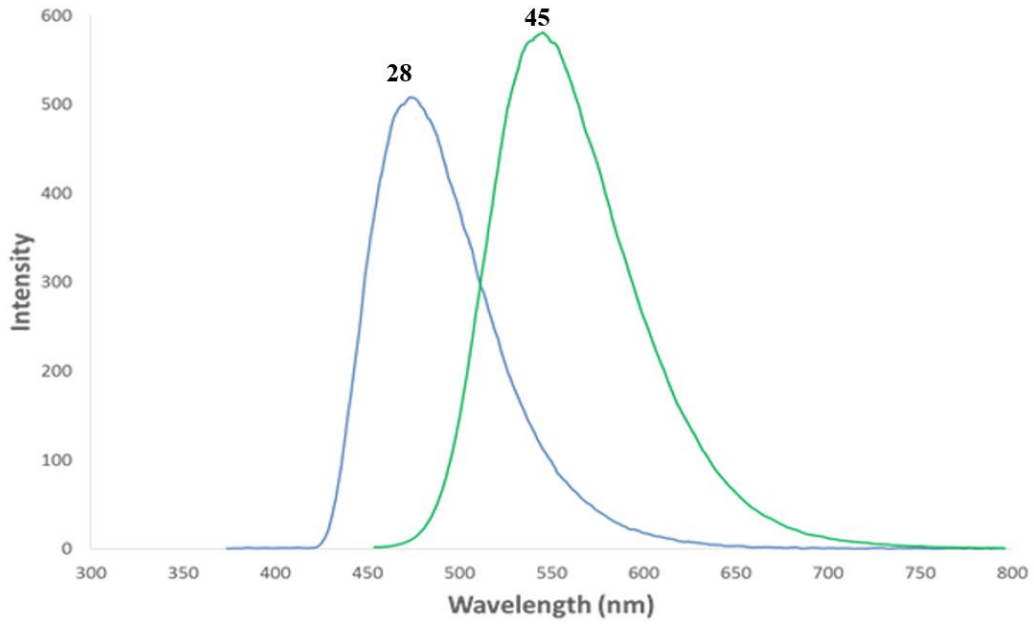

*Figure 2-11: The emission spectra of compound **28** (10 µM) and its fluorophore reference compound **45** in 10 mM phosphate buffer at pH 7.4*

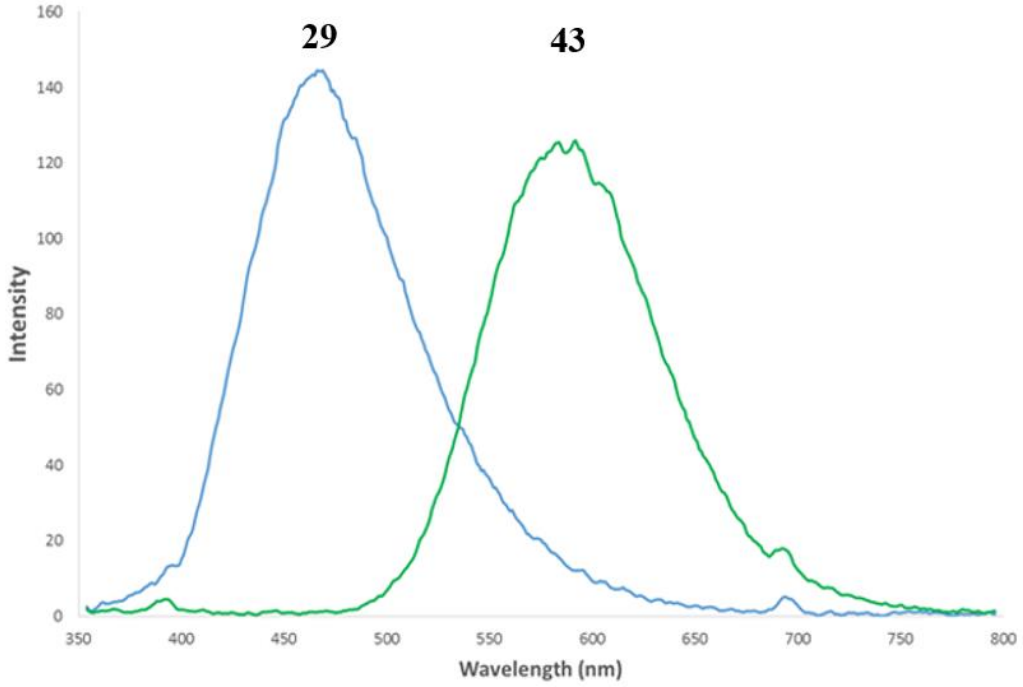

*Figure 2-12: The emission spectra of compound **29** (10 µM) and its fluorophore reference compound **43** in 10 mM phosphate buffer at pH 7.4*

2.3.2 NTR Response

Compound **29** not only shows lower absorption in UV/Visible spectrums than compound **28** but also shows lower intensity in the emission spectrums. So now we investigated their spectral properties when placed under reductive stress conditions by treatment with NTR (oxygen insensitive NTR expressed in *E. coli*).

The emission spectrums were measured in PBS (pH 7.4, 10 Mm) with 0.5% DMSO as co-solvent in the presence of NADPH (50 µM, as a cofactor of NTR) at 25 °C.

When treated compound **28** with 0.5 µg NTR, we can see an emission spectrum with the intensity change during times (figure 2-13). The emission maximum at 475 nm was decreased while the signal at 550 nm was a coherent increase, clearly visible to the naked eyes as a blue fluorescence to green fluorescence change in colour. After 20 mins, the fluorescence intensity at 550 nm was increased by more than 8-fold than before while the emission at 475 nm had decreased for 5-fold. The

colour changed from blue to green in fluorescence also proved the transformation from compound **28** to **45** while treated with NTR.

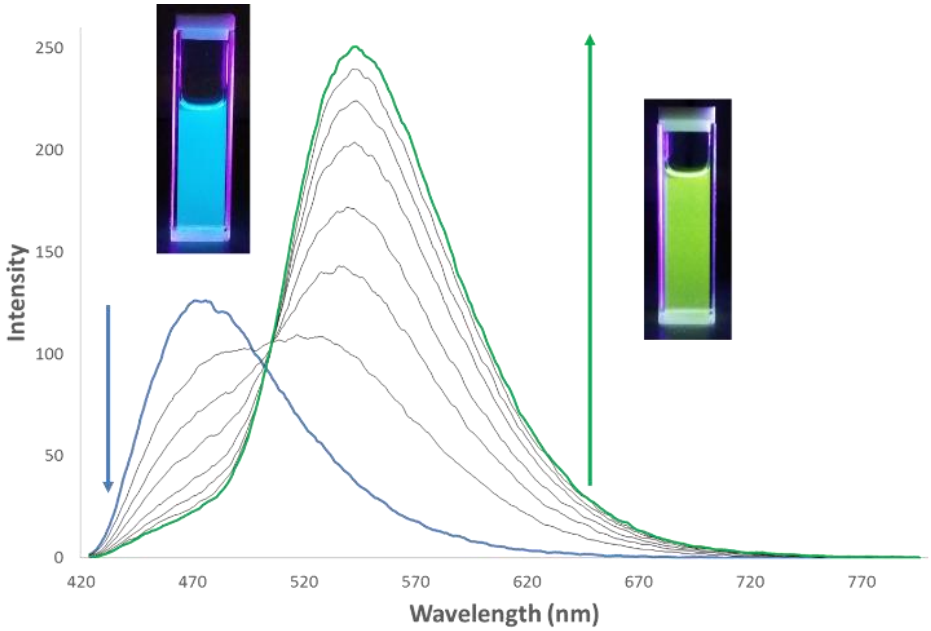

*Figure 2-13: Changes in the emission spectrum of compound **28** (10 µM) at various time points (0 - 25 mins) after addition of NTR (0.5 µg mL^{-1}). Insert, pictures beside the spectrum were the colour change of compound **28** when treated with NTR. The blue fluorescence on the left represents the colour at the beginning when treated with NTR; the green fluorescence on the right represents the colour of the compound and NTR after 20 minutes of reaction.*

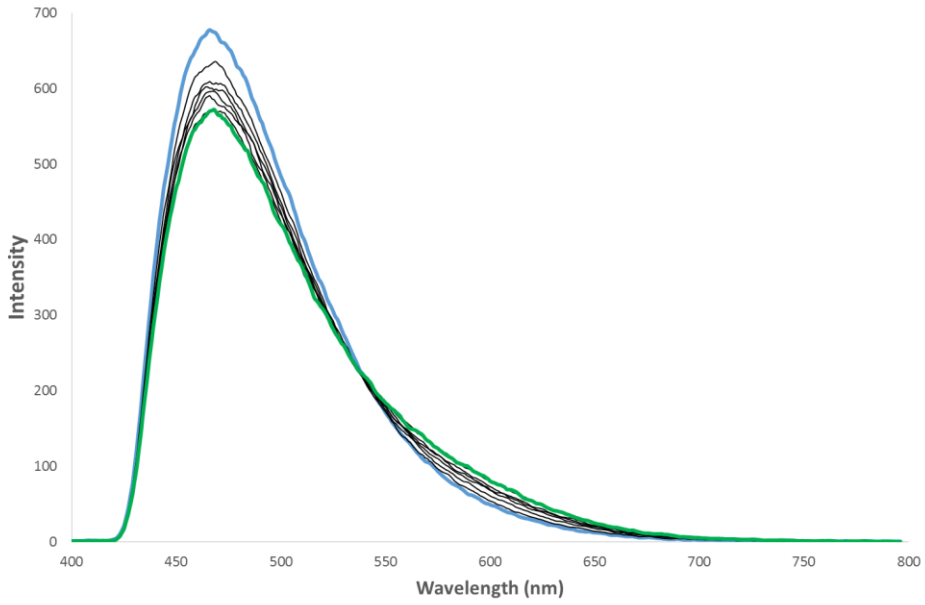

*Figure 2-14: Changes in the emission spectrum of compound **29** (10 µM) at various time points (0 - 25 mins) after addition of NTR (1 µg mL^{-1}).*

Interestingly, compound **29** did not have the same result as compound **28**, there was no fluorescence change when treated with NTR under the same conditions. The colour of compound **29** in the vial did not change after treating with NTR. Similar information can be seen on the emission spectrum of figure 2-14, we treated compound **29** with 0.5 µg of NTR in PBS, and the figure 2-14 here was emission spectrum with intensity change during time. Compound **29** had an emission maximum at 460 nm, and the emission intensity decreased slightly over time. Also a slight upward trend in emission intensity was observed at 590 nm. After 20 mins, the intensity of the signal at 460 nm decreased by 1/7, and the intensity of the signal at 590 nm increased by only 1/3. Although it cannot be said that the compound **29** does not react with the NTR at all, such a small change is difficult to detect. Visually, compound **29** showed blue fluorescence, but unlike compound **28**, it did not react with NTR to become green fluorescence, further demonstrating that compound **29** was not reacted with NTR effectively.

The emission spectra showed us the fluorescence intensity of compounds **28** and **29** and it preliminary proved that compound **28** can react effectively with NTR undergoes fluorescence changes and also showed that the emission intensity of

compound **29** varies little when treated with NTR during time. Resulting in the inability to determine whether compound **29** reacts with NTR by photophysical methods. Next, we used various other methods to confirm the fragmentation pathway of compound **28** and **29**.

2.4 ESI-LCMS Study

In order to further explore the change of compound **28** and **29** when treated with NTR in reductive stress condition, we also conducted a mass spectrometry to trace the reaction.

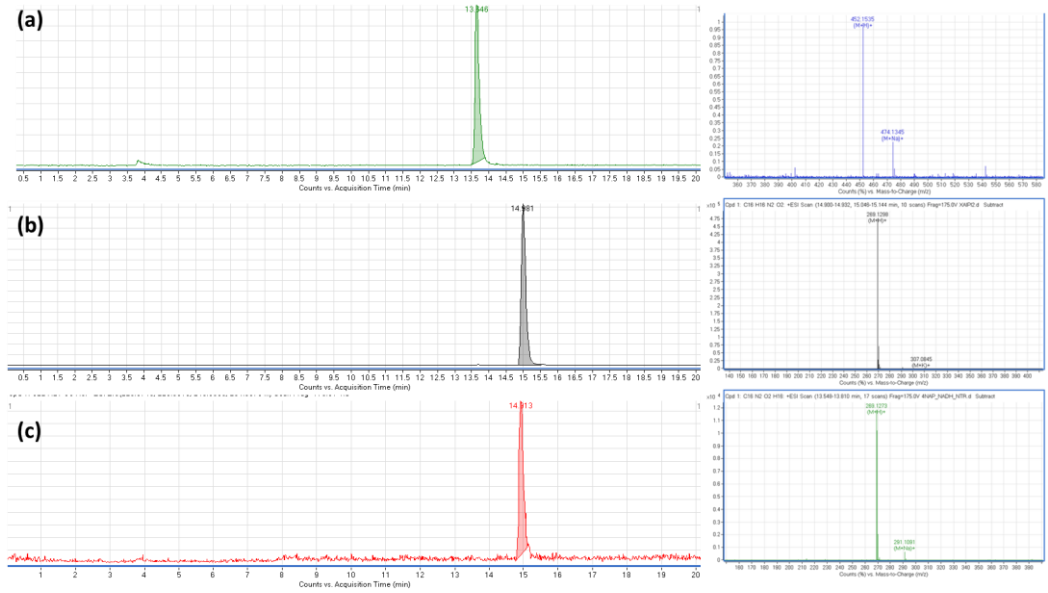

*Figure 2-15: Analytical LCMS traces of (a) compound **28**, (b) compound **45** and (c)compound **28** after treatment with NTR (1µg/mL) in the presence of NADH (500 µM); (0-100% acetonitrile over 20 min, 0.1% Formic Acid, λ = 254 nm); Calculated Mass of 1 $[M+H]^+$: 452.1565; Calculated Mass of 2 $[M+H]^+$: 269.1285*

As we can see from the figure 2-15, the peak in (a) represents the signal of **28** where the MS spectrum revealed peaks at m/z = 452.1535 and 474.1345 attributed to the $[M + H]^+$ and $[M + Na]^+$ ions of compound **28** respectively. The peak in (b) represents the signal of **45** where the MS spectrum revealed peaks at m/z = 269.13

and 307.08 attributed to the $[M + H]^+$ and $[M + K]^+$ ions of 50 respectively as reference. The peak in (c) was measured when compound **28** was treated with NTR and NADPH in PBS. Moreover, this peak revealed peaks at m/z = 269.13 and 291.10 which showed the $[M + H]^+$ and $[M + Na]^+$ ions of **45**. This result showed that when the compound **28** was added to the NTR, the signal of the original compound **28** disappeared and the signal of the compound **45** was detected. These three graphs fully illustrated that compound **28** can be quickly converted to its reference compound **45** when treated with NTR.

However, there was no fluorescence change when compound **29** was treated with NTR under the same condition while ESI-LCMS only gave rise to peaks at m/z = 452.15 and 474.13 attributed to the [M + H]+ and [M + Na]+ ions of the compound **29**, respectively.

In conclusion, with the detection of mass spectrometry, compound **28** was confirmed to be converted to compound **45** in the presence of NTR, indicating that compound **28** has a very high level of reactivity to oxygen sensitive NTR in the presence of NADPH to reduce its nitro group and goes through a chain break to form compound **45** and finally shift the fluorescence single from blue to green. On the other hand, there were no signal of compound **43** was found in the reaction of compound **29** with NTR. And since the intensity of emission spectrum was not changed. We infer that compound **29** does not react effectively with NTR.

2.5 Characteristic Detection of 28

2.5.1 Sensitivity Study

Considering the above results, we thought that substitution at the 4 -portion is the key element for this reaction, so we chose to concentrate our efforts on compound **28**. We also converted experiments to investigate the sensitivity of compound **28** to the enzyme by releasing the fluorophore in the presence of different concentrations of NTR ($0 – 5$ μg mL^{-1}).

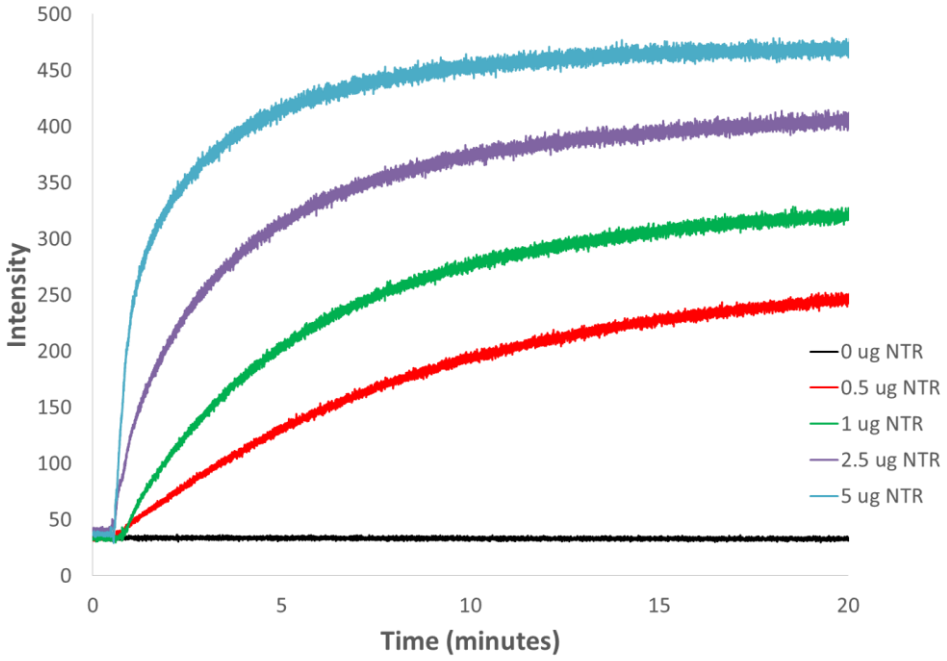

Figure 2-16: Plots of the change in emission intensity at 545 nm as a function of time after treatment with various concentrations of NTR in the presence of NADH (50 µM).

The same concentration of compound **28** was placed in 5 vials and different concentrations of NTR were added to each vials. Since we had determined that the reaction of compound **28** with NTR was fully capable of generating and formed compound **45**, we had recorded the emission intensity at 545 nm during the reaction, which corresponds exactly to the concentration of the compound **45**. And the higher the intensity represents the more formation of compound **45**. The shorter the time to reach a certain intensity, the faster the reaction rates.

From the figure 2-16 we can see that higher concentration of NTR can result in a faster increase in fluorescence intensity. As we increased the concentration of NTR the intensity goes higher and faster to reach the maximum value, which means more compound **28** had reacted with NTR when the concentration was increased and the more compound **28** was, the more it can help the reaction to proceed more quickly. When treated with 5 µg mL^{-1} of NTR, almost 90 % of compound **28** had transformed to compound **45** in 5 mins at 25 °C while it took almost 15 mins for the reaction to complete when the concentration of NTR was 0.5 µg mL^{-1}.

Moreover, the concentration of NTR from 0.5 µg mL^{-1} to 5 µg mL^{-1} gave a linear response whereby increasing the concentration of NTR gave rise to a rapid fluoresce modulation. Finally, in the absence of no response was observed demonstrating the stability of compound **28** under the mimicked biological conditions.

2.5.2 pH Study

The next experiment was to measure the reaction of compound **28** to NTR at different pH. As shown in the figure 2-17, we set different pH values of the environment (pH = 5 – 9) in different vials and inserted compound **28** and NTR with same concentration. The result indicated that compound **28** showed the highest activity between pH = 6 and 7, which demonstrated the applicability of compound **28** to a biological environment whereby it was shown to perform best at pH values consistent with those found in biological media.

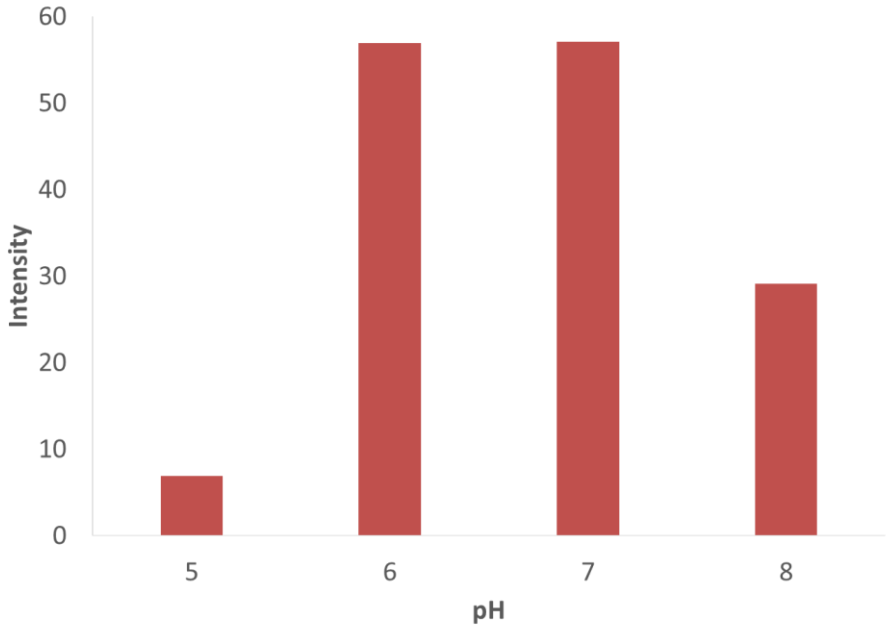

*Figure 2-17: Changes in the emission spectrum of compound **28** (10 µM) (λ_{ex} 345 nm) at various pH values*

2.5.3 Selectivity Study

Because of the diversity of substances in biological cells, our compound **28** was inevitable to be exposed to these biological interferents in cells. Therefore, the ability to effectively identify and eliminate the interference of these substances has become the primary problem. To this end we set an experiment to simulate the diversity of biological cells and we selected most of the representative substances (NaCl, $CaCl_2$, $MgCl_2$, glucose, H_2O_2, aspartic acid, lysine, serine, tyrosine and lysozyme) as interference items to detect the biological selectivity of the compound **28**. We added the same concentration of compound **28** in each substance, and we measured the emission intensity at the same wavelength after 20 mins.

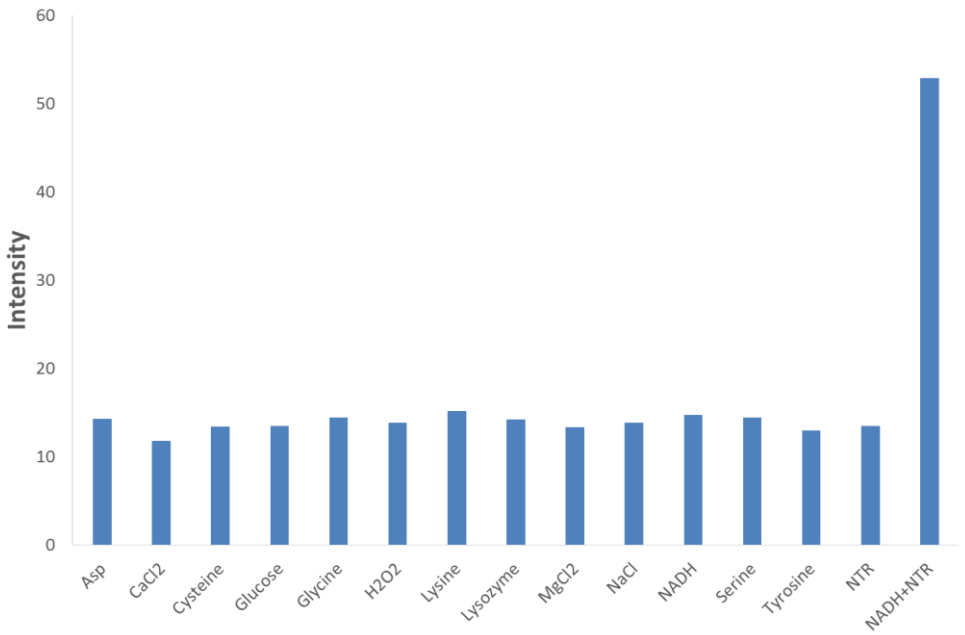

*Figure 2-18: Changes in the emission spectrum of compound **28** (10 μM) (λ_{ex} 345 nm) upon addition of various biological interferants.*

From the result of figure 2-18, compound **28** displayed a high level of both stability and selectivity towards NTR over all of the other species tested. Its emission intensity was almost three times more than in other substances. When compound **28** was in other substances inside, its material concentration is almost unchanged. In general, compound **28** exhibited a high stability and sensitivity in a simulated

biological tissue environment, moreover, it can find the target NTR very quickly under various interference and reduce the nitro group to amino group to release the fluorophore and finally shift the fluorescence.

2.6 Enzyme Study

2.6.1 Biological behaviour

In the above experiments we have discussed the spectral characteristics and the sensitivity of bioreduction of compound **28**, and the result was very positive. Our next test was to evaluate compound **28** as a biological probe for reductive stress in cells, to explore its ability to be internalised in target cells (These studies were conducted with the help of Dr. Sandra Bright carried out at TCD). Cellular environment was conducted in cervical cancer HeLa cells. We incubated live cells (0.5×10^5) with compound **28** (10 μM) at 37°C for 4 hrs (figure 2-19). Through the fluorescence confocal microscopy we obtained a clear result showing below. The compound **28** successfully attached to the cytoplasmic position within the cells, which emitted a strong blue fluorescence as an evidence of its presence in the cells. We also did the same experiment with its fluorophore group compound **45**. As a result, the compound **45** can also adhere to the cytoplasm of cells and emit a different but still strong fluorescence in the same environment. The rates of these compounds **28** and **45** get into the cells were also investigated by using flow cytometry in figure 2-20. The result indicated that both of them were shown to be rapidly taken up into cells and reaching their peak uptake within 15 mins and stay constant for a long while.

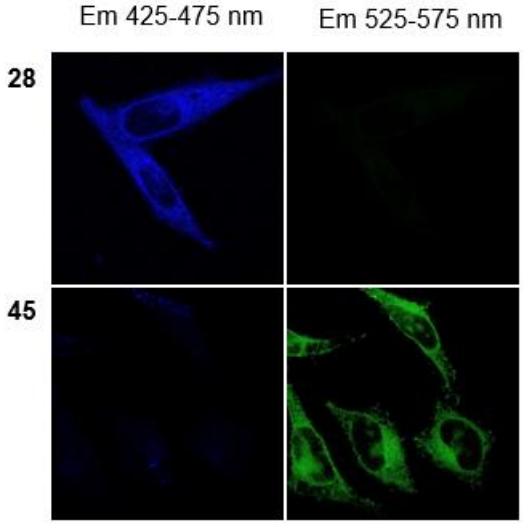

*Figure 2-19: Cellular localisation of compound **28** and **45** in HeLa cells at 37°C*

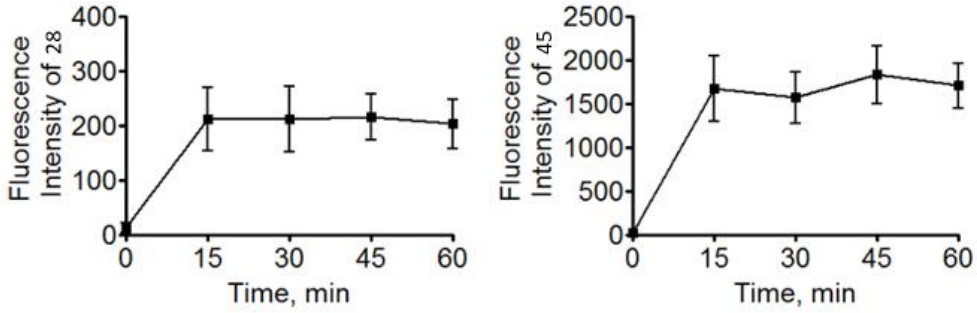

Figure 2-20: Cellular uptake determined by flow cytometry

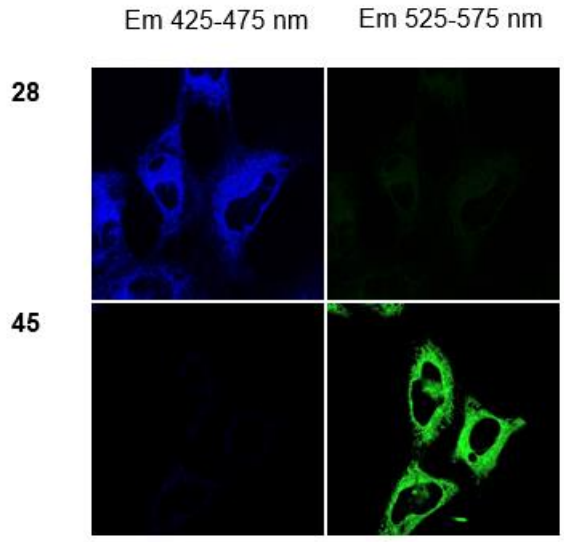

Figure 2-21: Cellular localisation at 4°C

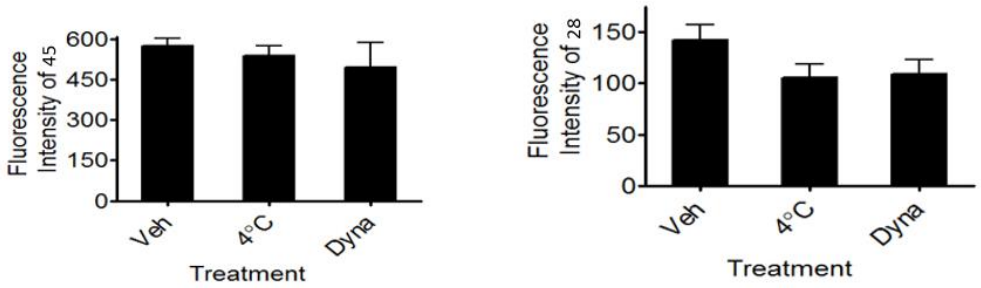

Figure 2-22: Passive diffusion and endocytosis determined by flow cytometry (Scale bar = 10 µm).

In order to explore the way the compound **28** enters the cells, we also carried out the following experiments. We injected compound **28** and its reference fluorophore compound **45** into HeLa cells at 4 °C to see if the cell fluorescence signal generation. Experiments showed that at such a low temperature we can still observe the fluorescence signal generated by compound **28** and **45** (Figure 2-21). The experiment also proved that the way compound **28** was getting into the cells

should be passive diffusion (Figure 2-22), since the diffusion which needs ATP, is inhibited at this low temperature. In agreement with this, we treated the cells with the general endocytosis inhibitor dynasore, and then put compound **28** and **45** into the cells, the result showed no effect on the uptake of compound **28** or **45**.

Compound	**IC_{50} value (μM)**
28	>75
29	6.5
45	45.6
43	35.3

*Table 2-1: Table summarising viability data of compounds **28**, **29**, **45** and **43** after treatment of HeLa cells for 24hrs (Scale bar = 10 μm).*

Cellular viability in the presence of **28**, **29** and **45**, **43** was also measured using an AlamarBlue assay (table 2-1). The result showed that the IC_{50} value of compound **28** could not be measured and was observed without any cytotoxicity. And similarly, compound **45** had observed a modest IC_{50} value of **29** μM when cells were treated for 24 hrs. This showed that compound **28** showing no observed toxicity to the cells and the same as the released compound **45**. While what interesting us was that compound **29** and **43** were shown to have increased toxicity with IC_{50} values of 7 μM and 35 μM respectively. Compound **29** was shown that it is not suitable for being developed as a probe for detecting hypoxia in cells, and the reason that its IC_{50} value is so low could be their structural similarities to the known anti-proliferative agent amonafide.

2.6.2 Ability of reduction in cells

With the biological behaviour of these compounds characterised we next wished to evaluate their abilities to monitor reductive stress in cells. Before the cell experiment we had some adjustments to the experiment environment. We treated HeLa cells with NTR (1 µg mL^{-1}) and its co-factor NADPH (0.5 M) before addition of compound **28** or **29** (10 µM) in order to mimic reductive stress on the cell population.

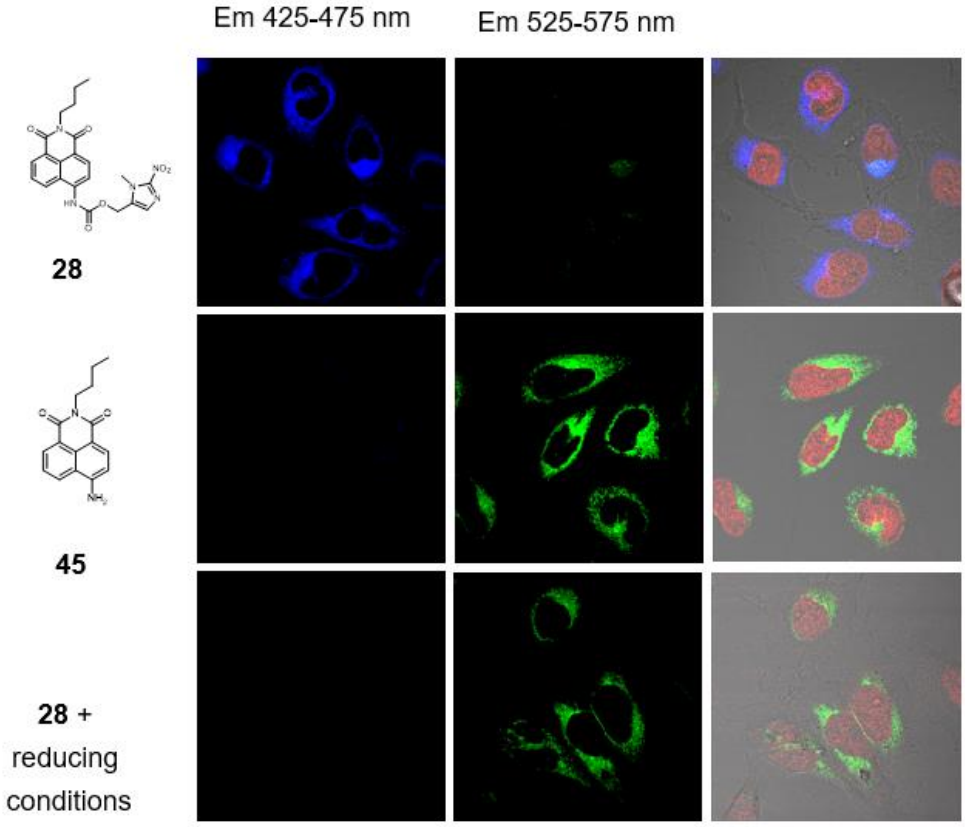

*Figure 2-23: Confocal laser scanning microscopy images of HeLa cells after treatment with compound **28**, **45** and **28** (10µM) under reducing conditions. Nuclear imaging with red nuclear stain, DRAQ5.*

As shown in Figure 2-23 Hela Cells treated with compound 28 (10 µM) under non-reducing conditions clearly exhibit blue fluorescence between 425 -475 nm while

under similar conditions cells treated with compound 45 (10 µM) show intense green fluorescence between 525 – 575 nm.

Upon subjecting Hela cells containing compound 28 (10 µM) to reducing conditions a rapid and obvious fluorescence change is observed whereby the blue fluorescence is quenched and the green fluorescence between 525 – 575 nm is switched on.

This result suggests the reduction of compound **28** to release compound **45** under reductive stress condition in cells was successful. The emission spectra of the compounds recorded within cells of figure 2-24 demonstrated that the λ_{max} of compound **28** was 465 nm (range 410 to 595 nm), whilst the λ_{max} of compound **45** was 512 nm (range from 456 to 661 nm). Incubation of compound **28** under reducing conditions in HeLa cells revealed a cellular λ_{max} of 512 nm (range 428 to 659 nm), again suggesting successful reduction of compound **28** under these cell culture conditions.

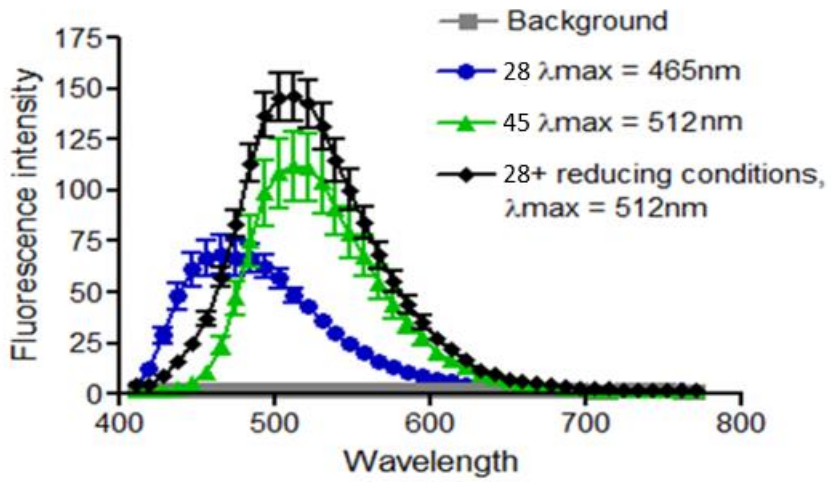

Figure 2-24: Emission spectra of treated cells measured using confocal microscopy.

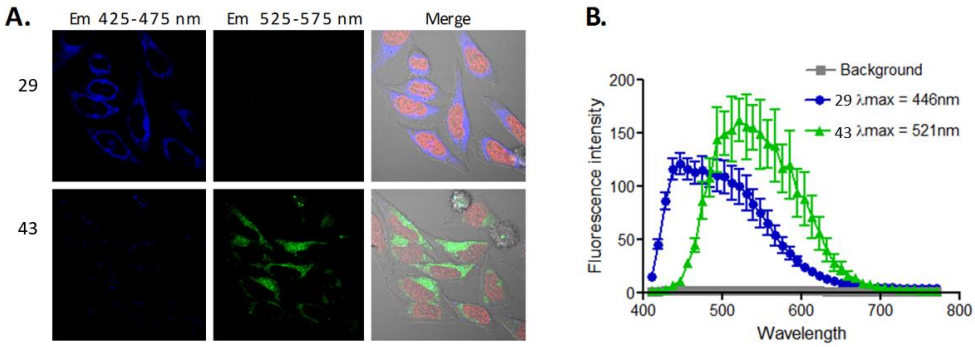

*Figure 2-25: Uptake of compound **29** and **43** (10 µM) by HeLa cells measured using confocal laser scanning microscopy (A) cellular localisation of compound **29** and **43** at 37°C, (B) emission spectra of treated cells measured using confocal microscopy.*

While same experiment conducted on compound **29**, which we injected **29** (10 µM) into HeLa cells and observed the fluorescence change. The emission spectra for compound **29** and reference compound **43** showed separate λ_{max} value of 446 nm and 521 nm respectively (figure 2-25 B). When compound **29** was injected in HeLa cells treated with NTR and NADPH as co effector, there was no fluorescence change we can receive from the cell, in other words, the blue fluorescence did not shift to green. And the emission spectra used to trace the experiment did not receive the any signal that compound **29** can emit the signal of λ_{max} value of 521 nm (range from 472 nm to 630 nm). This supports the results of the enzymatic spectroscopic studies described above which showed that treatment of **29** with NTR did not release **43**.

2.7 Conclusions

In summary, we have reported the synthesis of two 2-nitroimidazole-1,8-naphthalimide conjugates **28** and **29**. Of these two compounds, compound **28** showed high sensitivity and selectivity to NTR in cells and through a reduction - fragmentation mechanism, which showed a fluorescence response clearly visible

to the naked eye. However, compound **29**, although with similar structural features, did not show any reaction to NTR in reductive stress environment. Due to its high cytotoxicity, compound **29** does not seem to be suitable for NTR detection in hypoxia area in cells. In addition, we have demonstrated the applicability of compound **28** to cellular detection of reductive stress using both confocal microscopy and flow cytometry where compound **28** allows facile discrimination of cells under normal conditions and those under reductive stress. Considering that nitroreductase is widely studied in bacteria, as well as in yeast, trypanosomes and hypoxic tumors and other systems [55], the use of ratiometric probes for NTR such as compound **28** will provide new perspectives on the role of reductive stress in various diseases.

Chapter 3 : Naphthalimide fluorescent sensors for nitroreductase: Varying the nitroaromatic

3.1 Introduction

According to the previous chapter, we had successfully synthesized the compound **28** which can react well with the NTR enzyme. We used a number of methods to demonstrate that compound **28** was indeed capable of reacting with NTR, such as photophysical experiments, mass spectrometry, and fluorescence confocal microscopy. Compound **28** not only showed good selectivity to NTR but also the sensitivity increased with increasing concentration. It underwent a reduction and fragmentation and finally released the fluorophore. In contrast, compound **29** cannot react with NTR in the same environment. Therefore, considering the difference between compound **28** and compound **29** we assumed that the fluorescence sensor which can have a reaction with NTR in the case of the substitution on 4 position (Figure 3-1). With this assumption, we focused on compound **28** and attempted to increase the sensitivity of compound **28** by altering the substituents attached to the fluorophore and strived to synthesize more efficient hypoxic environment sensors.

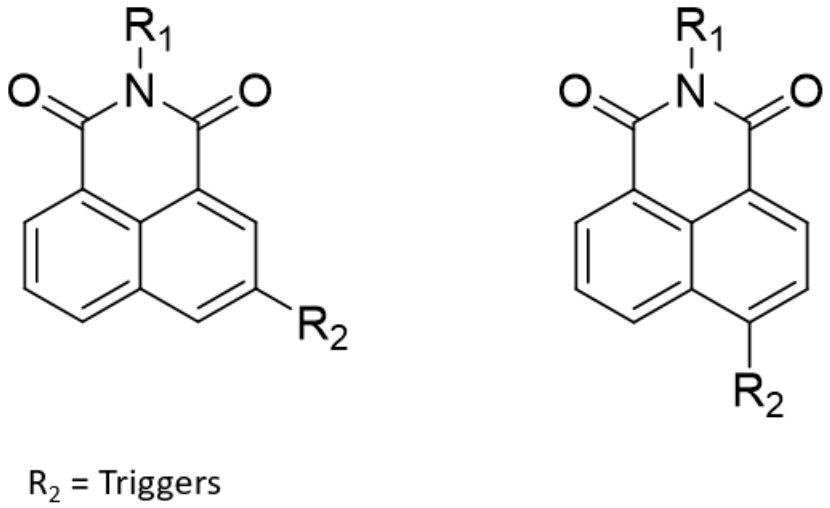

Figure 3-1: Substitution on 3 position of naphthalimide (left) and 4 position of naphthalimide (right)

On this basis, we decided to carry out some modifications to compound **28** in order to expect more efficient compounds. We intended changing the nitroaromatic triggers of compound **28**, taking advantage of other aromatic moieties such as nitrofuran, nitrobenzene and nitrothiophene shown in Figure 3-2. These functional groups have been shown to be readily oxidized by NTR in hypoxic environments. In the research of fluorescence sensors for NTR, nitrofuran, nitrobenzene and nitrothiophene are frequently used as NTR recognition groups. Such as in 2013 [41], Zhao and Co-workers published a fluorescence sensor based on resorufin and 5-nitrofuran to form the compound **11**, which reacted with NTR and finally release the fluorophore and shift the fluorescence single from colorless to pink. Same year in May, they published another fluorescence sensor based on nitrothiophene and resorufin as compound **12** [56]. Similar result showed that nitrothiophene can work as NTR recognition group. The last example is a nitrobenzene based fluorescence sensor for the detection of NTR. The nitrobenzene was reduced by NTR in the presence of NADHP and went through a 1,6-rearrangement and release a highly fluorescent dye [57]. With all these examples we are confident that nitrofuran, nitrobenzene, and nitrothiophene are fully capable of acting as NTR recognition groups. We expect the new compounds with these nitro substitutes not only to accomplish their work by reacting with NTR to alter the fluorescence signal but also have a higher activity.

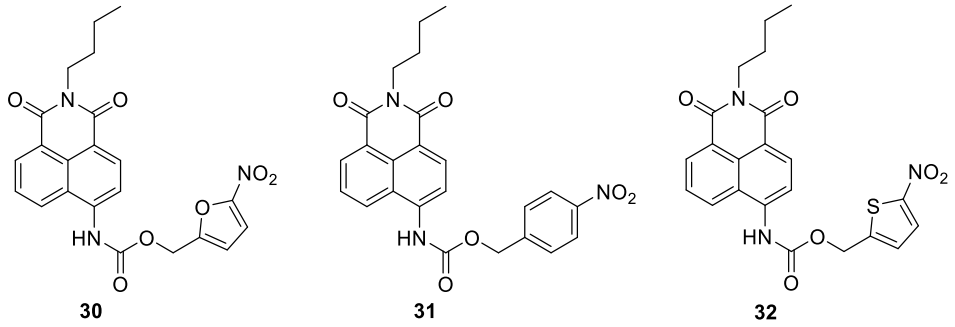

Figure 3-2: Target compounds for sensitivity improvement.

The overall aim of work presented in this chapter is to discuss the development and the improvement of compound **28**. Firstly, we will discuss the improvement of sensitivity for compound **28**, and some synthesis procedure will be mentioned.

Following by a comparison of the photophysical properties of the resulting compound and its response to the enzyme NTR. Then we will discuss the improvement of the biological conjugation of the compound **28**. As usual, we will mention the synthesis procedure of these derivatives. Finally, the reaction of the resulting compound to NTR will be mentioned.

3.2 Synthesis

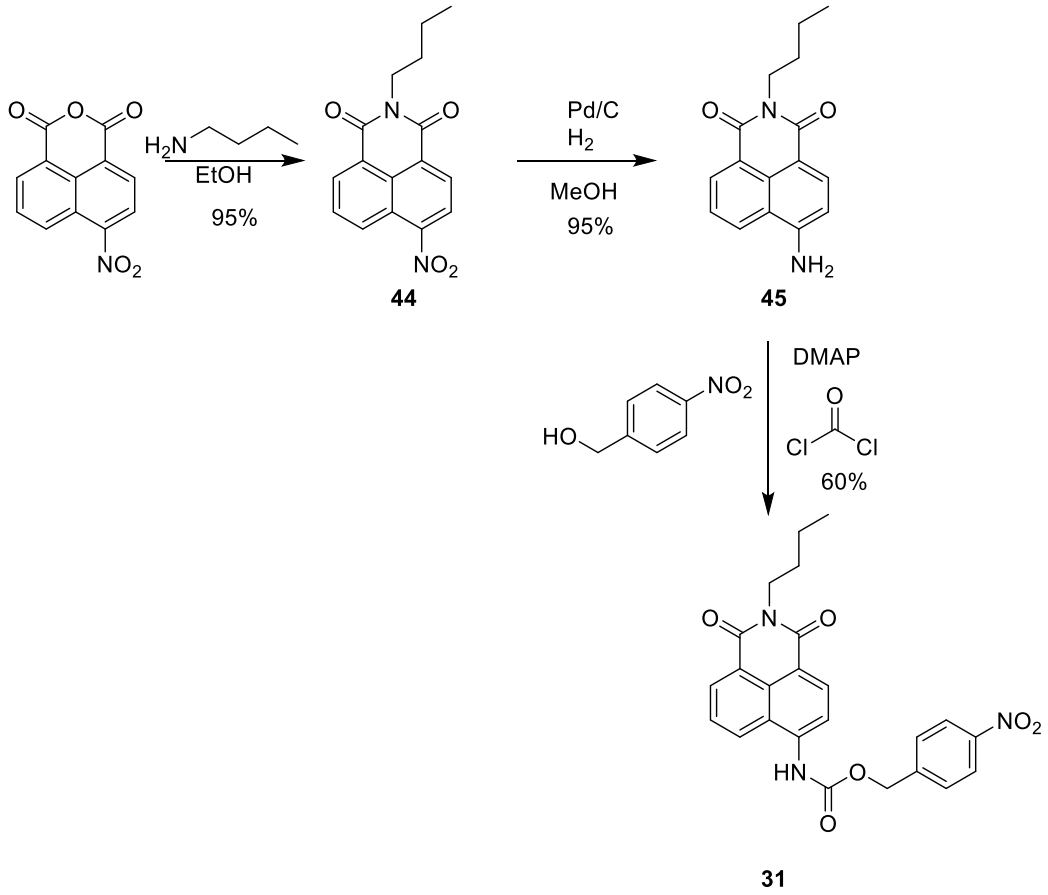

*Scheme 3-1: The synthesis of compound **31***

The synthesis of compound **31** showed in Scheme 3-1 was similar as the one with compound **28**, the only different was that we switched 4-nitrobenzene alcohol instead of compound **36**. The synthetic procedure had been mentioned in the

previous chapter, and the detailed synthesis process was outlined in Chapter 6, so it was not described here.

Compound **31** was characterised by ^{1}H NMR, melting point analysis, mass spectrometry, ^{13}C NMR and IR spectroscopy. The ^{1}H NMR spectrum is shown in Figure 3-3. Assignment of the peaks was achieved by H-H COSY and C-H COSY analysis.

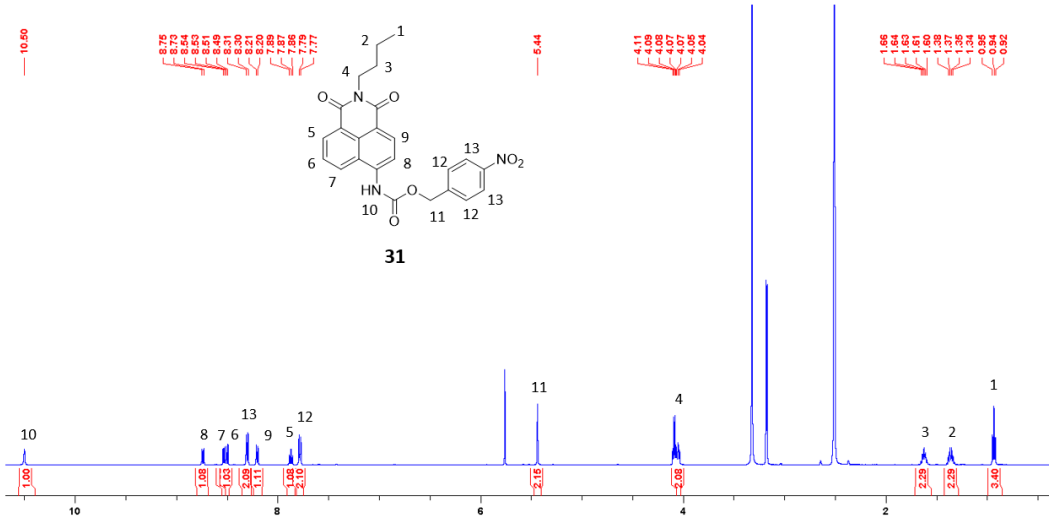

*Figure 3-3: The ^{1}H NMR spectrum of compound **31** (500 MHz, DMSO-d_6)*

In the ^{1}H NMR spectrum of compound **31 (**Figure 3-3**)**, we can clearly see 13 peaks which represent 13 different kinds of H in compound **31**. In general, peaks between 7 ppm to 9 ppm stand for the aromatic H while peaks between 0 ppm to 5 ppm indicated the aliphatic H. compound **31** has 7 different aromatic H and 5 different aliphatic H which was perfectly match the ^{1}H NMR spectrum.

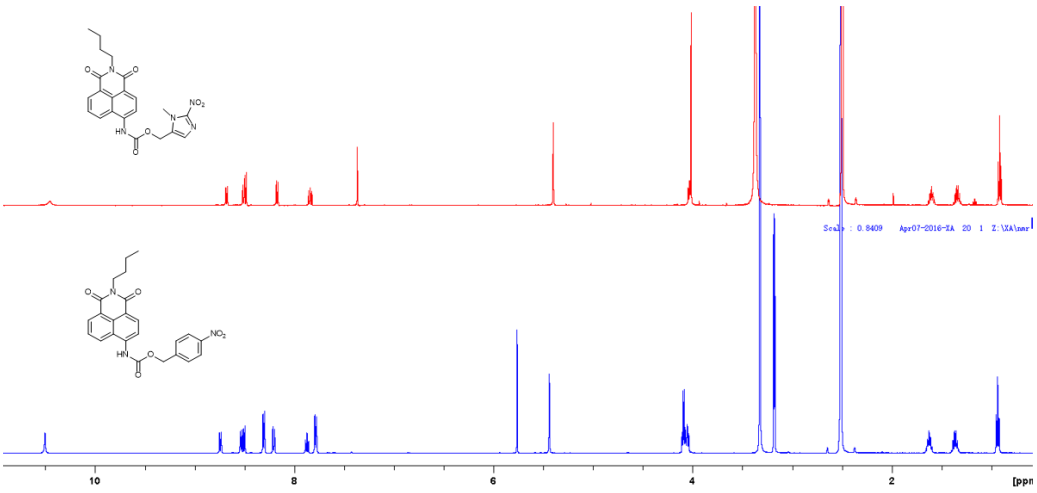

*Figure 3-4: The comparation of compound **28** and compound **31***

If we compared this spectrum of compound **31** with the spectrum of compound **28** in Figure 3-4 we can see the chemical shift of butyl group of compound **31** was same as the chemical shift of compound **28**. Even the chemical shifts of the CH_2 groups on the side of the two carbamates of the compounds were very similar. In the aromatic region, we can clearly see 5 different H signals integrated 1 which represent the H on the naphthalimide and two signals integrated to 2 which indicated the Hs on the nitrobenzene because the hydrogen on the benzene ring is symmetrical. Peak at 10.5 ppm integrated 1 indicated the hydrogen of NH because we did not see signal at this chemical shift in HSQC, which means there was no hydrogen connect to carbon and since there was a signal on ^{1}H NMR spectrum we can ensure that the chemical shift at 10.5 ppm was NH peak. Peak at 5.76 ppm was the solvent peak of DCM and signal at 3.17 ppm was the methanol peak. At this point, all of the signals corresponded to compound **31** and we did have reason to believe compound **31** had not been made successfully.

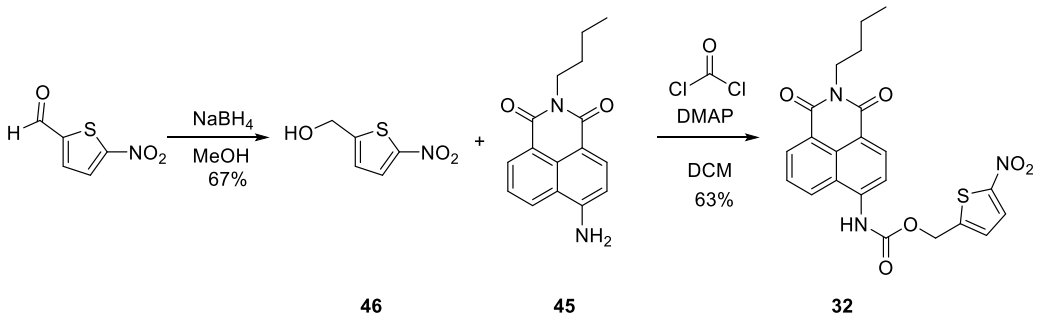

*Scheme 3-2: The synthesis of compound **32***

For the synthesis of compound **32** in Scheme 3-2, we used the same procedure as compound **28** but different starting material. In the synthesis of compound **32**, compound **46** was reduced from its aldehyde form 5-nitro-2-thiophenecarboxaldehyde using sodium borohydride. The ^{1}H NMR spectrum is shown below. With those starting materials in hand, compound **32** was synthesised as previously described.

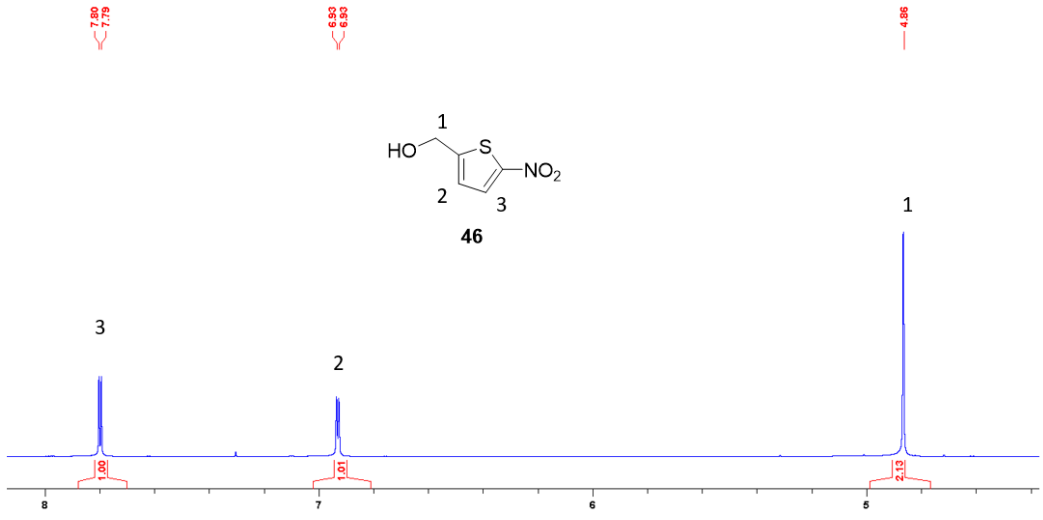

*Figure 3-5: The ^{1}H NMR spectrum of compound **46** (500 MHz, $CDCl_3$)*

From the spectrum shown in Figure 3-5, we can see there are three relevant peaks which indicated three different hydrogens of compound **46**. Peak at 4.85 ppm integrated to 2 represents H1 and peak at 7.93 ppm stands for H3 as it was more

close to electron withdrawing group which make the H more de-shielded. Peak at 6.91 ppm stands for the H2.

Compound **32** was characterised by ^{1}H NMR, melting point analysis, mass spectrometry, ^{13}C NMR and IR spectroscopy. The ^{1}H NMR spectrum was shown in Figure 3-6. Assignment of the peaks was achieved by H-H COSY and C-H COSY analysis.

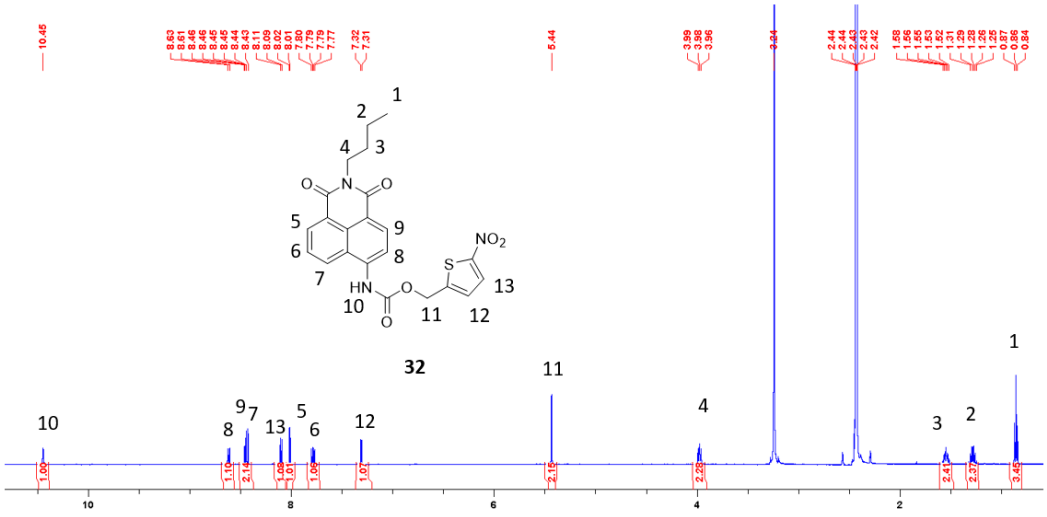

*Figure 3-6: The ^{1}H NMR spectrum of **32** (500 MHz, DMSO-d_6)*

From the ^{1}H NMR spectrum in Figure 3-6, peaks between 7 ppm to 9 ppm were signals of aromatic H on naphthalimide and thiofuran groups. While peak at 5.44 ppm was a singlet and integrated to 2 which represented the signal of H11. H1, H2, H3 and H4 represented the butyl group of compound **32**. The peak with chemical shift at 10.5 ppm was very similar as compound **31**, which was proved to be the single NH. In this situation, each peak stand for one single of compound **32**, therefore, we can ensure that compound **32** has been made successfully.

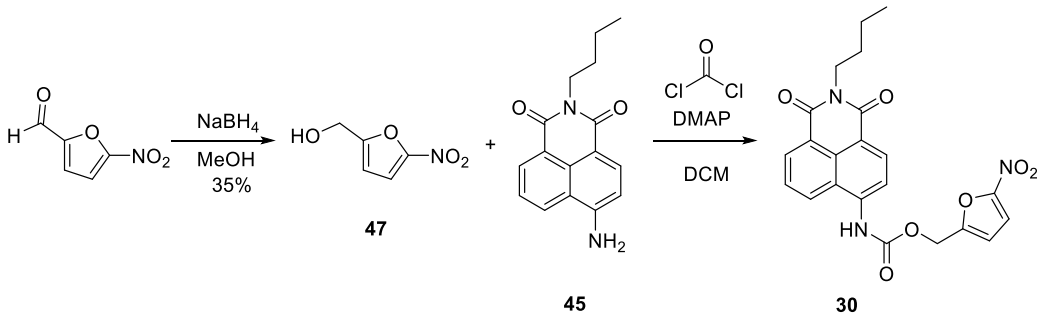

*Scheme 3-3: The idea path for the synthesis of compound **30***

The synthesis of compound **30** was just the same as compound **32** in Scheme 3-3, while the synthesis of the nitroaromatic trigger was successful by reducing the 5-nitrofuran-2-carbaldehyde to (5-nitrofuran-2-yl) methanol **47** with sodium borohydride in MeOH. The ^{1}H NMR is shown below in Figure 3-7.

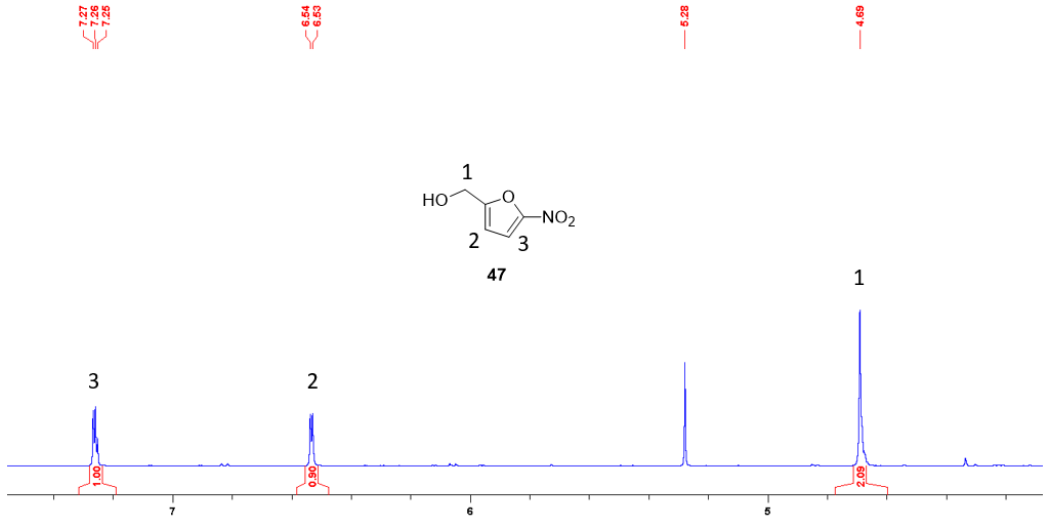

*Figure 3-7: The ^{1}H NMR spectrum of **47** (500 MHz, $CDCl_3$)*

The ^{1}H NMR spectrum was shown in Figure 3-7, compound **47** was very similar to compound **46** as it had three signals. Peak at 4.69 ppm integrated to 2 stands for H1 and peak at 7.26 ppm integrated 1 stands for H3 as it was more close to nitro group. Peak at 6.53 ppm stands for H2 and peak at 5.28 ppm was solvent DCM.

When we tried to combine the fluorophore with (5-nitrofuran-2-yl) methanol compound **47** through a carbamate linker. The compound **30** exhibited its high degree of instability and converted to its starting material again according to the

^{1}H NMR spectrum in Figure 3-8, there was no single at 10.5 ppm which means there was no NH peak formed and the Mass spec did not find the peak for compound **30**. Changed the experimental procedure by reacting the compound **47** with phosgene first and then the fluorophore was added. The result showed that it was still not working for compound **30**. Taken into account its instability, compound **30** would not be used as fluorescence sensor for NTR.

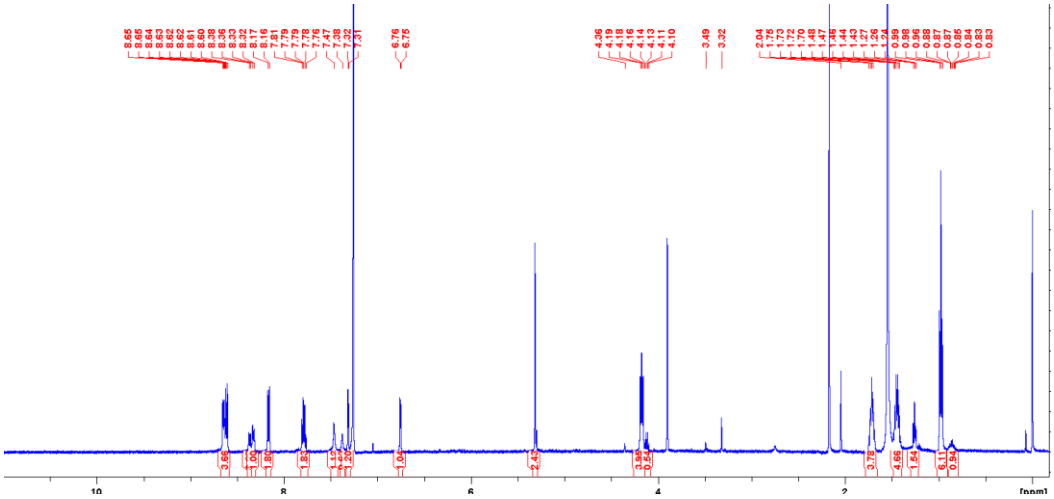

Figure 3-8: The ^{1}H NMR spectrum of the crude product after the reaction of Scheme 3-3 (500 MHz, $CDCl_3$)

Since compound **30** could not be made, our next wish was to compare compound **31** and **32** with compound **28** and **29** to find out the most sensitive probe to NTR.

3.3 Preliminary test for NTR

In this section, we investigated the spectral properties of **31** and **32** when placed under reductive stress conditions by treatment with NTR in the presence of NADH. And by comparing with the emission spectrums of those compounds, we wish to find out the most sensitive probe for NTR.

The emission spectrums were measured in PBS (pH 7.4, 10 Mm) with 0.5% DMSO as co-solvent in the presence of NADPH (50 μM, as a cofactor of NTR) at 25 °C.

We treated compound **32** with 0.5 µg NTR in the PBS and recorded the fluorescence change every 2 mins, herein we can see an emission spectrum (Figure 3-9) with intensity change over time. The emission maximum at 475 nm was slightly decreased during the time while the emission at 550 nm was increased. The experiment showed that compound **32** does react with NTR to some extent, but the intensity change was very small to observe. The fluorescence change of compound **32** was also very small, which was not easily visible to the naked eye.

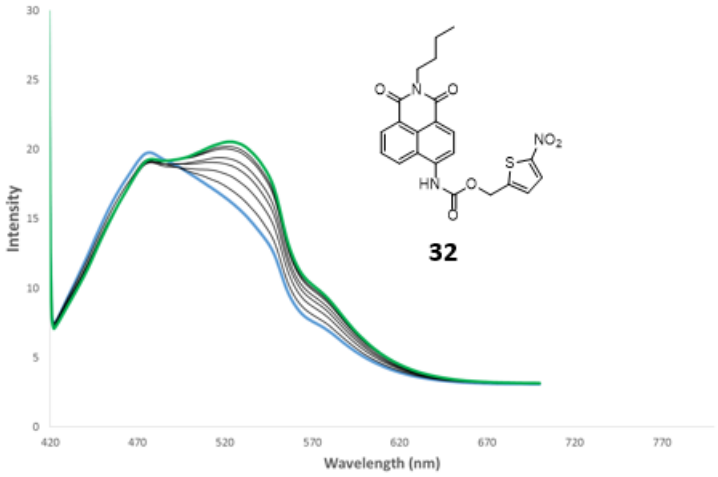

*Figure 3-9: Changes in the emission spectrum of **32** (10 µM) at various time points (0 - 25 mins) after addition of NTR (1 µg mL^{-1}).*

The same experiment was conducted with compound **31**, and we treated compound **31** (10 µM) with NTR (1 µg mL^{-1}) in the presence of NADH. The fluorescence intensity change was shown below in Figure 3-10. The emission maximum at 476 nm was seen to decrease while the emission at 550 nm was again increased. The emission intensity change at 476 nm showed that compound **31** does react with NTR but the magnitude of the change was very small. From the spectrum we knew that the intensity at 476 nm had a 3-fold decrease and there was also a 2-fold increase of intensity at 550 nm, which means that compound **31** was transferred to its fluorophore under the reaction of NTR.

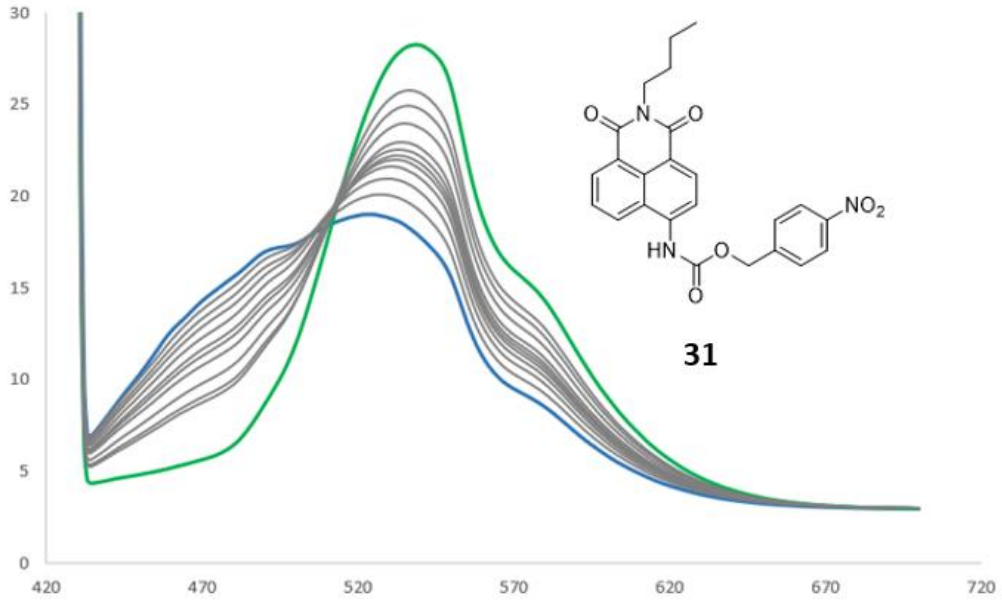

*Figure 3-10: Changes in the emission spectrum of **31** (10 µM) at various time points (0 - 25 mins) after addition of NTR (1 µg mL^{-1}).*

After having all the emission intensity change experiments, we compared all the emission spectrums together and assessed their sensitivity to NTR. Compound **28** and **29** was the first generation compounds and compound **32** and **31** was modified based on compound **28**.

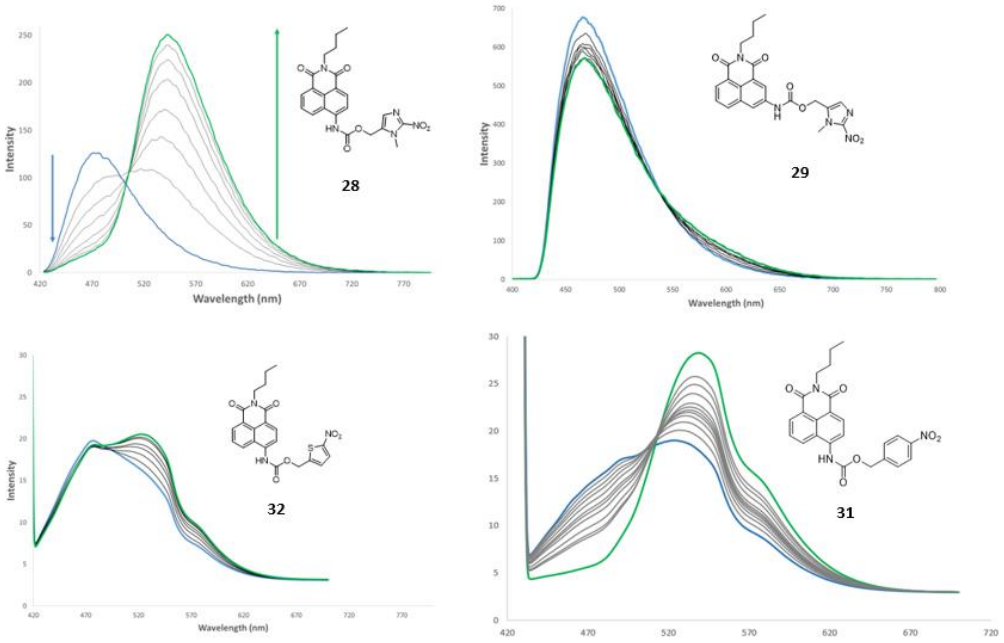

*Figure 3-11: Changes in the emission spectrum of **28, 29, 32** and **31** (10 μM) at various time points after addition NTR.*

In the comparison of Figure 3-11, we can clearly see those 4 compounds with their fluorescence change over time. Compound **29** has very little change at 460 nm and still very little change at 590 nm and after the MS experiment, we can indicate that compound **29** was not suitable as a substrate for NTR. The spectrum of compound **32** did not show any intensity change at 475 nm but there was a 30% increase in intensity at 550 nm. The situation of **31** was better than compound **32** while it had a 3-fold decrease signal at 476 nm and 2-fold intensity increase at 550 nm. Since compound **32** showed more or fewer changes in the response to NTR, compounds **32** were believed to be able to react with NTR to alter the fluorescence, but due to their relatively low sensitivity to NTR, a particularly high concentration of those compounds were required to show a significant fluorescence change. Compound **31** had a great response when reacted with NTR compared with compound **32** and **29**. However, the value of the intensity was quite low compared to the value of compound **28**, therefore, we believe compound **31** would have an affection with NTR only in a very high concentration environment. Among them, compound **28** showed the highest sensitivity to NTR as there was a 5 fold decrease of signal at 475 nm and an 8 fold increase of signal at 550 nm than before which gave a very

clear fluorescence change from blue to green. More importantly, in the reaction of compound **28** with NTR, the concentration of NTR was 0.5 μg mL^{-1}, which was lower than the reaction concentration of the other various test compounds (1 μg mL^{-1}), meaning that compound **28** requires only a smaller concentration to give higher reaction intensity.

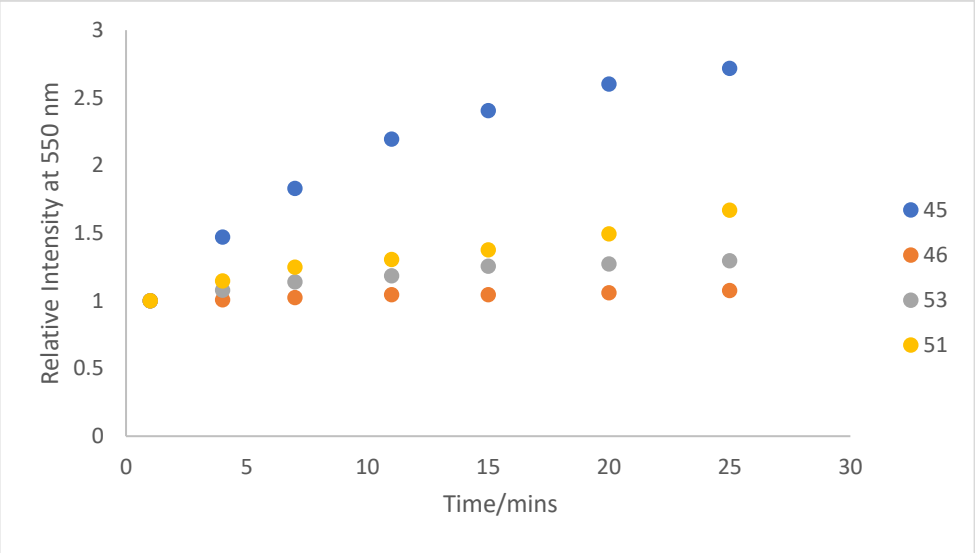

Figure 3-12: Relative Intensity change at 550 nm overtime for these 4 compounds

In order to make the comparison more clear, we took the intensity at 550 nm for all 4 compounds at different time and compared the trend of the intensity which showed in Figure 3-12. As we can see, compound **29** was almost a parallel line which means the intensity at 550 nm had nearly no change. The change of compound **32** was also very small while compound **31** had a relative higher change than compound **31** and compound **29**. Finally compound **28** showed the most sensitive change among these 4 compounds. This result also matched the observation above which compound **28** had the best activity with NTR.

3.4 Conclusion

Of all the tested compounds, compound **28** showed the highest chemical activity and reached the highest sensitivity with minimal concentration. We were convinced of the advantages of nitroimidazole as an NTR identification group and

compound **28** was studied as a major NTR probe. On the other hand, compound **31** showed the second best activity to NTR compared with compound **29** and compound **32**, the emission spectrum of compound **31** had great change when treated with NTR and compound **31** had transferred to its fluorophore during the change. However, if we compared the emission spectrum of compound **31** with the emission spectrum of compound **28** we can see a huge difference between the intensity values of each spectrum. Compound 45 had a 5-fold decrease of the signal at 475 nm while compound **31** had only 3-fold decrease of single at 476 nm, similarly, there was an 8-fold increase of signal at 550 nm for compound **28** when reacted with NTR compared with a 2-fold increase of single at 550 nm of compound **31**. This result showed that compound **28** had higher sensitivity for NTR than compound **31**.

Since compound **31** and **32** did not show very high sensitivity to NTR, we decided not to proceed with further study of them. Compound **28** still showed the strongest activity and was our main research focus. Next, we intended to make some structural modifications to compound **28**, without affecting its ability to recognise NTR while simultaneously enabling its conjugation to molecules of interest.

Chapter 4 : Naphthalimide fluorescent sensors for nitroreductase: A toolkit for bioconjugation

4.1 Introduction

In the former chapters, we knew that compound **28** had the highest sensitivity to NTR mediated reduction. The difference between compound **28** and other compounds under study was thought to be depended on the substitution pattern of the naphthalimide (substitution at the 4 position was found to be optimal) and the nitroaromatic trigger (2-nitroimidazole was found to be optimal). In this case, we turned our focus on the N-terminus of the compound **28**. We intended to modify the structure of compound **28** to enable bioconjugation of the NTR to important biomolecules or to attain selective uptake in subcellular organelles. The *N*-terminal consisting of n-butyl group could be changed to other substituents to enhance the ability of compound **28** to either undergo bioconjugation or to allow specific uptake (Figure 4-1). Tumor cells have a series of biological features, such as unlimited potential for replication, anti-growth inhibitory signal, anti-apoptotic, continued to produce proliferative signals, induce angiogenesis and invasion and metastasis, etc. [4]. Since mitochondria can regulate apoptosis of cells, most of mitochondria of tumor cells show abnormalities, such as poor permeability of the outer membrane, cannot be timely release of apoptotic signals, mitochondria also become the target of cancer treatment [58]. Mitochondria play an important role in cells: on the one hand, mitochondria are cells' energy factories that decompose carbohydrates to produce ATP, which provides most of the energy required for metabolism and movement of living organisms [59]; on the other hand, mitochondria participate in the process of apoptosis [60]. The drug targeting of mitochondria mainly includes lipophilic cations and mitochondrial protein import [61]. The main mitochondrial targeting ligands are triphenylphosphine (TPP) and its derivatives such as octadecyl triphenylphosphine (STPP), as well as gold ions and nitrogen heterocyclic complexes (NHCs), KLA polypeptide (KLAKLAK), αvβ3 family of polypeptides [62] [63]. Mitochondrial is important in hypoxic cancer research, as most of the reduced products form and accumulate in mitochondria [64]. If the compound can easily enter the mitochondria, then the

compound can more effectively react with the reducing substance such as nitroreductase. In order to further enhance the ability of compound **28** to target the mitochondrial, we envisioned the introduction of mitochondrial targeting of triphenylphosphine to make the probe more accurately reach its target.

In this section, we will discuss the synthesis of modified compounds based on compound **28** and the characterisation of those compounds to identify that all compounds needed were made successfully.

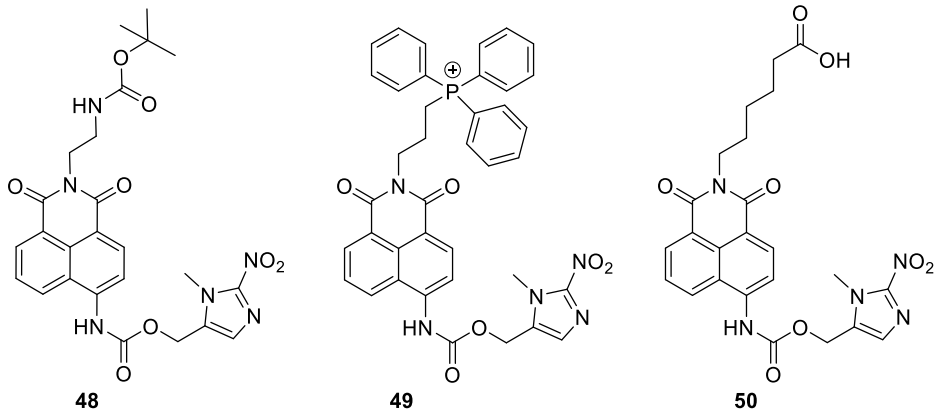

*Figure 4-1: Target compounds for bioconjugation based on compound **28***

4.2 Synthesis

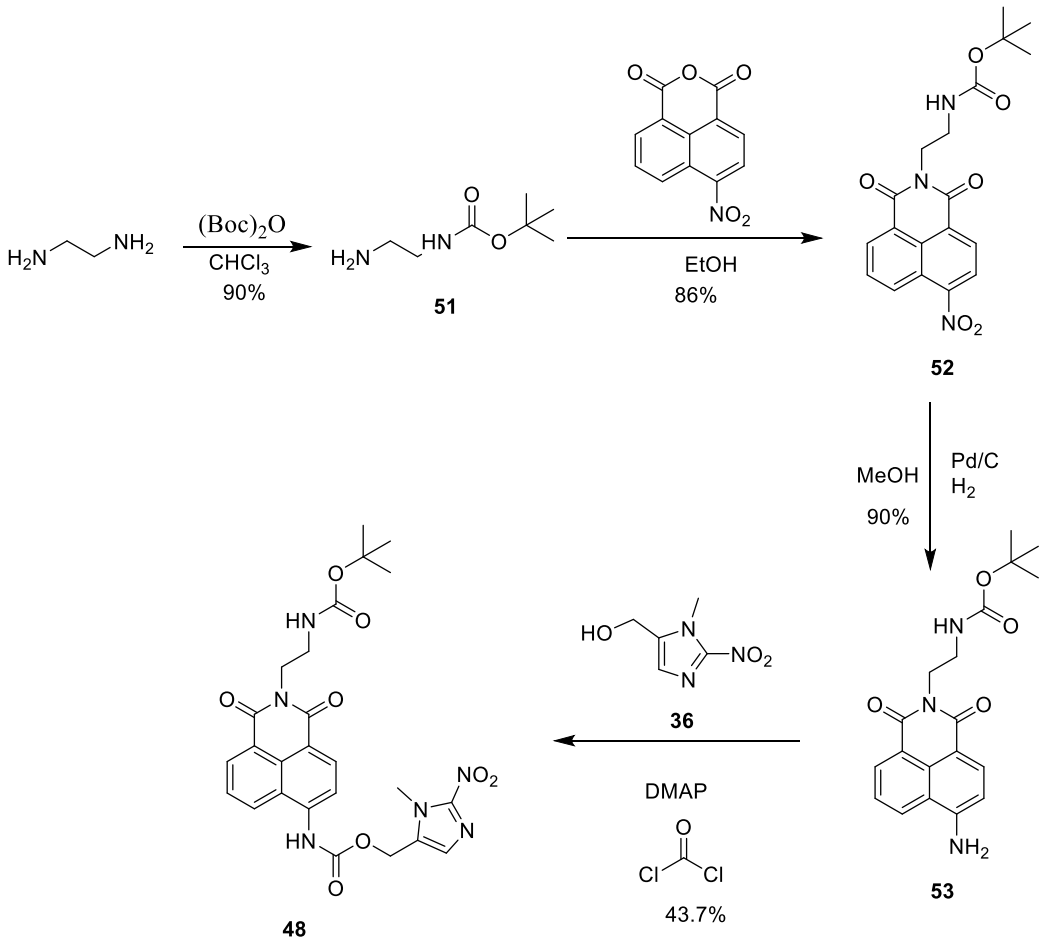

*Scheme 4-1: The synthesis of compound **48***

The synthesis of compound **48** shown in Scheme 4-1 was achieved using an intermediate in the synthetic pathway of 2-nitro-imidazole. The synthesis of compound **51** was achieved using ethyl diamine mono-protected using di-tert-butyl dicarbonate in chloroform to yield a colourless liquid in 90 % yield. Compound **51** was characterised by ^{1}H NMR, melting point analysis, mass spectrometry, ^{13}C NMR and IR spectroscopy. Assignment of the peaks was achieved by H-H COSY and C-H COSY analysis.

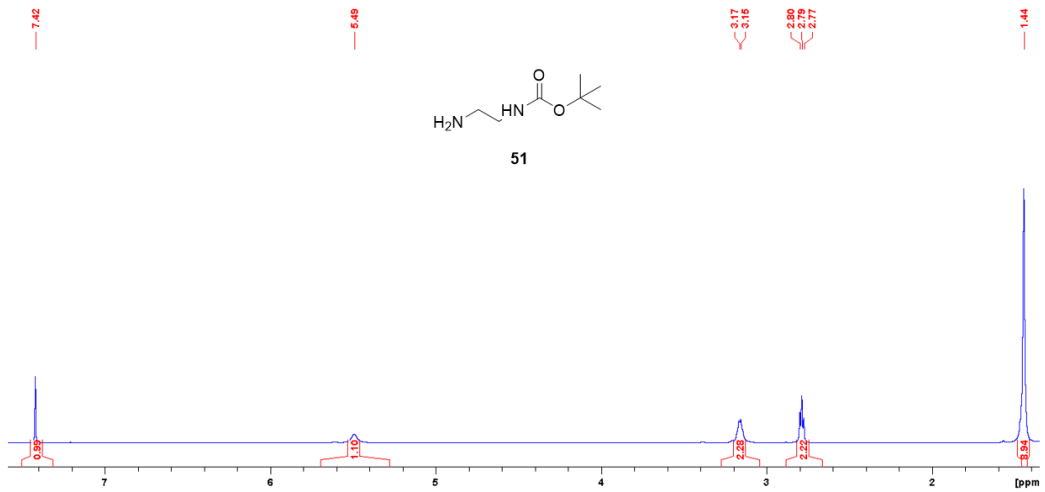

*Figure 4-2: The ^{1}H NMR spectrum of compound **51** (500 MHz, DMSO-d_6)*

From the spectrum in Figure 4-2, we can see 5 signals which represent 5 different H of compound **51**. Peak at 1.44 integrated 9 represents three CH_3 groups because they were in the same chemical environment. And peaks at 2.79 ppm and 3.15 ppm stand for 2 aliphatic H and since they all integrated 2, therefore, they represent the two CH_2 groups of compound **51**. Peak at 7.42 ppm stands for NH in the middle because it was more close to ester group which is an electron withdrawing group, so it will shift the NH to down field and finally, peak at 5.49 ppm stands for the other NH group.

The remaining scheme followed the same strategy as compound **28**, reacting with 4-nitro-1,8-naphthalic anhydride and reducing the nitro group with H_2 and Pd/C to form the fluorophore of compound **53**. Finally, compound **53** was reacting with compound **36** as previously described to form the final product compound **48**.

Compound **48** was characterised by ^{1}H NMR, melting point analysis, mass spectrometry, ^{13}C NMR and IR spectroscopy. Assignment of the peaks was achieved by H-H COSY and C-H COSY analysis. Successful formation of this trigger was also evident from accurate mass spectrometry.

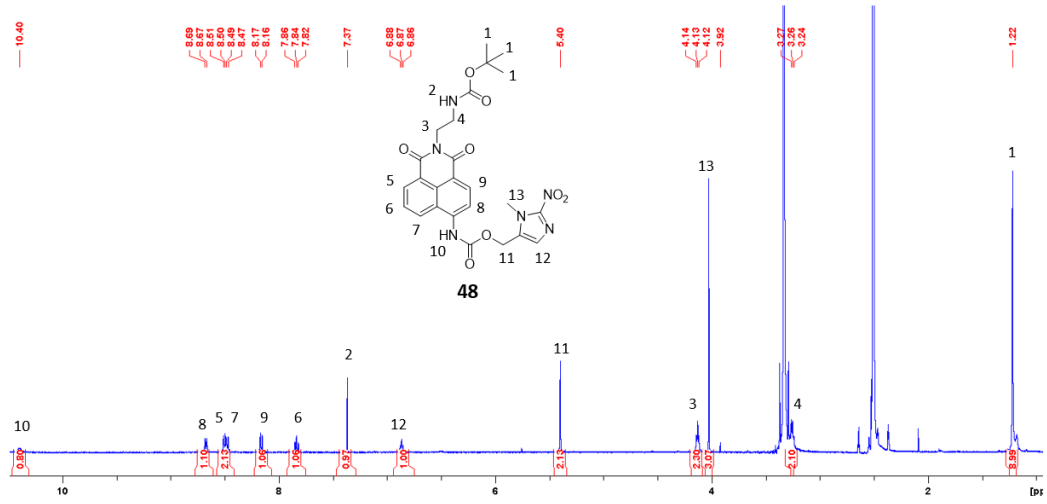

*Figure 4-3: The ^{1}H NMR spectrum of compound **48** (500 MHz, DMSO-d_6)*

As seen in Figure 4-3, there were some similar peaks compared with compound **51**. H1 stands for the signal at 1.22 ppm which integrated 9 and peaks at 3.24 ppm and 4.13 ppm stand for the 2 CH_2 groups of the diamine at the top compared with compound **51**. And the singlet peak at 7.37 ppm integrated 1 stands for H2. The rest peaks were similar as compound **28** while there were 6 aromatic peaks which match the H of compound **48** and peak at 10.4 stands for the other NH10 of compound **48**. Finally, the singlet peak at 5.4 ppm integrated to 2 stands for H11. From the two spectra were confident that compound **48** had been made successfully.

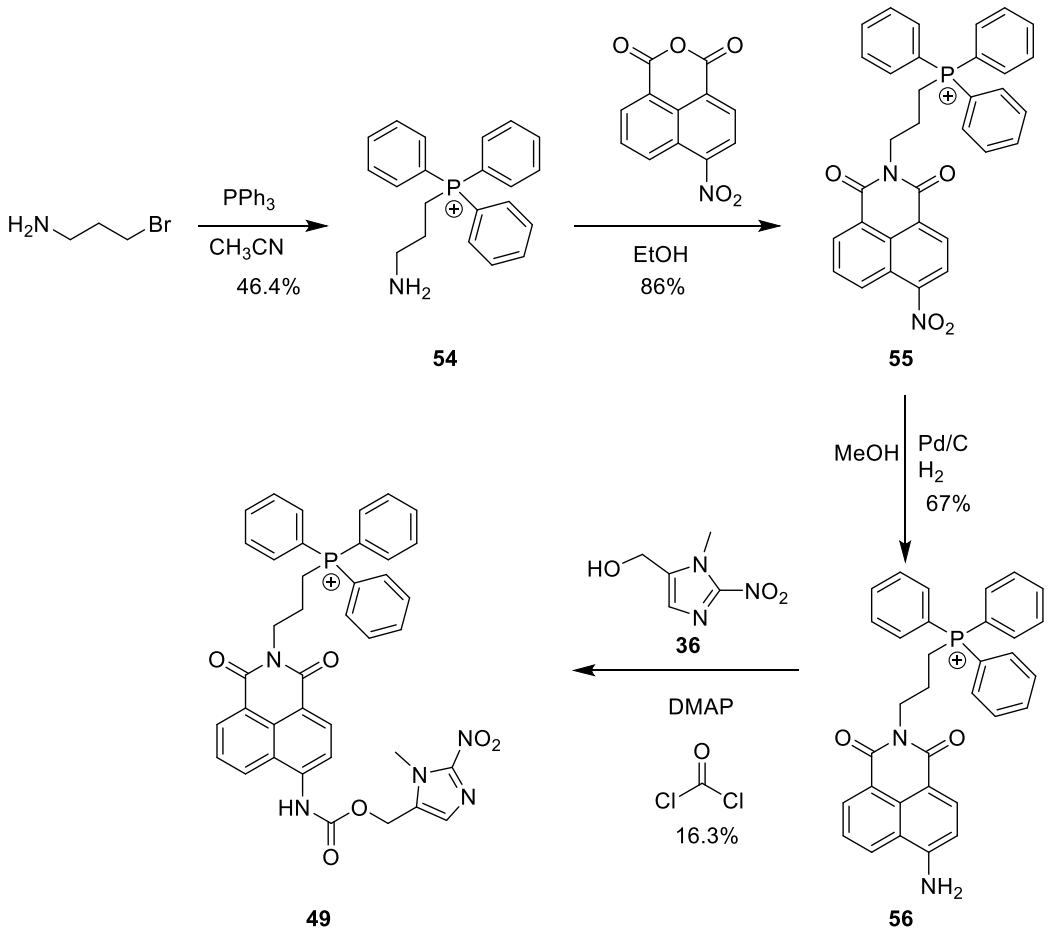

*Scheme 4-2: The synthesis of compound **49***

The synthesis of compound **49** in Scheme 4-2 also took us great efforts. The first step was introducing mitochondrial targeting of triphenylphosphine on the top of naphthalimide. We had tried 1-bromoethylamine to be the linker to connect the triphenylphosphine with 4-nitro-1,8-naphthalic anhydride (Scheme 4-3). With the 1-bromoethylamine as linker the reaction was unsuccessful, however, with the 1-bromopropylamine as linker the reaction was successful, the reason we thought was that the number of the carbon on the chain is too little and cannot afford two big molecules. The steric hindrance between macromolecules is also a reason that this compound is not working.

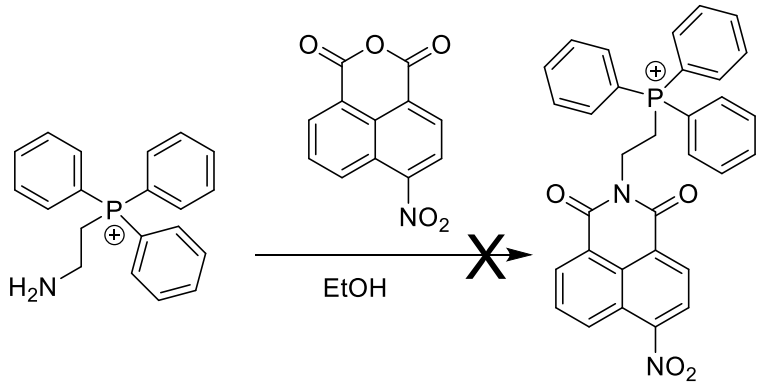

Scheme 4-3: Problems encountered in the experiment

Therefore, we chose 1-bromopropylamine to connect the triphenylphosphine. 1-bromopropylamine and triphenylphosphine were refluxed in CH_3CN for 24 hr. Cooled the solution to room temperature and heated the solution again to reflux to yield precipitate. Removed the solvent when it was cooled down and the solid was washed with DCM to yield a white compound **54** with 46.4 % yield.

With compound in hand, 4-nitro-1,8-naphthalic anhydride and compound **54** were reacted and after the reduction it formed compound **56**. Compound **56** was reacted with compound **36** in the presence of phosgene to make the final product compound **49**.

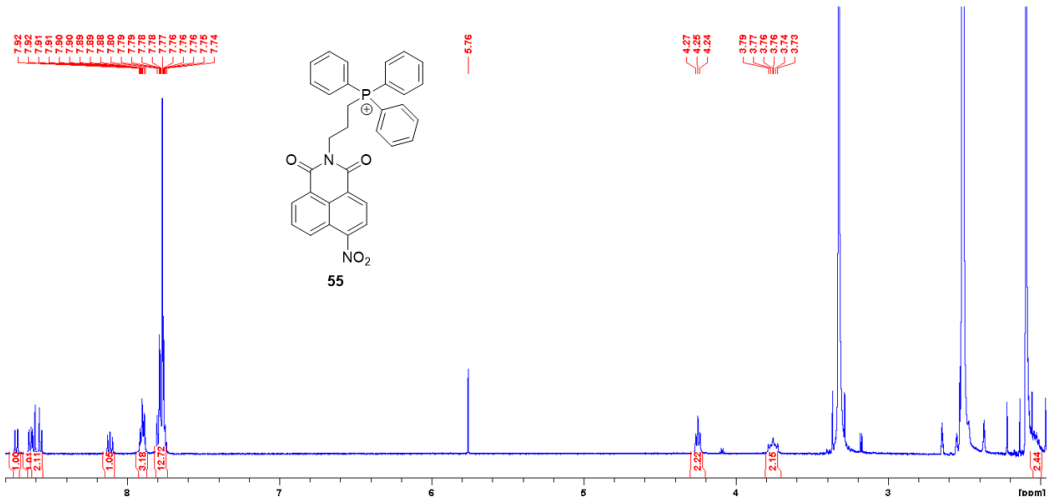

*Figure 4-4: The ^{1}H NMR spectrum of compound **55** (500 MHz, DMSO-d_6)*

Compound **49** was characterised by ^{1}H NMR, melting point analysis, mass spectrometry, ^{13}C NMR and IR spectroscopy. The ^{1}H NMR spectrum was shown

in figure below. Assignment of the peaks was achieved by H-H COSY and C-H COSY analysis. Successful formation of this trigger was also evident from accurate mass spectrometry.

We took compound **55** as an example, from the spectrum in Figure 4-4 we can see there were two signals which integrated 3 and 12 indicated the hydrogens of triphenylphosphine and there were also 5 signals at range 8 ppm to 9 ppm indicated those five aromatic hydrogens of the naphthalimide. There were also three signals at 4.25 ppm, 3.76 ppm and 2.01 ppm integrated 2 stand for those three CH_2 group of compound **55**. While peak at 5.76 ppm was the DCM solvent peak.

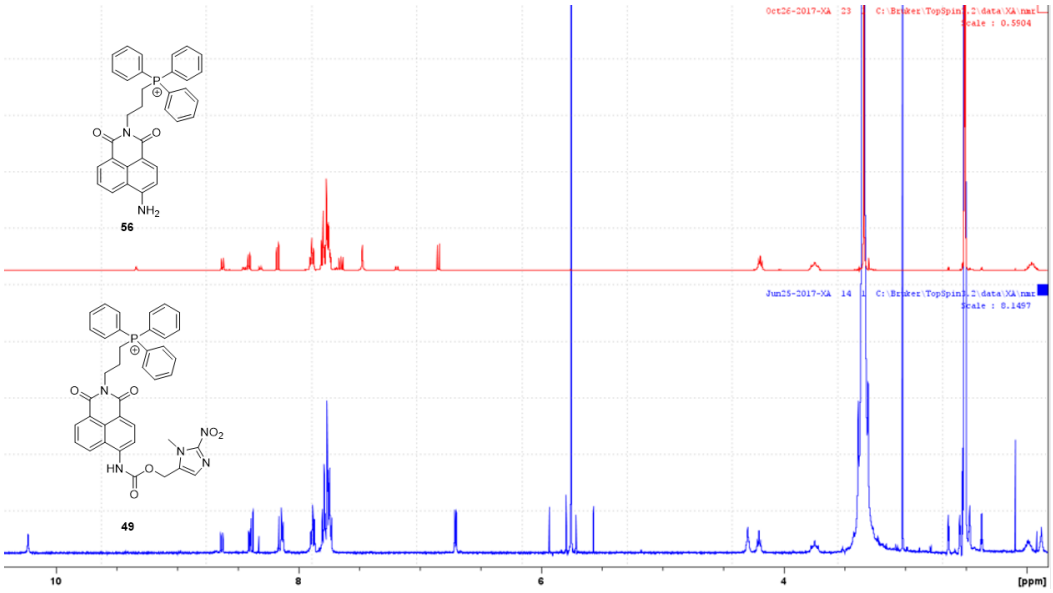

*Figure 4-5: The comparison of compound **56** and compound **49***

The Figure 4-5 was the comparison of compound **56** and **49**. From the figure we can see that there were few new signals show up of compound **49**. The peak at 10.3 ppm was singlet and integrated 1, from the HSQC in Figure 4-6 we did not see any single at this chemical shift, so we can certainty the single was the NH of compound **49**. And there were two aliphatic signals showed up at 6.7 ppm and 4.3 ppm which should be the CH_2 group and CH_3 group of the nitroimidazole group. Consider to this, we can make sure that compound **49** was made successfully. With the comparison of compound **56**, we can indicate the signals of this spectrum to each hydrogen of compound **49**.

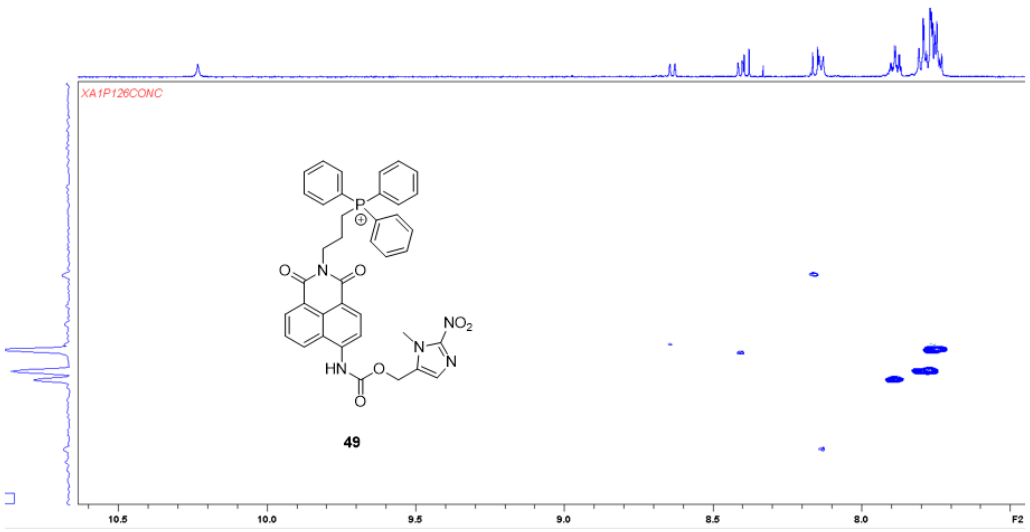

*Figure 4-6: The HSQC of compound **49** (500 MHz, DMSO-d_6)*

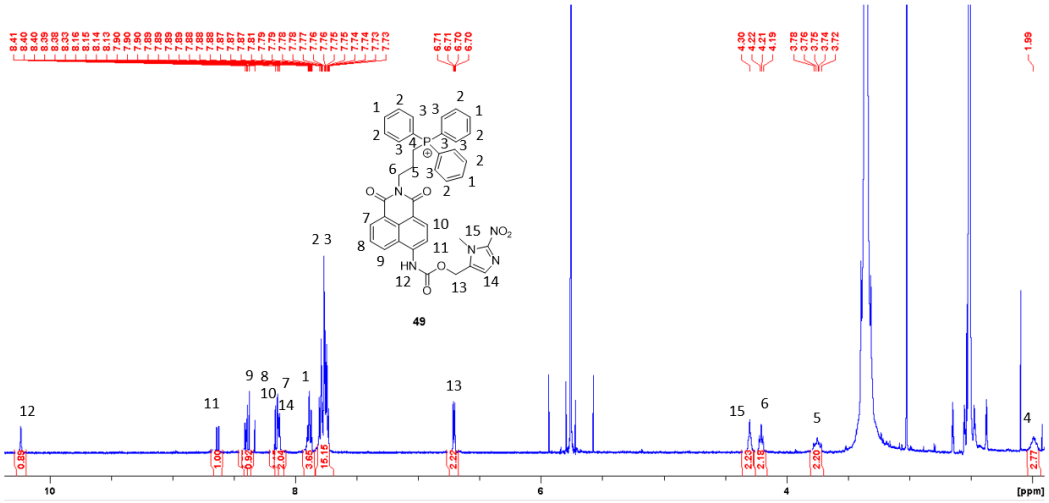

*Figure 4-7: ^{1}H NMR spectrum of compound **49** (500 MHz, DMSO-d_6).*

In Figure 4-7, peak at 7.9 ppm stands for H1 and peak at 7.76 ppm integrated 12 stand for H2 and H3. The peaks chemical shift at the range of 8 to 9 stand for the aromatic hydrogens H7, H8, H9, H10, H11 and H14 respectively. There is a big single at 5.6 ppm and some little singles around 5.6 ppm which indicate the peak of DCM and the satellite peaks of DCM. Peaks at 1.99 ppm, 3.72 ppm and 4.2 ppm stand for the propyl group of the compound **49** and peak at 6.7 ppm stand for H13 while peak at 4.3 ppm was H15. Finally, chemical shift at 10.3 ppm was the NH of compound **49**.

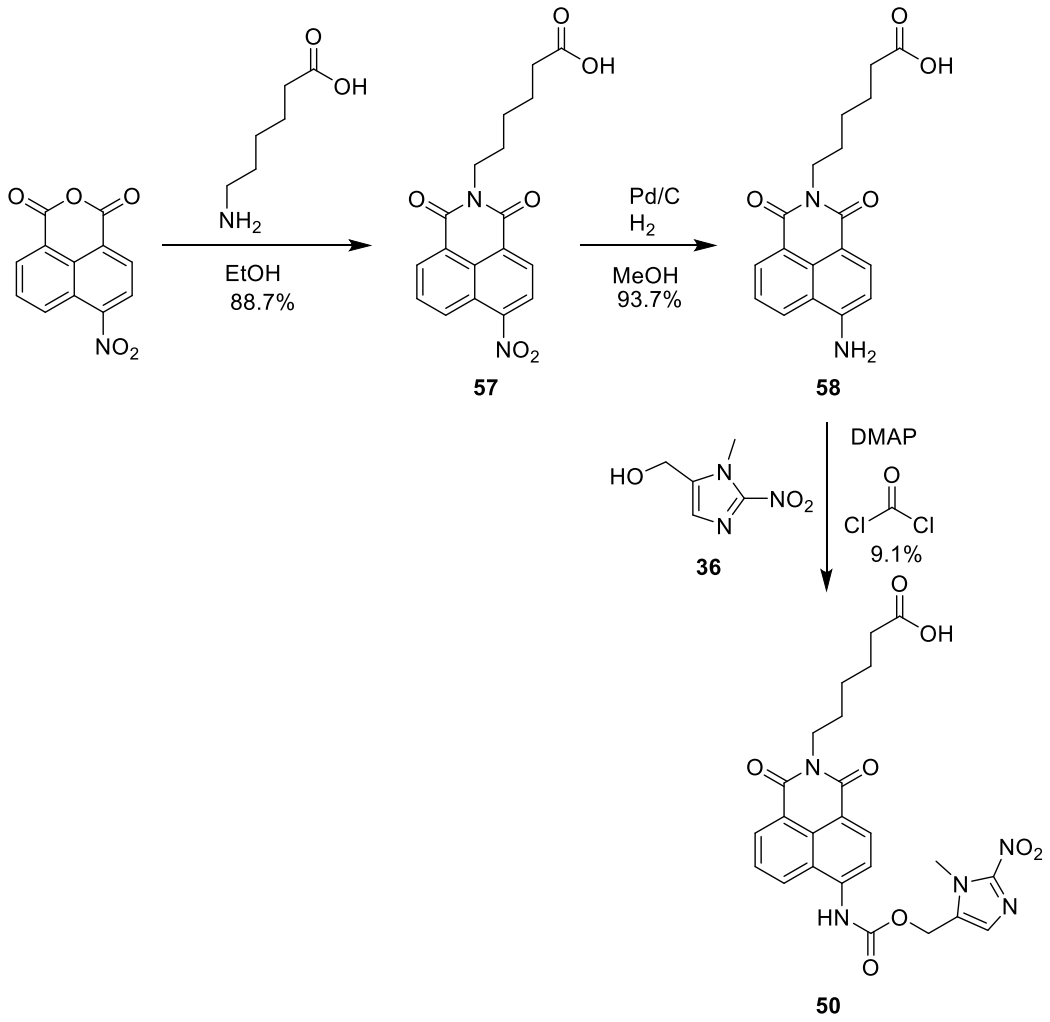

*Scheme 4-4: The synthesis of compound **50***

The synthesis of compound **50** shown in Scheme 4-4 was the same as compound **28**. However, due to the presence of carboxyl groups, compound **50** cannot be purified by passing through the column. So we used HPLC purification to make sure we got high purity compounds. The purification was performed using a mobile phase of 0.1% formic acid in water as solvent A and 0.1% formic acid in acetonitrile solvent B and a linear gradient of 0-100% B over 30 min.

Compound **50** was characterised by ^{1}H NMR, melting point analysis, mass spectrometry, ^{13}C NMR and IR spectroscopy. The ^{1}H NMR spectrum is shown in figure below. Assignment of the peaks was achieved by H-H COSY and C-H COSY analysis.

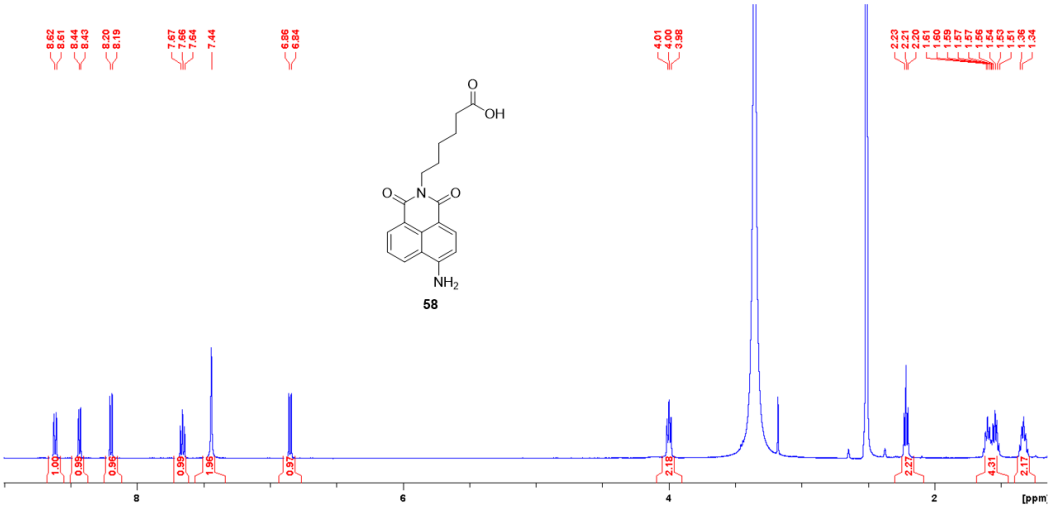

*Figure 4-8: The ^{1}H NMR spectrum of compound **58** (500 MHz, DMSO-d_6).*

We took compound **58** as reference. From the spectrum in Figure 4-8 we can see there were 5 aromatic signals which indicated those 5 aromatic hydrogens of compound **58** and there was a singlet which integrated 2 stand for the NH_2 group and there were 5 aliphatic signals which clearly stand for 5 CH_2 groups of compound **58**. This picture clearly showed the signal of each hydrogen of Compound **58**. Now we compared the spectrum of compound **58** with the spectrum of compound **50** we made to see if we can certainty our final compound was perfectly made.

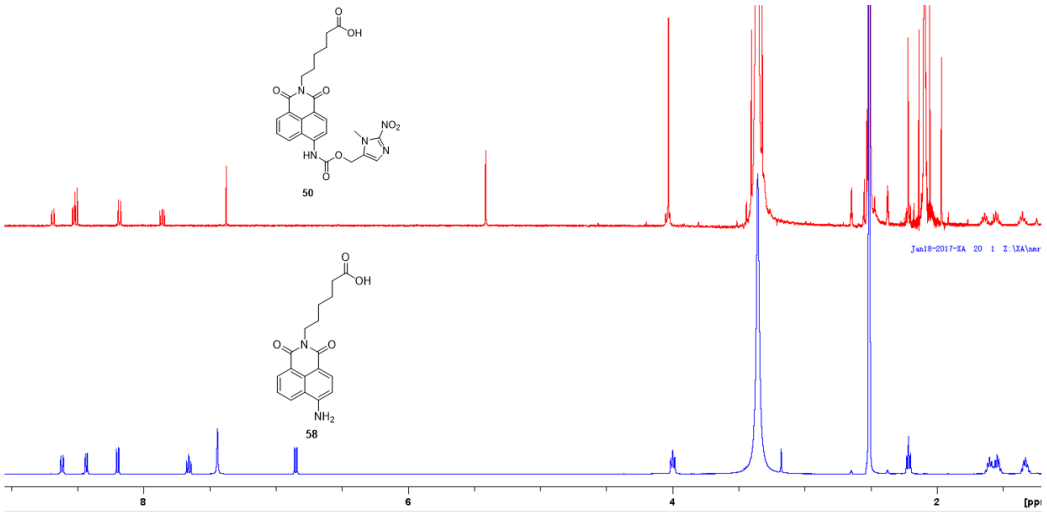

*Figure 4-9: The comparison of compound **50** and compound **58***

From the comparison in Figure 4-9 we knew that the aromatic hydrogens of compound **50** were moved to down field because the conjugation of carbamate linker lower the electron density of the naphthalimide group which cause de-shield and pushed the signal to down field. There were another aliphatic signals showed up from the spectrum of compound **50** which indicated the CH_2 and CH_3 groups of the nitroimidazole group. Finally there was an aliphatic signal at 2.2 ppm which was covered by the solvent acetone.

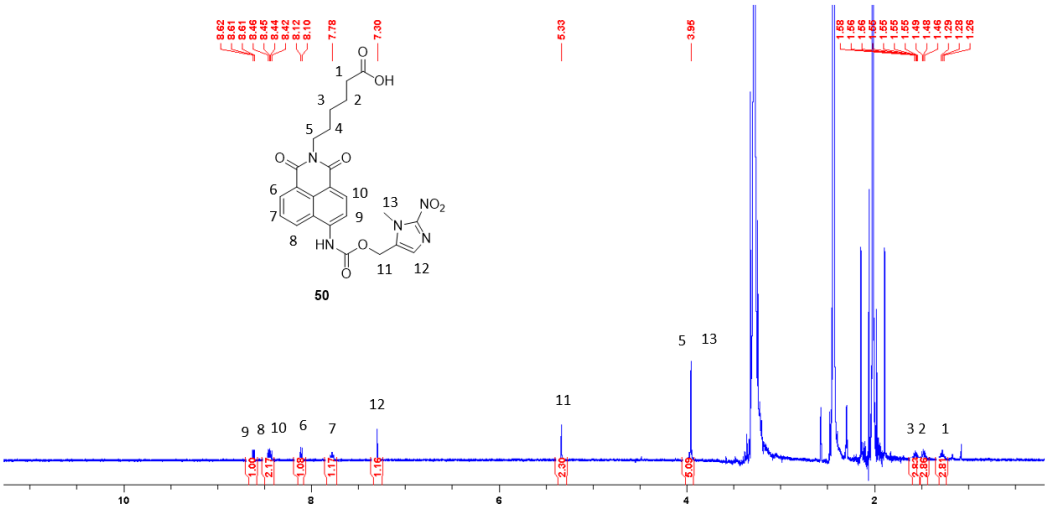

*Figure 4-10: The ^{1}H NMR spectrum of compound **50** (500 MHz, DMSO-d_6).*

Therefore, we can indicate the signals of compound **50**. In Figure 4-10, peak at 1.36 ppm, 1.54 ppm, 1.65 ppm and 4.03 ppm stand for H1, H2, H3 and H5. While there was still a signal at 4.03 ppm stand for H13. Peak at 5.41 integrated 2 stand for H11 and the singlet at 7.37 ppm indicated H12. The peak at 8.68 ppm stand for the H9 because it was more close to the carbamate linker and the triplet signal at 7.86 ppm was the H7. The NH peak was showed up at 10.5 ppm but it was overlapped by the base line. Hence we measured the Mass Spec to test our compound which shown in Figure 4-11.

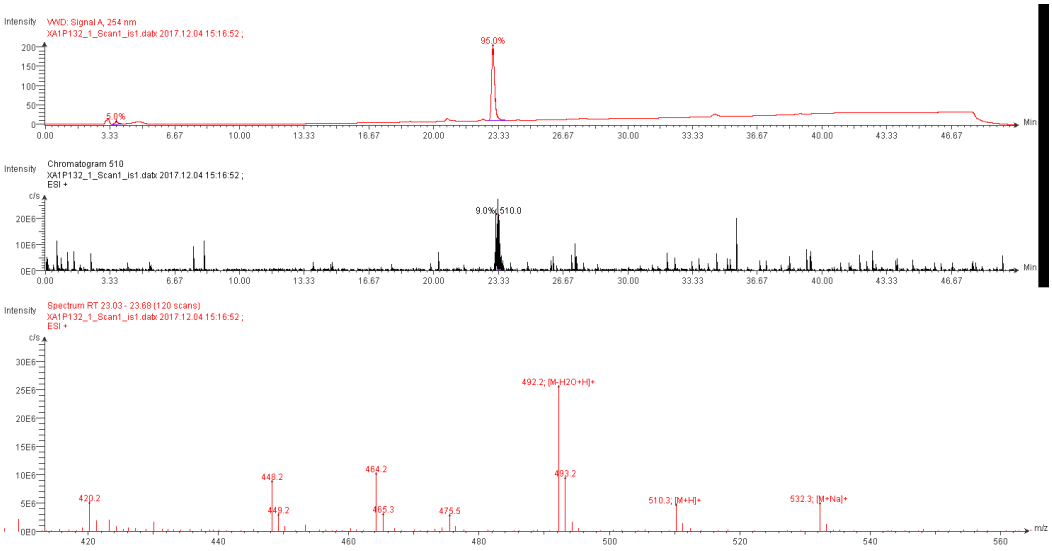

*Figure 4-11: Mass Spec of compound **50***

The first part of Figure 4-11 was the absorption of the compound **50**. And the second part was the ions detected at this absorption peak with the molecular weight of 510 (the molecular weight of compound **50** is 509), and the final part was the Mass spectrum of compound **50**. Here we can clearly see the signal that the compound **50** is ionized by hydrogen ions and sodium ions. Therefore, we may certainty say that compound **50** was made successfully.

4.3 Conclusion

After a series of modifications to compound **28**, compounds **48**, **49** and **50** were successfully synthesized. The key to the successful synthesis of these compounds is the selection of the correct synthesis procedure and the appropriate separation technique. For example, when triphenylphosphine was linked to naphthalene anhydride to form compound **55**, the length of the carbon chain was not enough would causes the two macromolecules to be too close together to form a steric hindrance and finally prevent the formation of compound. In the purification of compound **50**, the silica gel column adsorbs the compound on the column without obtaining the product, but if we used HPLC purification the pure product will show up easily. Overcoming the problems and difficulties encountered in synthetic

chemistry is the foundation of our progress, and the experience in these research processes has a profound influence for our future development.

These compounds are able to bind to biological macromolecules in vivo, providing a great help to compounds in targeting cells. We believe that changing the structure of the N-terminal of the compound will not affect the compounds' own sensitivity to NTR. Although NTR reactions have not been conducted to demonstrate the properties of these compounds, we are still fully confident in those compounds and we believe compounds **48**, **49**, **50** can all be used as NTR fluorescent sensors.

Chapter 5 Conclusion and Future work

Conclusion

In summary, during our research, we successfully synthesized compounds **28** and **29**, and we studied their photophysical properties, in addition, we also conducted a deep discussion on their fluorescence properties with NTR treated. The reason for the study of compounds **28** and **29** was to explore the important properties of the fluorescent sensors by comparing the similarities and differences between the two compounds. We kept the fluorophore and the nitro imidazole same but change the binding position to see if these two compounds have response to NTR (Figure 5-1).

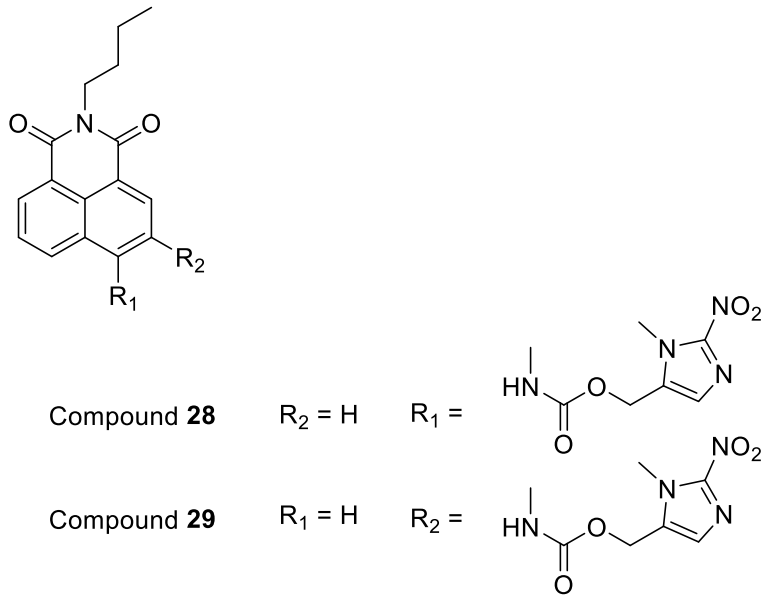

*Figure 5-1: The difference between compound **28** and compound **28***

On the other hand, in the experiment of enhancing the sensitivity of compound **28**, we further synthesized fluorescent probes based on different nitroaromatic triggers such as nitrobenzene and nitro thiofuran to form compounds **31** and **32** (Figure 5-2). We would like to find out which nitro aromatic trigger has the best response to NTR. The NTR reactions with them were also investigated.

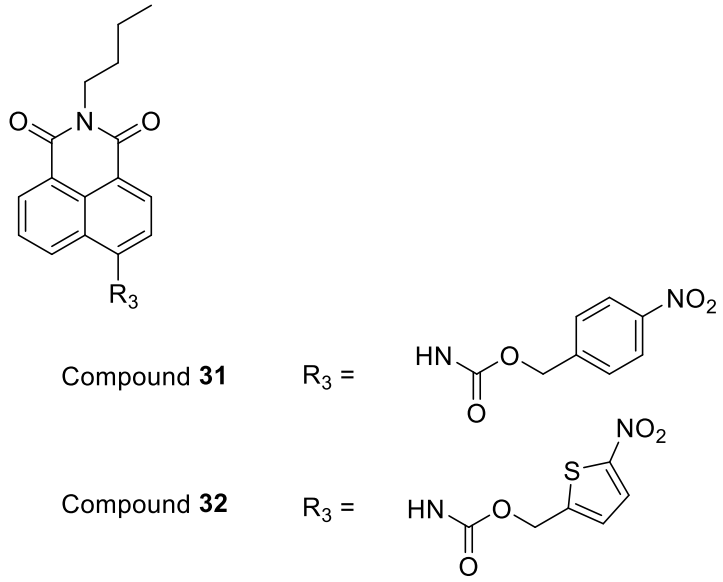

Figure 5-2: The change on the nitro aromatic triggers

Finally, we performed a bioconjugation experiment on compound **28** to improve the ability of compound **28** to bind to a given functional group (Figure 5-3). For this reason, we have successfully synthesized compounds **48**, **49** and **50** to adapt to the combination of various functional groups.

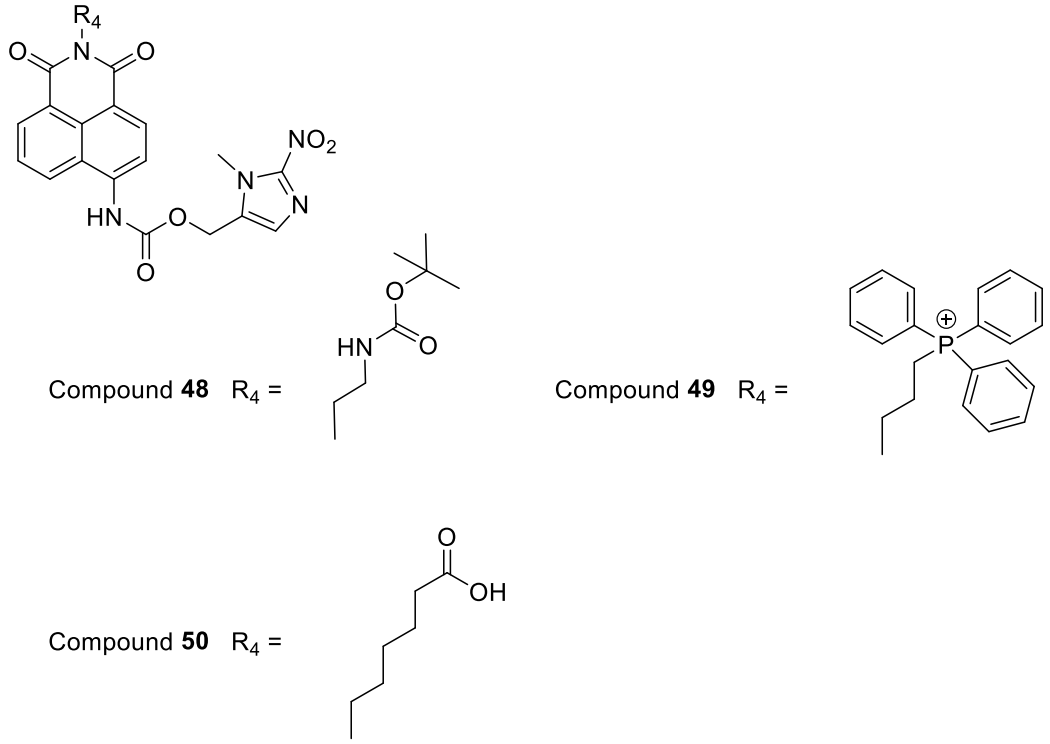

*Figure 5-3: Bioconjugation of compound **28***

In these experiments, we fully understand some of the important properties of the probe based on naphthalene anhydride as a fluorescent group: the compound made through 4-position substituted of naphthalimide has a more pronounced NTR response than the compound substituted at the 3-position. In the first set of experiments, compound **28** exhibited a very high sensitivity to NTR reactions. It was clearly shown by fluorescence emission spectroscopy that the compound **28** reacted rapidly under the action of NTR, eventually releasing the fluorophore through a bond breaking and rearrangement reaction and finally change the fluorescence signal. On the other hand, compound **29** did not show any change in fluorescence intensity under the action of NTR. We therefore determined that the substitution of naphthalene 4 position is the key to the reaction with NTR.

Through biological experiments, we know that compound **28** was transported into cells by passive transport, which means that compound **28** can enter cells without any energy retention.

In addition, during the NTR sensitivity experiment, we tested all the compounds we made from different nitroaromatic triggers with NTR and recorded their fluorescence intensity. We found that compound **28** had the best change during reacting with NTR while there was no particularly strong fluorescence change of the fluorescent probes synthesized by other aromatic nitro substituents at the same concentration. Therefore, we concluded that nitroimidazole as an NTR recognition factor has the advantage that other aromatic nitro compounds cannot be replaced.

These experiments confirmed the advantage of compound **28** in the detection of hypoxic tumors. Similarly, the novel compounds **48**, **49** and **50** synthesized on the basis of compound **28** are also highly promising as tumor fluorescent probes to play an important role in this field.

Future work

The successful NTR reaction of compound **28** with HeLa cells demonstrated that the potential value of compound **28** as a hypoxia fluorescent probe. Our next phase of research will focus on the detection of hypoxia in living tissues. Although the optical imaging technology has its own unique advantages, it has not been widely

used in clinical practice. An important reason is the lack of suitable for in vivo tissue hypoxia probe. During the hypoxia probe research, people mainly using adherent cells to react with the probes. While there is a huge difference between adherent cells and three-dimensional living tissue. Probes which show great affection in adherent cells might not have the same result in living tissue due to the tissue permeability and other issues that it cannot penetrate the tumor hypoxia centre. Therefore, increasing the solubility of compounds is an important way to solve the problem. When it comes to increasing the solubility of the compounds, we envisaged that the polarity of the compounds could be increased by the introduction of polar functional groups. Another way to increase the solubility is to form coordination complex or salt of the compound by the reaction of hydrotropic agent.

In the meantime, we would like to change the structure of compound **28** by exchanging the nitroaromatic trigger to the N terminal to form a set of novel fluorescence compounds (Figure 5-4).

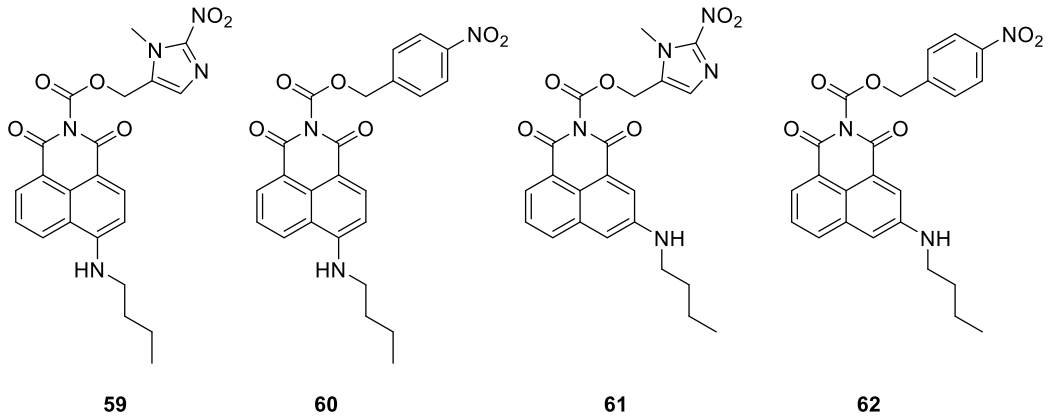

59 **60** **61** **62**

Figure 5-4: Novel fluorescence sensors in the future

Also, we could modify the nitro aromatic triggers to not only act as the NTR recognition group but also can carry some drug molecules into the cells (Figure 5-5). In this case, the nitro aromatic triggers can connect to some drug molecules and once the compound reacts with NTR in cells it will bring the drug molecule into the cells as well.

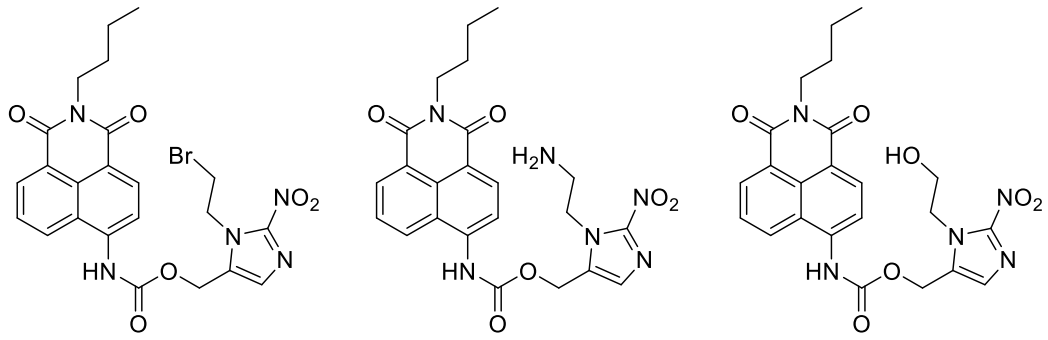

Figure 5-5: Novel fluorescence sensors by modifying the nitroaromatic triggers

Chapter 6 Experiments

6.1 General remarks

^{1}H NMR spectra were recorded using a Bruker Avance III 500 at a frequency of 500.13 MHz, and are reported as parts per million (ppm) with either DMSO-*d*$_6$ (δ_H 2.50 ppm) or $CDCl_3$ (δ_H 7.26 ppm) as an internal reference. The data are reported as chemical shift (δ), multiplicity (br = broad, s = singlet, d = doublet, t = triplet, m = multiplet), coupling constant (*J* Hz) and relative integral. ^{13}C NMR spectra were recorded using a Bruker Avance III 500 at a frequency of 125.76 MHz and are reported as parts per million (ppm) with either DMSO-*d*$_6$ (δ_H 39.5 ppm) or $CDCl_3$ (δ_H 77.2 ppm) as an internal reference. High resolution ESI spectra were recorded on an Agilent 6310 LCMS TOF. Analytical TLC was performed using pre-coated silica gel plates (Merck Kieselgel 60 F254). Microwave irradiation of reaction mixtures was performed using a CEM Discover SP microwave controlled by Synergy^{TM} software.

6.2 Materials and Methods for Biological Experiments:

6.2.1 Nitroreductase Studies

Fluorescence titrations were carried out using a Cary Eclipse Fluorescence Spectrometer or a Jasco FP6300 spectrofluorimeter. A stock solution of the fluorescent probe under study was prepared in DMSO before being diluted in a 3 mL quartz fluorescence cell to a final concentration of 1×10^{-5} M with NADH (50 μM) in 10 mM phosphate buffer solution (PBS) where the total amount of DMSO present was < 0.1%. Spectroscopic titrations were performed by additions of aliquots of a 1 μg/μL Nitroreductase (from Escherichia coli, ≥90% (SDS-PAGE), recombinant, expressed in E. coli), followed by either continuous scanning of a single wavelength or by intermittent fluorescence spectra recorded from 400 nm to 750 nm. Typically, 0 up to 24 μg/mL of NTR was added to the solution. ESI-LCMS studies were conducted on an Agilent 6310 LCMS TOF with samples prepared to a final concentration of 1×10^{-3} M with NADH (50 μM) in 10 mM

phosphate buffer solution (PBS) where the total amount of DMSO present was < 0.1%.

6.2.2 Cell culture

HeLa cells were grown in Dulbecco's Modified Eagle Medium supplemented with 10% fetal bovine serum and 50 µg/ml penicillin/streptomycin at 37˚C in a humidified atmosphere of 5% CO_2. For reducing conditions, compounds were pre-treated for 3 hrs with nitroreductase and its cofactor NADH before being added to cells. For endocytosis studies, cells were pre-treated for 3hrs with 100 µM dynasore.

6.2.3 Viability assay

$5x10^3$ cells/well were seeded in a 96-well plate and treated with the respective compound for 24 h. Alamar Blue (20 µl) (BioSource) was then added to each well and incubated for 4 h. Fluorescence was read using at 590 nm (excitation 544 nm). The control untreated cells represented 100% cell viability. All data points (expressed as means ± S.E.M.) were analysed using GRAPHPAD Prism (version 4) software (Graphpad software Inc., San Diego, CA).

6.2.4 Confocal microscopy

HeLa cells were seeded at a density of 1 x 10^5 cells /2 mL and left for 24 h before the required treatment. Cells were then washed twice, stained with the red nuclear stain DRAQ5 and analysed by live confocal microscopy using an Olympus FV1000 point scanning microscope with a 60x oil immersion lens with an NA (numerical aperture) of 1.42. The software used to collect images was FluoView Version 7.1 software. Compounds were excited by a 405 nm argon laser, emission 425-475 and 525-575 nm. DRAQ5 was excited by a 633 nm laser, emission >650 nm. For spectra, emission from 410 to 770 nm was quantified using a Leica SP8 confocal microscope (60X oil immersion lens), excitation 405 nm.

6.2.5 Flow cytometry

Following the required treatment, cells were trypsinised, washed twice with PBS, resuspended in 400 µL of ice cold PBS and assayed for flow cytometry (FACS CyAn, Bectin Dickson). Analysis was performed using appropriate gates, counting 10,000 cells and the FlowJo software package. The compounds were excited by a 405 nm laser, emission filters 425 nm-475nm and 510 nm-550nm.

6.3 Experimental procedure

3-nitro-*N*-butyl-1,8-naphthalimide (42)

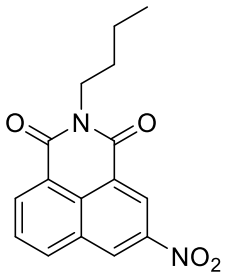

3-nitro-1,8-naphthalic anhydride (1 g, 4.1 mmol, 1 eq.) and butyl amine (0.31 g, 0.406 ml, 4.1 mmol, 1 eq.) were dissolved in EtOH (17 mL) before being heated at 110 ^{o}C for 1 hr under microwave irradiation. The mixture was allowed to cool to room temperature before the solvent was removed under reduced pressure. The resulting residue was purified by column chromatography eluting with DCM. The purified product was isolated as a cream solid (1.2 g, 97% yield). **^{1}H NMR** (500 MHz, DMSO-d_6) σ 9.41 (d, 1H, J = 2.3 Hz), 8.89 (d, 1H, J = 2.3Hz), 8.72 (dd, 1H, J = 8.4/0.82 Hz), 8.62 (dd, 1H, J = 7.4/1.2 Hz), 8.01 (dt, 1H, J = 7.4/0.75 Hz), 4.03 (t, 2H, J = 7.49 Hz), 1.62 (qu, 2H, J = 7.48 Hz), 1.36 (sex, 2H, J = 7.47 Hz), 0.93 (t, 3H, J = 7.47 Hz); **^{13}C NMR** (125 MHz, DMSO-d_6): 163.24, 162.73, 146.29, 136.74, 134.38, 131.31, 130.12, 129.97, 129.71, 124.48, 123.32, 123.04, 29.99, 20.25, 14.19; **HRMS** (ESI): Calculated for $C_{16}H_{15}N_2O_4$ $[M+H]^+$, expected: 299.1035, observed: 299.1026, PPM: 3.03; **ν_{max} (film)/cm^{-1}:** 3089.47, 2965.46, 2937.14, 2876.14, 1993.10, 1837.2, 1707.12, 1598.98, 1547.54, 1508.57, 1462.63, 1437.21, 1418.73, 1352.05, 1327.24, 1267.73, 1241.87, 1203.19. **MP:** 130~136 ^{o}C.

3-amino-*N*-butyl-1,8-naphthalimide (43)

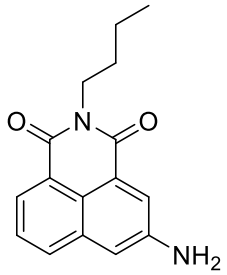

3-nitro-*N*-butyl-1,8-naphthalimide (1.2g, 4 mmol, 1 eq.) was dissolved in MeOH (70 ml) before Pd/C (0.25 g) was added and the reaction was placed under an atmosphere of H_2. The reaction was allowed to proceed for 2 hrs before being filtered through a pad of celite. The solvent was removed under reduced pressure to yield a bright yellow solid. (1.05 g, 98% yield) **^{1}H NMR** (500 MHz, DMSO-d_6) σ 8.13 (dd, 1H, J = 7.12/1.13Hz), 8.08 (dd, 1H, J = 8.4/1.0Hz), 8.02 (d, 1H, J = 2.32Hz), 7.67 (dt, 1H, J = 7.3/1.03Hz), 7.34 (d, 1H, J = 2.32Hz), 6.04 (s, 1H), 4.08 (t, 2H, J = 7.4Hz), 1.65 (qu, 2H, J = 7.32Hz), 1.41 (sex, 2H, J = 7.48Hz), 0.98 (t, 3H, J = 7.48Hz). **^{13}C NMR** (125 MHz, DMSO-d_6): 164.24, 164.05, 148.34, 134.02, 131.92, 127.42, 125.88, 123.04, 122.24, 122.18, 121.04, 112.18, 79.42, 30.17, 20.27, 14.19; **HRMS** (ESI): Calculated for $C_{16}H_{17}N_2O_2$ $[M+H]^+$, expected: 269.1298, observed: 269.1285, PPM: 4.86; **ν_{max} (film)/cm^{-1}:** 3467.96, 3364.16, 3065.44, 2959.11, 2863.58, 1691.26, 1652.47, 1629.40, 1580.68, 1516.78, 1449.69, 1388.59, 1341.53, 1306.06, 1218.14. **MP:** 150~162 ^{o}C.

(2-Butyl-1,3-dioxo-2,3-dihydro-1H-benzo[de]isoquinolin-5-yl)-carbamic acid 3-methyl-2-nitro-3H-imidazol-4-ylmethyl ester (29)

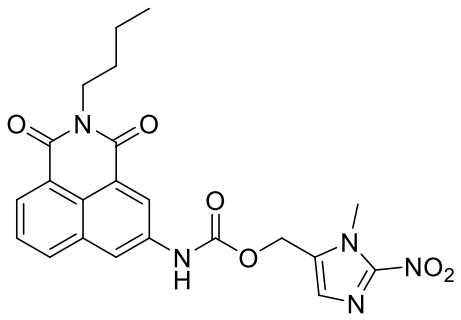

3-amino-*N*-butyl-1,8-naphthalimide (48 mg, 0.18 mmol, 1 eq.) and DMAP (66 mg, 0.54 mmol, 3 eq.) were dissolved in anhydrous DCM (20 mL) and placed under an argon atmosphere. The reaction was cooled to -10°C using an ice and salt bath before phosgene solution (15 wt. % in toluene; 0.7 ml, 1.07 mmol, 6 eq.) was added dropwise and the reaction mixture was allowed warm to room temperature and stirred for 4 hrs. The reaction mixture was reduced to dryness by bubbling with argon before the residue was redissolved in anhydrous DCM and cooled to 0 °C (20 mL). (3-Methyl-2-nitro-3H-imidazol-4-yl)-methanol **3** (84 mg, 0.53 mmol, 3 eq) was added and the reaction was allowed to return to room temp before being stirred overnight under an argon atmosphere. The reaction was quenched with water (10 mL) and extracted with DCM (3 x 10 ml). The resulting organic layer was dried over $MgSO_4$ before the solvent was removed under reduced pressure. The resulting residue was purified by column chromatography eluting with EtOAc/Pet Ether (6:4 to 8:2) to yield a beige solid. (51 mg, 63% yield) **^{1}H NMR** (500 MHz, $CDCl_3$) σ 8.56 (brs, 1H, NH), 8.5 (d, 1H, J = 7.4Hz), 8.3 (d, 1H, J = 2.3Hz), 8.16 (d, 1H, J = 8.3Hz), 7.75 (t, 1H, J = 7.5Hz), 7.32 (s, 1H), 7.08 (s, 1H), 5.31 (s, 2H), 4.16 (t,2H, J = 7.6Hz), 4.11 (s, 3H), 1.7 (qu, 2H, J = 7.4), 1.44 (sex, 2H, J = 7.5), 0.97 (t, 3H, J = 7.4Hz). **^{13}C NMR** (125 MHz, $CDCl_3$): 163.86, 163.60, 153.36, 146.62, 138.24, 134.01, 133.55, 132.60, 129.46, 129.38, 128.18, 124.24, 123.63, 123.36, 122.36, 120.12, 56.06, 34.79, 30.10, 20.27, 14.20; **HRMS** (ESI): Calculated for $C_{22}H_{22}O_6N_5$ $[M+H]^+$, expected: 452.1543, observed: 452.1562, PPM: -4.76; **ν_{max} (film)/cm^{-1}:** 3414.37, 2960.13, 1738.57, 1699.25, 1655.81, 1626.98, 1562.83, 1490.27, 1467.33, 1432.17, 1345.74, 1272.53, 1226.28, 1176.74, 1135.72, 1067.69, 1037.12, 837.81, 783.86. **MP:** 212 ^{o}C.

4-nitro-*N*-butyl-1,8-naphthalimide (44)

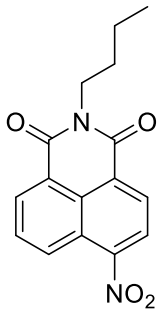

4-nitro-1,8-naphthalic anhydride (1 g, 4.1 mmol, 1 eq.) and butyl amine (0.31 g, 0.406 ml, 4.1 mmol 1 eq.) were dissolved in EtOH (17 mL) before being heated at 110 ^{o}C for 1 hr under microwave irradiation. The mixture was allowed to cool to room temperature before the solvent was removed under reduced pressure. The resulting residue was purified by column chromatography eluting with DCM. The purified product was isolated as a cream solid (1.18 g, 95% yield). **^{1}H NMR** (500 MHz, DMSO-d_6) σ 8.58 (dd, 1H, J = 8.65/0.84Hz), 8.51 (dd, 1H, J = 7.34/0.8Hz), 8.48 (d, 1H, J = 8.1Hz), 8.46 (t, 1H, J = 7.8Hz), 7.99 (dd, 1H, J = 7.62/0.86Hz), 3.98 (t, 2H, J = 7.58Hz), 1.59 (qu, 2H, J = 7.45Hz), 1.35 (sex, 2H, J = 7.42Hz), 0.92 (t, 3H, J = 7.42Hz). **^{13}C NMR** (500 MHz, DMSO-d_6): 163.24, 162.44, 149.39, 132.06, 130.50, 129.99, 129.09, 128.60, 126.89, 124.68, 123.05, 122.99, 29.91, 20.25, 14.15; **HRMS** (ESI): Calculated for $C_{16}H_{15}N_2O_4$ $[M+H]^+$, expected: 299.1025, observed: 299.1026, PPM: -0.4; **ν_{max} (film)/cm^{-1}:** 3106.27, 3069.79, 3040.62, 2961.54, 2873.57, 1949.06, 1708.53, 1654.57, 1623.75, 1583.15, 1529.35, 1461.93, 1439.21, 1408.28, 1346.72, 1269.49, 1231.81, 1188.64, 1082.40. **MP:** 104~108 ^{o}C.

4-amino-*N*-butyl-1,8-naphthalimide (45)

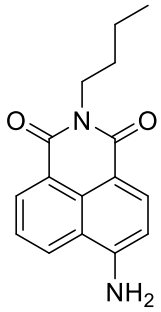

4-nitro-*N*-butyl-1,8-naphthalimide (1.1g, 3.7 mmol, 1 eq.) was dissolved in MeOH (70 ml) before Pd/C (0.25 g) was added and the reaction was placed under an atmosphere of H_2. The reaction was allowed to proceed for 2 hrs before being filtered through a pad of celite. The solvent was removed under reduced pressure to yield a bright yellow solid. (1.02 g, 95% yield) **^{1}H NMR** (500 MHz, DMSO-d_6) σ 8.59 (dd, 1H, J = 8.45/0.89Hz), 8.41 (dd, 1H, J = 7.33/0.85Hz), 8.18 (d, 1H, J = 8.4Hz), 7.63 (dd, 1H, J = 7.48/0.83Hz), 7.43 (s, 2H), 6.82 (d, 1H, J = 8.4Hz), 3.99 (t, 2H, J = 748Hz), 1.56 (qu, 2H, J = .48Hz), 1.31 (sex, 2H, J = 7.48Hz), 0.9 (t, 3H, J = 7.48Hz); **^{13}C NMR** (125 MHz, DMSO-d_6): 163.94, 163.40, 153.86, 140.79, 133.47, 132.13, 131.46, 129.74, 129.51, 128.80, 126.99, 124.48, 122.76, 117.91, 56.48, 34.82, 30.14, 20.28, 14.21; **HRMS** (ESI): Calculated for $C_{16}H_{17}N_2O_2$ $[M+H]^+$, expected: 269.1273, observed: 269.1285, PPM: -4.33; **ν_{max} (film)/cm^{-1}:** 3410.38, 3356.55, 3254.13, 2957.81, 2930.08, 2861.62, 1676.07, 1636.78, 1613.97, 1575.31, 1528.50, 1480.40, 1431.25, 1378.83, 1362.04, 1304.33, 1244.87, 1115.97, 1077.63. **MP:** 178~186 °C.

(2-Butyl-1,3-dioxo-2,3-dihydro-1H-benzo[de]isoquinolin-6-yl)-carbamic acid 3-methyl-2-nitro-3H-imidazol-4-ylmethyl ester (28)

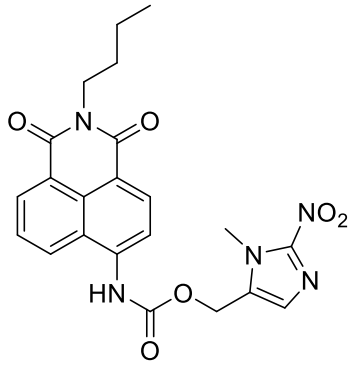

4-amino-*N*-butyl-1,8-naphthalimide (48 mg, 0.18 mmol, 1 eq.) and DMAP (66 mg, 0.54 mmol, 3 eq.) were dissolved in anhydrous DCM (20 mL) and placed under an argon atmosphere. The reaction was cooled to -10°C using an ice and salt bath before phosgene solution (15 wt. % in toluene; 0.7 ml, 1.07 mmol, 6 eq.) was added dropwise and the reaction mixture was allowed warm to room temperature and stirred for 4 hrs. The reaction mixture was reduced to dryness by bubbling with argon before the residue was redissolved in anhydrous DCM and cooled to 0 °C (20 mL). (3-Methyl-2-nitro-3H-imidazol-4-yl)-methanol **3** (84 mg, 0.53 mmol, 3 eq) was added and the reaction was allowed to return to room temp before being stirred overnight under an argon atmosphere. The reaction was quenched with water (10 mL) and extracted with DCM (3 x 10 ml). The resulting organic layer was dried over $MgSO_4$ before the solvent was removed under reduced pressure. The resulting residue was purified by column chromatography eluting with EtOAc/Pet Ether (6:4 to 8:2) to yield a beige solid (55 mg, 68% yield). **^{1}H NMR** (500 MHz, DMSO-d_6) σ 10.45 (Bs, NH), 8.67 (dd, 1H, J = 8.59/1.0Hz), 8.5 (dd, 1H, J = 7.26/0.9Hz), 8.48 (d, 1H, J = 8.24Hz), 8.17 (d, 1H, J = 8.27Hz), 7.84 (dt, 1H, J = 7.38/1.2Hz), 7.36 (s,1H), 5.39 (s, 2H), 4.02 (t,2H, J = 7.74Hz), 4.01 (s, 3H), 1.6 (qu, 2H, J = 7.5Hz), 1.34 (sex, 2H, J = 7.48Hz), 0.92 (t, 3H, J = 7.47Hz); **^{13}C NMR** (500 MHz, DMSO-d_6): 163.94, 163.40, 153.86, 140.79, 133.47, 132.13, 131.46, 129.74, 129.51, 128.80, 126.99, 124.48, 122.76, 117.91, 56.48, 34.82, 30.14, 20.28, 14.21; **HRMS** (ESI): Calculated for $C_{22}H_{22}O_6N_5$ $[M+H]^+$, expected: 452.1536, observed: 452.1565, PPM: -6.26; **ν_{max} (film)/cm^{-1}:** 3444.50, 3234.96, 2928.75, 2870.81, 1698.32, 1654.59, 1592.32, 1542.07, 1486.61, 1390.09, 1358.23, 1228.60, 1181.95. **MP:** 230~242 ºC.

(2-Butyl-1,3-dioxo-2,3-dihydro-1H-benzo[de]isoquinolin-6-yl)-carbamic acid 4-nitro-benzyl ester (31)

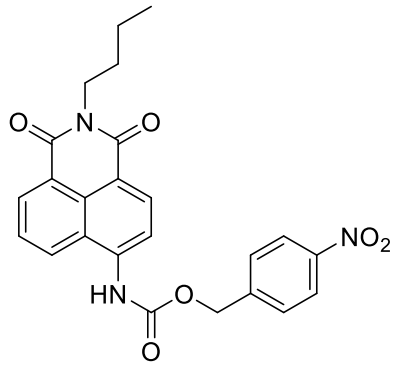

4-amino-*N*-butyl-1,8-naphthalimide (60 mg, 0.22 mmol, 1 eq.) and DMAP (82 mg, 0.67 mmol, 3 eq.) were dissolved in anhydrous DCM (20 mL) and placed under an argon atmosphere. The reaction was cooled to -10°C using an ice and salt bath before phosgene solution (15 wt. % in toluene; 1.0 ml, 1.33 mmol, 6 eq.) was added dropwise and the reaction mixture was allowed warm to room temperature and stirred for 4 hrs. The reaction mixture was reduced to dryness by bubbling with argon before the residue was redissolved in anhydrous DCM and cooled to 0 °C (20 mL). 4-nitrobenzyl alcohol (103 mg, 0.67 mmol, 3 eq.) was added and the reaction was allowed to return to room temp before being stirred overnight under an argon atmosphere. The reaction was quenched with water (10 mL) and was extracted with DCM (3 x 10 ml). The resulting organic layer was dried over $MgSO_4$ before the solvent was removed under reduced pressure. The resulting residue was purified by column chromatography eluting with MeOH/DCM (0:100 to 4:96) to yield a beige solid (60 mg, 60% yield). **^{1}H NMR** (500 MHz, DMSO-d_6) σ 10.50 (s, NH), 8.74 (d, 1H, J = 8.68Hz), 8.54 (d, 1H, J = 7.28Hz), 8.5 (d, 1H, J = 8.29Hz), 8.3 (d, 2H, J = 8.46Hz), 8.2 (d, 1H, J = 8.1Hz), 7.87 (t, 1H, J = 7.83Hz), 7.78 (d, 2H, 8.47Hz), 4.08 (dd, 2H, 5.24Hz), 4.05 (t, 2H, 7.42Hz), 1.63 (qu, 2H, J = 7.51Hz), 1.36 (sex, 2H, J = 7.77Hz), 0.94 (t, 3H, J = 7.4Hz). **^{13}C NMR** (125 MHz, DMSO-d_6): 163.96, 163.41, 147.66, 144.66, 132.15, 131.43, 129.07, 126.94, 124.13, 65.76, 55.38, 49.07, 40.61, 30.16, 20.28, 14.29. **HRMS** (ESI): Calculated for $C_{24}H_{21}N_3O_6$ $[M+H]^+$, expected: 447.1435, observed: 447.143, PPM: 0.95; **ν_{max} (film)/cm^{-1}:** 3309.52, 2956.91, 2872.62, 1707.63, 1694.55, 1646.75, 1621.35,

1593.24, 1544.41, 1518.43, 1447.13, 1393.43, 1365.32, 1346.34, 1224.021065.63. **MP:** 240~244 ^{o}C.

(5-nitrothiophen-2-yl)methanol (46)

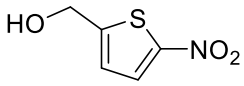

A solution of 5-nitrothiophene-2-carbaldehyde (1.05g, 1 mmol, 1 eq) and methanol (10 ml) was stirred at 0 °C with ice bath. Sodium borohydride (0.446 g, 1.5 mmol, 1,5 eq) was added slowly. The mixture was stirred overnight at room temperature. Solvent was removed by vacuo, then water (20 ml) was added. The resulting mixture was extracted with DCM (3 * 30 ml). The extracts were washed with water (3 * 30 ml) and brine (3 * 30 ml). Dried the organic layer with $MgSO_4$ and removed the solvent to yield a black liquid (0.703 g, 67% yield). **^{1}H NMR** (500 MHz, Chloroform-d) σ 7.793 (d, 1 H, J = 4.15 Hz), 6.91 (d, 1 H, J = 4.12 Hz), 4.855 (d, 2 H, J = 2.56 Hz); **^{13}C NMR** (125 MHz, Chloroform-d): 153.7632, 150.7806, 128.7298, 123.4825, 60.4389; **HRMS** (ESI): Calculated for $C_5H_5NO_3S$ $[M+H]^+$, expected: 158.999, observed: 158.9983, PPM: -4.63; **ν_{max} (film)/cm^{-1}:** 3846.95, 3400.52, 3107.59, 2929.12, 2871.4, 2666.33, 2461.46, 2374.99, 2304.62, 2162.18, 2071.44, 1809.39, 1678.80, 1634.44, 1206.63, 1160.27.

(5-nitrothiophen-2-yl)methyl(2-butyl-1,3-dioxo-2,3-dihydro-1H-benzo[de]isoquinolin-6-yl)carbamate (32)

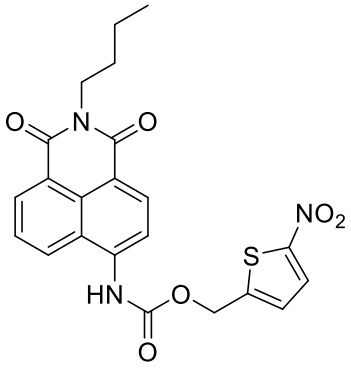

4-amino-*N*-butyl-1,8-naphthalimide (60 mg, 0.224 mmol, 1 eq.) and DMAP (82.11 mg, 0.672 mmol, 3 eq.) were dissolved in anhydrous DCM (20 mL) and placed under an argon atmosphere. The reaction was cooled to -10°C using an ice and salt bath before phosgene solution (15 wt. % in toluene; 1.0 ml, 1.33 mmol, 6 eq.) was added dropwise and the reaction mixture was allowed warm to room temperature and stirred for 4 hrs. The reaction mixture was reduced to dryness by bubbling with argon before the residue was redissolved in anhydrous DCM and cooled to 0 °C (20 mL). (5-nitrothiophen-2-yl)methanol (107 mg, 0.672 mmol, 3 eq.) was added and the reaction was allowed to return to room temp before being stirred overnight under an argon atmosphere. The reaction was quenched with water (10 mL) and was extracted with DCM (3 x 10 ml). The resulting organic layer was dried over $MgSO_4$ before the solvent was removed under reduced pressure. The resulting residue was purified by column chromatography eluting with EtOAc/Pet Ether (1:1) to yield a beige solid (63 mg, 63% yield).). **^{1}H NMR** (500 MHz, DMSO-d_6) σ 8.64 (d, 1 H, J = 7.16 Hz), 8.61 (d, 1 H, J = 8.12 Hz), 8.32 (d, 1 H, J = 8.46 Hz), 8.17 (d, 1 H, J = 8.19 Hz), 7.83 (d, 1 H, J = 3.57 Hz), 7.79 (t, 1 H, J = 7.52 Hz), 7.47(s, NH), 7.125 (d, 1 H, J = 3.93 Hz), 4.17 (t, 2 H, J = 7.48 Hz), 1.71 (qu, 2 H, J = 7.02 Hz), 1.44 (sex, 2 H, J = 7.34 Hz), 0.97 (t, 3 H, J = 7.06 Hz); **^{13}C NMR** (125 MHz, DMSO-d_6): 164.027, 163.553, 145.08, 138.00, 132.28, 131.362, 128.211, 127.351, 126.924, 125.663, 123.65, 118.716, 61.69, 40.29, 30.218, 20.39, 13.8376; **HRMS** (ESI): Calculated for $C_{22}H_{19}N_3O_6S$ $[M+H]^+$, expected: 453.0995, observed: 453.0999, PPM: 1.07; **ν_{max} (film)/cm^{-1}:** 3328.62, 3063.72, 2960.44, 1711.21, 1694.5, 1621.04, 1593.16, 1553.99, 1510.99, 1445.63, 1394.59, 1346.39, 1244.32, 1225.71.

(2-Amino-ethyl)-carbamic acid tert-butyl ester (51) [65]

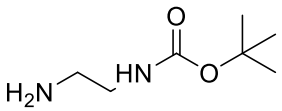

To a 250 ml of round bottom flask was added ethyl diamine (13.4Ml, 200mmol) in CHCl3 (100Ml). A solution of Di-tert-butyl dicarbonate (4.4 g, 20mmol) in CHCl3 (50 ml) was added dropwise over 2 hours at 0 ^{o}C. Stirred at RT for 24 hours. The mixture was washed with brine. The organic layer was washed with H2O. dried with MgSO4 and concentrated in vacuum to yield a colorless liquid (2.89 g, 90% yield). **^{1}H NMR** (500 MHz, DMSO-d_6) σ 7.417 (s, NH), 5.49 (s, NH), 3.156 (d, 2 H, J = 5.37 Hz), 2.786 (t, 2 H, J = 5.91 Hz), 1.44 (s, 9 H); **^{13}C NMR** (125 MHz, DMSO-d_6): 156.2326, 78.8123, 77.456, 77.4, 77.2, 76.94, 68.34; **HRMS (ESI):** Calculated for $C_7H_{16}O_2N_2$ [M+H]+, expected: 160.1217, observed: 160.1212, PPM: 2.99.

[2-(6-Nitro-1,3-dioxo-1H,3H-benzo[de]isoquinolin-2-yl)-ethyl]-carbamic acid tert-butyl ester (52)

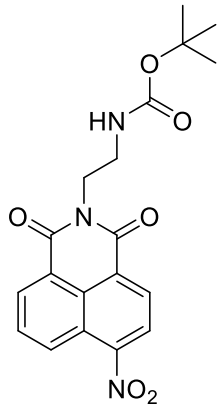

4-nitro-1,8-naphthalic anhydride (0.4 g, 1.65 mmol, 1 eq.) and (2-Amino-ethyl)-carbamic acid tert-butyl ester (0.263 g, 263 ul, 1.65 mmol, 1 eq.) were dissolved in EtOH (14 mL) before being heated at 110 ^{o}C for 1 hr under microwave irradiation. The mixture was allowed to cool to room temperature before the solvent was removed under reduced pressure. The resulting residue was purified by column chromatography eluting with pure dichloromethane to 3% methanol in

dichloromethane. The purified product was isolated as a cream yellow solid (0.566 g, 86.01% yield). **^{1}H NMR (500 MHz, DMSO-d$_6$) σ** 8.846 (d, 1 H, J = 8.9 Hz), 8.749 (d, 1 H, J = 7.29 Hz), 8.705 (d, 1 H, J = 7.95 Hz), 8.4 (d, 1 H, J = 8.09 Hz), 7.98 (t, 1 H, J = 8.49 Hz), 4.85 (s, NH), 4.37 (t, 2 H, J = 5.35 Hz), 3.55 (d, 2 H, J = 5.14 Hz), 1.237 (s, 9 H); **^{13}C NMR** (125 MHz, DMSO-d$_6$): 136.6366, 156.2874, 149.5733, 132.0410, 130.5680, 129.0647, 128.9660, 124.6667, 123.1953, 77.9744, 38.0379, 28.5142; **HRMS** (ESI): Calculated for $C_{19}H_{19}O_6N_3$ [M+H]+, expected: 385.1276, observed: 385.1274, PPM: 0.56; **νmax (film)/cm^{-1}:** 3400.79, 3070.24, 2977.06, 2935.65, 1719.09, 1701.93, 1623.19, 1583.90, 1524.01, 1447.90, 1410.74, 1366.32, 1341.39, 1272.94, 1233.68, 1192.60.

[2-(6-Amino-1,3-dioxo-1H,3H-benzo[de]isoquinolin-2-yl)-ethyl]-carbamic acid tert-butyl ester (53)

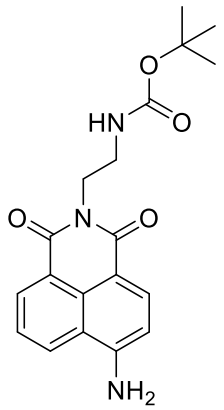

[2-(6-Nitro-1,3-dioxo-1H,3H-benzo[de]isoquinolin-2-yl)-ethyl]-carbamic acid tert-butyl ester (0.4g, 1.038 mmol, 1 eq.) was dissolved in MeOH (70 ml) before Pd/C (0.2 g) was added and the reaction was placed under an atmosphere of H_2. The reaction was allowed to proceed for 4 hrs before being filtered through a pad of celite. The solvent was removed under reduced pressure to yield a mustard solid (0.33 g, 90% yield). **^{1}H NMR (500 MHz, DMSO-d$_6$) σ** 8.604 (d, 1 H, J = 8.39 Hz), 8.42 (d, 1 H, J = 7.05 Hz), 8.191 (d, 1 H, J = 8.39 Hz), 7.6539 (t, 1 H, J = 7.59 Hz), 7.3839 (s, 2 NH), 6.84 (d, 1 H, J = 8.47 Hz), 4.097 (t, 2 H, J = 5.95 Hz), 3.22 (q, 2 H, J = 6.2 Hz), 1.379 (s, NH), 1.2683 (s, 9 H); **^{13}C NMR** (125 MHz, DMSO-

d_6): 164.4716, 163.5858, 156.1299, 152.9727, 134.2628, 131.2949, 130.3129, 129.5576, 124.3589, 122.5508, 119.8571, 108.5024, 108.4046, 77.8726, 38.5433, 28.6136; **HRMS** (ESI): Calculated for $C_{19}H_{21}O_4N_3$ [M+H]+, expected: 355.1557, observed: 355.1532, PPM: 7.07; **νmax (film)/cm^{-1}:** 3366.18, 3257.63, 2976.80, 1701.80, 1677.65, 1659.51, 1634.51, 1528.80, 1480.76, 1447.57, 1427.25, 1368.58, 1273.04, 1246.82, 1170.18.

[2-(2-tert-Butoxycarbonylamino-ethyl)-1,3-dioxo-2,3-dihydro-1H-benzo[de]isoquinolin-6-yl]-carbamic acid 5-methyl-4-nitro-cyclopenta-1,3-dienylmethyl ester (34)

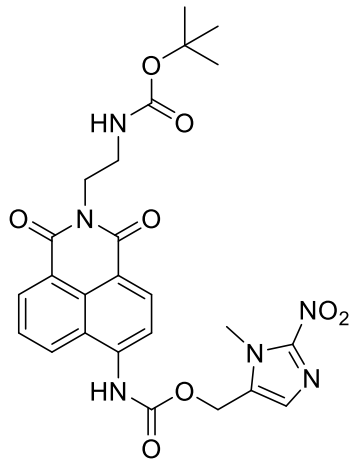

[2-(6-Amino-1,3-dioxo-1H,3H-benzo[de]isoquinolin-2-yl)-ethyl]-carbamic acid tert-butyl ester (53.27 mg, 0.15 mmol, 1 eq.) and DMAP (54.9 mg, 0.45 mmol, 3 eq.) were dissolved in anhydrous DCM (20 mL) and placed under an argon atmosphere. The reaction was cooled to -10°C using an ice and salt bath before phosgene solution (15 wt. % in toluene; 0.6 ml, 0.9 mmol, 6 eq.) was added dropwise and the reaction mixture was allowed warm to 0°C and stirred for 4 hrs. The reaction mixture was reduced to dryness by bubbling with argon before the residue was redissolved in anhydrous DCM and cooled to 0 °C (20 mL). (3-Methyl-2-nitro-3H-imidazol-4-yl)-methanol (70.7 mg, 0.45 mmol, 3 eq) was added and the reaction was allowed to return to room temp before being stirred overnight under an argon atmosphere. The reaction was quenched with water (10 mL) and extracted with DCM (3 x 10 ml). The resulting organic layer was dried

over $MgSO_4$ before the solvent was removed under reduced pressure. The resulting residue was purified by column chromatography eluting with Methanol/Dichloromethane (0:100 to 5:95) to yield a beige solid (35 mg, 43.7% yield). . **^{1}H NMR (500 MHz, DMSO-d_6) σ** 10.4 (s, NH), 8.677 (d, 1 H, J = 8.8 Hz), 8.5 (d, 1 H, J = 7.33 Hz), 8.48 (d, 1 H, J = 8.01 Hz), 8.1667 (d, 1 H, J = 8.13 Hz), 7.84 (t, 1 H, J = 7.65 Hz), 7.37 (s, NH), 6.868 (t, 1 H, J = 6.72 Hz), 5.4 (s, 2 H), 4.133 (t, 2 H, J = 6.13 Hz), 4.03 (s, 3 H), 3.26 (q, 2 H, J = 5.81 Hz), 1.223 (s, 9 H); **^{13}C NMR** (125 MHz, DMSO-d_6): 164.18, 163.63, 156.24, 153.92, 146.62, 133.52, 131.89, 131.24, 129.53, 129.47, 128.97, 126.85, 123.04, 119.07, 77.92, 56.46, 39.45, 38.25, 34.80, 28.52; **HRMS** (ESI): Calculated for $C_{25}H_{26}O_8N_6$ [M+H]+, expected: 538.1821, observed: 538.1812, PPM: 1.67; **νmax (film)/cm^{-1}:** 3386.43, 2977.00, 1742.88, 1690.60, 1654.27, 1592.06, 1547.60, 1496.41, 1427.17, 1387.29, 1368.27, 1352.74, 1242.34, 1204.44.

(3-Amino-propyl)-triphenyl-phosphonium (54)

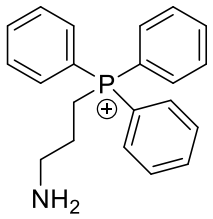

3-Bromo-propylamine (1.25 g, 5.719 mmol, 1 eq) and Triphenyl-phosphane (1.5 g, 5.719 mmol, 1 eq) were refluxed in acetonitrile (40 ml) for 24 hours. After the reaction, a white precipitate formed. Cooled down to RT and filtered the solid which was washed with dichloromethane (3 x 10 ml). finally yield a white solid. (0.849 g, 46.4% yield). **^{1}H NMR** (500 MHz, DMSO-d_6) σ 7.94 (m, 3 H), 7.81 (m, 12 H), 7.66 (s, 2 NH), 3.669 (t, 2 H, J = 15.37 Hz), 2.96 (t, 2 H, J = 7.93 Hz), 1.81 (sex, 2 H, J = 7.8 Hz); **^{13}C NMR** (125 MHz, DMSO-d_6): 135.6313, 135.6077, 134.1169, 134.0355, 130.9202, 130.8206, 118.8527, 118.1672, 20.6346, 18.9292, 18.5066; **HRMS** (ESI): Calculated for $C_{21}H_{23}NP$ [M+H]+, expected: 320.1556, observed: 320.1568, PPM: -3.82; **νmax (film)/cm^{-1}:** 3417.28, 2817.28, 2742.44,

2064.51, 1612.05, 1586.92, 1518.01, 1481.96, 1434.32, 1398.16, 1314.84, 1156.16, 1110.91, 995.27.

6-Nitro-2-[3-(triphenyl-l5-phosphanyl)-propyl]-benzo[de]isoquinoline-1,3-dione (55)

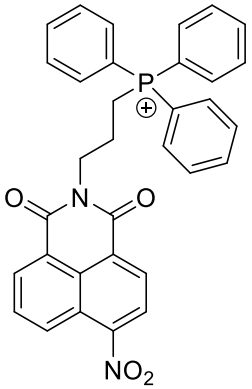

(3-Amino-propyl)-triphenyl-phosphonium (0.235 g, 0.734 mmol, 1 eq.) and 4-nitro-1,8-naphthalic anhydride (0.179 g, 0.734 mmol, 1 eq.) and trimethylamine (204.3 ul, 1.468 mmol, 2 eq) were dissolved in EtOH (14 mL) before being heated at 110 ^{o}C for 1 hr under microwave irradiation. The mixture was allowed to cool to room temperature before the solvent was removed under reduced pressure. The resulting residue was purified by column chromatography eluting with pure dichloromethane to 5% methanol in dichloromethane. The purified product was isolated as a yellow solid (0.566 g, 86.01% yield). **^{1}H NMR** (500 MHz, DMSO-d_6) σ 8.37 (dd, 1 H, J = 8.61/ 0.8 Hz), 8.64 (d, 1 H, J = 7.44 Hz), 8.59 (dd, 2 H, J = 14.28/ 8.17 Hz), 8.114 (dd, 1 H, J = 8.09/ 1.38 Hz), 7.9 (m, 3 H), 7.77 (m, 12 H), 4.25 (t, 2 H, J = 7.13 Hz), 3.75 (sex, 2 H, J = 5.82 Hz), 2.033 (sex, 2 H, J = 7.51 Hz); **^{13}C NMR** (125 MHz, DMSO-d_6): 163.76, 135.45, 134.14, 134.06, 132.11, 130.78, 130.68, 130.6, 130.0, 127.37, 124.67, 123.51, 119.08, 118.4, 9.33; **HRMS** (ESI): Calculated for $C_{33}H_{26}O_4N_2P$ [M+H]+, expected: 545.1598, observed: 545.163, PPM: -5.89; **νmax (film)/cm^{-1}:** 3422.11, 2936.96, 2677.07, 1705.43, 1664.94, 1585.8, 1526.05, 1437.82, 1345.84, 1250.93, 1113.21, 1033.75.

6-Amino-2-[3-(triphenyl-l5-phosphanyl)-propyl]-benzo[de]isoquinoline-1,3-dione (56)

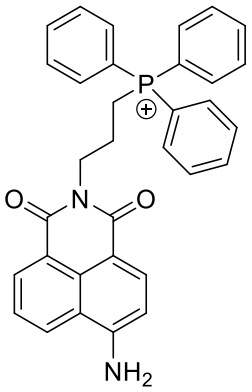

6-Nitro-2-[3-(triphenyl-l5-phosphanyl)-propyl]-benzo[de]isoquinoline-1,3-dione (0.4 g, 0.75 mmol, 1 eq.) was dissolved in MeOH (70 ml) before Pd/C (0.2 g) was added and the reaction was placed under an atmosphere of H_2. The reaction was allowed to proceed for 4 hrs before being filtered through a pad of celite. The solvent was removed under reduced pressure to yield a mustard solid (0.253g, 67% yield). **^{1}H NMR** (500 MHz, DMSO-d_6) σ 8.631 (dd, 1 H, J = 8.53/ 1.24 Hz), 8.4 (dd, 1 H, J = 7.38/ 1.11 Hz), 8.17 (d, 1 H, J = 8.45 Hz), 7.89 (m, 3 H), 7.77 (m, 12 H), 7.65 (t, 1 H, J = 7.87 Hz), 7.48 (s, 2H), 6.84 (d, 1 H, J = 8.34 Hz), 4.2 (t, 2 H, J = 7.27 Hz), 3.74 (qu, 2 H, J = 3.8 Hz), 1.96 (qu, 2 H, J = 7.89 Hz); **^{13}C NMR** (125 MHz, DMSO-d_6): 164.46, 163.49, 135.4, 134.48, 134.16, 134.08, 131.52, 130.74, 130.64, 130.33, 129.86, 124.43, 122.32, 119.84, 119.14, 118.45, 108.61, 107.98; **HRMS** (ESI): Calculated for $C_{33}H_{28}O_2N_2P$ [M+H]+, expected: 515.1862, observed: 515.1888, PPM: -5.05; **νmax (film)/cm^{-1}:** 3420.05, 3161.39, 1678.30, 1637.77, 1583.40, 1528.98, 1481.68, 1437.97, 1380.78, 1363.33, 1307.61, 1251.00, 1113.46.

{1,3-Dioxo-2-[3-(triphenyl-l5-phosphanyl)-propyl]-2,3-dihydro-1H-benzo[de]isoquinolin-6-yl}-carbamic acid 3-methyl-2-nitro-3H-imidazol-4-ylmethyl ester (35)

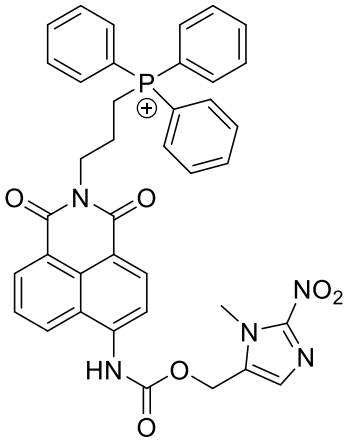

6-Amino-2-[3-(triphenyl-l5-phosphanyl)-propyl]-benzo[de]isoquinoline-1,3-dione (77.25 mg, 0.15 mmol, 1 eq.) and DMAP (54.98 mg, 0.45 mmol, 3 eq.) were dissolved in anhydrous DCM (20 mL) and placed under an argon atmosphere. The reaction was cooled to -10°C using an ice and salt bath before phosgene solution (15 wt. % in toluene; 0.6 ml, 0.9 mmol, 6 eq.) was added dropwise and the reaction mixture was allowed warm to 0°C and stirred for 4 hrs. The reaction mixture was reduced to dryness by bubbling with argon before the residue was redissolved in anhydrous DCM and cooled to 0 °C (20 mL). (3-Methyl-2-nitro-3H-imidazol-4-yl)-methanol (70.7 mg, 0.45 mmol, 3 eq) was added and the reaction was allowed to return to room temp before being stirred overnight under an argon atmosphere. The reaction was quenched with water (10 mL) and extracted with DCM (3 x 10 ml). The resulting organic layer was dried over $MgSO_4$ before the solvent was removed under reduced pressure. The resulting residue was purified by column chromatography eluting with Methanol/Dichloromethane (0:100 to 5:95) to yield a beige solid (17 mg, 16.3% yield). **^{1}H NMR** (500 MHz, DMSO-d_6) σ 10.23 (s, NH), 8.63 (dd, 1 H, J = 7.64/1.02 Hz), 8.40 (dd, 1 H, J = 6.47/0.75 Hz), 8.38 (d, 1 H, J = 8.23 Hz), 8.15 (d, 1 H, J = 8.34 Hz), 8.13 (d, 2 H, J = 6.78 Hz), 7.88 (m, 3 H), 7.76 (M, 12 H), 6.70 (dd, 2 H, J = 1.48/3.85 Hz), 4.299 (t, 2 H, J = 5.56 Hz), 4.20 (t, 2 H, J = 6.99 Hz), 3.75 (qu, 2 H, J = 6.79 Hz), 1.985 (t, 3 H, J = 4.89 Hz); **^{13}C NMR** (125 MHz, DMSO-d_6): 163.03, 162.388, 154.511, 153.981, 144.486, 134.085, 132.703, 132.624, 130.769, 129.565, 129.465, 124. 668, 117.581, 116.896, 114.66, 105.57, 49.75, 38.44, 24.97; **HRMS** (ESI): Calculated for $C_{39}H_{33}O_6N_5P$ [M+H]+, expected: 698.2169, observed: 698.2241, PPM:1.03; **νmax (film)/cm^{-1}:** 3416.92, 2923.49, 1726.22, 1693.35, 1650.65, 1587.65, 1542.51, 1438.09, 1391.55, 1363.68, 1212.60, 1108.33.

6-(6-Nitro-1,3-dioxo-1H,3H-benzo[de]isoquinolin-2-yl)-hexanoic acid (57)

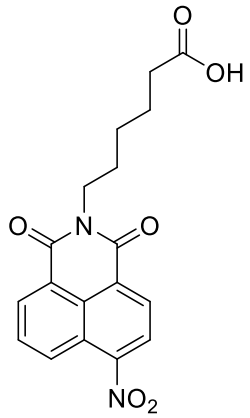

6-Amino-hexanoic acid (0.404 g, 3.084 mmol, 1 eq.) and 4-nitro-1, 8-naphthalic anhydride (0.75 g, 3.084 mmol, 1 eq.) were dissolved in EtOH (15 mL) before being heated at 110 ºC for 1 hr under microwave irradiation. The mixture was allowed to cool to room temperature before the solvent was removed under reduced pressure. The resulting residue was purified by column chromatography eluting with pure dichloromethane to 5% methanol in dichloromethane. The purified product was isolated as an orange solid (0.9743 g, 88.74% yield). **^{1}H NMR** (500 MHz, DMSO-d_6) σ 8.84 (d, 1 H, J = 8.72 Hz), 8.74 (d, 1 H, J = 7.38 Hz), 8.695 (d, 1 H, J = 8.13 Hz), 8.409 (d, 1 H, J = 7.89 Hz), 7.992 (t, 1 H, J = 7.89 Hz), 4.196 (t, 2 H, J = 7.196 Hz), 2.38 (t, 2 H, J = 7.38 Hz), 1.75 (m, 4 H), 1.495 (qu, 2 H, J = 7.72); **^{13}C NMR** (125 MHz, DMSO-d_6): 163.3252, 162.5042, 149.6122, 132.4993, 129.9637, 129.8619, 139.3619, 129.1181, 126.981, 123.9221, 123.7088, 123.0075, 40.542, 27.6088, 26.4552, 24.3196; ; **HRMS** (ESI): Calculated for $C_{18}H_{16}O_6N_2$ [M+H]+, expected: 379.0901, observed: 379.0984, PPM: 2.91; **νmax (film)/cm^{-1}:** 3078.02, 2943.60, 2865.89, 1703.30, 1624.88, 1593.97, 1583.18, 1521.67, 1460.75, 1437.15, 1410.20, 1339.84, 1261.87, 1230.39, 1182.72, 1157.54, 1121.24, 1079.16.

6-(6-Amino-1,3-dioxo-1H,3H-benzo[de]isoquinolin-2-yl)-hexanoic acid (58)

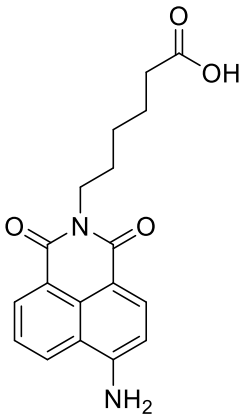

6-(6-Nitro-1,3-dioxo-1H,3H-benzo[de]isoquinolin-2-yl)-hexanoic acid (07.g, 1.9662 mmol, 1 eq.) was dissolved in MeOH (45 ml) before Pd/C (0.2 g) was added and the reaction was placed under an atmosphere of H_2. The reaction was allowed to proceed for 4 hrs before being filtered through a pad of celite. The solvent was removed under reduced pressure to yield a brownish red solid (0.6 g, 93.75 % yield). **^{1}H NMR** (500 MHz, DMSO-d_6) σ 8.618 (d, 1 H, J = 8.48 Hz), 8.434 (d, 1 H, J = 7.07 Hz), 8.198 (d, 1 H, J = 8.48 Hz), 7.66 (t, 1 H, J = 7.46Hz), 7.441 (s, 2 NH), 6.849 (d, 1 H, J = 8.5 Hz), 3.997 (t, 2 H, J = 7.48 Hz), 2.21 (t, 2 H, J = 7.48 Hz), 1.6 (qu, 2 H, J = 7.4 Hz), 1.54 (qu, 2 H, J = 7.4 Hz), 1.32 (qu, 2 H, J = 8.07 Hz); **^{13}C NMR** (125 MHz, DMSO-d_6): 174.9314, 164.2348, 163.3670, 153.171, 134.4343, 131.4837, 130.1530, 129.7605, 124.4667, 122.2607, 119.8384, 108.6363, 108.0192, 34.0072, 27.9025, 26.5495, 24.7321; **HRMS** (ESI): Calculated for $C_{18}H_{18}O_4N_2$ [M+H]+, expected: 326.1262, observed: 326.1267, PPM: -1.52; **νmax (film)/cm^{-1}:** 3429.86, 3358.01, 3243.00, 2949.90, 2855.03, 1750.98, 1651.27, 1623.59, 1606.81, 1532.14, 1482.77, 1454.40, 1432.92, 1376.46, 1310.12, 1248.28.

6-[6-(3-Methyl-2-nitro-3H-imidazol-4-ylmethoxycarbonylamino)-1,3-dioxo-1H,3H-benzo[de]isoquinolin-2-yl]-hexanoic acid (33)

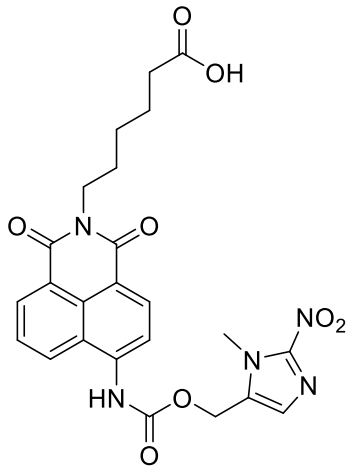

6-(6-Amino-1,3-dioxo-1H,3H-benzo[de]isoquinolin-2-yl)-hexanoic acid (48.918 mg, 0.15 mmol, 1 eq.) and DMAP (54.98 mg, 0.45 mmol, 3 eq.) were dissolved in anhydrous DCM (20 mL) and placed under an argon atmosphere. The reaction was cooled to -10°C using an ice and salt bath before phosgene solution (15 wt. % in toluene; 0.6 ml, 0.9 mmol, 6 eq.) was added dropwise and the reaction mixture was allowed warm to 0°C and stirred for 4 hrs. The reaction mixture was reduced to dryness by bubbling with argon before the residue was redissolved in anhydrous DCM and cooled to 0 °C (20 mL). (3-Methyl-2-nitro-3H-imidazol-4-yl)-methanol (70.7 mg, 0.45 mmol, 3 eq) was added and the reaction was allowed to return to room temp before being stirred overnight under an argon atmosphere. The reaction was extracted with DCM (3 x 10 ml). The resulting organic layer was dried over $MgSO_4$ before the solvent was removed under reduced pressure. The resulting residue was purified by HPLC Technique eluting with water/acetonitrile from 1 : 0 to 0 : 1 to yield the pare yellow solid (7 mg, 9.1% yield) **^{1}H NMR** (500 MHz, DMSO-d_6) σ 8.68 (dd, 1 H, J = 8.61/1.03 Hz), 8.52 (dd, 1 H, J = 7.28/1.03 Hz), 8.5 (d, 1 H, J = 8.3 Hz), 8.18 (d, 1 H, J = 8.08 Hz), 7.85 (dd, 1 H, J = 1.17/7.4 Hz), 7.37 (s, 1 H), 5.41 (s, 2 H), 4.035 (t, 2 H, J = 7.17 Hz), 4.03 (s, 3 H), 1.64 (qu, 2 H, J = 7.68 Hz), 1.55 (qu, 2 H, J = 7.87 Hz), 1.35 (qu, 2 H, J = 8.56 Hz)); **^{13}C NMR** (125 MHz, DMSO-d_6): 163.39, 157.39, 139.46, 139.14, 133.49, 129.48, 129.15, 128.65, 127.06, 107.41, 55.37, 53.39, 34.84, 34.61, 34.58, 33.48, 26.28, 24.49; **HRMS** (ESI): Calculated for $C_{24}H_{23}O_8N_5$ [M+H]+, expected: 509.1539, observed: 509.1547, PPM: -1.46; **νmax (film)/cm^{-1}:** 3410.26, 3347.58, 3101.01, 2953.86, 1740.33, 1701.24, 1690.50, 1592.41, 1487.64, 1377.63, 1369.72, 1354.60, 1245.35, 1205.34

2-Amino-3-methyl-3H-imidazole-4-carboxylic acid ethyl ester (39)

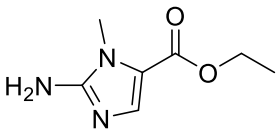

30 ml of Ethyl formate was added to 100 ml round bottle flask with sarcosine ethyl ester hydrochloride (2 g, 13.01 mmol, 1 eq) in it. Slowly added potassium tert butoxide (2.19 g, 19.53 mmol, 1.5 eq) to flask for 0.5 hr and stirred for 2 hr at room temperature. In addition, potassium tert-butoxide (2.91 g, 26.04 mmol, 2 eq) was added at 10 C for 2 hr. 30 ml of brine and 10 ml of toluene were added. Mixed and filtered the aqueous layer, which was washed with toluene (10 ml * 2) to remove Ethyl formate. 5.5 ml of conc HCl and Ethylene glycol (3.5 g, 19.515 mmol, 1.5 eq) were added, stirred for 1 hr at 58 C. Sodium acetate (8 g, 97.5 mmol, 7.49 eq) was added in the flask to adjust the ph to 4.5. Cyanamide (1.09 g, 26.02 mmol, 2 eq) was added and the reaction was stirred for 2 hr at 87 C. After the reaction, cool down the solvent with ice bath. 30% Sodium hydroxide solution was used to adjust the ph to 9. Keep the solution for 10 mins and then filtered the solid to yield pare yellow compound (1.45 g, 66.2 % yield). **^{1}H NMR** (500 MHz, DMSO-d_6) σ 7.28 (s, 1 H), 6.1889 (S, 2 NH), 4.156 (q, 2 H, J = 7.12 Hz), 3.5258 (s, 3 H), 1.239 (t, 3 H, J = 7.12 Hz); **^{13}C NMR** (125 MHz, DMSO-d_6): 160.2032, 154.8042, 136.5759, 117.3921, 59.3449, 30.6925, 14.8355; **HRMS** (ESI): Calculated for $C_7H_{11}O_3N_2$ [M+H]+, expected: 169.0851, observed: 169.0851, PPM: 0.01; **νmax (film)/cm^{-1}:** 3394.02, 3133.32, 2987.61, 1547.62, 1480.84, 1460.16, 1380.70, 1349.74, 1304.94, 1247.22, 1213.03, 1172.40, 1127.78, 1110.33.

3-Methyl-2-nitro-3H-imidazole-4-carboxylic acid ethyl ester (40)

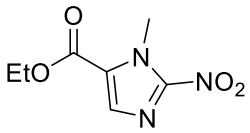

To an aqueous solution of sodium nitrite (6 ml, 4.08 g, 59.2 mmol, 10 eq) was added aminoimodazole (1 g, 5.92 mmol, 1 eq) in acetic acid (10 ml) in a dropwise manner. This reaction was stirred for 4 hr at room temperature when there was no nitrogen gas evolved. The organic layer was extracted with dichloromethane (2 * 10 ml), washed with brine (1 *20 ml) and saturated aqueous solution of sodium sulfite (1 * 20 ml), dried with magnesium sulfate, and filtered. The filtrate was concentrated in vacuo, and the product was purified by silica gel column chromatography, eluting with dichloromethane, to yield a white crystal (0.8 g, 69.7 % yield). **^{1}H NMR** (500 MHz, DMSO-d_6) σ 7.79 (s, 1 H), 4.34 (q, 2 H, J = 7.06 Hz), 4.188 (s, 3 H), 1.327 (t, 3 H, J = 7.14 Hz); **^{13}C NMR** (125 MHz, DMSO-d_6): 159.2626, 134.2536, 126.5996, 61.90, 55.35, 35.7, 14.45; **HRMS** (ESI): Calculated for $C_7H_9O_4N_3$ [M+H]+, expected: 199.0604, observed: 199.0593, PPM: 5.7; **νmax (film)/cm^{-1}:** 3433.14, 2984.44, 1554.60, 1521.61, 1488.95, 1422.68, 1367.58, 1332.08, 1286.76, 1241.99, 1183.37, 1144.26, 1105.38.

3-Methyl-2-nitro-3H-imidazole-4-carboxylic acid (41)

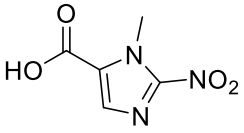

To 3-Methyl-2-nitro-3H-imidazole-4-carboxylic acid ethyl ester (563 mg, 2.814 mmol, 1 eq), was added a 1 N aqueous solution of NaOH (0.6 g in 15 ml water), and the resulting suspension was stirred for O/N. After this time the reaction solution was acidified to ph 1 using conc HCl, resulting the formation of white precipitate. The organic compound was extracted with EtOAc (5 * 20 ml), the organic layers combined and dried over MgSO4, and filtered. The filterate was

concentrated in vacuo, to finally yield a white solid (417 mg, 87 % yield). **^{1}H NMR** (500 MHz, DMSO-d_6) σ 7.73 (s, 1 H), 4.19 (s, 3 H); **^{13}C NMR** (125 MHz, DMSO-d_6): 160.8163, 134.1750, 127.5690, 35.5296, 34.7931; **HRMS** (ESI): Calculated for $C_5H_5O_4N_3$ [M+H]+, expected: 171.0264, observed: 171.028, PPM: -8.88; **νmax (film)/cm^{-1}:** 3417.52, 3147.68, 2856.25, 2541.83, 1850.15, 1171.20, 1558.62, 1522.81, 1489.13, 1435.84, 1363.41, 1328.62, 1287.35, 1247.06, 1177.86, 1109.83.

(3-Methyl-2-nitro-3H-imidazol-4-yl)-methanol (36)

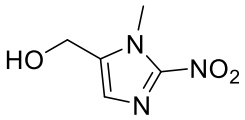

To a 100 ml round bottom flask with anhydride THF (30 ml) at -15 C with salt/ice bath, was added 3-Methyl-2-nitro-3H-imidazole-4-carboxylic acid (363 mg, 2.123 mmol, 1 eq) and trimethylamine (0.504 ml, 3.609 mmol, 1.7 eq). Isobutyl Chloroformate (0.44 ml, 3.396 mmol, 1.6 eq) was added dropsied during 10 min. The reaction was stirred for 1 hr at -15 C. Sodium borohydride (401.53 mg, 10.614 mmol, 5 eq) was added and keep stirring for 5 min, then 15 ml water was added slowly (if bubble come out, then wait for a while until bubble was gone and the temperature back to – 5 C). Kept the reaction at 0 C for 1 hr. The reaction was filtered to remove the precipitate which was washed with THF. Combined the organic layer and then separated the aqueous layer, and dried the organic layer with MgSO4, and removed the solvent to yield the yellow solid (167 mg, 50.1 % yield). **^{1}H NMR** (500 MHz, DMSO-d_6) σ 7.12 (s, 1 H), 5.499 (t, 1 H, J = 5.46 Hz), 4.545 (dd, 2 H, J = 5.45/ 0.3 Hz), 3.92 (s, 3 H); **^{13}C NMR** (125 MHz, DMSO-d_6): 139.1334, 127.0317, 61.2139, 34.5766, 23.6741; **HRMS** (ESI): Calculated for $C_5H_7O_3N_3$ [M+H]+, expected: 157.0488, observed: 157.0487, PPM: 0.62; **ν_{max} (film)/cm^{-1}:** 3255.43, 2965.39, 1748.04, 1540.11, 1494.33, 1468.35, 1397.20, 1362.13, 1331.34, 1277.34, 1242.07, 1188.88, 1124.27, 1042.72.

References

[1] Adams, J.M. and Cory, S, “The Bcl-2 apoptotic switch in cancer development and therapy.,” *Oncogene,* vol. 26, p. 1324–1337, 2007.

[2] Devita VT Jr, Rosenberg SA, “Two Hundred Years of Cancer Research,” *N Engl J Med,* vol. 366(23), pp. 2207-2214, 2012.

[3] Douglas Hanahan,Robert AWeinberg, “The Hallmarks of Cancer,” *Cell,* vol. 100, pp. 57-70, 2000.

[4] Douglas Hanahan, Robert A. Weinberg, “Hallmarks of Cancer: The Next Generation,” *Cell,* vol. 144, p. 646–674, 2011.

[5] Fedi, P., Tronick, S.R., and Aaronson, S.A, *Cancer Medicine,* p. 41–64, 1997.

[6] R. Weinberg, “ The retinoblastoma protein and cell cycle control,” *Cell,* vol. 81, p. 323–330, 1995.

[7] A. Levine, “p53, the cellular gatekeeper for growth and division,” *Cell,* vol. 88(3), pp. 323-331, 1997.

[8] Wright, W.E., Pereira-Smith, O.M., and Shay, J.W. , “Reversible cellular senescence: implications for immortalization of normal human diploid fibroblasts.,” *Mol. Cell. Biol,* vol. 9, p. 3088–3092, 1989.

[9] Bryan, T.M., Englezou, A., Gupta, J., Bacchetti, S., and Reddel, R.R., “Telomere elongation in immortal human cells without detectable telomerase activity.,” *EMBO J.,* vol. 14, p. 4240–4248, 1995.

[10] Volpert, O.V., Dameron, K.M., and Bouck, N., “Sequential development of an angiogenic phenotype by human fibroblasts progressing to tumorigenicity.,” *Oncogene,* vol. 14, p. 1495–1502, 1997.

[11] Christofori, G., Naik, P., and Hanahan, D., “A second signalsupplied by insulin-like growth factor II in oncogene-induced tumorigenesis.,” *Nature,* vol. 369, p. 414–418, 1994.

[12] Holmgren, L., Szeles, A., Rajnavolgyi, E., Folkman, J., Klein, G.,Ernberg, I., and Falk, K.I., “Horizontal transfer of DNA by theuptake of apoptotic bodies.,” *Blood ,* vol. 93, p. 3956–3963, 1999.

[13] Gilkes, Daniele M., Gregg L. Semenza, and Denis Wirtz., “Hypoxia and the extracellular matrix: drivers of tumour metastasis.,” *Nature Reviews Cancer,* vol. 14.6, pp. 430-439, 2014.

[14] Sorg BS, Hardee ME, Agarwal N, Moeller BJ, Dewhirst MW., “Spectral imaging facilitates visualization and measurements of unstable and abnormal microvascular oxygen transport in tumours.,” *J Biomed Opt,* vol. 13, p. 014026, 2008.

[15] Casazza A, Di Conza G, Wenes M, et al. , “Tumor stroma:a complexity dic tated by the hypoxic tumor microenvironment[J],” *Oncogene,* vol. 33(14), pp. 1743-1754, 2014.

[16] Pries AR, Cornelissen AJ, Sloot AA, et al. , “Structural adaptation and heterogeneity of normal and tumor microvascular networks[J],” *PLoS Comput Biol,* vol. 5(5), p. 1000394, 2009.

[17] Vaupel P, Harrison L. , “Tumor hypoxia:causative factors, compensatory mechanisms, and cellular response[J].,” *Oncologist,* vol. 9(Suppl 5), pp. 4-9, 2004.

[18] Yu Chen; Longqin Hu;, *Medicinal Research Reviews,* vol. 29, pp. 29-64, 2009.

[19] Yuhao Li; Yun Sun; Jiachang Li; Qianqian Su; Wei Yuan; Yu Dai; Chunmiao Han; Qiuhong Wang; Wei Feng; Fuyou Li; , *J. Am. Chem. Soc.,* vol. 137, pp. 6407-6416, 2015.

[20] C. Bayer, P. Vaupel, , *Journal of Radiation Oncology, Biology, Physics, ,* vol. 188, pp. 616-627, 2012.

[21] Xiao Hui Wang; Guo ren Yang; ; Chinese Journal of Oncoradiology 2009, Vol 2 No 2, “A Compendium for the Progress in the Principium and Imaging of Tumor Hypoxia,” *CONTEMPORARY MEDICINE,* vol. 15, p. 8, 2009.

[22] M. R. Horsman, “Measurement of tumor oxygenation,,” *Int, J. Radiat. Oncol. Biol. Phys. ,* vol. 42, pp. 701-704, 1998.

[23] Delides GS1, Venizelos J, Révész L., “Vascularization and curability of stage III and IV nasopharyngeal tumors.,” *J Cancer Res Clin Oncol.,* vol. 114, pp. 321-323, 1988.

[24] James A. Raleigh, Mark W. Dewhirst, Donald E. Thrall, “Measuring tumor hypoxia,” *seminars in radiat oncol,* vol. 6, pp. 37-45, 1996.

[25] F. S. Gold P, “ Demonstration of tumor specific antigen in human colonic carcinoma by immunologic tolerance and absorption techniques [J].,” *Exp Med, ,* vol. 12 (7), pp. 439-442, 1965.

[26] JiongWei Pan, Zhuo Cao, *J of Radioimmunology* , vol. 26 (3), pp. 293-296, 2013.

[27] Yagihashi A, Asanuma K, Kobayashi D, et al. , "autoantibodies to surviving in patients with chronic hepatitis and hepatocellular carcinoma [J].," *Autoilnlnunity,,* vol. 38 (6): , pp. 445-448., 2005, .

[28] Salsi V, Ferrari S, Ferraresi R, et al. , "HOXD13 binds DNA replication origins to promote origin licensing and is inhibited by geminin [J].," *Mol Cell Biol, ,* vol. 29 (21), pp. 5775-5788, 2009, .

[29] S. G. a. J. K. M. A. J. Varghese, *Cancer Res,* Vols. 36, , pp. 3761-3765., 1976, .

[30] C. B. Brezden, L. Horn, R. A. McClelland and A. M. Rauth, , *Biochem. Pharmacol.,* Vols. 56,, pp. 335-344., 1998, .

[31] W. A. Denny, *Future Oncol,* vol. 6, pp. 419-428, 2010.

[32] S. Kizaka-Kondoh and H. Konse-Nagasawa, , *Cancer Sci,* vol. 100, p. 1366–1373, 2009.

[33] J. Wu, B. Kwon, W. Liu, E. V. Anslyn, P. Wang and J. S. Kim, , *Chem. Rev.,* Vols. 115, , p. 7893–7943., 2015, .

[34] Z. Yang, J. Cao, Y. He, J. H. Yang, T. Kim, X. Peng and J. S. Kim, , *Chem. Soc. Rev., ,* Vols. 43, , p. 4563–4601., 2014, .

[35] G. N. Parkinson, J. V. Skelly and S. Neidle,, *J. Med. Chem., ,* Vols. 43, , p. 3624–3631., 2000,.

[36] E. M. Williams, R. F. Little, A. M. Mowday, M. H. Rich, J. V. E. ChanHyams, J. N. Copp, J. B. Smaill, A. V. Patterson and D. F. Ackerley, , *Biochem. J., ,* Vols. 471, , p. 131–153., 2015, .

[37] R. B. P. Elmes, *ChemComm, ,* vol. 10., p. 1039, 2016.

[38] P. L. Olive and R. E. Durand, , *Cancer Res., ,* Vols. 43, , p. 3276–3280, 1983, .

[39] Zhan Rong Liu, Yonghe Tang, An Xu, Weiying Lin; , *Biosensors and Bioelectronics,,* Vols. Vol 89, Part 2, pp. 853-858, 2017,.

[40] L. Cui, Y. Zhong, W. Zhu, Y. Xu, Q. Du, X. Wang, X. Qian and Y. Xiao, , *Org. Lett., ,* Vols. 13, , p. 928–931., 2011, .

[41] Z. Li, X. Li, X. Gao, Y. Zhang, W. Shi and H. Ma, , *Anal. Chem., ,* Vols. 85, , pp. 3926-3932., 2013, .

[42] Chen, W.; Li, Z.; Shi, W.; Ma, H. M. , *Chem. Commun. (Cambridge, U.K.)* , Vols. 48, , p. 2809−2811., 2012, .

[43] Zhang, Y. Y.; Chen, W.; Feng, D.; Shi, W.; Li, X. H.; Ma, H. M. , *Analyst* , Vols. 137, , p. 716−721. , 2012, .

[44] M. Dai, W. Zhu, Y. Xu, X. Qian, Y. Liu, Y. Li and Y. You, , *J. Fluoresc.*, Vols. 18, , pp. 591-597., 2008,.

[45] J. Xu, S. Sun, Q. Li, Y. Yue, Y. Li and S. Shao, *Analyst,*, Vols. 140,, p. 574–581, 2015.

[46] A. Harriman, L. J. Mallon, G. Ulrich and R. Ziessel,, *Chemphyschem,* vol. 8, pp. 1207-1214, 2007.

[47] D. Wang, R. Miyamoto, Y. Shiraishi and T. Hirai, *langmuir,* vol. 25, pp. 13176-13182, 2009.

[48] J. Xu, Q. Li, Y. Yue, Y. Guo and S. Shao, *Biosens. Bioelectron,* vol. 56, pp. 58-63, 2014.

[49] Y. Li, Y. Sun, J. Li, Q. Su, W. Yuan, Y. Dai, C. Han, Q. Wang, W. Feng and F. Li, , *J. Am. Chem. Soc,* vol. 137, p. 6407–6416, 2015,.

[50] T. Guo, L. Cui, J. Shen, W. Zhu, Y. Xu and X. Qian, , *Chem. Commun,* Vols. 49, , p. 10820., 2013, .

[51] S. Wang, H. Liu, J. Mack, J. Tian, B. Zou, H. Lu, Z. Li, J. Jiang and Z. Shen, *Chem. Commun,* vol. 51, p. 13389, 2015.

[52] A. Rajapakse and K. S. Gates, , *J. Org. Chem,* vol. 77, p. 3531–3537, 2012.

[53] Lei Cui, Ye Zhong, Weiping Zhu, Yufang Xu, Qingshan Du, Xin Wang, Xuhong Qian and Yi Xiao,, *Org. Lett,* vol. 13 (5), p. 928–931, 2011.

[54] Liam J. O'Connor, Cindy Cazares-Körner, Jaideep Saha, Charles N. G. Evans, Michael R. L. Stratford, Ester M. Hammond and Stuart J. Conway, “Efficient synthesis of 2-nitroimidazole derivatives and the bioreductive clinical candidate Evofosfamide (TH-302,” *Org. Chem. Front,* vol. 2, pp. 1026-1029, 2015.

[55] R. H. G. F. e. a. Bourgeois M, *Nucl Med Rev,* vol. 14, pp. 90-95, 2011.

[56] A. Chevalier, Y. Zhang, O. M. Khdour, J. B. Kaye and S. M. Hecht,, *J. Am. Chem. Soc,* vol. 138, p. 12009., 2016.

[57] Z. Li, X. Gao, W. Shi, X. Li and H. Ma, *Chem. Commun,* vol. 49, p. 5859, 2013.

[58] T. Guo, L. Cui, J. Shen, W. Zhu, Y. Xu and X. Qian, *Chem. Commun*, vol. 49, p. 10820–10822, 2013.

[59] HAN Min, LI Chang, GUO Wang-wei, LIU Hui-na, LIANG Wen-quan, GAO Jian-qing., " Mitochondrial drug delivery for cancer therapy[J].," *Acta Pharm Sin,,* vol. 51(2), pp. 257-263, 2016.

[60] Newmeyer DD, Ferguson-Miller S., " Mitochondria:releas-ing power for life and unleashing the machineries of death[J]," *Cell,* vol. 112, pp. 481-490, 2003.

[61] Zupančič Š, Kocbek P, Gulrez Zariwala M, et al. , "Design and development of novel mitochondrial targeted nanocarriers, DQAsomes for curcumin inhalation[J]," *Mol Pharm*, vol. 11, pp. 2334-2345, 2014.

[62] Chang J, Jung HJ, Park HJ, et al., "Cell-permeable mitochon-drial ubiquinol-cytochrome c reductase binding protein induces angiogenesis in vitro and in vivo[J].," *Cancer Lett,* vol. 366, pp. 52-60, 2015.

[63] Carroll B, Korolchuk VI, Sarkar S. , "Amino acids and auto-phagy:cross-talk and co-operation to control cellular homeostasis[J]," *Amino Acids,* vol. 47, pp. 2065-2088, 2015.

[64] Biswas S, Dodwadkar NS, Deshpande PP, et al., "Liposomes loaded with paclitaxel and modified with novel triphenylphos-phonium-PEG-PE conjugate possess low toxicity, target mito-chondria and demonstrate enhanced antitumor effects in vitro and in vivo[J].," *J Control Release,* vol. 159, pp. 393-402, 2012.

[65] Arnaud Chevalier, Yanmin Zhang, Omar M. Khdour, Justin B. Kaye, and Sidney M. Hecht, "Mitochondrial Nitroreductase Activity Enables Selective Imaging and Therapeutic Targeting," *J. Am. Chem. Soc,* vol. 138 (37), p. 12009–12012, 2016.

[66] Barros, R. C.; Gelens, E.; Bulten, E.; Tuin, A.; de Jong, M. R.; Kuijer, R.; van Kooten, T. G., *J. Biomed. Mater. Res,* 2017.

Chapter 7 Appendix

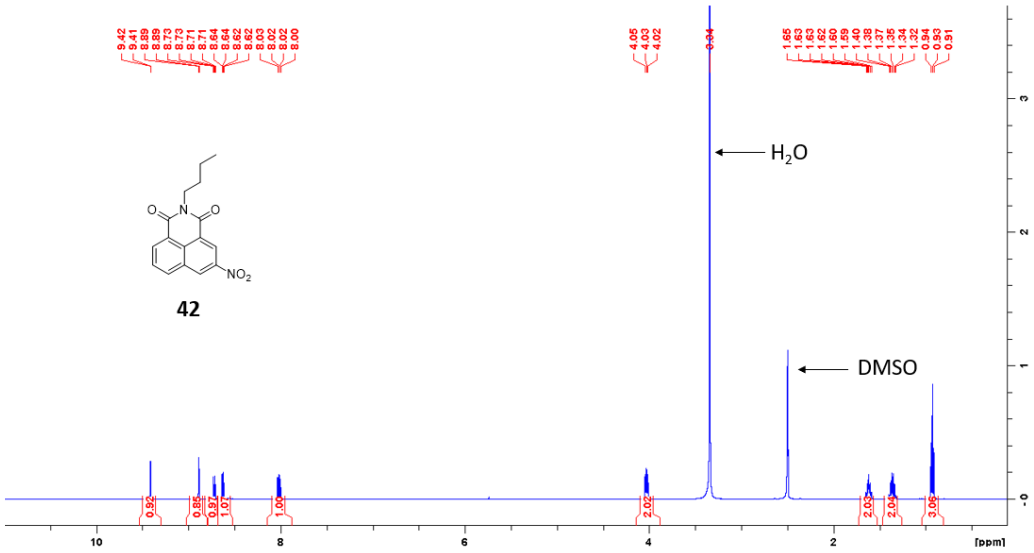

*Figure 7-1: The ^{1}H NMR spectrum of compound **42** (500 MHz, DMSO-d_6)*

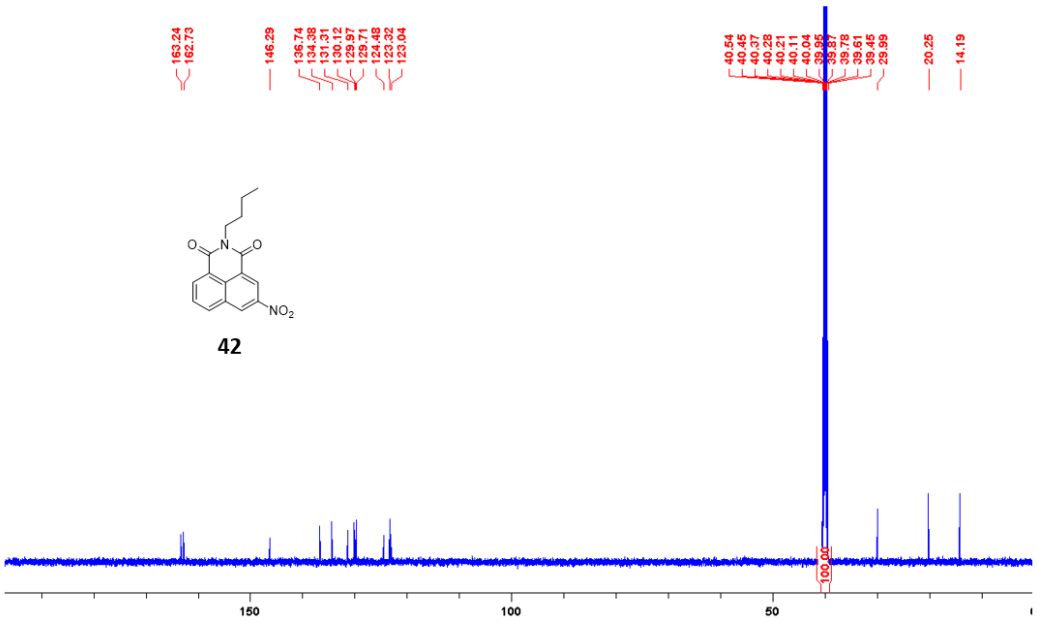

*Figure 7-2: The ^{13}C NMR spectrum of compound **42** (125 MHz, DMSO-d_6)*

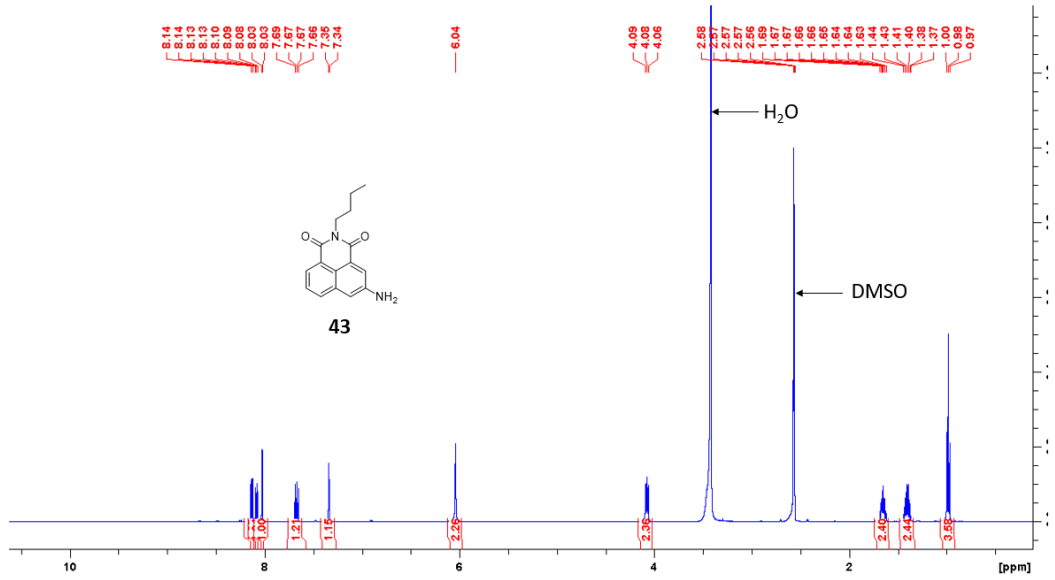

*Figure 7-3: The ^{1}H NMR spectrum of compound **43** (500 MHz, DMSO-d_6)*

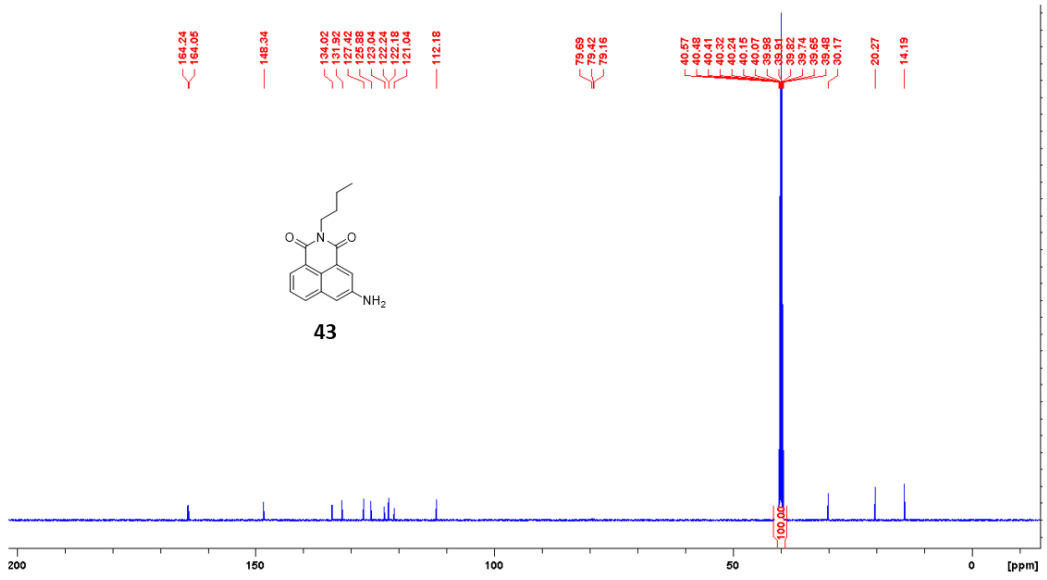

*Figure 7-4: The ^{13}C NMR spectrum of compound **43** (125 MHz, DMSO-d_6)*

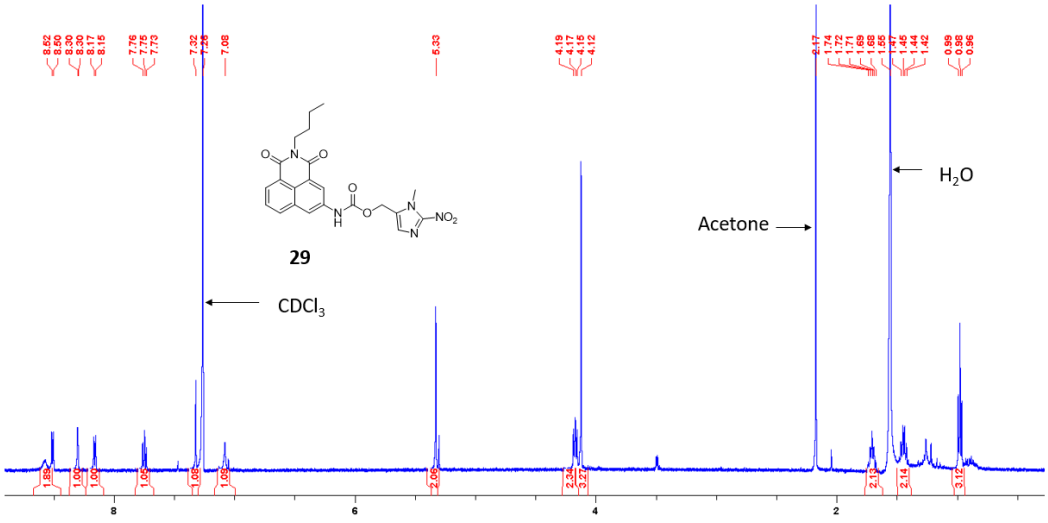

*Figure 7-5: The ^{1}H NMR spectrum of compound **29** (500 MHz, $CDCl_3$)*

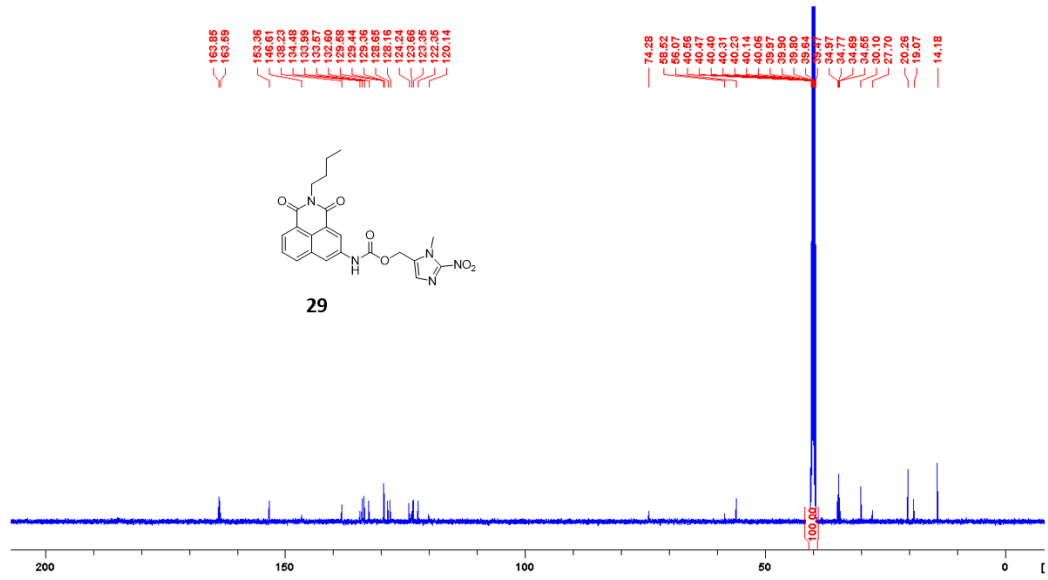

*Figure 7-6: The ^{13}C NMR spectrum of compound **29** (125 MHz, $CDCl_3$)*

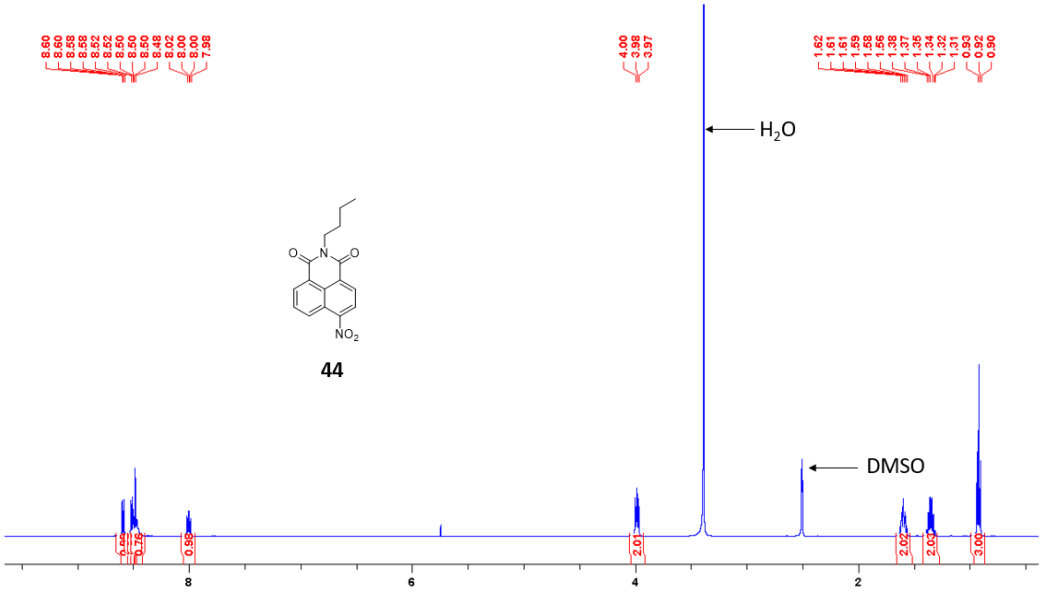

*Figure 7-7: The ^{1}H NMR spectrum of compound **44** (500 MHz, DMSO-d_6)*

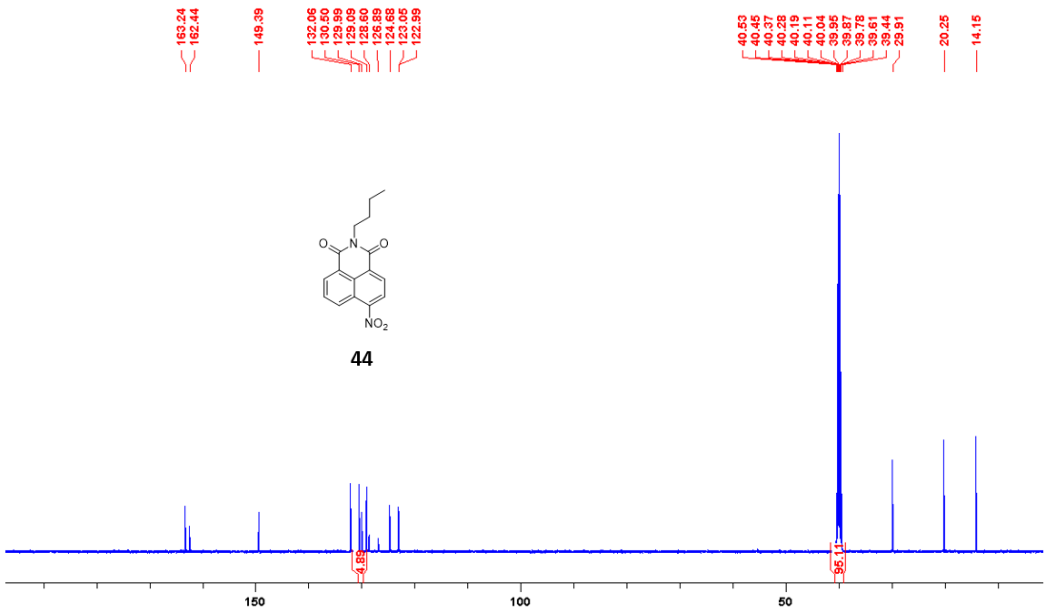

*Figure 7-8: The ^{13}C NMR spectrum of compound **44** (125 MHz, DMSO-d_6)*

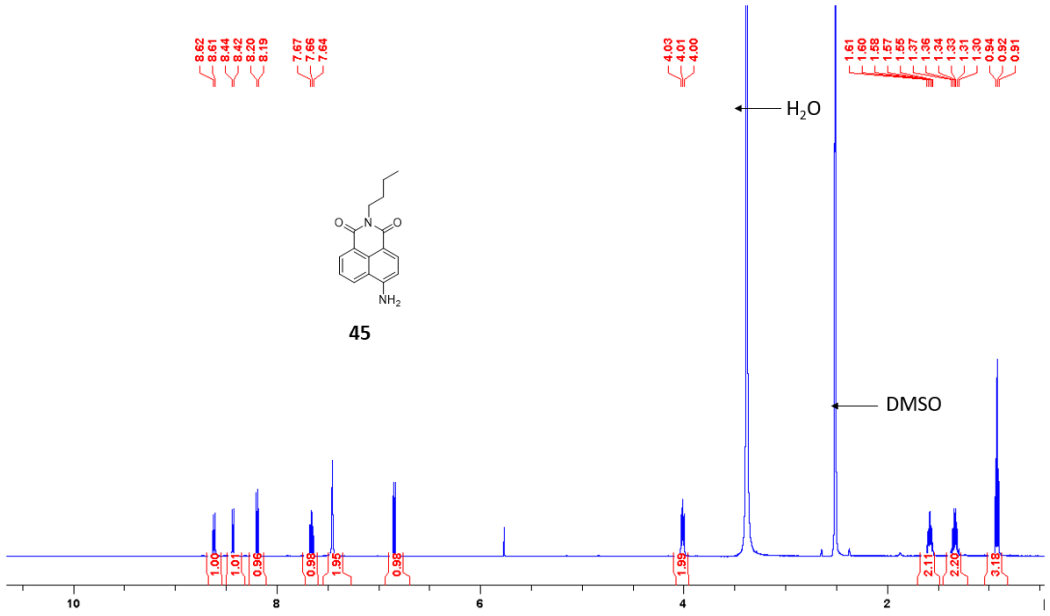

*Figure 7-9: The ^{1}H NMR spectrum of compound **45** (500 MHz, DMSO-d_6)*

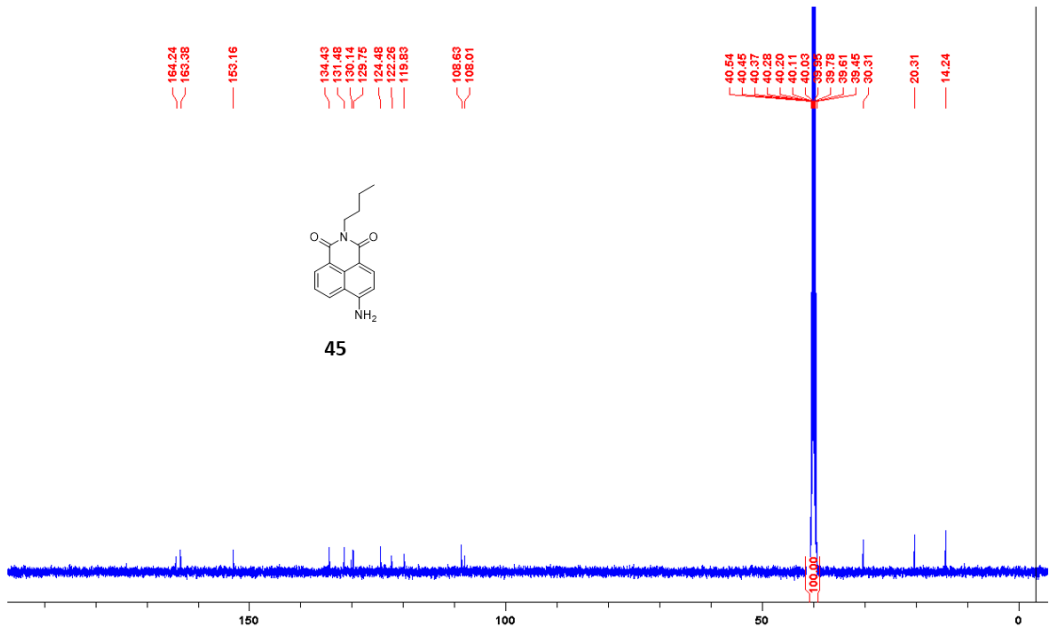

*Figure 7-10: The ^{13}C NMR spectrum of compound **45** (125 MHz, DMSO-d_6)*

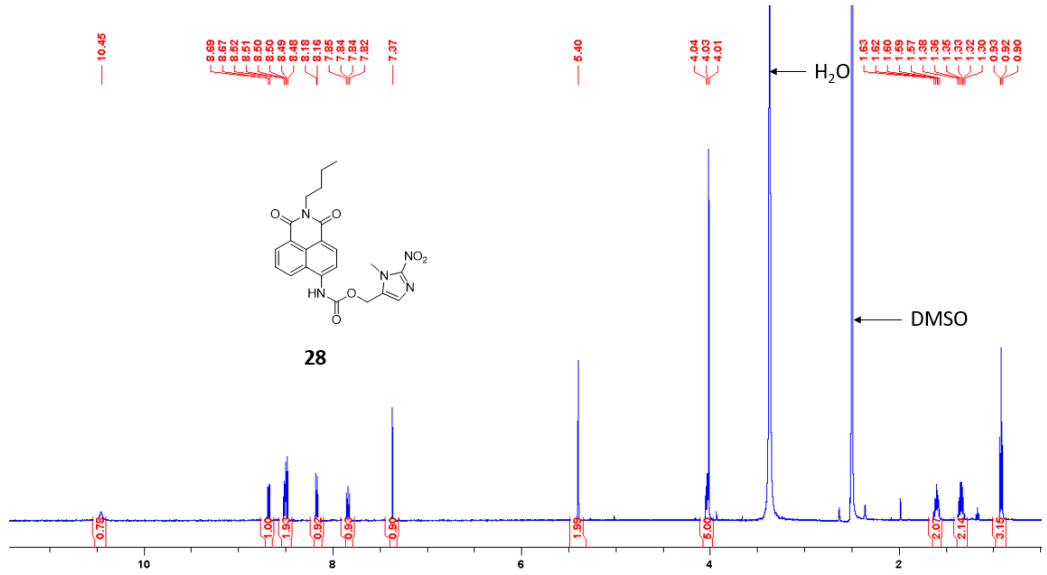

*Figure 7-11: The ^{1}H NMR spectrum of compound **28** (500 MHz, DMSO-d_6)*

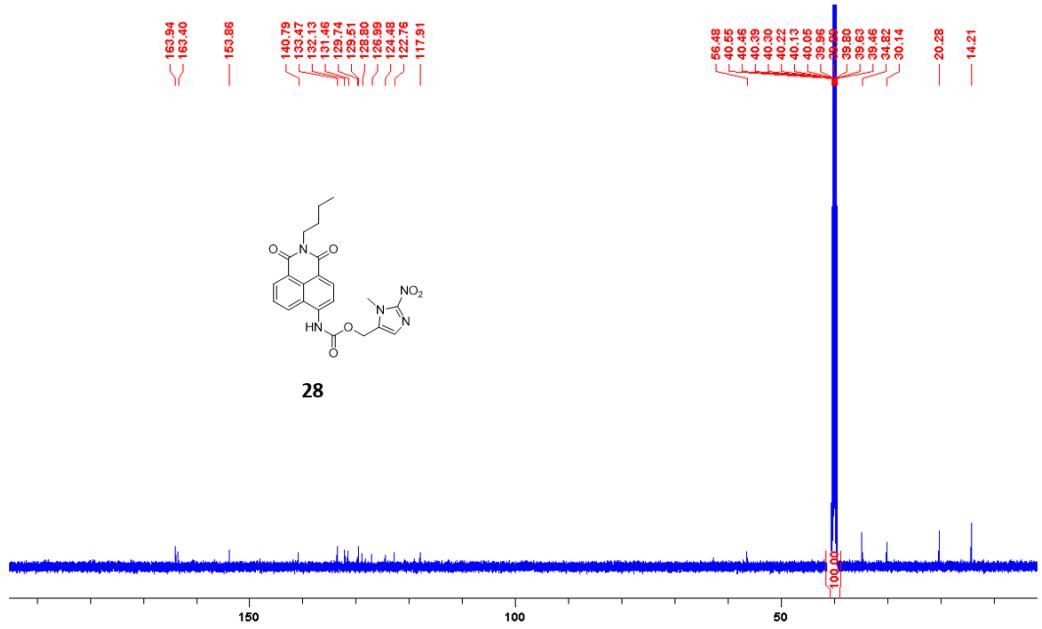

*Figure 7-12: The ^{13}C NMR spectrum of compound **28** (125 MHz, DMSO-d_6)*

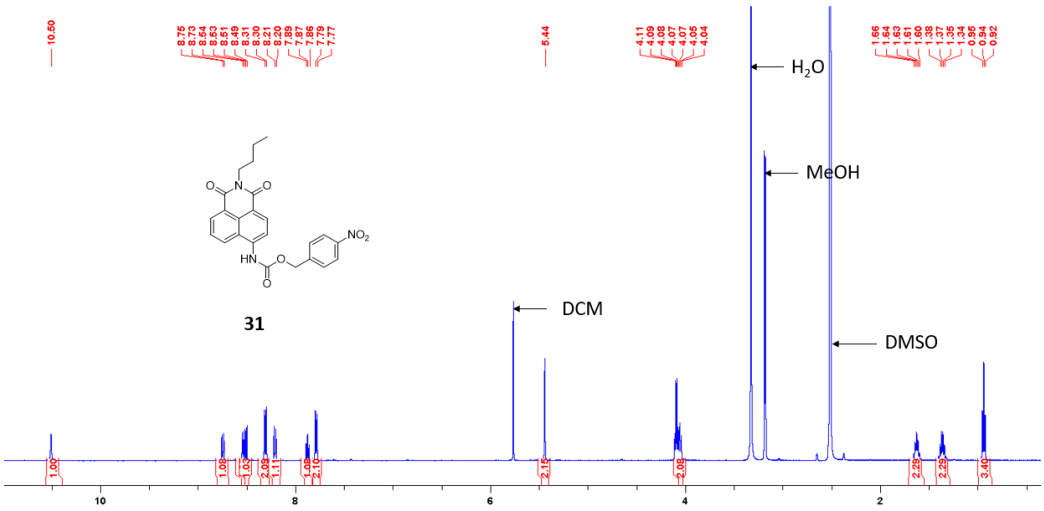

*Figure 7-13: The ^{1}H NMR spectrum of compound **31** (500 MHz, DMSO-d_6)*

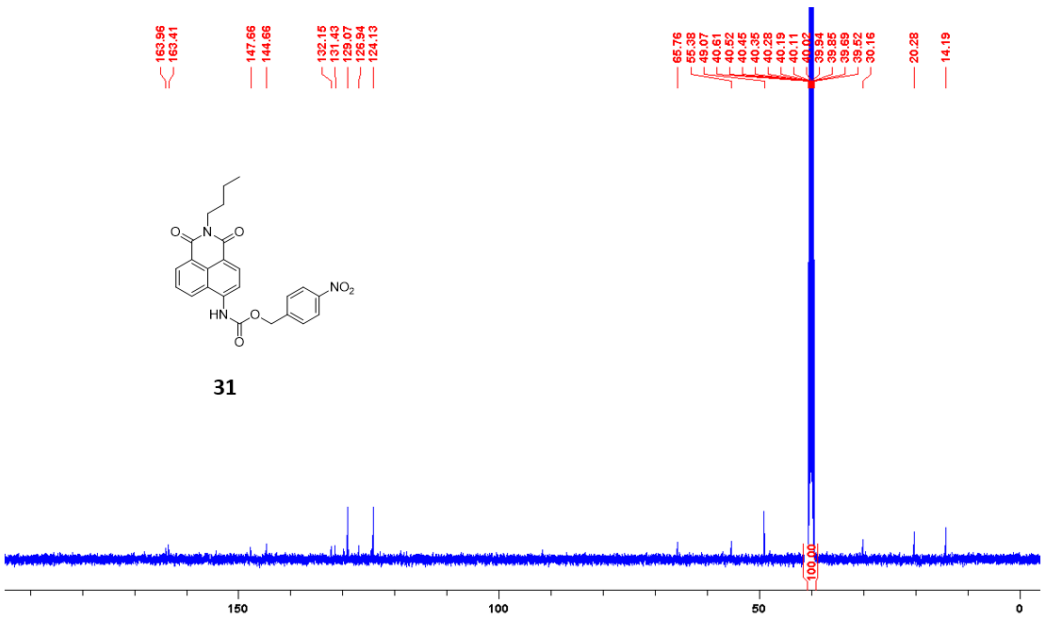

*Figure 7-14: The ^{13}C NMR spectrum of compound **31** (125 MHz, DMSO-d_6)*

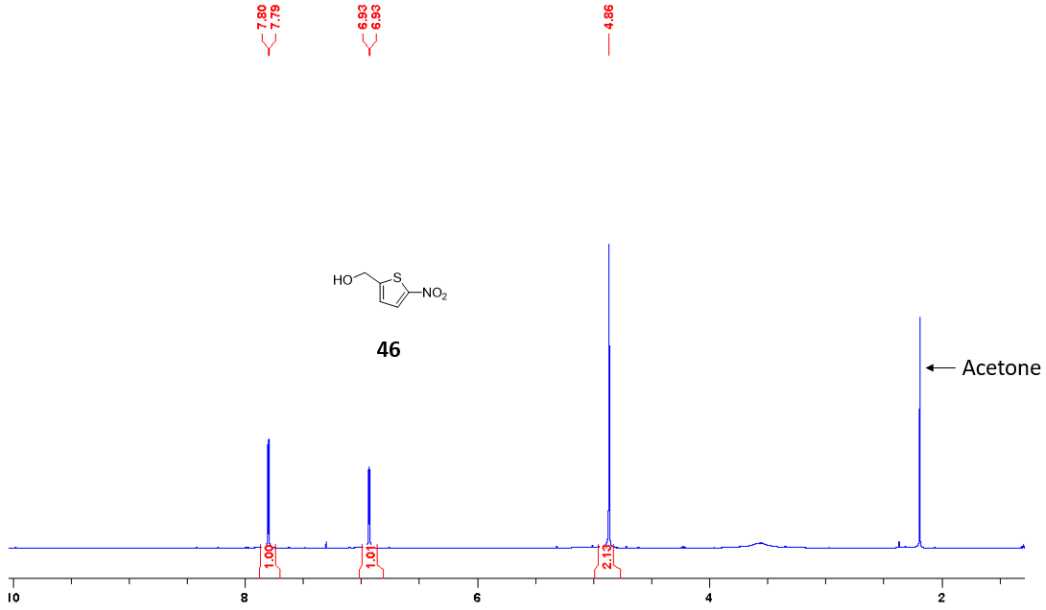

*Figure 7-15: The ^{1}H NMR spectrum of compound **46** (500 MHz, $CDCl_3$)*

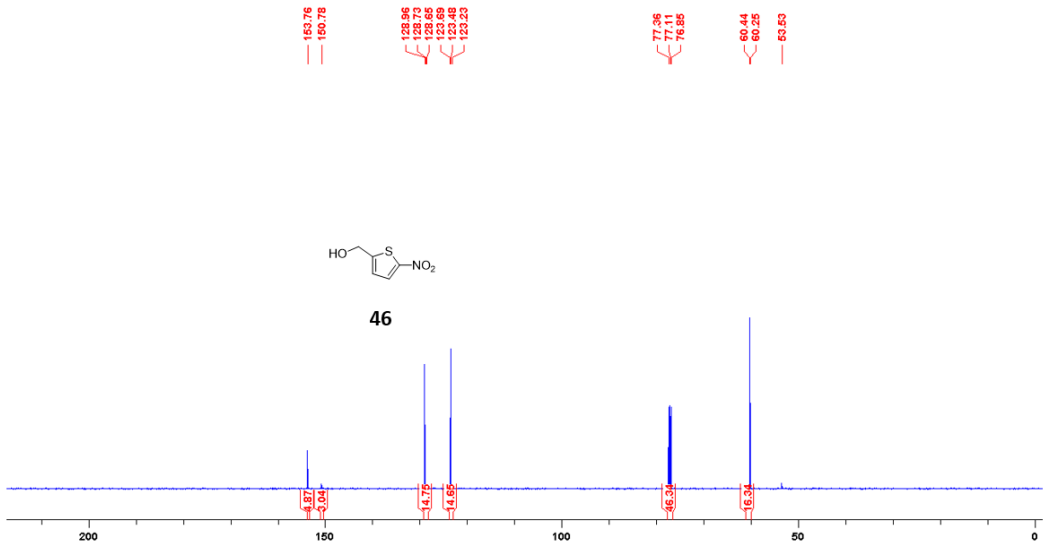

*Figure 7-16: The ^{13}C NMR spectrum of compound **46** (125 MHz, $CDCl_3$)*

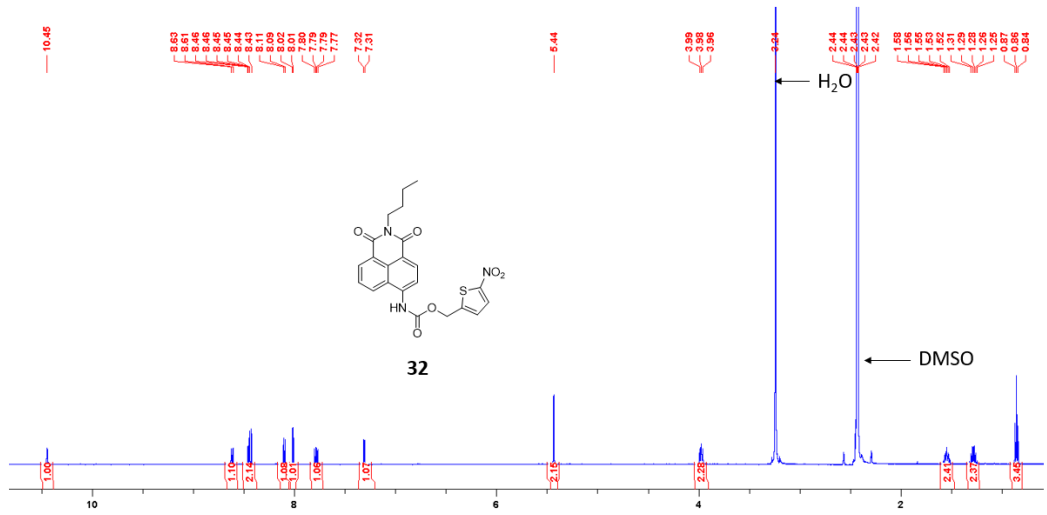

*Figure 7-17: The ^{1}H NMR spectrum of compound **32** (500 MHz, DMSO-d_6)*

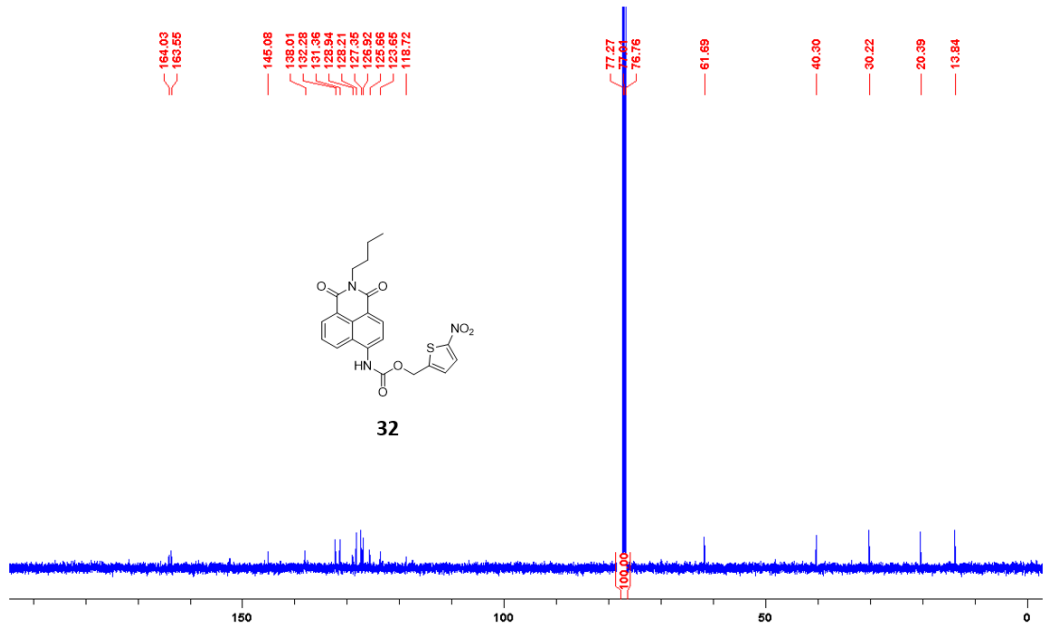

*Figure 7-18: The ^{13}C NMR spectrum of compound **32** (125 MHz, DMSO-d_6)*

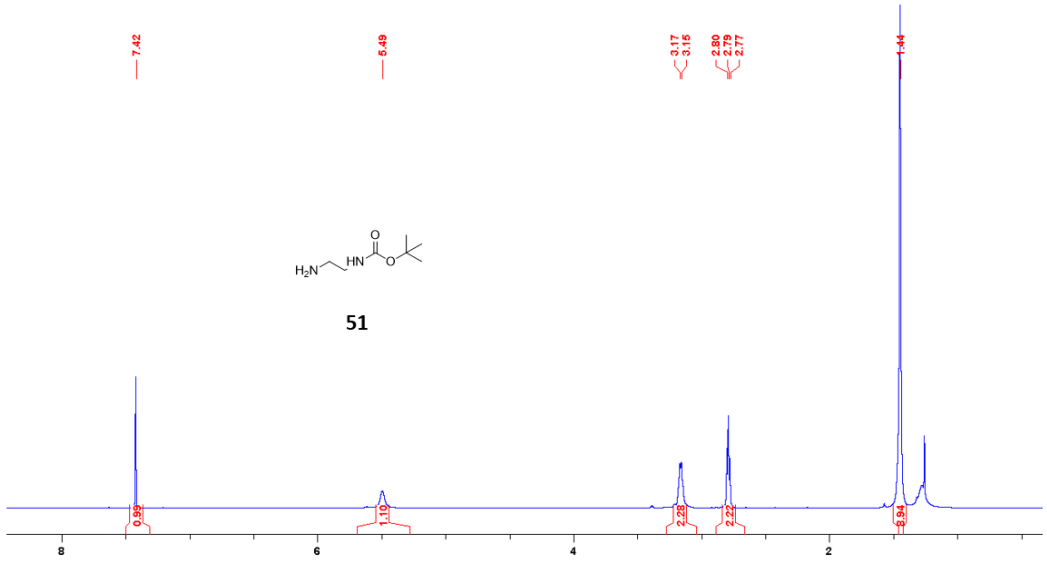

*Figure 7-19: The ^{1}H NMR spectrum of compound **51** (500 MHz, DMSO-d_6)*

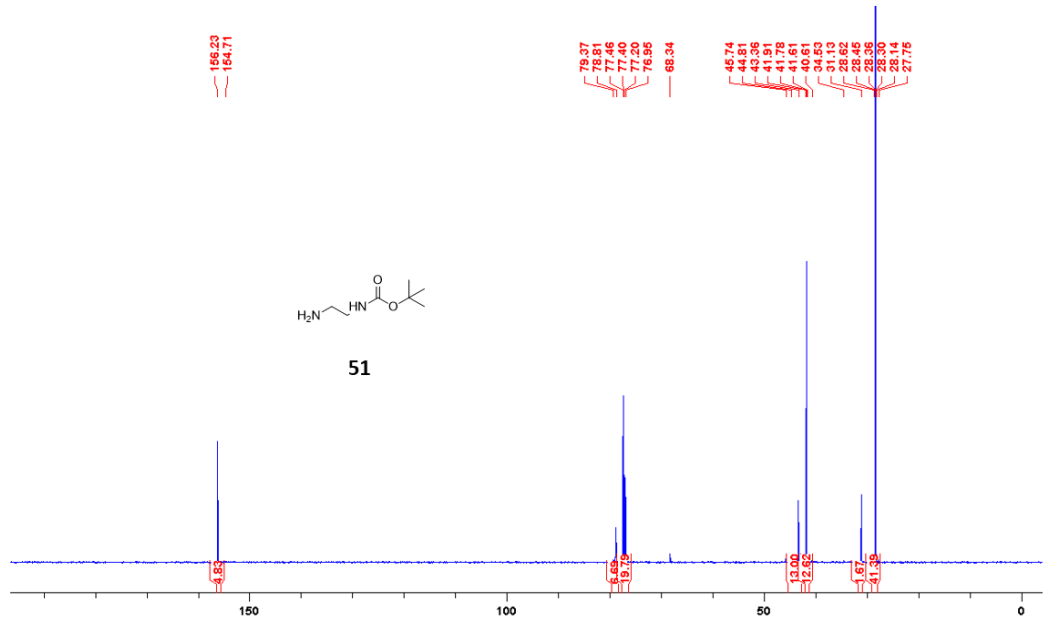

*Figure 7-20: The ^{13}C NMR spectrum of compound **51** (125 MHz, DMSO-d_6)*

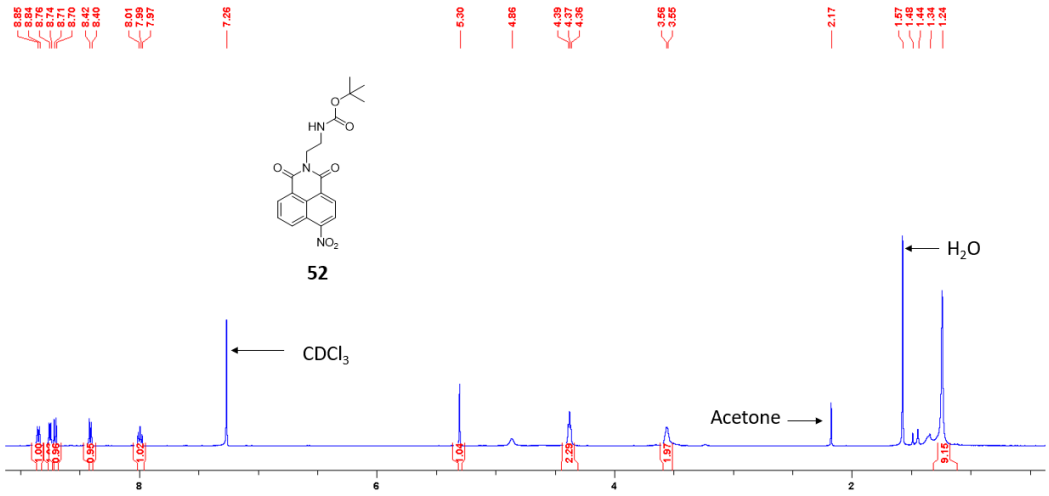

*Figure 7-21: The ^{1}H NMR spectrum of compound **52** (500 MHz, $CDCl_3$)*

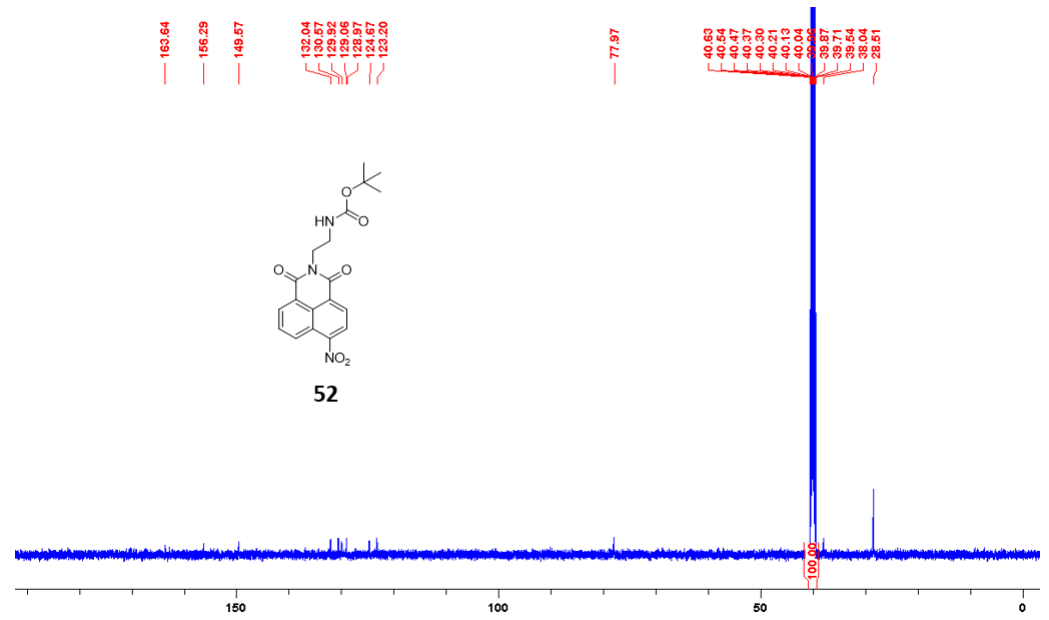

*Figure 7-22: The ^{13}C NMR spectrum of compound **52** (500 MHz, $CDCl_3$)*

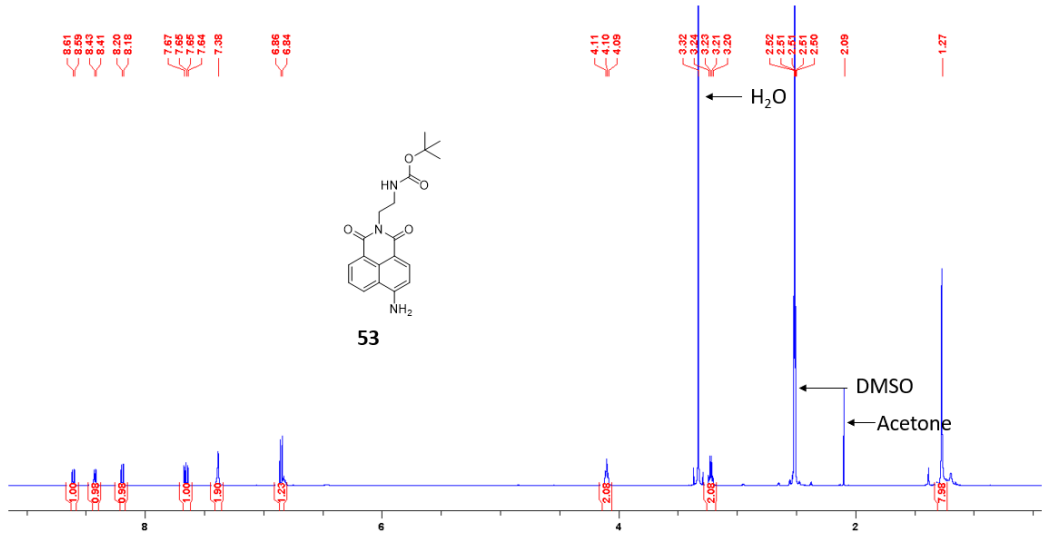

*Figure 7-23: The ^{1}H NMR spectrum of compound **53** (500 MHz, DMSO-d_6)*

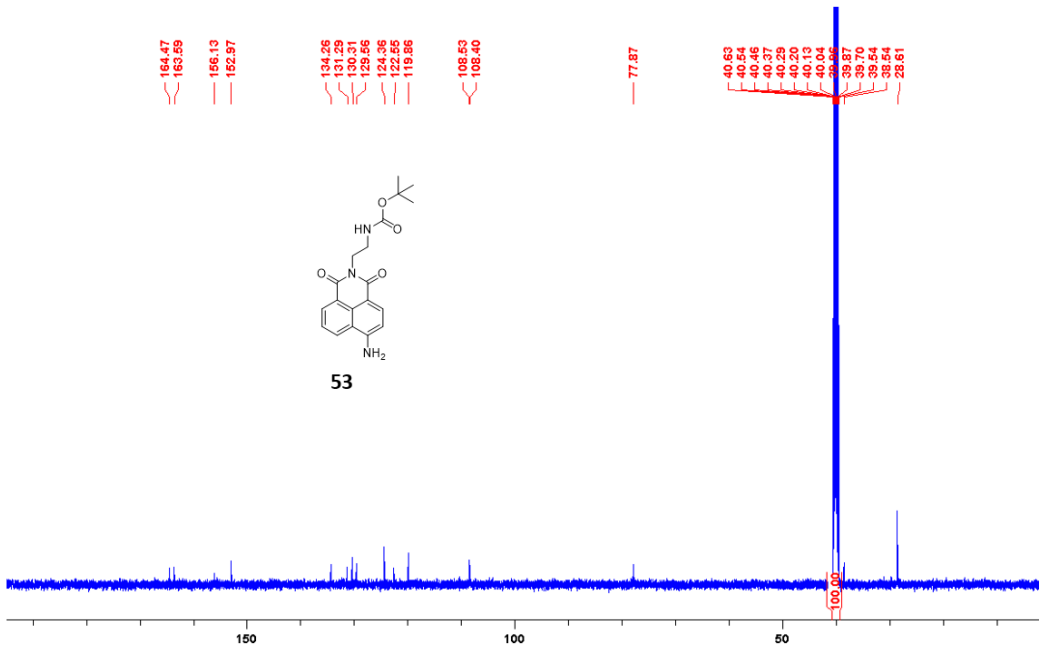

*Figure 7-24: The ^{13}C NMR spectrum of compound **53** (125 MHz, DMSO-d_6)*

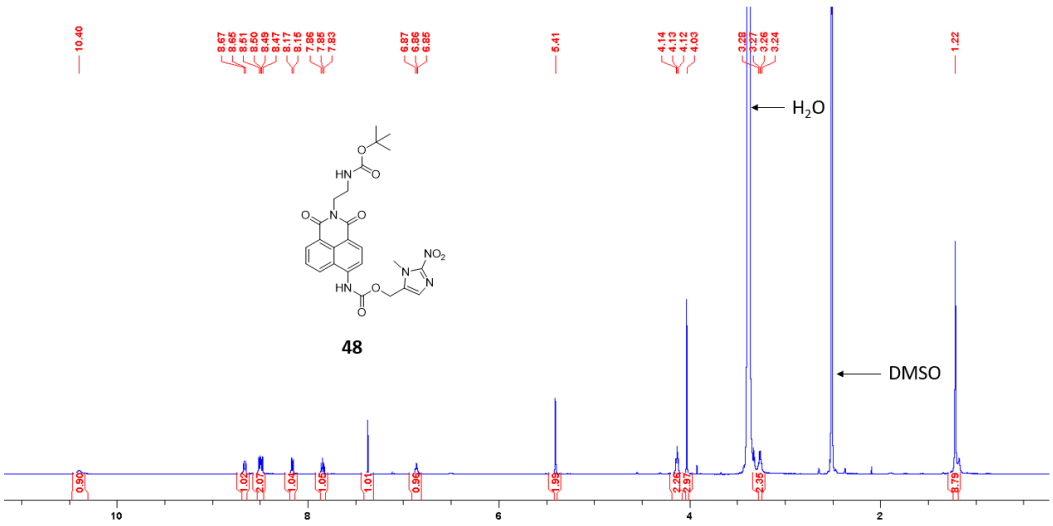

*Figure 7-25: The ^{1}H NMR spectrum of compound **48** (500 MHz, DMSO-d_6)*

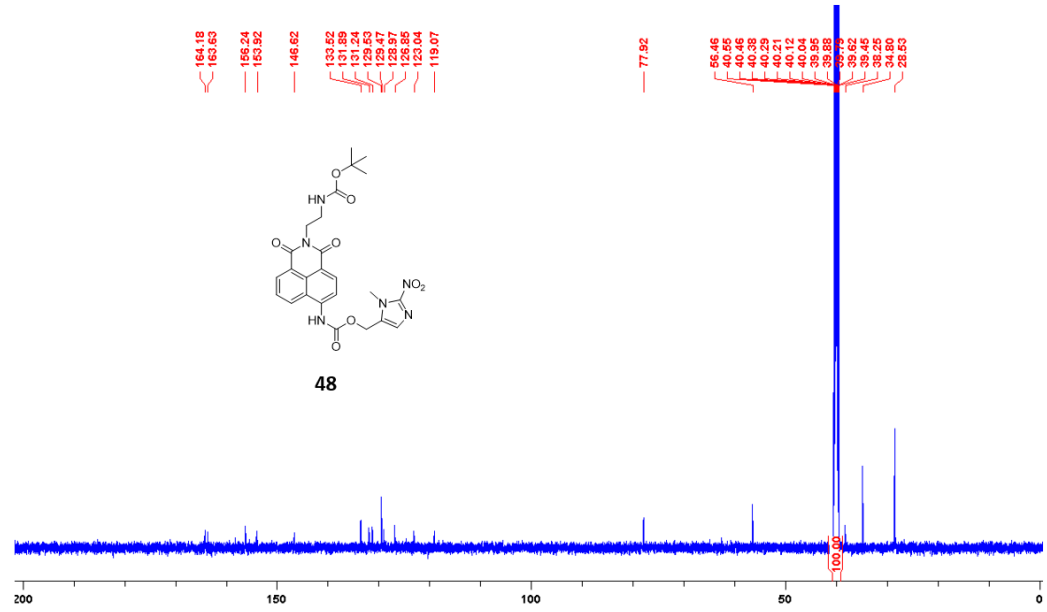

*Figure 7-26: The ^{13}C NMR spectrum of compound **48** (125 MHz, DMSO-d_6)*

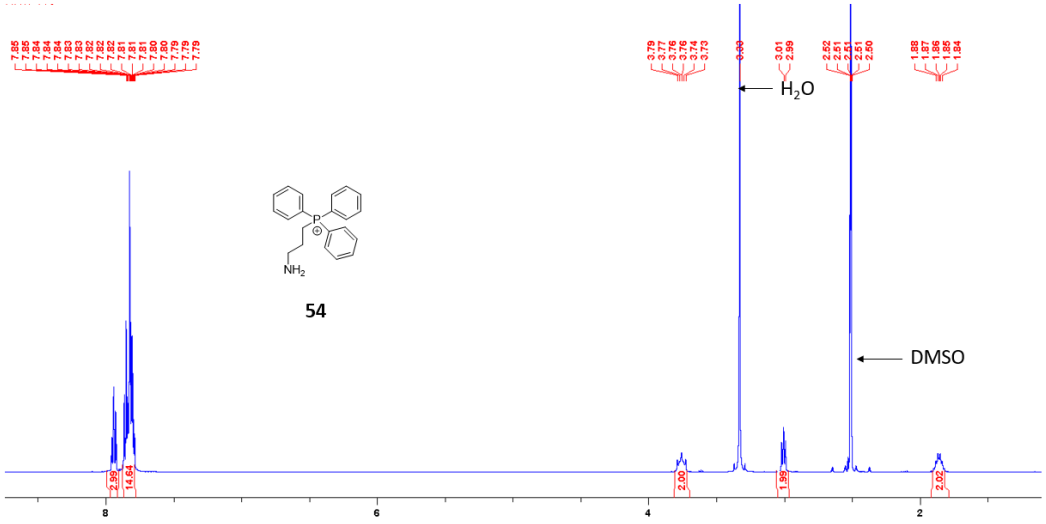

*Figure 7-27: The ^{1}H NMR spectrum of compound **54** (500 MHz, DMSO-d_6)*

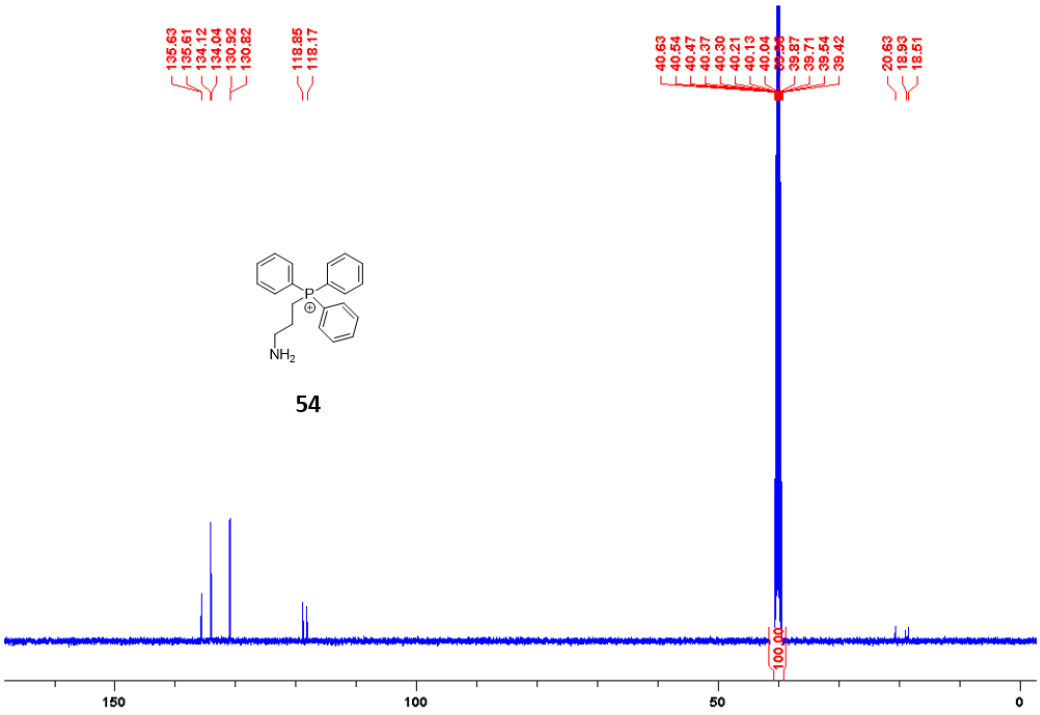

*Figure 7-28: The ^{13}C NMR spectrum of compound **54** (125 MHz, DMSO-d_6)*

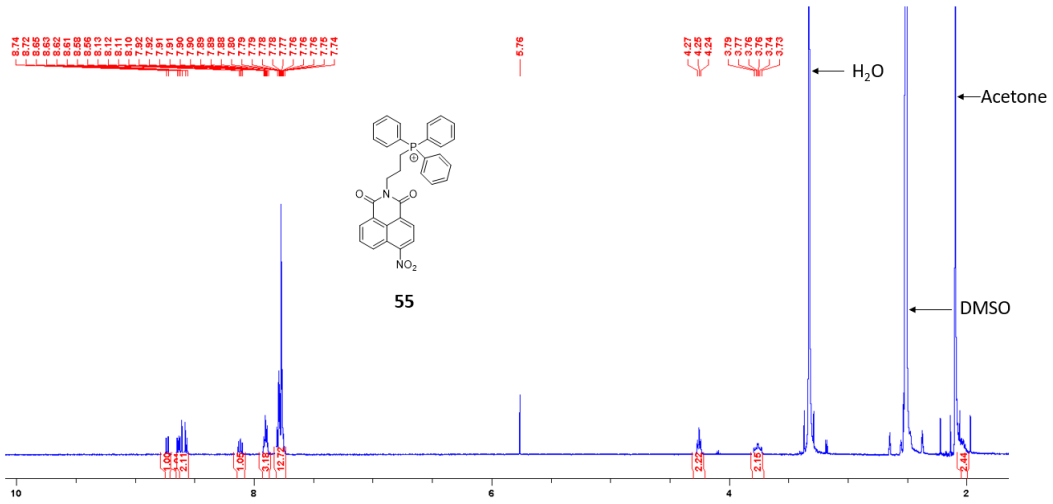

*Figure 7-29: The ^{1}H NMR spectrum of compound **55** (500 MHz, DMSO-d_6)*

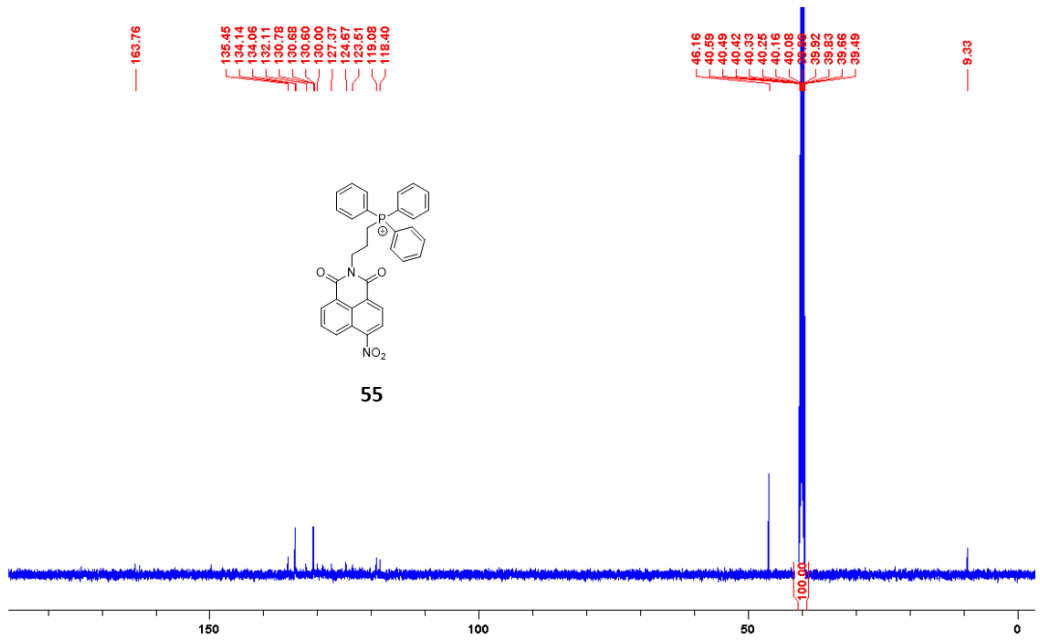

*Figure 7-30: The ^{13}C NMR spectrum of compound **55** (125 MHz, DMSO-d_6)*

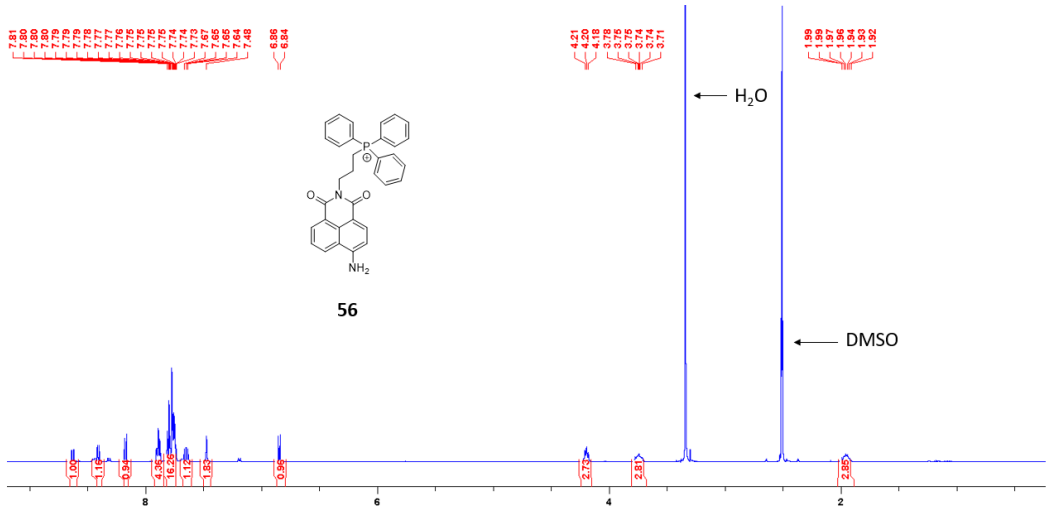

*Figure 7-31: The ^{1}H NMR spectrum of compound **56** (500 MHz, DMSO-d_6)*

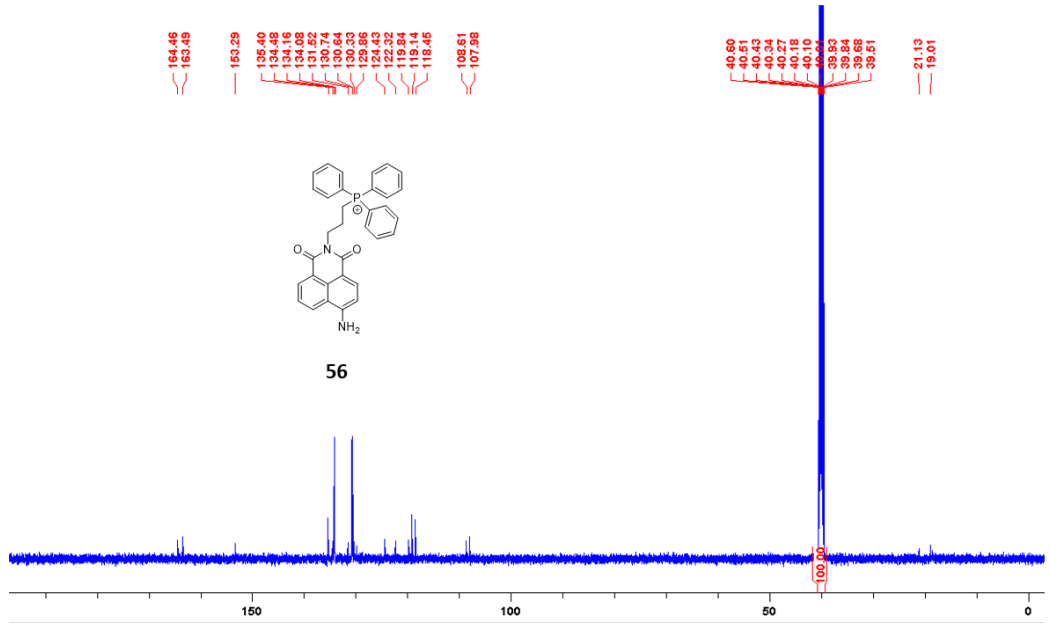

*Figure 7-32: The ^{13}C NMR spectrum of compound **56** (125 MHz, DMSO-d_6)*

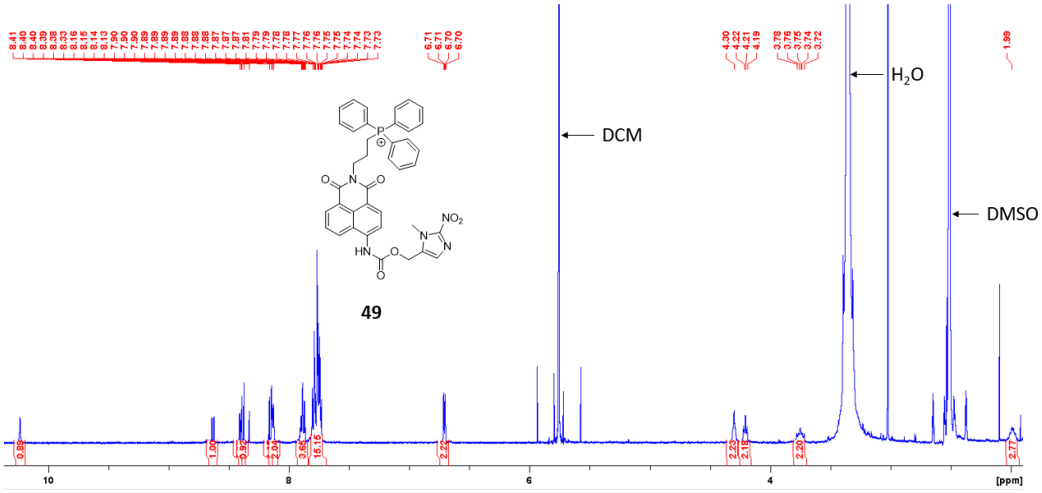

*Figure 7-33: The ^{1}H NMR spectrum of compound **49** (500 MHz, DMSO-d_6)*

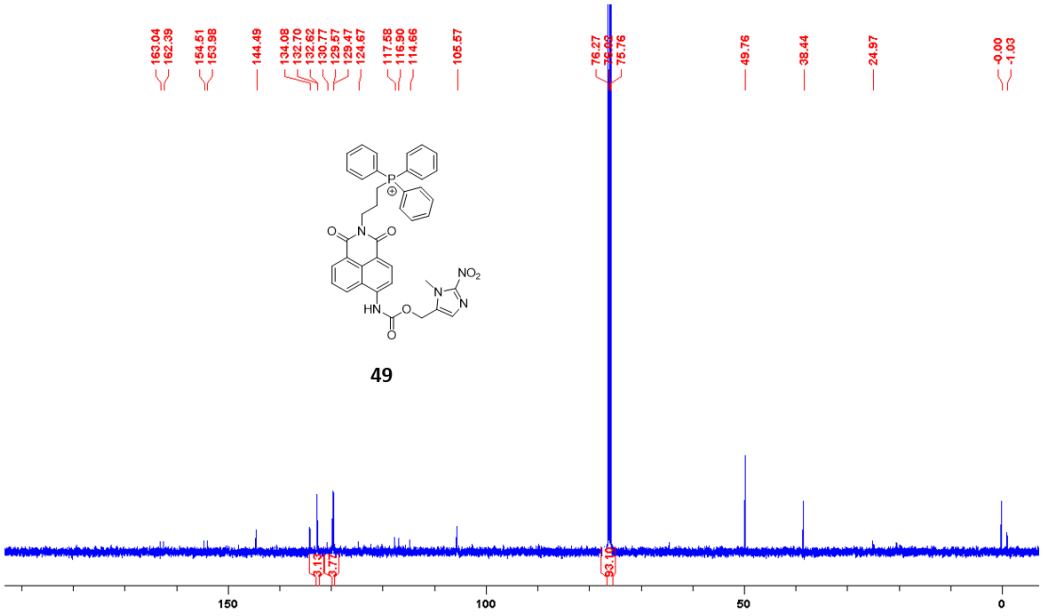

*Figure 7-34: The ^{13}C NMR spectrum of compound **49** (125 MHz, DMSO-d_6)*

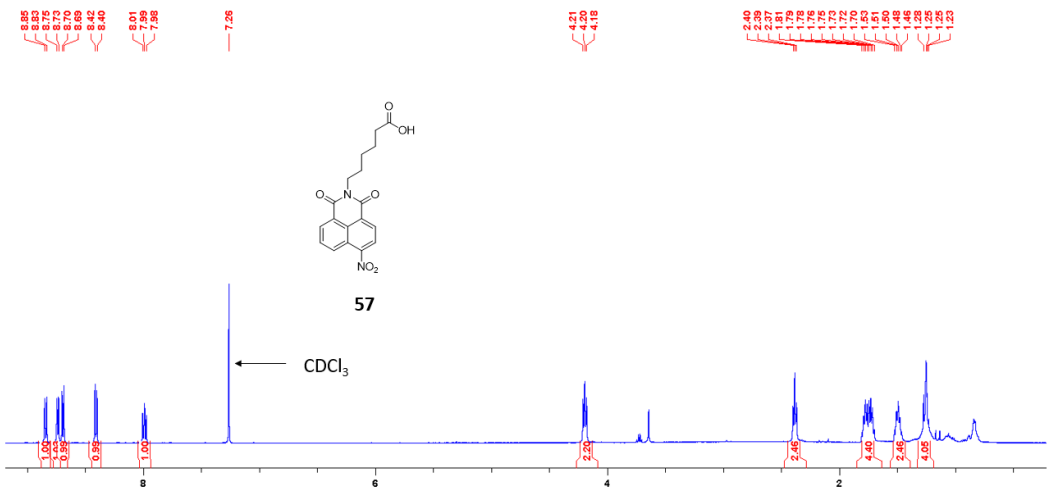

*Figure 7-35: The ^{1}H NMR spectrum of compound **57** (500 MHz, $CDCl_3$)*

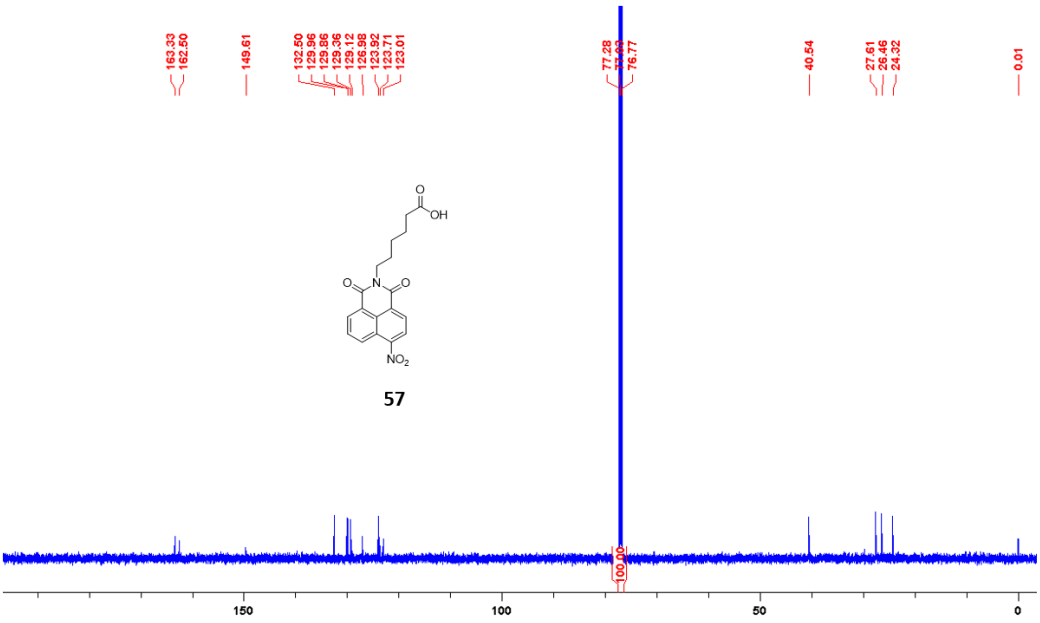

*Figure 7-36: The ^{13}C NMR spectrum of compound **57** (125 MHz, $CDCl_3$)*

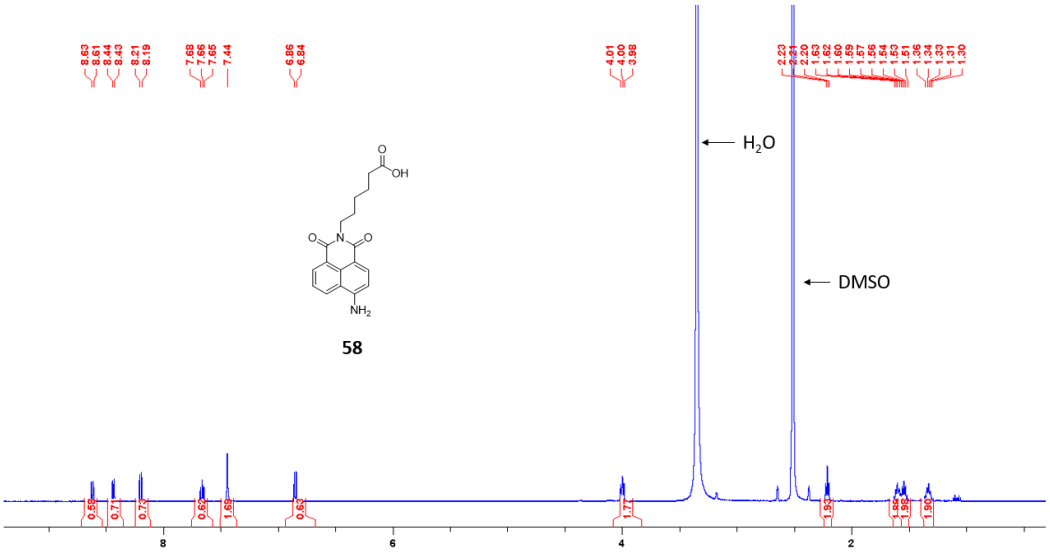

*Figure 7-37: The ^{1}H NMR spectrum of compound **58** (500 MHz, DMSO-d_6)*

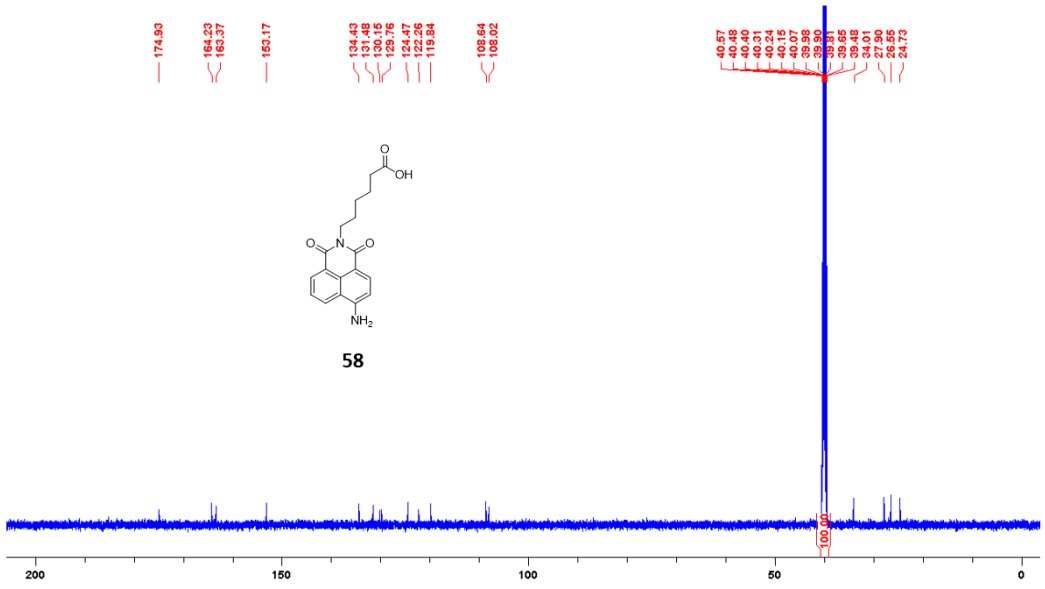

*Figure 7-38: The ^{13}C NMR spectrum of compound **58** (125 MHz, DMSO-d_6)*

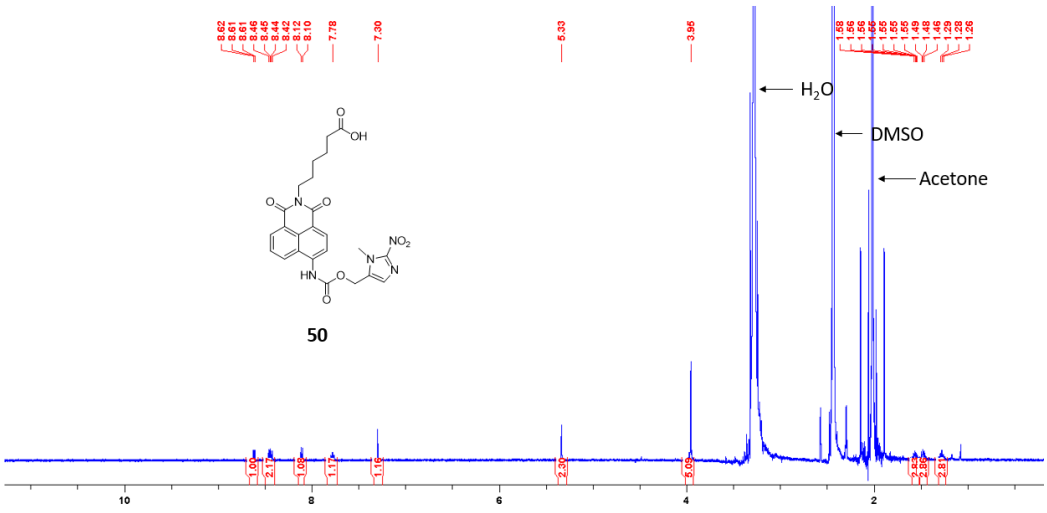

*Figure 7-39: The ^{1}H NMR spectrum of compound **50** (500 MHz, DMSO-d_6)*

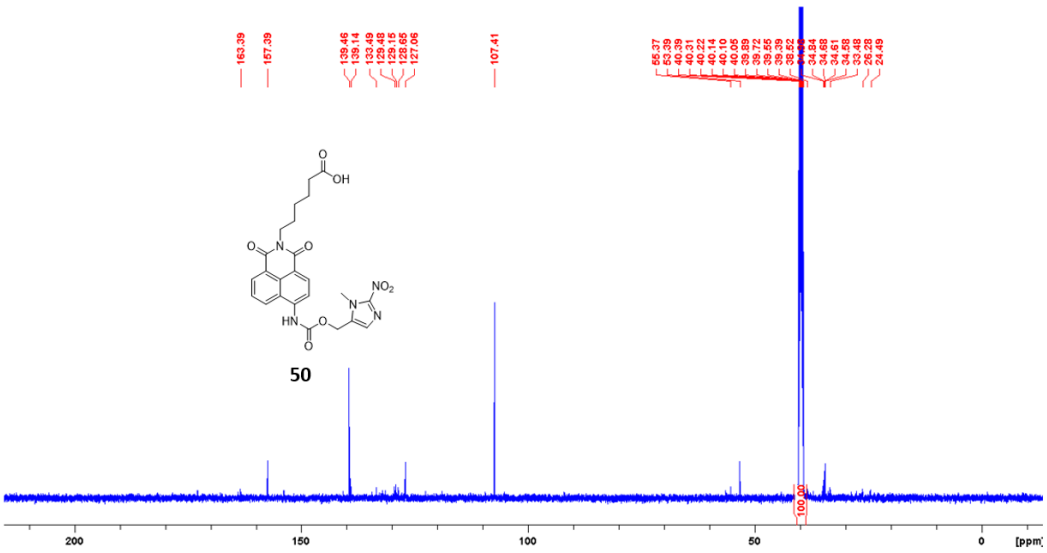

*Figure 7-40: The ^{13}C NMR spectrum of compound **50** (500 MHz, DMSO-d_6)*

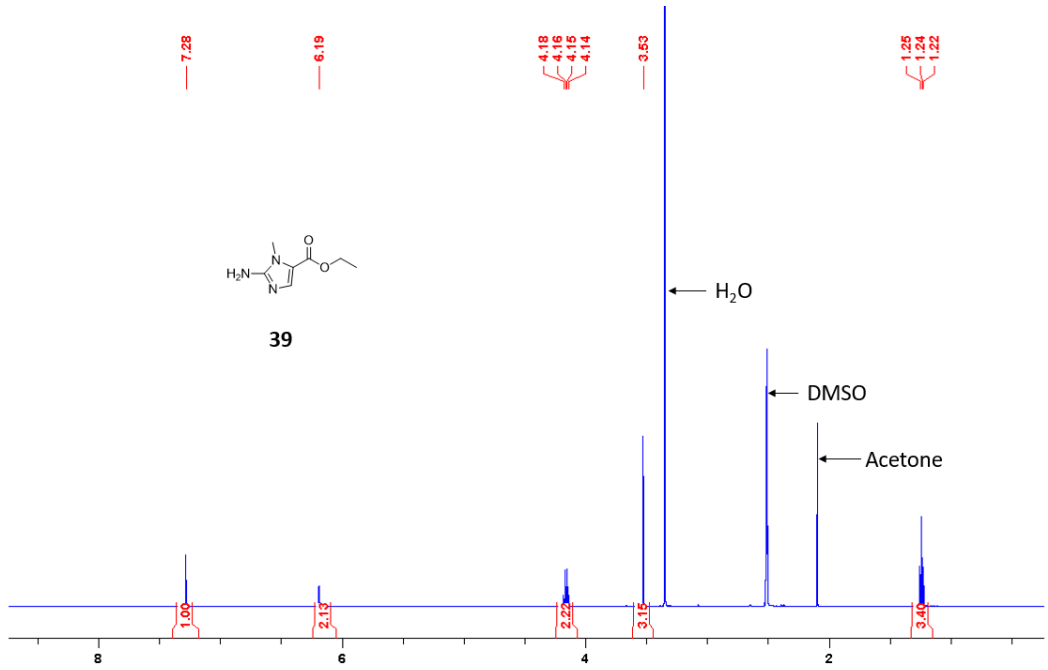

*Figure 7-41: The ^{1}H NMR spectrum of compound **39** (500 MHz, DMSO-d_6)*

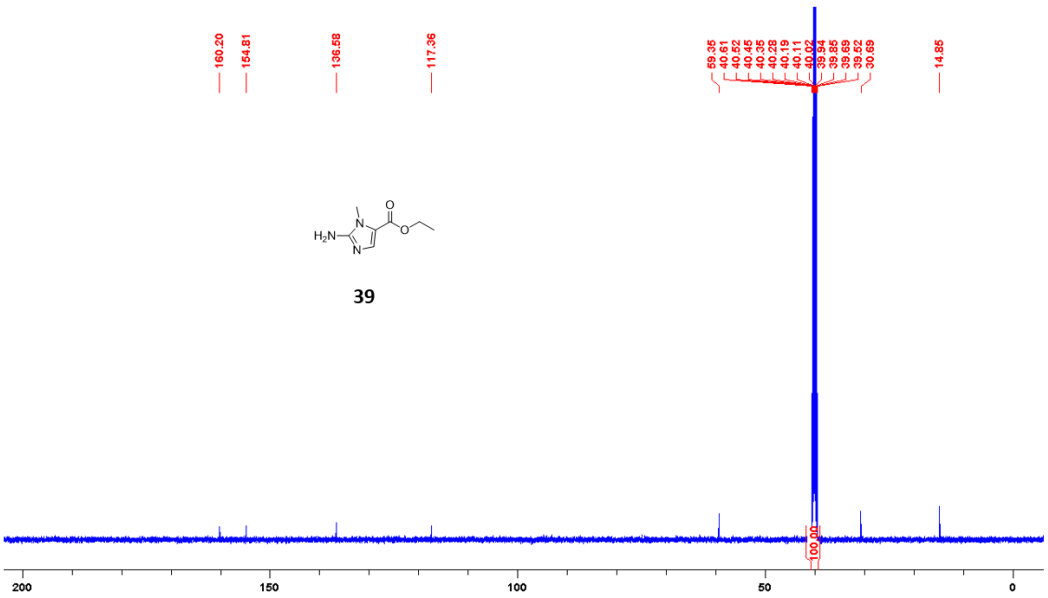

*Figure 7-42: The ^{13}C NMR spectrum of compound **39** (125 MHz, DMSO-d_6)*

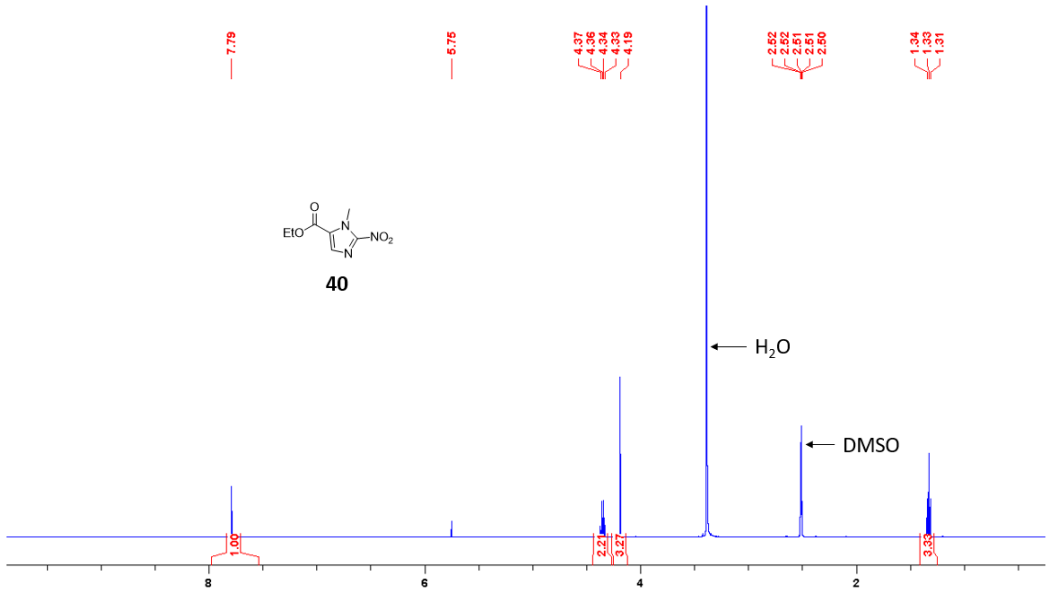

*Figure 7-43: The ^{1}H NMR spectrum of compound **40** (500 MHz, DMSO-d_6)*

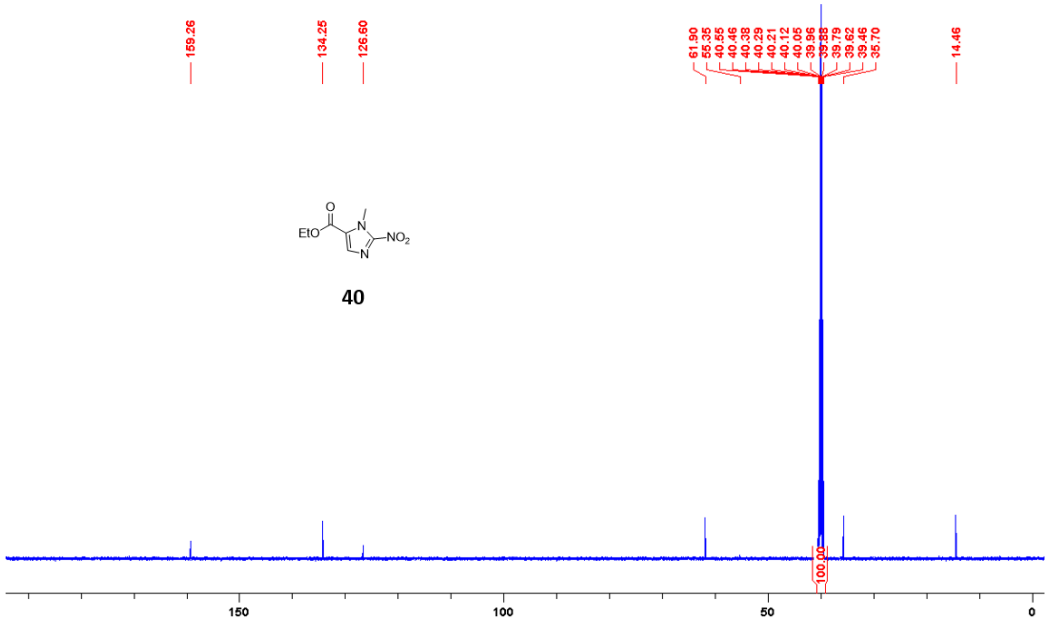

*Figure 7-44: The ^{13}C NMR spectrum of compound **40** (500 MHz, DMSO-d_6)*

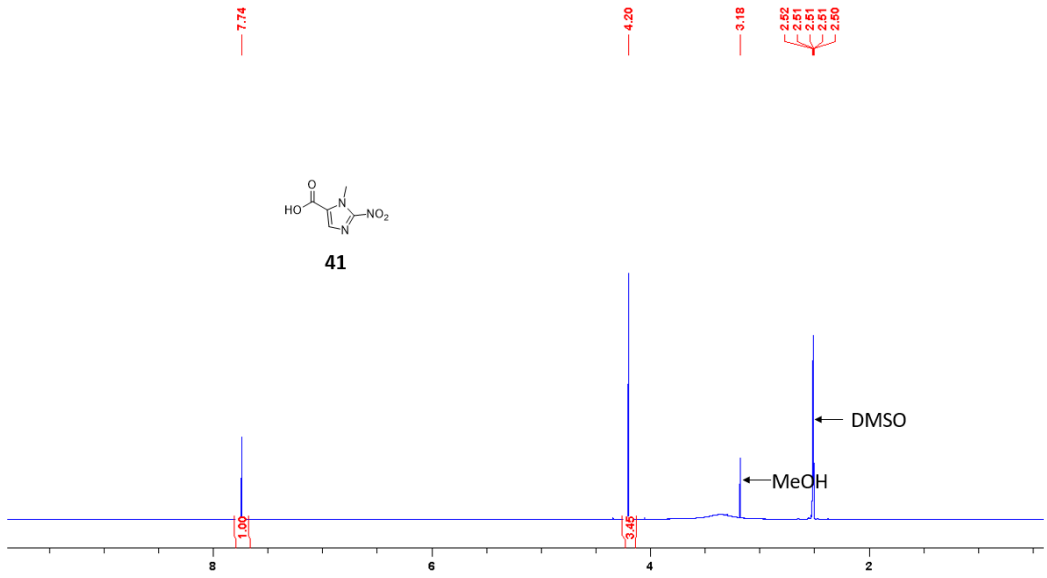

*Figure 7-45: The ^{1}H NMR spectrum of compound **41** (500 MHz, DMSO-d_6)*

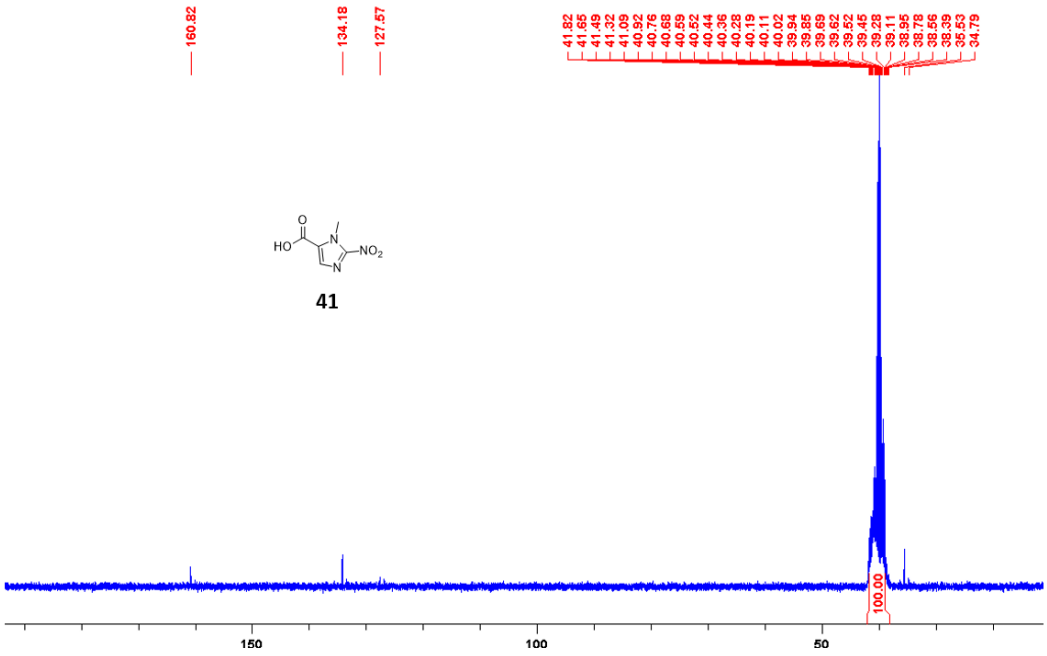

*Figure 7-46: The ^{13}C NMR spectrum of compound **41** (500 MHz, DMSO-d_6)*

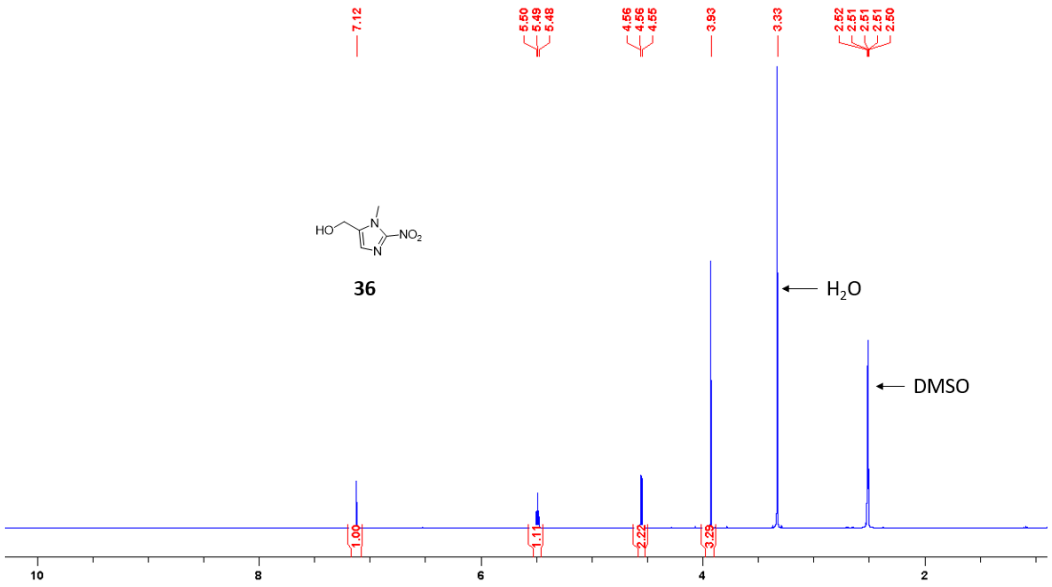

*Figure 7-47: The ^{1}H NMR spectrum of compound **36** (500 MHz, DMSO-d_6)*

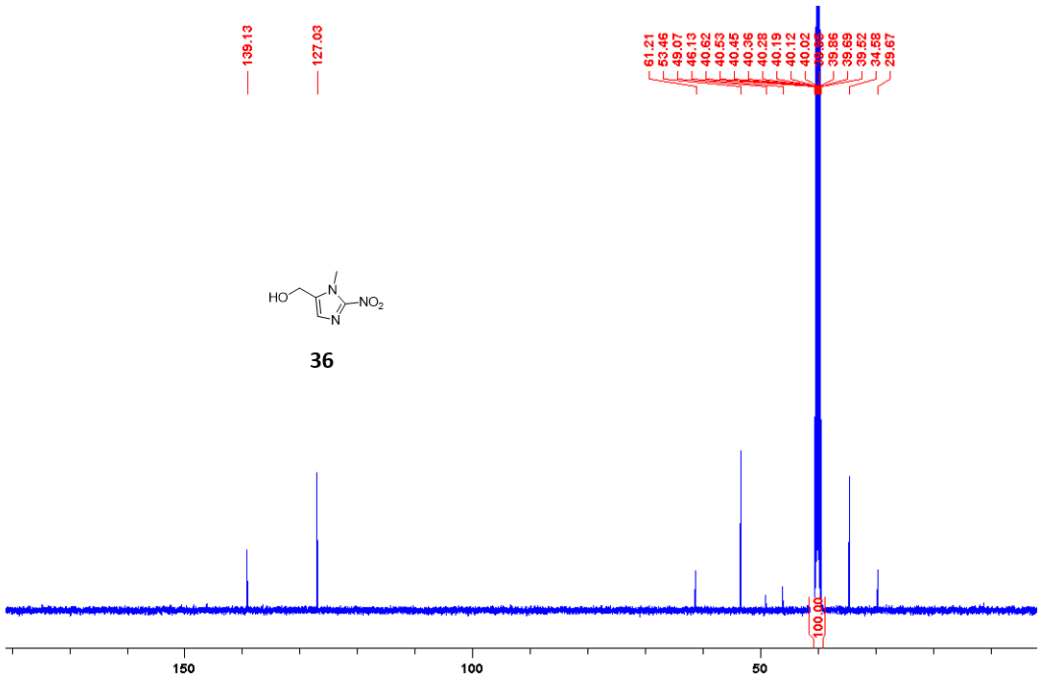

*Figure 7-48: The ^{13}C NMR spectrum of compound **36** (500 MHz, DMSO-d_6)*